This thesis is submitted for the degree of Doctor of Philosophy

By

Manar Essam Mohamed Khalifa

Title

Understanding Receptor-mediated Spillover of Rabies Virus Across Different Mammalian Hosts

Under supervision of

Prof. Muhammad Munir

Division of Biomedical and Life Sciences, Lancaster University, Lancaster, United Kingdom

Dr. Leonie Unterholzner

Division of Biomedical and Life Sciences,

Lancaster University

June 2023

Abstract

Rabies is a lethal viral zoonotic disease causing up to 59,000 human deaths annually. Recent studies have identified several cellular receptors for rabies virus (RV) entry and internalization. However, none of these receptors was identified as indispensable for RV entry. To better understand the preference of RV receptors *in vivo*, we established a cellular model using a replication-competent vesicular stomatitis virus (VSV). In this model, the VSV-G surface glycoprotein was replaced with the RV-G (Rabies Virus Glycoprotein) surface glycoprotein fused with a green fluorescent protein (GFP). To investigate the specific role of RV receptors in promoting RV entry, we identified that HaCaT cell line is refractory for RV infection. By studying the role of RV receptors in HaCaT cells, we identified ITGB1, mGluR2, and nAChR as potential receptors for RV entry and replication. Consequently, further studies involved generating knockout (KO) cell lines corresponding to each of these receptors. Surprisingly, RV was still able to enter and replicate in the generated KO cell lines, yet the replication and entry of RV in KO cells lacking mGluR2 and ITGB1 were significantly reduced; respectively. These findings suggest that RV employ binding to these receptors in series rather than sequentially. To gain more understanding of whether RV employ similar receptor preference among human, dog, and bats. We utilized the rVSV-dG-RV-G-GFP in A549 (lung human cells), Pa-Br (brain bat cells), and MDCK (dog kidney cells) cell lines that overexpress receptor orthologs from their respective species. Our findings revealed distinct receptor utilization by RV depending on the cell type. In human cells, human ITGB1 increased virus entry, while the nAChR enhanced virus replication. In bat cells, ectopic expression of nAChR allowed enhanced virus entry and internalization. While MDCK cells overexpressing ITGB1 enhanced the levels of virus entry and replication. These observations suggest that the RV receptor might be influenced by underlying pathways during the interaction between the virus and receptor in different cell lines. In conclusion, our study provides insights into the complex relationship between RV and its host receptors, uncovering distinct receptor preferences and emphasizing the significance of host-specific factors in virus entry and replication.

Declaration of originality

I declare that the content of this thesis is my own work and has not been submitted by myself in substantially the same form for the award of a higher degree elsewhere. Any sections of the thesis which have been published have been clearly identified.

Manar Khalifa

Table of Contents

List of Figures

List of Tables

List of Abbreviations

7 TMD	Seven Transmembrane helices
ABLV	Australian bat lyssavirus
ABLV	Australian Bat Lyssavirus
ANOVA	Analysis of variance
Aravan lyssavirus	ARAV
ASGR1	Asialo-glycoprotein receptor 1
Bokeloh bat lyssavirus	BBLV
CCR5	chemokine receptor
CDC	Centre for Disease Control and Prevention
cDNA	Complementary deoxyribonucleic acid
CER	chicken embryo-related
CMC	Carboxy methyl cellulose
CME	Clathrin mediated endocytosis
CPE	Cytopathic effect
CRD	cysteine-rich domain
CRISPR	Clustered regularly interspaced short palindromic repeat
cRNA	complementary RNA
CT	Cycle threshold
DAPI	4',6-diamidino-2-phenylindole
DMEM	Dulbecco's Modified Eagle Medium
DMSO	Dimethyl sulphoxide
DNA	Deoxyribonucleic acid
DRGs	dorsal root ganglia
DUUV	Duvenhage lyssavirus
EBLV-2	European bat 2 lyssavirus
ECSRT	endosomal sorting complex required for transport
EDTA	Ethylene diamine tetra acetic acid
ER	Endoplasmic reticulum

ERA-GFP	Evelyn-Rokitnicki-Abelseth-green fluorescence protein
FC	Flow cytometry
FELV-A	Feline leukaemia virus subtype A
FELV-C	Feline leukaemia virus subtype C
FFT	Fast Fourier transform
FITC	Fluorescein isothiocyanate
FN	Fibronectin
FWD	Forward
G	Glycoprotein
GBLV	Gannoruwa bat lyssavirus
GFP	Green Fluorescent protein
HA	Hemagglutinin protein
HCV	Hepatitis C-virus
HDCV	human diploid cell vaccine
HIV-1	Human immunodeficiency virus type 1
hpi	Hour post infection
I/C	Intra cerebral
I/M	intramuscular
Ikoma lyssavirus	IKOV
Immunofluorescence assay	IFA
IP	Immunoprecipitation
Irkut Virus	IRKV
ITGB1	Integrin beta 1
JAK-STAT	Janus kinase signal transducer and activator of transcription
kDa	Kilo Dalton
KHUV	Khujand lyssavirus
KO	Knockout
KBLV	Kotohlahti bat lyssavirus

KREMEN 1	Kringle domain-containing transmembrane protein 1
L	Large protein
LBV	Lagos bat lyssavirus
LBD	Ligand binding domain
LLBV	Lleida bat lyssavirus
M	Matrix protein
mGlUR2	Metabotropic Glutamate Receptor 2
min	minute
mNGS	Metagenomic next-generation sequencing
MOI	Multiplicity of infection
Mokola lyssavirus	MOKV
mRNA	Messenger RNA
N	Nucleoprotein protein
NA	Neuraminidase protein
nAChR	Nicotine acetyl choline receptor
NCAM	Neural cell adhesion Molecule
NFW	Nuclease free water
ng	Nanogram
NGF	nerve growth factor
ORF	Open reading frame
ORV	Oral rabies vaccine
P	Phosphoprotein
pAb	Polyclonal antibody
PAGE	Polyacrylamide gel electrophoresis
PBS	Phosphate buffered saline
PBST	Phosphate buffered saline-tween 20
PCECV	purified chick embryo cells vaccine
PCR	Polymerase chain reaction
PDB	Protein database
PFU	Plaque forming unit

pmol	Pico moles
PVDF	polyvinylidene fluoride
RBD	receptor binding domain
rc	Replication competent
RdRp	RNA dependent RNA Polymerase
REV	Reverse
RFP	Red fluoresence protein
rFPV	Recombinant fowl pox virus
RGD	Arg-Gly-Asp
RIG	Rabies Immunoglobulin
RNA	Ribonucleic acid
RNP	Ribonucleoprotein
RT-qPCR	Reverse Transcription-quantitative Polymerase Chain Reaction
RV	Rabies Virus
SARS-CoV-2	Severe Acute Respiratory Syndrome Coronavirus-2
SDS	Sodium dodecyl sulphate
SEM	Standard errors of mean
sgRNA	Single guide RNA
SHIBV	Shimoni bat lyssavirus
siRNA	short interfering RNA
SOC	Super Optimal broth with Catabolite repression
SpCas9	Streptococcus Pyogenes Cas 9
SRV	Semple rabies vaccine
STAT1	Signal transducer and activator of transcription 1
SV40	Simian virus 40
TEMED	Tetramethyl ethylenediamine
TIDE	Tracking Of indels by Decomposition
TM	Transmembrane
UV	Ultraviolet

V	Voltage
VPS	vacoular protein sorting
VSV	Vesicular stomatitis virus
VWA	The von Willebrand A
WCBV	West Caucasian bat lyssavirus
WHO	World Health Organization
WT	Wildtype
x g	times gravitational force
µg	Microgram
µL	Microliter

Acknowledgment

I would like to thank my supervisors Prof. Muhammad Munir and Dr. Leonie Unterholzner for their continuous support and guidance throughout my PhD project.

I would also like to acknowledge all the staff members, technical staff, Ph.D. students, and postdocs in our group and in the Biomedical and Life Science department for their continuous support.

I am indebted to my colleagues and friends, especially Mahmoud, Julianne, Emily and Nadia for their support, encouragement, and understanding throughout this challenging academic journey.

I am so grateful for the British Council and the Egyptian Mission Sector for funding my PhD project.

1 General Introduction

1.1 Rabies virus structure

Rabies is a lethal zoonotic viral disease which causes serious behavioural changes and neurological disorders in a wide range of hosts with a high fatality rate up to 100% (Hueffer et al., 2017). Rabies virus (RV) is bullet-shaped with a size of approximately 200 nm. The viral genome encodes five transcriptional units for nucleocapsid protein (N), phosphoprotein (P), matrix protein (M), glycoprotein (G), and RNA-dependent RNA polymerase or large protein (L) (Jackson, 2013). The genes are organized in the following order: 3'-N-P-M-G-L-5'. The N, P and L proteins encapsulate the RNA genome forming the ribonucleoprotein (RNP), which acts as a template for viral replication and transcription. The RNP together with P and L form the viral replication complex, which is surrounded by a lipid bilayer containing the viral G protein protruding as spikes from the viral surface **(Figure 1.1)**. The M protein has been proposed to bridge the RNP and the cytoplasmic domain (CD) of G protein to form the bullet-shaped virion (Pulmanausahakul et al., 2008).

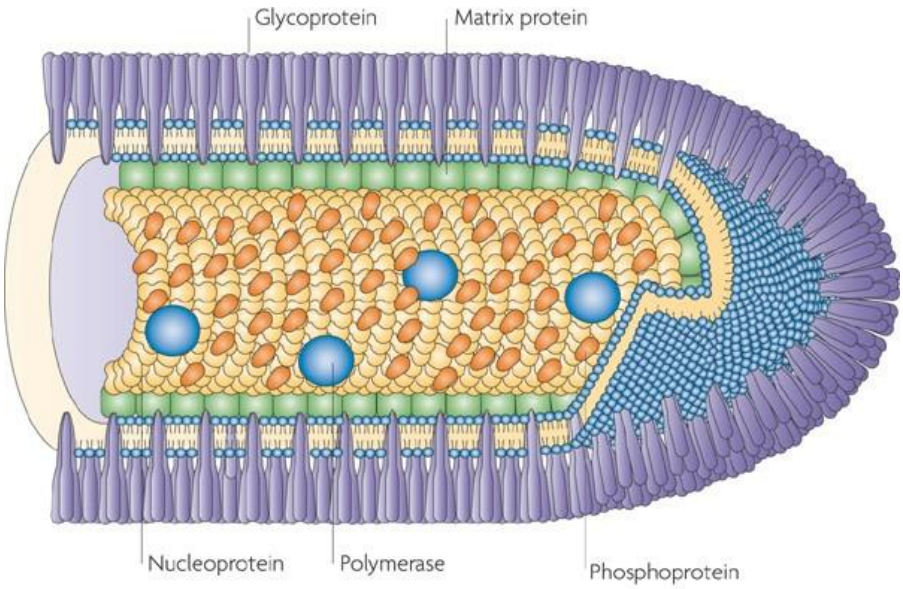

Figure 1.1 The structure of the rabies virus particle.

The viral genome, consists of negative-stranded RNA, is tightly enclosed within the nucleoprotein (yellow), and forms the ribonucleoprotein (RNP). The RNP is associated with two other viral proteins: the viral polymerase (blue) and the phosphoprotein (orange), constituting the internal core or capsid. The capsid is surrounded by a membrane derived from the host cell. This membrane is linked to two additional viral proteins: the matrix protein (green), and the glycoprotein which is arranged in a trimeric structure (purple). The figure is adapted from previous publication (Schnell et al., 2010).

1.2 Classification and distribution of lyssaviruses

The *Rhaboviridae* family constitutes one of the most ecologically diverse families among RNA viruses (Walker et al., 2015). Recently, there has been a significant expansion within the *Rhabdoviridae* family (Shepherd et al., 2023). The classification of viruses within this family is increasingly based solely on genetic sequence information, with less emphasis on biological characteristics for phylogenetic categorization (Shepherd et al., 2023). Utilizing the metagenomic next-generation sequencing (mNGS) for the discovery of new rhabdovirus sequences, has led to the reorganization of the family into 45 genera and 275 virus species distributed among three large subfamilies*: Alpharhabdovirinae, Betarhabdovirinae and Gammarhabdovirinae* (Walker et al., 2015). Based on the phylogenetic analysis of the L protein the *Alpharhabdovirina* subfamily includes 31 genera of viruses, including the genera most associated with human diseases as *Lyssavirus, Vesiculovirus, Tibrovirus and Ledantevirus* **(Figure 1.2)** (Walker et al., 2022). It is worth noting that several genera exhibited predominant associations with specific animal groups such as bats (e.g., ledanteviruses, lyssaviruses), for ungulates (e.g., tibroviruses, vesiculoviruses) (Walker et al., 2015). Notably, several viruses belonging to the *Alpharhabdovirinae* subfamily, including *Lyssavirus*, *Tibrovirus*, *Vesiculovirus*, and *Ledantevirus*, have been associated with human diseases (Shepherd et al., 2023) .

Rabies virus (RV) is an enveloped negative single stranded RNA virus and belongs to genus *Lyssavirus*, phylogroup I of the family *Rhabdoviridae* (Jackson, 2013). Lyssaviruses are divided into three distinct phylogroups based on serum cross reactivity against viral proteins: phylogroup I, II and III comprising 16 virus species (Banyard and Fooks, 2020) **(Figure 1.3)**. Most of the lyssaviruses belonging to phylogroup I, cause viral encephalitis in humans such as European bat 2 lyssavirus (EBLV), Gannoruwa bat lyssavirus (GBLV) and Australian bat lyssavirus (ABLV) (Fooks et al., 2021). Six lyssaviruses are known to be circulating in Europe: EBLV-1 and EBLV-2 which are prevalent in chiropteran host ; Bokeloh bat lyssavirus (BBLV), which was detected in Natterer's bats in Germany and France; Kotohlahti bat lyssavirus (KBLV), for which there is genetic evidence linked to the Brandt's bat in Finland; West Caucasian bat lyssavirus (WCBV),was isolated from a Bent Winged bat in the Caucasus mountains; and Lleida bat lyssavirus (LLEBV), which

was isolated in Bent Winged bats in both Spain and France (Banyard and Fooks, 2020).The WCBV and LLEBV are among the most genetically distinct from all other European lyssaviruses (Banyard and Fooks, 2020). Additionally, three Eurasian viruses have been characterized, all originating from bats: Aravan lyssavirus (ARAV) in Kyrgyzstan, Khujand lyssavirus (KHUV) which has been isolated in Tajikistan, and Irkut virus (IRKV) that has been isolated in Eastern Siberia (Banyard and Fooks, 2020). Across the Old World, several other lyssaviruses have been identified, including: Lagos bat lyssavirus (LBV), which was found in various bat species across sub-Saharan Africa; Mokola lyssavirus (MOKV), which was known to be prevalent across Africa; Duvenhage lyssavirus (DUVV), was initially isolated from a fatal human bat bite case in Kenya in 1971 and subsequently from fruit bats in South Africa; and Shimoni bat lyssavirus (SHIBV), which was initially isolated in 2009 from a Commerson's leaf-nosed bat in Kenya. Most recently, Ikoma lyssavirus (IKOV) was isolated from an African Civet in Tanzania in 2010, and although found in a terrestrial carnivore, it is believed that it has originated from bats (Fisher et al., 2018). In Australia, only the ABLV has been reported and has been isolated from five different bat species since its initial discovery in 1996 (Banyard and Fooks, 2020). In Asia, only GBLV, has been reported, found in Fruit bats in Sri Lanka in 2014 and 2015 (Fisher et al., 2018).

Figure 1.2 Maximum likelihood phylogenetic tree analysis of 100 rhabdovirus L protein sequences.

Maximum likelihood phylogeny of the *Alpharhabdovirinae* subfamily based on the alignment of trimmed L amino acid sequences. The scale bar on the tree corresponds to the number of amino acid substitutions per site, and nodes receiving substantial support, exceeding 70, are indicated by black circles, as

determined through 1000 bootstrap replicates. Orange text refers to viruses linked to human infections. The figure is adapted from previous study (Shepherd et al., 2023).

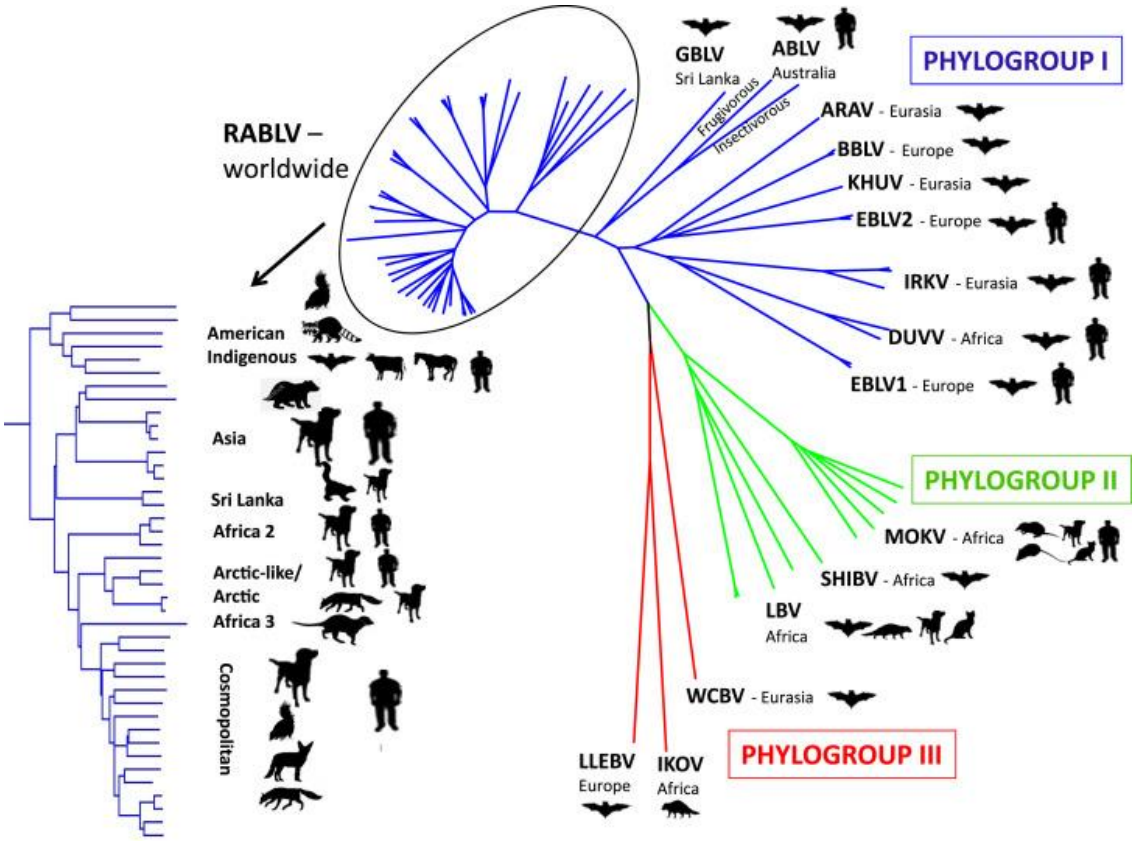

Figure 1.3 Phylogenetic relatedness of lyssaviruses

Lyssaviruses are classified into 3 phylogroups (I-III) based on the serum cross reactivity against the viral proteins and genetic sequence differences. The geographical area and the primary host are indicated for each of the lyssaviruses. Abbreviations: European bat lyssavirus (EBLV-1-EBLV-2), Gannoruwa bat lyssavirus (GBLV); Australian bat lyssavirus (ABLV); Bokeloh bat lyssavirus (BBLV); Kotohlahti bat lyssavirus (KBLV); West Caucasian bat lyssavirus (WCBV); Lleida bat lyssavirus (LLEBV); Aravan lyssavirus (ARAV); Khujand lyssavirus (KHUV); Irkut virus (IRKV); Lagos bat lyssavirus (LBV),; Mokola lyssavirus (MOKV); Duvenhage lyssavirus (DUVV); Shimoni bat lyssavirus (SHIBV); Ikoma lyssavirus (IKOV); Australian Bat Lyssavirus (ABLV).

1.3 Rabies virus replication cycle

1.3.1 Rabies virus entry into the cells

Understanding the mechanism by which RV replicates and induce infection into cells is crucial for future therapeutic implications. Viral entry into cells is regarded as the mechanism by which the cells are unlocked allowing the release of the viral genome and replication (Finke and Conzelmann, 2005). Since the RV infection is usually introduced through a bite or scratch from infected animal, thus the RV infection typically starts in

muscle tissues (Fisher et al., 2019). The RV entry depend on the viral surface components as glycoprotein in RV, where G protein is the surface protein for RV receptors binding (Grove and Marsh, 2011). As previously reported, multiple cellular receptors have been known to be involved in RV entry as the integrin beta 1 (ITGB1), metabotropic glutamate receptor 2 (mGluR2), nicotinic acetylcholine receptor (nAChR), neural cell adhesion molecule (NCAM) and the tumour necrosis factor receptor (p75NTR) (Lafon, 2005). However, none of these receptors have been known to be indispensable for RV entry.

The binding between the RV-G protein and the cellular receptors allow the RV internalization into the endocytic zones via the receptor mediated endocytosis (Fooks et al., 2017). Previous studies have reported that the RV uptake into cells occur through receptor mediated endocytosis through exhibiting properties of endocytic vesicles to migrate (Xu et al., 2015). RV transportation to clathrin coated pits is accomplished through actin enriched cell surface protrusions known as filopodia. This has been proven through the observation of production and elongation of filopodia following infection with RV which enhanced RV uptake (Xu et al., 2015). The mechanism by which RV is internalized into endosome occurs through its attachment to the cell membrane, in which they invaginate forming vesicle which bind to new forming vesicle forming tensile force, thereby, facilitating the detachment from the cell membrane and allowing its entry to the cytoplasm (Xu et al., 2015). The uptake of RV in neuronal and non-neuronal cells was known to be achieved by clathrin coated endocytosis which can be validated by their transport and co packaging with transferrin (Piccinotti et al., 2013). Subsequently, the cellular transport systems were used by RV to incorporate their genomes to cellular compartments for replication. Elucidating if the G protein attachment to specific receptors may influence the mechanism by which viral particle associates with clathrin mediated endocytosis needs further investigation (Piccinotti et al., 2013) **(Figure 1.4)**.

1.3.2 Clathrin-mediated endocytosis, fusion and uncoating

Upon the specific binding between the RV-G and the cellular receptors, the virus internalization occurs. Clustering of the cell surface receptors activates downstream signalling pathways (Guo et al., 2019). RV, like many viruses that enter the cells through

endocytosis, gets transported to the endosomes. In the endosomes, the RV utilize the low pH for membrane fusion and release of their genetic material into the cytoplasm (Grove and Marsh, 2011). Owing to the surface localization of the G protein, it plays a crucial role in the viral fusion (Pulmanausahakul et al., 2008). Unlike other viruses, fusion of RV does not necessitate the presence of components as cholesterol or sphingolipids. The low pH in the early endosomes (pH 5.8-6.0) resulted in conformational changes of G protein, facilitating the fusion of the viral envelope with the endosomal membrane (Gaudin et al., 1999). Interestingly, it was previously shown that fusion of RV with the endosomes limited the display of RV components on cell surface, allowing their evasion to the immune cell (Grove and Marsh, 2011). After the fusion between RV and the endosomal membrane, uncoating of the viral genome proceeds, resulting in the release of the viral ribonucleoprotein (RNP) into the cytosol (Fooks et al., 2017).

1.3.3 Transcription, translation, and replication of RV

RV transcription and replication events occur in the cytoplasm as shown in figure 4. Transcription begins as the L and P proteins (polymerase complex) binds to the nucleocapsid at the 3' end and produce leader RNA that is short RNA molecule, which is neither capped nor polyadenylated (Albertini et al., 2008). Consequently, the polymerase transcribed the nucleoprotein mRNA which become polyadenylated and capped by the viral polymerase complex. Subsequently, mono-cistronic mRNA is synthesized for each of the viral proteins. Afterwards, a full lengthy positive-strand RNA copies are produced with the L protein known as complementary RNA (cRNA) without cap or poly (A) tails but bind to the L-P complex and are encapsulated with nucleoprotein. New nucleocapsids are formed from the cRNA which serve as templates to produce new negative strands RNA genomes to be encapsulated by N protein (Albertini et al., 2008). All viral proteins are translated in ribosomes except the G protein which is translated thought the endoplasmic reticulum. During subsequent stages, the M protein alters the function of the RNA polymerase complex (consisting of enzymatic subunit L and cofactor P) from transcriptase activity to a replicase activity (Fooks et al., 2017). Nucleoproteins cannot bind to the cellular RNA and only bind viral RNA due to the formed N-P complex where phosphoprotein acts as a chaperone for the N protein, preventing its self-aggregation (Albertini et al., 2008). Replication starts once enough

quantities of the nucleoprotein capable of encapsulating the replicated viral genomes are available (Albertini et al., 2008).

1.3.4 Assembly and release of RV

Upon replication, the assembly of the replication products including the RNA genomes and the nucleoprotein occurs to form the RNP (Fooks et al., 2017) .The RV M protein is known for its role in mediating the assembly and budding processes. Previous study has demonstrated that the M protein oligomerization allows the high binding affinity between the M protein and the lipid bilayer, resulting in increased membrane curvature and subsequently virus release (Okumura and Harty, 2011). The detachment between virus and cell occurs through late budding domain (L) in M protein. The L domain of M protein is located at the N-terminal of M protein (35-38 a.a) possessing four main motifs which bind with the host proteins (Okumura and Harty, 2011). Binding with the host proteins involved in the host endosomal sorting complex required for transport (ESCRT) pathway recruits the cellular vacoular protein sorting (VPS) machinery to the budding site of RV, allowing the viral egression (Okumura and Harty, 2011). The newly synthesized RNP are then recognized by M protein where they bind in the cytoplasm. Subsequently, G protein which possesses has exocytic activity, accumulates at the plasma membrane. Simultaneously, the M protein congregates at the cytoplasmic side of the G enriched microdomains generating a lattice structure. This arrangement contributes to the membrane curvature forming the bud site (Okumura and Harty, 2011). Further, the condensation of M-RNP and the microdomains with excess G protein facilitated the outward curvature of the membrane and virion budding (Okumura and Harty, 2011). While RV initially spreads in a retrograde manner, during the late phase of infection, RV reverses its transport direction and moves in an anterograde manner out of the CNS, moving towards the periphery. The anterograde spread, particularly occurs to the salivary glands where the virus can be transmitted through bites from infected hosts, allowing the spread of infection(Fisher et al., 2019).

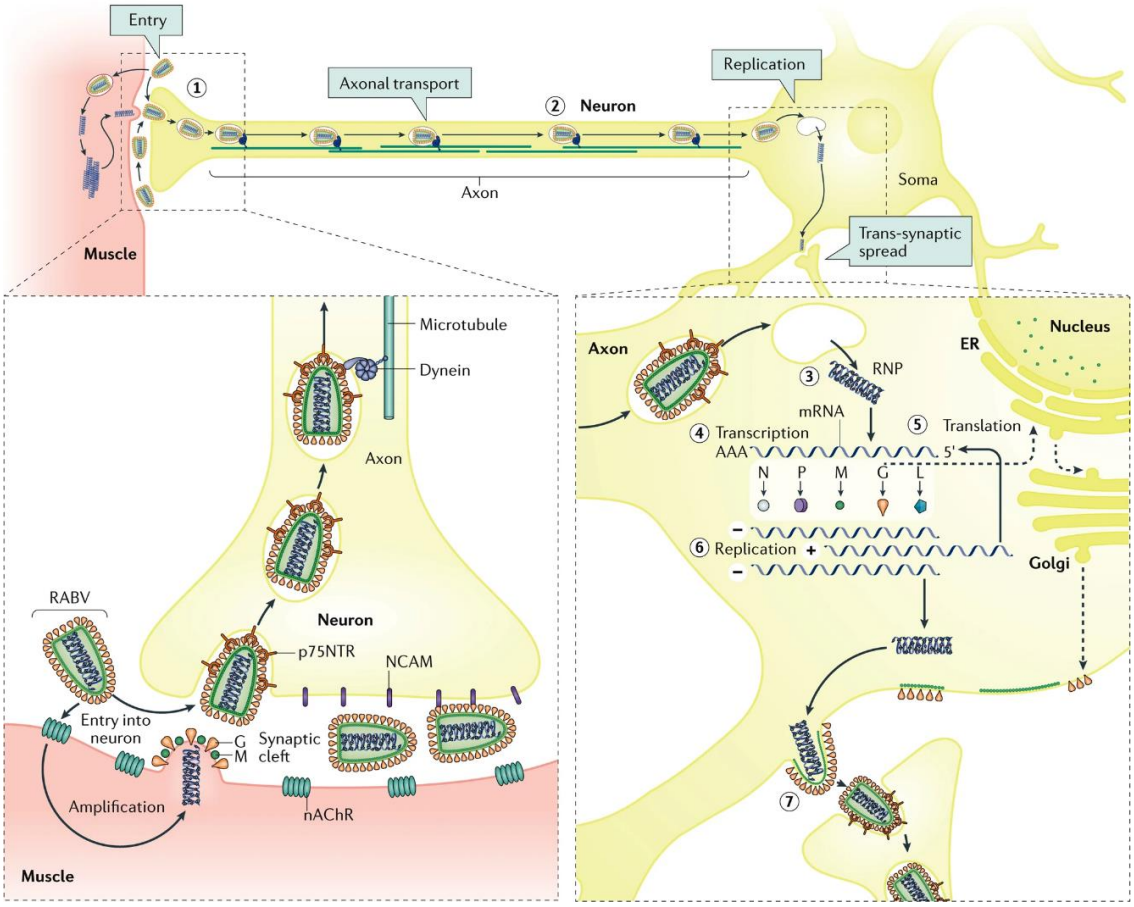

Figure 1.4 Rabies virus spread and replication cycle.

Upon the virus receptor-mediated endocytosis at the presynaptic membrane ***(step 1),*** *the virion undertakes retrograde axonal transport towards the neuron soma* ***(step 2).*** *Within the neuron soma, the ribonucleoprotein (RNP) is released from the endocytic vesicle* ***(step 3).*** *Primary transcription yields 5'-capped and polyadenylated viral mRNAs, facilitated by the viral associated large RNA polymerase protein (L) and phosphoprotein (P)* ***(step 4).*** *Viral proteins translation occurs in the cytoplasm, except for the G protein which is translated through the endoplasmic reticulum (ER) Golgi network* ***(step 5)****. Replication of full-length RNA genomes occurs* ***(step 6).*** *The negative-sense RNA genome undergoes transcription into, positive-sense RNA strands, followed by transcription into full-length, negative-sense RNA strands. Newly formed RNPs serve as templates for further RNA synthesis or be encapsulated into progeny virions. Assembly and budding of virions are primarily mediated by the M protein. The M protein oligomerization enhances its binding affinity for the lipid bilayer, influencing membrane curvature, RNP encapsulation, and virus egress* ***(step 7)****. The transport of the G protein to the budding sites occurs via the secretory pathway, including translation at the rough ER and transport through the Golgi apparatus. The figure is adapted from previous publication (Fooks et al., 2017).*

1.4 Rabies virus pathogenesis

Rabies is regarded the most lethal viral disease, with fatality rate approximately 100% (Okumura and Harty 2011). All mammals can be infected with rabies with special concern to dogs which cause over 99% of rabies human deaths in developing countries (Hampson et al. 2015). Several reservoirs maintain RV including multiple species from carnivores and chiropteran which differ according to the geographical distribution (Troupin et al. 2016). The spread of RV mostly occurs through bite or scratch wounds where it spreads to nerve terminals through either the skin or skeletal muscle which are rich in nerve endings (motor, sensory or visceral) and enters at tips of peripheral nerves where Schwann cells are absent (since they are not susceptible to RV). Upon entry into peripheral neurons, centripetal spread occurs where the virus is transported in the neuron axon to the spinal cord via either sensory or motor neurons (Begeman et al. 2018). RV use both retrograde and anterograde transport systems where in retrograde, the virus is transported from terminal branches to the cell body, while anterograde transport system occurs after the virus replication when the virus travels from the cell body to the synapse. One prominent difference between both routes is that the retrograde virus transport is dynein-dependent while the anterograde is kinesin-dependent (Begeman et al. 2018). Upon reaching the spinal cord, the virus spreads to various parts of the brain, then further centrifugal spread of RV via peripheral nerves to different organs as salivary glands occur to be excreted through the bite and enable its transmission to another host (Begeman et al. 2018).

The pathogenesis of RV differs among carnivores and bats in many aspects. Primarily, the tissue exposed to the virus following the bite differs from carnivores to bats. Carnivores own long teeth, so the bite is likely to go deeply through the skin into underlying skeletal muscle. While bat bites normally will not go beyond the skin.

Another main difference was observed in the centrifugal RV transport which was observed in mucous cells of salivary glands in both natural and experimental RV infected carnivores. On the other hand, bat RV was also detected in tongue surface and in the epithelium of the salivary glands(Begeman et al. 2018). Highlighting that in infected bats, tongue epithelium may be one site for virus excretion as well.

Interestingly, humans acquiring bat and dog related RV differ in the clinical signs presented. Primarily, dog related RV is mostly acquired in humans through deep bites, on the contrary bat related RV was most probably acquired through superficial bat bites (Begeman et al. 2018).

The site of RV exposure is critical for determination of the types of nerves involved for entry of peripheral nervous system. In addition to affecting the route by which RV reaches the spinal cord. This can explain the low manifestation of clinical signs with bat related RV (Begeman et al. 2018). Applying the following concepts *in vitro* may give insights to the difference of tissue preference among bat related RV and dog related RV from neuronal or non-neuronal cells (Begeman et al. 2018).

1.5 Control measures relative to the human deaths' cases of RV

Dog mediated rabies is known to cause up to 59,000 human deaths all over the world every year with billions of humans at substantial risk of being infected. Africa and Asia represent the greatest continents at risk where rabies is being ignored with no sufficient preventive and control measures for the spread of the disease (Wunner and Briggs, 2010). While in USA, bats pose the greatest threat of domestically acquired rabies. Since 2000, they caused around 81.6% of rabies infections in humans (Blackburn et al., 2022). Currently the applied regimen of the post exposure prophylaxis (PEP) as recommended by the WHO, involved proper wound cleansing with soap and water and recommended virucidal if available. Followed by the infiltration of the Rabies Immunoglobulin (RIG) around the wound and administration of the rest of the RIG intramuscular (I/M). The I/M administration of either the purified chick embryo cells vaccine (PCECV) or the human diploid cell vaccine (HDCV) vaccines on days 0,3,7 and 14th day of exposure. In case of vaccinated individuals, the same regimen was applied without the RIG and vaccines only administered on day 0 and third day after exposure (Tarantola et al., 2019).

While rabies typically exhibits high mortality rates, there have been reports of approximately seven individuals who survived the rabies virus infection (Reznik et al., 2020). Intriguingly, six of these individuals had received vaccinations before the onset of their illness, potentially mitigating the severity of the disease (Reznik et al., 2020). In the seventh case, a 15-year-old girl, who had contracted rabies through a bat bite on

her right hand, underwent treatment using a clinical protocol known as the Milwaukee protocol, initially introduced in 2004 (Hoffman et al., 2005). This clinical approach involves introducing a medically induced coma in the patient, followed by the administration of antiviral drugs, ketamine, and amantadine. Notably, this patient developed neutralizing antibodies within 48 hours of treatment, consequently the patient survived the rabies infection (Hoffman et al., 2005). However, it is worth mentioning that at least 31 other patients did not survive despite treatment with the Milwaukee protocol (Zeiler and Jackson, 2015), thus it has been recently opined to abandon implying this protocol (Zeiler and Jackson, 2015).

Considerable progress in rabies antiviral drugs (Jochmans and Neyts, 2019) and genetically engineered vaccines (Natesan et al., 2023) has been made to control RV. However, there exists a knowledge gap regarding the effectiveness of these antiviral drugs and vaccines in controlling the disease.

This section focuses on establishing a relationship between the progress made in control programs in China and USA and its correlation with the RV fatality rate among humans. The situation in China and USA was addressed in this study due to their acquisition of robust surveillance systems represented by the Centre for Disease Control and Prevention (CDC) that enable comprehensive data monitoring in both countries. Additionally, these two countries belong to different continents with distinct rabies reservoirs. This geographical distinction provides valuable insights for comparative assessments of the RV situation.

1.5.1 Control measure and number of cases in USA 1960-2020

Upon collecting and analysing the reports of the human fatalities caused by rabies in the USA between 1960 and 2020. A decline in the number of deaths during the period from 1980 to 1999 (36 cases) was reported, in comparison to the preceding years from 1960 to 1980 (38 cases). However, strikingly, an increase in the human deaths was observed from 2000 to 2020, reaching a total of 52 cases. It has been documented that out of the 32 human fatalities reported between 1980 and 1996, none of the individuals who were exposed to the RV received a complete prophylactic treatment following their exposure (Noah et al., 1998). During the period spanning from 1960 to 1979, a total of

16 cases were exposed to rabies, and administered the post-exposure prophylaxis (PEP), all except one individual who received the PEP died. The remaining 20 cases who did not receive PEP, all died except for one person who survived (Anderson et al., 1984). The analysis of rabies virus variants responsible for the 52 human deaths in the USA reveals a clear pattern; over 61.5% of these fatalities from 2000 to 2020 were attributed to bats. In contrast, approximately 14 cases were caused by dogs, acquired by patients in the Philippines or India (Ma et al., 2021). Remarkably, in 2021, there has been a surge in the number of human deaths in which five human deaths were reported. This represents the highest number of reported cases since 1960 in which one or two cases were reported each year **(Figure 1.5)** (Blackburn et al., 2022).

The decrease in dog rabies cases in USA has been achieved through controlling dogs as animal reservoir of rabies in USA through vaccination programs with specific regard to the oral rabies vaccine (ORV) (Slate et al., 2009).

The experimental use of the ORV use has started mid 1990s with expansion for implementation of the ORV programs between 1998-2003 with the aim of preventing the spread of terrestrial rabies virus variants (Slate et al., 2005). The reduction in human fatalities observed during the 1980-1999 period might have been attributed to the experimental use followed by use of the oral rabies vaccines for vaccination of the wildlife animals as raccoons since 1990. The ORV has been approved in the form of baits distributed by ground personnel and air. Approximately 6.5 million baits have been distributed to confine the racoon rabies.

When investigating the relationship between vaccine development and the mortality rate of rabies, it becomes evident that the availability of vaccines or PEP only is not the sole determinant factor in preventing deaths. In certain instances, fatalities occur even when PEP is available, primarily due to the initial exposure resulting from unnoticed contact or bites with infected animals. This is particularly prevalent with bats, as their bites or scratches are often too small to be detected by the patient, leading to infection going unnoticed and consequently result in delayed administration of the PEP (Ma et al., 2021).

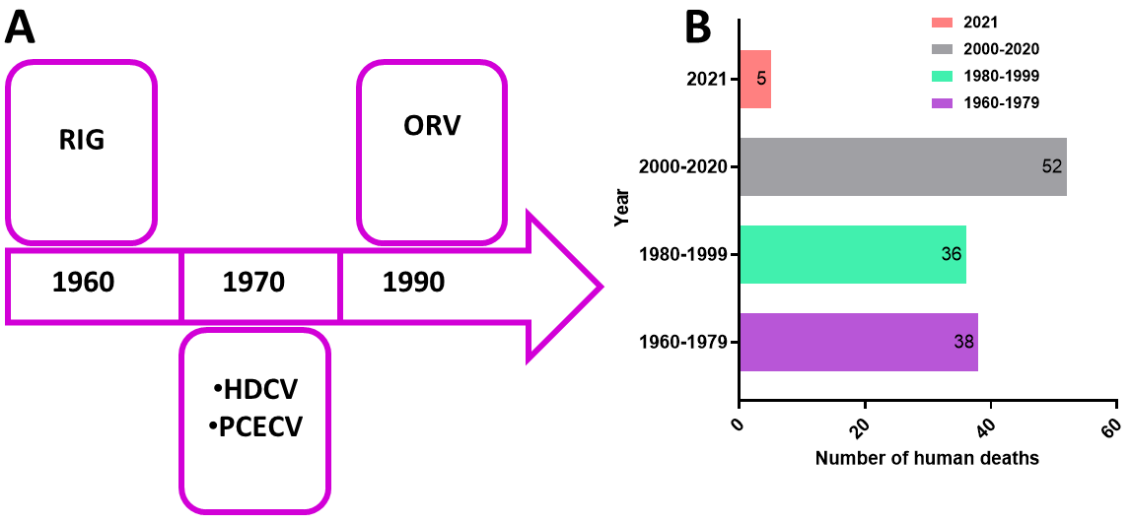

Figure 1.5 Rabies human cases and vaccine development in USA

(A) *A schematic representation illustrating the key advancements in preventive measures in U.S.A that could have impacted the occurrence of human rabies cases. (**B**) Graph showing the rabies death cases in humans-United states during 1960-2021. Abbreviation: RIG; Rabies Immunoglobulin HDCV; human diploid cell vaccine, PCECV; purified chick embryo cells vaccine, ORV, oral rabies vaccine*

1.5.2 Control measure and number of cases in China 1960-2020

China represents the second highest human fatality rate caused by dog-mediated rabies (Song et al., 2009). Since 1949, China implemented a national reporting system in which rabies was among the initial list of notifiable diseases (Tao et al., 2021).

In China, from 2000 to 2020, there was a significant rise in the number of rabies cases, with the highest levels observed in 2007, causing 3,307 human deaths cases(Tao et al., 2021). This increase in cases has been linked to the replacement of the concentrated rabies vaccines with a purified version. As a result, many individuals in rural areas, who were exposed to rabies, were unable to afford the expensive purified vaccine (Zhou et al., 2016). Despite, this peak in human cases in 2007, the mortality rate among humans during the 2000-2020 period was lower compared to 1980-1999 (**Figure 1.6)**. Several factors might have contributed to this decline. Firstly, the adoption of the Zagreb regimen in 2010 allowed for the administration of the PEP in four doses (two on day 0, one on day 7, and the final dose on day 21), which resulted in reducing the number of clinic visits for the patients, compared to the Essen regimen that required five visits (Ren et al., 2015). Furthermore, in 2009, the Ministry of Health in China, introduced the new rural cooperative medical service (NRCMS) reimbursement program. This program

covered the costs of PEP to alleviate the financial burden in rural areas(Song et al., 2014). The 1980-1990 period witnessed the highest recorded fatality rate, with an estimated 57,751 human deaths (Tao et al., 2021). This could potentially be associated with the delayed registration and the introduction of RIG in China which was approved for use in China by 1994 (Yin et al., 2013). Additionally, in the late 1970s, there has been an increase in dog ownership in Chinese households with a consistent lack of dog vaccination(Ren et al., 2015). This could potentially account for the significant rise in human deaths observed during this period (Qiao et al., 2021).

Currently, China is recognized as a prominent producer and consumer of rabies vaccines, manufacturing over 10 million doses and having the ability to export to other Asian countries. Nevertheless, instances of treatment failures can arise occasionally, primarily due to inadequate storage of vaccines within the cold chain. Additionally, there have been also reports documenting the substitution of vaccines with water in certain rural regions (Hu et al., 2009).

Comparative analysis of the human fatalities caused by rabies in humans between China and USA, it is evident that China has a significantly higher human deaths rate compared to the United States. This disparity could be explained by the fact that in the USA, approximately 16,000 to 39,000 people receive PEP annually without displaying any symptoms (Vaidya et al., 2010). Additionally, the presence of freely roaming stray dogs, which are challenging to vaccinate or manage, contributes to the situation in China (Shen et al., 2023). In addition, the challenges of accessing PEP in China, can be attributed to its limited availability in rural areas or insufficient awareness(Song et al., 2014). In China, the vaccination of dogs and cats in is primarily conducted using an inactivated vaccine. However, this vaccination method covers only a third of the dog and cat population in the country. Furthermore, there is currently no availability of oral rabies vaccines to control the spread of the disease among wildlife and stray animals in China(Fan et al., 2022).

Taken together, it can be inferred that despite the progress made in rabies antiviral drugs (Jochmans and Neyts, 2019) and genetically engineered vaccines (Natesan et al., 2023). None of these advancements have resulted in a reduction in rabies infection cases in China or the USA. This could be assigned to the lengthy approval process for

such vaccines. For that reason, considerable attention should be directed towards potentially involving the use of oral vaccines to target wildlife animals and an increase in awareness about rabies prevention. Besides, enhancing the accessibility of PEP in rural regions and making it more affordable for utilization. Furthermore, it is crucial to prioritize the understanding of the host-virus interactions in various hosts, as this knowledge can potentially lead to the development of structure-guided antiviral treatments that would be more efficacious in controlling the disease.

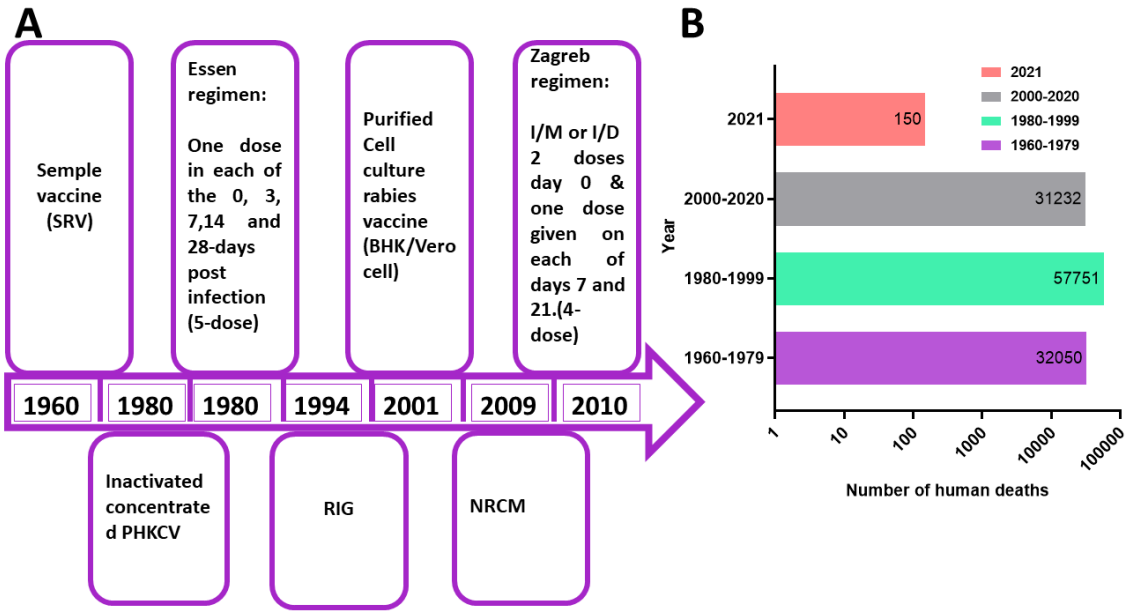

Figure 1.6 Rabies human cases and vaccine development in China

(A) *A schematic representation illustrating the key advancements in rabies preventive measures in China that could have impacted the occurrence of human rabies cases. (**B**) Graph showing the rabies death cases in humans-China 1960-2021. Abbreviation: RIG; Rabies Immunoglobulin; PCECV; purified chick embryo cells vaccine, ORV, oral rabies vaccine, NRCM; new rural cooperative medical*

1.6 Spillover

RV is characterized by its ability to infect all mammals and maintaining the infection cycles only within distinct host species among Carnivores and Chiropteran (Mollentze et al., 2014). Generally, RV can acquire stable infection cycles within different susceptible species, resulting in transmission of the virus through bites. Stable infection cycles are commonly observed in carnivores such as skunks, dogs, foxes, and racoons **(Figure 1.7)**. Alternatively, RV may cross species barrier causing sporadic disease cases with no further transmission events promoting epidemics (Holmes et al., 2002). This phenomenon is known as spillover and is defined as the ability of the pathogen to

establish infection from mammals to humans (Plowright et al., 2017). In this section we will list the factors contributing to spillover events.

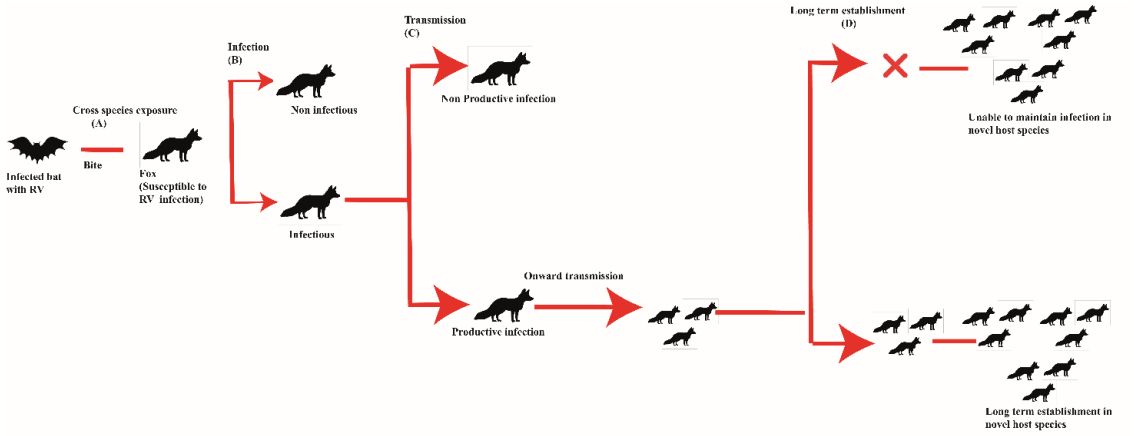

Figure 1.7. Schematic representation of spillover events of RV

For RV spillover to occur, four main steps are required. ***(A).*** *Cross species exposure* ***(B).*** *Infection* ***(C).*** *Transmission****. (D).*** *Long term establishment.*

1.6.1 Ecological factors: facilitate the cross-species transmission such as the cross species contact rate.

One of the main factors affecting success of the spillover events is the presence and density of the potential rabies reservoirs and their susceptible hosts (Astorga et al., 2015). In most cases, rabies variants from the spillover events did not result in stable infection cycles in the new host species mostly due to human intervention to disrupt the transmission cycle (Astorga et al., 2015).

Factors affecting the contact rate between the rabies reservoir and the new susceptible species are referred to as the barriers to spillover. These factors have a direct impact on the prevalence of spillover events. Some of these factors include the density and distribution of the reservoir, the intensity of infection within the reservoir, the ability of the infection to survive and spread to other hosts, and the extent of human exposure to the infection (Plowright et al., 2017). Based on the primary rabies virus reservoir in each country, nations implement varying control strategies to prevent spillover events. For instance, in Chile, bats are the principal rabies reservoirs including the *Lasiurus cinereus* and *Tadarida brasiliensis* species. Thus, strategies focusing on dog restrictions would not be critical as Chile has been declared free of dog-related rabies (Astorga et al., 2015). On the other hand, in Asian and African countries which represent the major global

burden of the dog-mediated rabies. Significant control strategies involving dog elimination and vaccination are crucial to effectively control the disease (Athingo et al., 2020). Therefore, it is crucial to understand the ecological factors that influence disease spillover within each country to effectively control the spread of the disease. The control of the ecological factors might include reducing the contact with the susceptible hosts and ensuring their vaccination, as well as immunizing wildlife species that serve as reservoirs for rabies (Escobar et al., 2023).

1.6.2 Evolutionary viral factors: the capability of the pathogen to infect novel host.

1.6.2.1 Structure of RV G protein

Owing to the location of G protein on the viral surface of RV, it is considered the key determinant of tissue tropism (Yang et al., 2020). RV exhibits a broad host spectrum, highlighting the importance of G protein in interacting with multiple host receptors (Jackson, 2013). RV- G protein is classified as class III virus fusion protein based on the conformational structures and the mechanism by which the virus fuses with the cell membrane (Rey and Lok, 2018; Leroy et al., 2020). The RV-G protein is translated on membrane-bound ribosomes and inserted co-translationally into the endoplasmic reticulum (ER) in an unfolded form. Folding of the transmembrane proteins occur in three topologically and biochemically distinct environments: the ER lumen, the ER membrane, and the cytosol. The RV G protein is composed of three domains; ectodomain (a.a 1-439) exist as homotrimer, transmembrane domain (TMD) (a.a 440-461) and the cytoplasmic domain in the inner membrane(CD) (a.a 462-504) which can fold independently of each other, extending in the cytoplasm of infected cells and play the role in interacting with the M protein for virus assembly. The RV-G ectodomain was further classified into four functional domains: lateral domain I, trimerization domain II, pH domain III and fusion domain IV (Both et al., 2012; Ng et al., 2022). Three different states have been demonstrated for the G protein. The native state (n) which is detected at the virus surface and is known to be responsible for receptor binding. The activated hydrophobic state (A) interacts with the target membrane as the primary step in the fusion process, and the fusion-inactive conformation state (I) (Gaudin et al., 1999). These distinct states are governed by pH equilibrium where the “I” state is triggered by

low pH forming longer conformation than that in “n” state. Rendering them antigenically different (Gaudin et al., 1999). Cleavage of the signal peptide triggers the mature glycoprotein. The G protein undergoes common cellular protein modification processes, whereby carbohydrates (glycans) are attached to specific amino acid side chains in proteins, resulting in establishment of glycoproteins. Appropriate folding of G proteins is dependent on the N-glycosylation sites, where they increase the solubility of folding intermediates and facilitates the interaction of folding intermediates with chaperones (Wojczyk et al., 2005).

1.6.2.2 Surface viral protein mutations and its role in cross species transmission

Viruses undergo mutations to adapt and recognize the cellular receptors orthologs in the new host species. The mutations in the surface glycoprotein can affect its interaction with host receptors and influence the virus ability to infect and replicate in distinct species (Kuzmin et al., 2012). Since rabies G protein is associated with the virus neurotropism, receptor binding, production of neutralizing antibody and host adaptation. The substitutions in the glycoprotein can potentially enhance the affinity of the virus for receptors in a new host species, allowing for successful transmission and adaptation (Callaway et al., 2022). Understanding the specific glycoprotein substitutions involved in cross-species transmission is important for studying the dynamics of rabies spread and developing strategies for prevention and control.

Viral genome adaptation can occur following cross-species transmission to enhance the virus's fitness in the new host. These changes are driven by selective pressures that facilitate adaptation to the new host environment. Alternatively, mutations may occur prior to cross-species transmission, enabling the virus to readily circulate in new host species (Kuzmin et al., 2012). One example of pre-host shift adaptation in the G protein sequence was the substitution of specific a.a (serine to threonine) at position 242 in the G protein's ectodomain. This substitution allowed bat RV to transmit to carnivore RV (Kuzmin et al., 2012).

One model demonstrating the cross-species transmission because of the mutation in the G protein was exemplified in a previous study (Ding et al., 2017). The study showed that the substitution of the lysine (Lys) residue 333 with arginine (Arg) has facilitated the adaptation of the G protein to carnivores rather than to bats (Ding et al., 2017). These

adaptations of the G protein from bats to carnivores might have occurred as the region encompassing the a.a. residues 181-431 plays a crucial role in determining host tropism and neuro-invasion. Specifically, a.a residues 330 and 333 within this region are known for their involvement in receptor recognition (Tuffereau et al., 1998a).

Additionally, further adaptation of the G protein to the new host species (carnivores) has been achieved through homologous recombination. The recombination event took place between the fusion domain IV of the G protein from bats (forming the stem of the hairpin conformation) and the lateral domain, trimerization domain, and pH domain from skunk RV (comprising 84% of the G protein head). This recombination resulted in enhanced capability of the resulting variant for evasion of the immune response owing to the role of the pH domain in altering the ability to escape neutralizing antibodies (Borucki et al., 2013)

A recent study has categorized RV strains into four antigenic groups based on the sequences of the G protein and their ability to be neutralized by vaccine-induced sera, namely GAgV1, GAgV2, GAgV3, and GAgV4. Through a comparative sequence analysis of these antigenic groups, it was observed that the GAgV4 group exhibited a higher number of substitutions compared to the other antigenic groups. Specifically, three amino acid substitutions were observed in positions 113, 164, and 254 of the G protein. It is worth noting that most of the strains listed in this group were associated with bat-related RV, and they displayed the lowest level of neutralization compared to the other antigenic groups. These substitutions may be linked to host shift events, indicating a potential role in facilitating the transmission of RV between different host species (Cai et al., 2022). It is also, noteworthy, that those substitutions were all located in the G protein ectodomain (Cai et al., 2022).

Table 1-1 Summarizing the RV-G antigenic groups and the differences in the corresponding a.a.

Antigenic group	Amino acid & position
GAgV1	254-P

GAgV2	254-P
GAgV3	113-H 164-V 254-P
GAgV4	113-Q/H 164-I/V 254-S/H

1.6.2.3 Glycosylation on the viral surface proteins

The N-linked glycosylation (NLG) is a post translational modification for surface glycoproteins which is acquired during virus evolution (Li et al., 2021). Glycosylation can modulate the function and structure of proteins through their effect on intermolecular interactions (Marth and Grewal, 2008). The acquisition of glycosylation by the glycoprotein can serve as a protective shield, preventing it from binding to antibodies (Feng et al., 2022).

Numerous studies have demonstrated the evolution of seasonal influenza because of either an increase or loss of the glycosylation sites (Wei et al., 2010; Kim et al., 2018). An example of acquiring more glycosylation sites was observed during the 2016 influenza virus pandemic, specifically with the H1N1 strain. During the 2016 pandemic, the hemagglutinin (HA) protein displayed glycosylation at amino acid position 179. This modification allowed the virus to evade the immune response generated during the previous 2009 pandemic and consequently increased its activity (Kim et al., 2018). Further evidence for the role of the glycosylation, was demonstrated in the H3N3 virus which was de-glycosylated at position 499 that allowed the virus transmission from wild birds to pigs (Chauhan and Gordon, 2021). Cross species transmission resulted from loss of glycosylation sites was further demonstrated. In H5N1 influenza virus, the HA, acquired a mutation (Thr 160 Ala) which resulted in loss of glycosylation site in position

158-160. The loss of the glycosylation site was responsible for the H5N1 virus transmission from ducks to guinea pigs (Gao et al., 2009).

In the context of rabies, further research is required to identify and understand the role of the glycosylation pattern of rabies G protein that facilitates its cross-species transmission among different mammalian hosts and assessing their impact on viral entry and replication and immune recognition. This will give insight into the contribution of glycosylation to rabies spillover and develop strategies to mitigate the risks associated with spillover.

1.6.3 Phylogenetic relatedness of the donor and recipient hosts

The phylogenetic relatedness between the reservoir and the susceptible host has been reported to affect the zoonotic potential of the viruses in respect to their virulence and their onward transmission in the susceptible hosts. A previous study demonstrated that viruses transmitted from the host species distantly related to humans Chiropteran, displayed less likelihood of causing human-to-human transmission owing to harbouring highly virulent viruses. In contrast, the mammalian reservoirs closely related to humans displayed a higher likelihood of facilitating the onward human-to-human transmission of the viruses. Additionally, viruses transmitted to humans from reservoirs that are phylogenetically distant exhibited higher degree of fatalities compared to those transmitted from closely related reservoirs (Guth et al., 2019).

1.6.4 Receptor availability and glycosylation and expression in different hosts

1.6.4.1 Receptors availability for virus entry

Cellular receptors are regarded as the primary pathway through which virus can gain access to the host cellular compartments. Addressing the ways by which virus can enter the host cells using the viral attachment proteins is considered the most fundamental aspects in viral invasion of the host cells (Maginnis, 2018a).

RV is known to interact with wide range of receptors by which it enters cells among different host species. In this regard, elucidating the preferences of RV to bind and attach to certain types of receptors is a point of interest which open insights into controlling such mechanisms. From this perspective, several studies focused on

elucidating the role of the most well-known RV receptors for RV entry which are nAChR, NCAM, p75NTR, mGluR2 and ITGB1 and TRf1 **(Figure 1.8)** (Guo et al., 2019)**.**

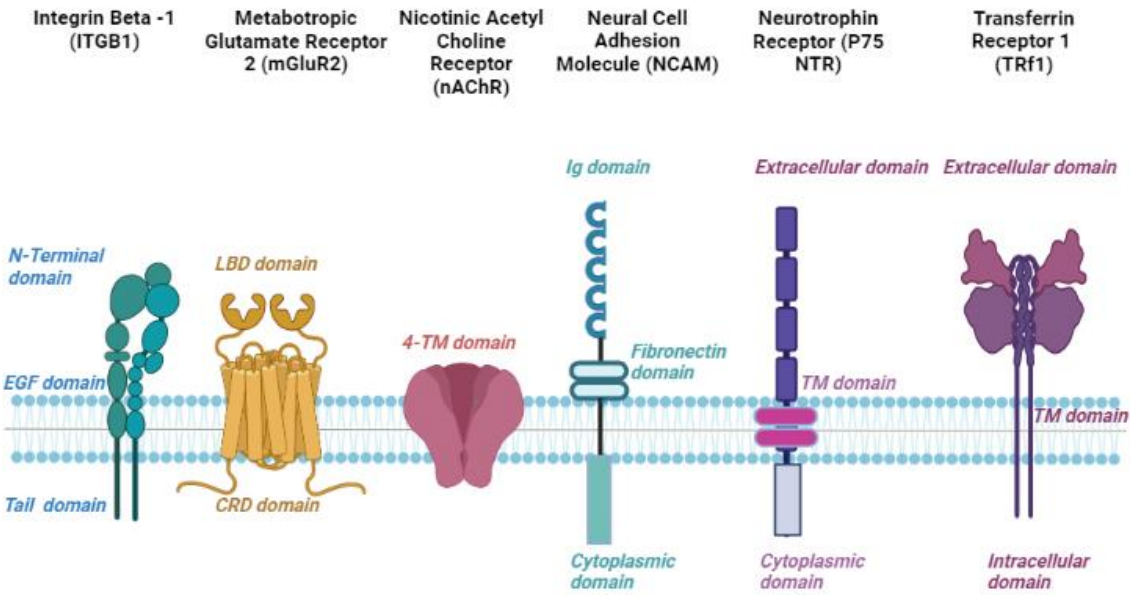

Figure 1.8 Schematic diagram of the RV receptors

Created with BioRender.com. Abbreviations: EGF domain: epidermal growth factor like domain. CRD domain: cysteine-rich domain, TM domain transmembrane domain, Ig: Immunoglobulin domain.

1.6.4.1.1 Nicotinic acetylcholine Receptor (nAChR)

Principally, the muscular form of the nicotinic acetyl choline (nAChR) receptor was the first discovered receptor for RV (Lentz et al., 1982; Lafon, 2005). It has been documented that RV attaches at the postsynaptic membrane of neuromuscular junctions where nAChR accumulates(Lafon, 2005). The nAChR belongs to the neurotransmitter ligated ion channels superfamily which shows high affinity to the neurotoxin; alpha bungarotoxin (α-BTX). The localization of RV antigens at the neuromuscular junctions (abundant in nAChR), following intramuscular injection (I/M) of the RV into mice has demonstrated that the nAChR is a cellular receptor for RV Subsequent experiments confirmed those results, through the partial inhibition of RV infection observed upon binding of the nAChR to the *α*-BTX (Lentz et al., 1982). Further studies determined that the interaction site of nAChR with RV G protein involved the amino acid (a.a) residues 173-204 within nAChR alpha subunit (Lentz, 1990; Lafon, 2005) Neuronal and muscular cells express the nAChR which is formed of five subunits constituting the hetero pentameric organization of nAChR which are α1, β1, d, γ, and ε

(Edson X et al. 2009) **(Figure 1.9)**. Interestingly, each of those subunits has four transmembrane domains; both the N- and C-termini are in the extracellular space. While the large cytoplasmic domain is located between the third and fourth transmembrane domains with a conserved tyrosine a.a residue. Phosphorylation of the tyrosine residue plays a role in the determining the nAChR distribution at neuromuscular junctions and the rate of receptor sensitivity. Further that the phosphorylation of tyrosine residue plays a role in clustering of nAChR. Consequently, more attention to the role of that residue should be taken in consideration. Hence, this might be involved in susceptibility of nAChR expressing cells to RV infection (Thomas and Smart, 2005).

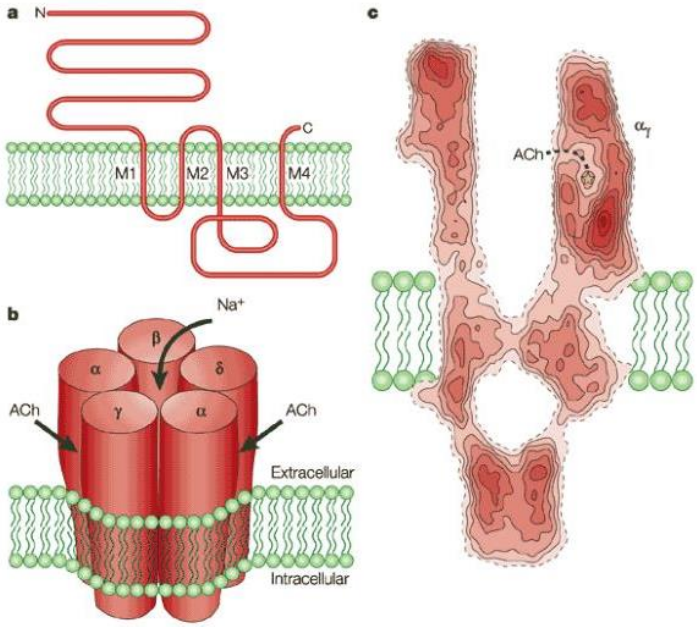

Figure 1.9 The pentameric nicotinic acetylcholine receptor structure

(a) The membrane-spanning pattern of receptor subunits. (b) An illustration of the overall structure, depicting the arrangement of subunits in the muscle-type receptor, the positions of the two acetylcholine (ACh)-binding sites (between an α- and a γ-subunit, and an α- and a δ-subunit), and the central channel for cation conduction. (c) A cross-sectional view of the receptor's 4.6-Å structure obtained through electron microscopy of tubular crystals of Torpedo membrane frozen in ice. The figure is adapted from a previous publication (Karlin, 2002).

1.6.4.1.2 Neural cell adhesion molecule (NCAM)

The neural cell adhesion molecule (CD56) belongs to the cell adhesion glycoproteins of the immunoglobulin (Ig) superfamily (Skog et al., 2016). NCAM is transcribed from a

single gene and three main isoforms are generated upon alternative mRNA splicing of 120, 140 and 180 kDa molecular masses (Horstkorte et al., 2012). NCAM has three main domains: extracellular, transmembrane, and cytoplasmic domains **(Figure 1.10)**. The extracellular domain consists of five immunoglobulins (Ig) like domains and two type III fibronectin-like domains. All the NCAM isoforms have a similar extracellular domain, while only NCAM 140 and NCAM 180 have both the cytoplasmic and transmembrane domains which link them to the membrane, while NCAM 120 subunit is linked to the membrane via the glycol phosphatidylinositol- transmembrane anchor (GPI) (Thoulouze et al., 1998). The accumulation of NCAM in pre- and post-synaptic regions as well as in neuromuscular junctions render them involved in synaptogenesis and mediate the transport and accumulation of synaptic organelles at the sites of synapse formation (Matthias and Horstkorte, 2006). It has been previously demonstrated that the surface expression of NCAM, decreased the RV. Additionally, most of the cells susceptible to RV infection were shown to express NCAM. While the resistant cell lines such as primary cortical cell cultures derived from NCAM deficient mice did not support RV infection into cells (Thoulouze et al., 1998; Lafon, 2005). NCAM was regarded as the second discovered receptor for RV through observing increased susceptibility to RV laboratory strain CVS (challenge virus standard) infection upon transfecting cells with NCAM. On the other hand, reduced RV susceptibility was reported upon blocking NCAM action through antibodies. Moreover, previous *in vivo* studies indicated a decreased RV progression in NCAM-deficient mice (Thoulouze et al., 1998; Hotta et al., 2006). Despite the enhanced RV attachment in the hepato-erythropoietic porphyria cells (HEP) over-expressing the NCAM-120, a distinctly lower RV replication was observed in the cells over-expressing NCAM-120 compared to those expressing NCAM-140. This was associated with the upregulation of the IFN-ß gene in cells expressing NCAM-120, but not NCAM -140 (Hotta et al., 2006).

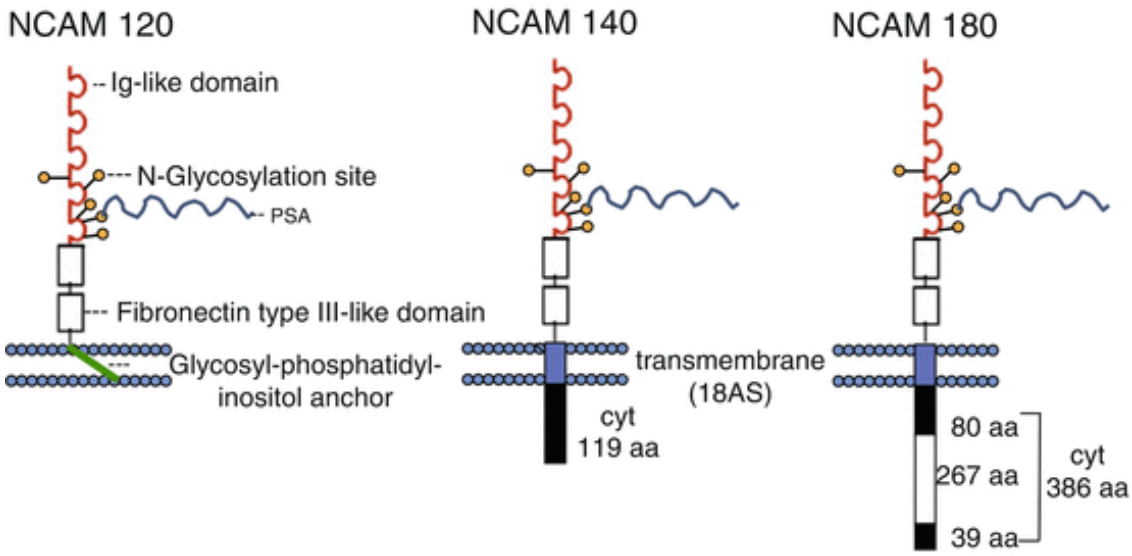

Figure 1.10 Schematic representation of the NCAM Isoforms

NCAM-120, NCAM 140 and NCAM 180. This figure is adapted from a previous study (Horstkorte et al., 2012). Abbreviations: Ig Immunoglobulin like domain, a.a : amino acid.

1.6.4.1.3 p75 NTR neurotrophic receptor (NTR)

The p75NTR, is a type I transmembrane protein which was considered the first identified receptor for p75 nerve growth factor (NGF) belonging to tumour necrosis factor receptor family (TNF) (Cragnolini and Friedman, 2008).The p75NTR are dimers, constituted from N-Terminal ectodomain comprising four cysteine rich domains (CRD) each made up of six cysteine residues along with transmembrane and intracellular domains. The intracellular domain is further composed of chopper and death domains which plays role in the intracellular trafficking **(Figure 1.11)** (Barker, 1998; Almeida and Duarte, 2014). The p75 NTR are abundantly expressed during the development or injury in neurons and glia cells, however, the p75 is not highly expressed in normal adult brain (Cragnolini and Friedman, 2008). The p75NTR receptors influence multiple cellular functions as the myelination of Schwann cells which highly express p75NTR, in addition to, their role in regulating the astrocytes proliferation during injury. Moreover, the p75NTR is expressed in nonneuronal cells as microglia cells and tanycyte where it is involved in maintenance of integrity of blood brain barrier. Interestingly, it was previously reported that cells expressing p75NTR in sub ventricular zone could be differentiated from neurogenic into glial progenitors' cells in cases of injury (Cragnolini and Friedman, 2008).

The p75NTR has been initially demonstrated as RV receptor when the BSR cells (a clone of baby hamster kidney cell) showed susceptibility to the non-adapted fox isolate of RV. More evidence was obtained upon the co precipitation of both the p75 and the RV-G proteins with anti G antibodies. (Tuffereau et al., 1998b). Further studies have also identified the interaction of the G protein to the first CRD domain in the p75 NTR, where the interaction with the G protein was completely abolished with substituting the p75 Gln 33 a.a with Glu confirming the trimeric G protein act as a high affinity ligand for the non-neurotrophins binding site in p75 (Langevin et al., 2002).

Further explanation of the receptor role of the p75NTR in RV infection was exemplified in the facilitated RV internalization through RV binding to the p75NTR positive endosomes at the axon tip which facilitated the axonal transport process. The binding of RV to p75NTR enhances faster route to reach central nervous system (CNS) through the transport of viral particles in a retrograde axonal transport. This could be explained as both RV and p75NTR are known to be internalized through clathrin mediated endocytosis (CME), where they bind to each other. Upon binding, both the RV and p75NTR form endocytic compartments, which subsequently induces low pH within the endocytic compartments, which promotes conformational changes in RV G protein. The conformational change in the RV-G protein sends signal for RV-p75NTR complex allowing the accelerated transport (Gluska et al., 2014). Thus, the role of the p75 is not limited to the initial binding with the RV-G, but also accelerating the RV long distance transport in the axons. The importance of studying long distance transport to CNS has pivotal role in successful establishment of RV in CNS which subsequently affect the RV transmission to other organisms (Finke and Conzelmann, 2005). Despite the demonstrated role in p75 receptor facilitating the uptake of the RV into the cells, other study demonstrated that mice with deleted extracellular membrane of the p75 which was known for its binding with the RV-G were still showing susceptibility to RV infection. The findings in this study, demonstrated that the role of the p75 is not essential in RV infection of primary neurons and that other receptors are mediating the RV entry into the cells (Tuffereau et al., 2007).

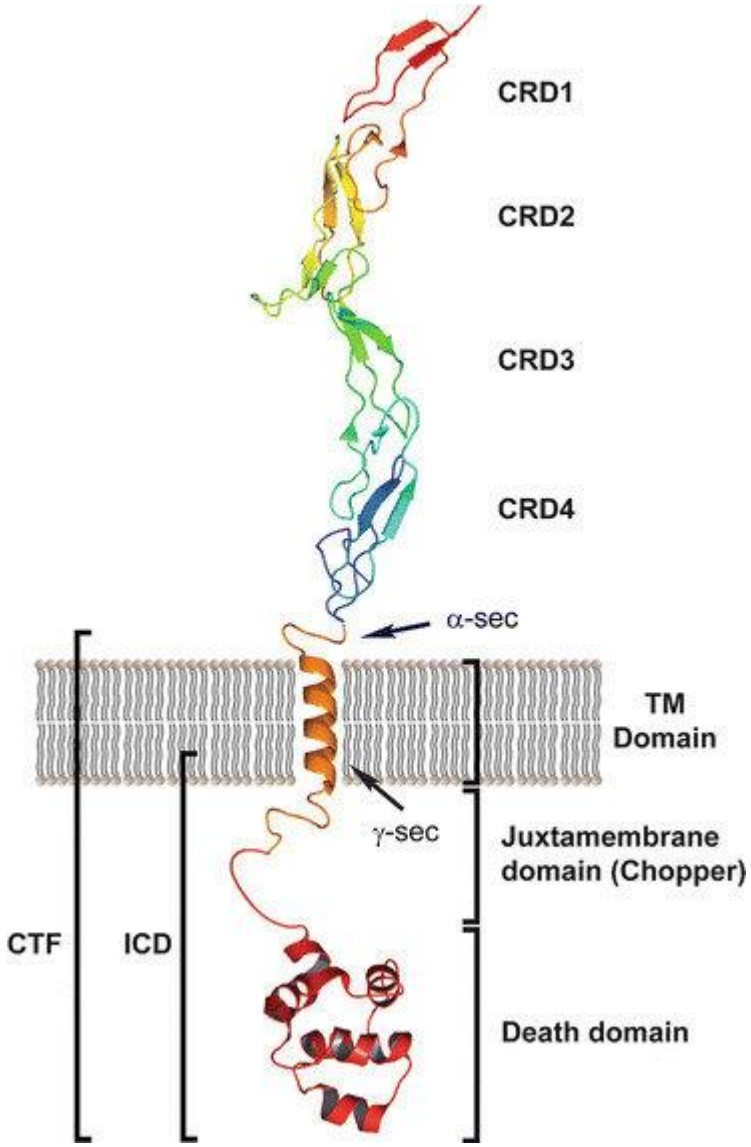

Figure 1.11 The p75 NTR protein structure

The p75 composed of 4-CRD domains, TM domain and intracellular domain. The intracellular domain is comprised of chopper and death domains. Abbreviations: CRD: cysteine-rich domain, TM domain: transmembrane domain, CTF C-terminal fragment, ICD intracellular domain

1.6.4.1.4 Metabotropic Glutamate Receptor subtype 2 (mGluR2)

Glutamate receptors belong to the G coupled receptors superfamily (GPCRs), they are considered as the most common excitatory neurotransmitters within the nervous system regulating neuronal and synaptic transmission. Glutamate receptors are widely expressed in central and peripheral nervous system (Mazzitelli et al., 2018). The metabotropic glutamate receptors have eight different subtypes which are classified into three groups (I-III). Metabotropic glutamate receptor 2 (mGluR2) belongs to group II which are expressed in pain related neural processing elements in peripheral synaptic

and super synaptic regions and are involved in pain modulation (Mazzitelli et al., 2018). The structure of mGluR2 is characterized by the extracellular region which is composed of the ligand binding domain (LBD) and CRD, followed by the transmembrane domain which is formed of seven transmembrane helices **(Figure 1.12)** (Mazzitelli et al., 2018). A global small interfering RNA (siRNA) strategy has been employed targeting 21,585 mRNA to determine key host factors for RV on human embryonic kidney cell line (HEK293) cells (Wang et al., 2018). Accordingly, the mGluR2 was identified as a novel RV cellular receptor. As previously described, infecting mouse neuroblastoma cell line. (N2a), HEK293 and human neuroblastoma cells (SK-N-SH) with recombinant Evelyn-Rokitnicki-Abelseth-green fluorescence protein (ERA-GFP) virus strain (RV strain) showed less virus replication upon mGluR2 knockdown from cells. Whereas the cells overexpressing the mGluR2, enhanced the RV replication, compared to un transfected cells. Moreover, the physical interaction between the mGluR2 and the RV-G was demonstrated through the co-immunoprecipitation (Co-IP) and pull-down assays.

Despite the crucial role played by the mGluR2 in RV entry, it is not essential for RV. Since the mGluR2 knockdown in mice resulted in 45% of mice deaths because of RV infection, demonstrating that RV utilized other receptors (Wang et al., 2022).

The mGluR2 and RV were demonstrated to colocalize in the late and early endosomes, however, the underlying mechanism was not explained. A recent study demonstrated that upon the interaction of the RV with the mGluR2, the virus receptor complex migrates to the pre-existing clathrin coated pits (CCP) that contain the transferrin receptor 1 (TRf1) in which the endocytic signalling of the TRf1 facilitates the entry of the virus into cells (Wang et al., 2022).

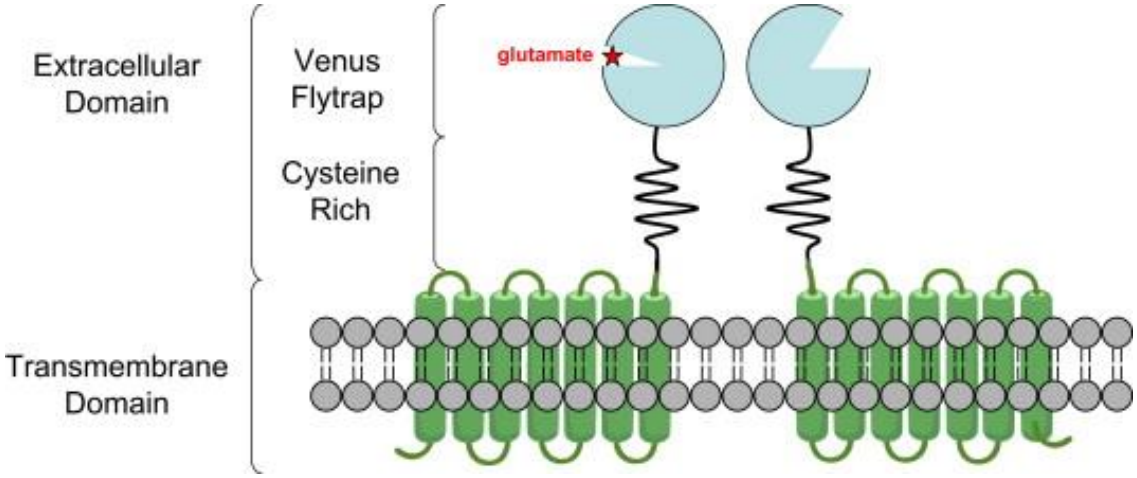

Figure 1.12 Schematic diagram illustrating the mGluR structure.

The mGluR is composed of a transmembrane domain spanning the seven transmembrane domain and an extracellular domain that includes the "Venus's flytrap" and "Cysteine-rich" regions, as illustrated in the diagram provided. The figure is adapted from previous publication (Topiol et al., 2011)

1.6.4.1.5 Integrin beta 1 (ITGB1)

ITGB1 is a heterodimer and type I transmembrane cell surface molecules that regulate cell structure, and behaviour affecting their differentiation and proliferation (Kapp et al., 2017). The receptor is known for its role in mediating the entry of many viruses such as Ebola virus, parvovirus, cytomegalovirus and reoviruses. Integrins are known for their role in development of peripheral and central nervous systems since they are expressed in muscle and cerebral cortex (Kapp et al., 2017).

ITGB1 possess two transmembrane subunits: one alpha and one beta subunit connecting between the intracellular cytoskeleton and pericellular extracellular matrix cytoskeletons (Kapp et al., 2017) as shown in **(Figure 1.13)**. ITGB1 has been the most recently identified RV receptor through siRNA strategy which revealed low infection rates of ERA strain upon ITGB1 knockdown on HEK293 and N2a cells. Previous studies have indicated that the overexpression of ITGB1 increased RV infection which highlighted the importance of ITGB1 as RV key host factor (Shuai et al., 2020). In addition, a recent study was able to identify the interacting domain between ITGB1 and RV-G through CO-IP, where it has been concluded that ITGB1 ectodomain (1-728 a.a) and ERA G ectodomain (20-459 a.a) interact with each other (Shuai et al., 2020). Both cytoplasmic and transmembrane domains showed no role in interaction between both ITGB1 and RV G protein. A previous study has reported the low levels of ITGB1 upon

N2a cells infection with RV, indicating its internalization with RV during infection where they colocalize in early and late endosomes. Consequently, confirming the crucial role of ITGB1 for RV entry into cells was carried out through blocking ITGB1 effect with antibodies. It has been observed that ERA-GFP RV infection was decreased in HEK293 and N2a cells upon ITGB1 antibody blockade, supporting the role if ITGB1 as RV receptor.

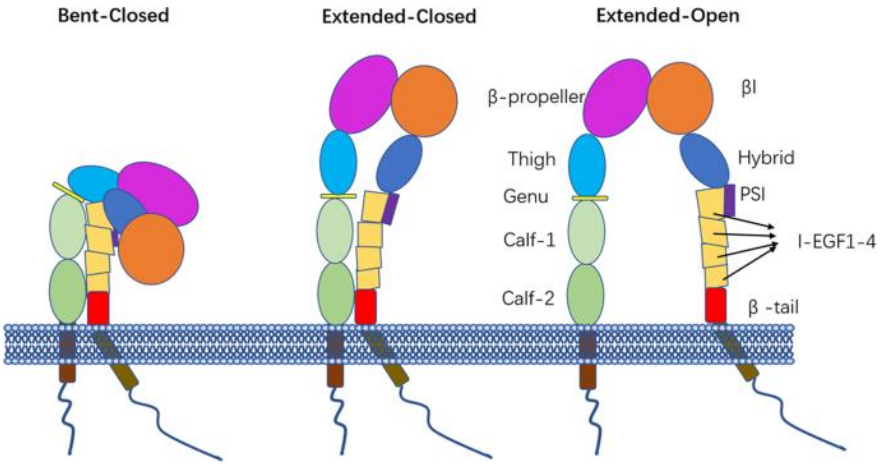

Figure 1.13 A schematic diagram representing the structure of integrins and its conformational changes.

The α- and β-subunits of integrin comprise the extracellular, transmembrane, and the intracellular domains. The extracellular domain is divided into multiple smaller domains. The figure has been adapted from (Nevo, 2010).

1.6.4.2 Role of the host factors sequence conservation and glycosylation in spillover events

Host cellular factors may have a minor influence compared to other factors in driving the transmission of the virus across distinct species. One explanation for this is that host cellular genes involved in virus entry exhibit a high degree of conservation among various species, primarily due to evolutionary constraints imposed on these genes. This conservation in gene sequences can be linked to the involvement of these proteins in multifunctional roles. However, certain cellular proteins undergo continuous sequence changes in consequence to adaptations to the changing external environment. This phenomenon is particularly prominent in genes associated with defending the cells against new pathogens or to the genes involved with interaction with certain viruses (Warren and Sawyer, 2019).

Collectively, for a virus to successfully enter a new host species, the virus might bind to a receptor protein that is highly conserved among the species. This has been clearly exemplified in recent study that demonstrated the effectiveness of SARS-CoV-2 in binding to the ACE2 receptor since it represents the principal host factor influencing its ability to establish infection among distinct species due to its high sequence conservation among susceptible hosts (Conceicao et al., 2020).

An intriguing observation was made regarding the closely related ACE2 sequences in rats and hamsters, revealing different interactions with SARS-CoV-2. While the rat ACE2 did not facilitate binding with SARS-CoV-2, the hamster ACE2 enabled viral binding. This discrepancy was attributed to multiple substitutions identified in the interaction interface of the receptor binding domain (RBD), which contributed to the variability in SARS-CoV-2 binding to these receptors (Conceicao et al., 2020). These findings underscored the significance of not only a highly conserved receptor sequence between donor and recipient species could allow virus spillover, but also highlighted the importance of a similar interaction site with the receptor for successful virus transmission across species barriers, suggesting that sequence similarity among the surface receptors may play a role in determining susceptibility to certain viruses, potentially equalizing susceptibility across species. However, the absence of virus infection in certain species despite high receptor sequence similarity could be attributed to the utilization of multiple receptors by the virus or the presence of species-specific restriction mechanisms, such as innate immunity. Recent studies have provided confirmation for the first hypothesis, demonstrating that SARS-CoV-2 does not solely rely on ACE2 for its entry. These studies have revealed the involvement of alternative functional receptors, namely Asialo-glycoprotein receptor 1 (ASGR1) and Kringle domain-containing transmembrane protein 1(KREMEN)1, in mediating the ACE2-independent virus entry (Johnson et al., 2020).

1.6.4.2.1 Receptors glycosylation

The glycosylation of the surface receptors is recognized as one of the factors influencing the cross-species transmission of viruses. This post-translational modification of receptors, particularly those involved in viral attachment and entry, can impact the ability of a virus to bind and infect cells from distinct species The entry of influenza virus

into host cells is initiated by the interaction between its surface protein hemagglutinin (HA) and sialic acid receptors. The glycosylation patterns of these receptors contribute to the transmission dynamics of the virus between human and avian populations. Specifically, avian influenza viruses prefer binding to sialic acid linked to galactose via α-2,3 linkage, found in avian hosts, whereas human influenza viruses exhibit a preference for α-2,6 sialic acids, commonly present in human respiratory tissues (Kumlin et al., 2008). Mutations occurring in the surface protein known as hemagglutinin (HA) of influenza viruses are responsible for the cross-species transmission of the virus. These mutations lead to changes in the binding affinity of avian influenza viruses (AIV) for several types of sialic acids. Notably, subtypes H2 and H3 of AIV underwent two specific mutations that enabled them to switch their preference from avian-type sialic acids to human-type sialic acids (Kim et al., 2018). There are no previous studies reporting the role of RV receptors glycosylation in mediating virus cross-species transmission.

1.6.5 The onward transmission of single infection to a member of the same species.

The onward transmission of the virus depends on host density and contact rates between same species. Furthermore, the ability of a new strain to replicate and shed in the new host also determines its ability to be transmitted to members of the same species. Onward transmission does not guarantee the maintenance of the virus to species such as in low population densities cross species transmission may decrease by reducing the contact exposure among the species (Plowright et al., 2017).

1.6.6 The ability for long term transmission and maintenance of infection.

The long-term virus transmission is influenced by the density and growth rate of newly affected species. Besides the ability of the virus to modify the host behaviour and balance the replication and transmission of the new strain, concluding that this stage is more dependent on phylogenetic relatedness of species rather than ecological overlap. Commonly infected species showed variation in host association among viral lineages because of the interspecific contact rate between the reservoir host and that the spillover transmission should be dependent on the ecological overlap rather than phylogenetic relatedness (Mollentze et al., 2014).

1.7 Aims of this Project

RV is known for its wide host range and spillover events. Despite the availability of substantial information on RV infectivity, there is a gap in understanding the mechanism by which the G protein can interact with different receptors for initiation of infection. The aim of this project is to identify the essential receptor that influences the RV differential species and cellular tropism with primary focus on human, bat, and dog hosts.

- In this project, we aim to compare the protein sequences corresponding to the RV receptors in human, dog, and bats. Together with i*n silico* prediction of the interaction between the RV-G and the receptor orthologs (human, dog, and bats). This section was published at the start of the project (Khalifa et al., 2021).
- Further to the *in silico* analysis, we aim to investigate whether proteins encoding the RV receptors in *P.alecto* bat species have a functional role in RV entry (**Chapter 3).**
- For studying the host susceptibility and RV receptor preference, we aim to establish an *in vitro* cellular model. This model involves the generation and characterization of replication competent VSV carrying the RV-G surface protein, along with identification of a non-permissive cell line lacking host factors necessary for RV replication to allow studying the receptor preference of RV (**Chapter 4)**.
- To transiently express the RV receptors individually or in combinations in the identified resistance cell line which will consequently allow selection of receptors with potential role in promoting RV entry and replication for knockout studies. This will allow the identification of the essential RV receptors essential in RV entry and replication **(chapter 5)**
- Explore the role of receptor orthologs of *Homo sapiens, Canis. familiaris* and P.alecto in rVSV-dG-RV-G-GFP infection and entry, and investigate the differential tropism of RV in human, dog, and bat cell lines to determine if the RV utilizes similar receptors in different cell lines **(Chapter 6).**
- Investigate additional factors, beyond the receptors, that influence RV replication in Pa-BR cells such as host attachment factors and RV viral proteins such as phosphoprotein and matrix proteins **(Chapter 7)**

It is anticipated that the proposed research plan will generate data which will enable understanding the receptor utilization mechanism of RV and its differential tropism among human, dog, and bats.

2 Chapter 2 Methods

2.1 Methods

2.1.1 Bioinformatics methods

2.1.1.1 Construction of Data Sets

To investigate the differences among RV receptors in distinct species, protein sequences were retrieved from NCBI by BLAST search. All sequences for each of the proteins were downloaded and collated in a FASTA format.

2.1.1.2 Alignment of the Protein Sequences

Multiple sequence alignment for protein sequences of host receptors were performed using DNASTAR Laser Gene version 17.0.2.1 using the MUSCLE method (Burland, 2000).

2.1.1.3 Domain Organization for RV Receptors

Domain organization for different RV receptors in distinct species were analysed by Pfam (http://pfam.xfam.org) (Mitchell et al., 2015; Finn et al., 2016) InterPro (http://www.ebi.ac.uk/interpro/). Schematic diagrams for domains in the different protein receptors have been represented by PROTTER software (Omasits et al., 2014).

2.1.1.4 3D Structure Model Building and Quality Assessment

The 3D structure models for RV receptors, ITGB1, mGluR2, nAChR, and NCAM proteins, were generated using I-TASSER (Yang et al., 2010). The 3D structures generated by I-TASSER were based upon threading, fragment assembly, and iteration. The best model was selected according to the confidence score (C-score) which represented the quality of predicted models by I-TASSER. The C-score range was between (−5 and −2), where the higher the C-score, the higher the confidence of a model and vice versa. After predicting the protein model, structure and stereochemical analyses were performed and the predicted 3D structures were visualized and annotated using PyMOL software (DeLano, 2002).

2.1.1.5 Molecular Docking Simulations

The predicted structures were used for protein-protein docking studies using GRAMM-X software (Tovchigrechko and Vakser, 2006a) .Docking studies were performed for the Egyptian RV-G protein against each of RV receptors from human, dog, and black fruit

bat. In addition, *in silico* interactions between RV-G protein related to bat strain were mapped with different receptors.

2.1.1.6 Analysis of the Docking Complex

The docking complexes obtained from GRAMM-X were uploaded to PDBsum (Laskowski et al., 2018) and PDBePISA (Battle, 2016) servers for analysis of the protein-protein interactions. Identification of hydrogen bonds, interacting interfaces, nonbonded contacts, salt bridges, Gibb' free energy of binding (ΔG^{int}, kcal/mol), pores, and tunnels in protein complexes were carried out. Mapping of the docking complexes was performed using PYMOL software (DeLano, 2002).

2.1.2 Molecular biology methods

2.1.2.1 **Amplification of the RV-G insert using Polymerase chain reaction (PCR):**

Component	Amount (25 µL)	Final concentration
Plasmid	1 µL	100 ng
Q5 DNA polymerase enzyme	0.25 µL	0.02 U/µL
10 mM REV primer	1.25 µL	0.5 µM
10 mM FWD. primer	1.25 µL	0.5 µM
10 mM dNTPs	0.5 µL	200 µM
5X Q5 reaction buffer	5 µL	1X
Q5 GC enhancer	5 µL	1X
Nuclease-free water (NFW)	up to 25 µL	

Thermocycler conditions were set as described in the appendix.

2.1.2.2 Analysis of PCR/restriction digestion products by agarose gel electrophoresis

The agarose gel electrophoresis was performed as previously described (Michael R. Green, 2012). The 1X TAE buffer was prepared by adding 5 mL of the 10X TAE buffer stock solution to 45 mL of distilled autoclaved water. A 0.6% agarose gel was prepared by dissolving 0.3 grams of Ultrapure agarose gel in 50 mL of 1X TAE buffer. The agarose solution was heated in an autoclave for 1 minute to facilitate solubilization. While leaving the agarose solution to cool down, the gel casting tray was assembled, and the comb was placed After cooling of the gel, the gel red stain (nucleic acid stain) was added

at a ratio of 10 µL per 50 mL of agarose solution. The samples were then mixed with 6X gel loading dye and loaded in the wells (10 µL). One well was kept for loading the Gene Ruler 1 kb DNA ladder. The chamber was covered, and the apparatus was connected to the power supply. The gel was electrophoresed at 100 volts for 30 minutes – 1 hour in 1X TAE running buffer, and the visualization of the gel was performed using a Gel-doc machine. For cutting specific bands, the gel was examined using the UV transilluminator.

2.1.2.3 Purification of PCR product from the agarose gel

The purification of PCR product or DNA was performed according to the manufacturer's instructions using the Gene JET Gel Extraction Kit. Upon performing the agarose gel electrophoresis, excising the DNA band of interest was performed using a razor blade. Then the gel slice was placed in a pre-weighed Eppendorf tube and the binding buffer was added at a 1:1 volume of buffer (µL): gel (mg). Followed by incubation of the gel mixture on a heat block at 65 °C till the gel completely dissolved. Then the solubilized gel was transferred into Gene-JET purification column and centrifuged for 1 min. at 12,000 x g and the flow through was discarded. Afterwards, 700 µL of wash buffer was added to the column and centrifuged again at the same speed while discarding the flow through. Re-centrifugation of the empty column was carried out to remove any residual buffer from the column. DNA was eluted by adding 30- 50 µL of warmed elution buffer added at the centre of the column and left to stand for 5 minutes at room temperature. Then the tube was centrifuged at 12,000 x g for 2 minutes. Purified DNA concentration was measured using a Nano-Drop 2000c spectrophotometer.

2.1.2.4 Restriction Digestion reaction of the vector/PCR product/purified plasmids

After purifying the PCR product or purified plasmids, restriction digestion reactions for the PCR product and vector were carried out.

Component	Amount (50 µL)	Final concentration
NFW	up to 50 µL	
PCR product	19 µL	1 µg
MluI-HF enzyme	1 µL	

NheI-HF enzyme	1 µL
10X CutSmart® Buffer	5 µL

Component	Amount (50 µL)	Final concentration
NFW	up to 50 µL	
Vector	2 µL	1 µg
MluI-HF enzyme	1 µL	
NheI-HF enzyme	1 µL	
10X CutSmart® Buffer	5 µL	1X

Upon spinning the tubes for 10-20 sec, the restriction digestion reactions were incubated at 37 °C for overnight, followed by heat inactivation according to the manufacturer's instructions. Then followed by, running the restriction digest in agarose gel electrophoresis along with the DNA ladder.

2.1.2.5 Ligation of linearized vector/PCR product

The ligation of the linearized vector, PCR products or annealed oligos was carried out according to the manufacturer instructions.

Component	Amount (10 µL)
NFW	up to 10 µL
Vector	2 µL
DNA insert	1 µL
10X T4 DNA ligase buffer	1 µL
T4 DNA ligase enzyme	1 µL

The ratio of vector: DNA insert was used at 1:3. The tube was gently spun for mixing the reagents. The reaction was incubated at 16 °C overnight followed by heat inactivation of reaction at 65 °C for 10 minutes**.**

2.1.2.6 Transforming the competent E. coli.

The chemically competent *E. coli* was used to transform the ligation reaction or plasmid DNA. Thawing the chemically competent vial was performed on ice. In a circular manner, the ligation mixture (1-20 µL) or the plasmid DNA (50 ng) was added to 50 µL of DH5-alpha E. coli competent cells and kept on ice for 30 minutes. After incubation, the transformation mixture was heat shocked at 42 °C for 45 seconds. Samples were then transferred on ice again for 10 minutes. Transformation mixture was mixed with pre-heated 250 µL of SOC medium and then incubated for 1 hr at 37 °C in shaking incubator. In the meantime, preparation of the agar plates with the selective bacterial media was carried out by dissolving the LB agar in the microwave. When reaching 55 °C, final concentration of ampicillin was added (100 µg/mL). Then LB gar was poured into the petri dishes and kept solidifying at room temperature. Following the incubation, 50 µL of the transformation mixture was plated on the prepared LB agar plates followed by incubation overnight at 37 °C. Control plates were included in all experiments. The following day, the plates were checked for colonies. Single, well-defined colonies were picked and incubated in 5 mL LB broth containing 100 µg/mL ampicillin overnight in a shaking incubator at 37 °C. The following day, 4.5 mL of the bacterial culture was used for plasmid purification. The rest of the culture (0.5 mL) was mixed with the preservation medium and stored at -80 °C for future use.

2.1.2.7 Verification of bacterial transformants using Colony PCR

One mL of bacterial culture was centrifuged at 13,000 x g for 10 minutes. The supernatant was discarded, and the pellet was resuspended in 40 µL TAE buffer with mixing. The tubes were incubated at 100 °C for 10 minutes in bench incubator. Samples were centrifuged at 13,000 x g for 5 minutes and the DNA containing supernatant was transferred to new microfuge tube to be used as the template DNA. Gene specific primers were used, and the reaction mixture was prepared as follows:

Component	Amount (25 µL)	Final concentration
DNA template	1 µL	50-100 ng
Dream-Taq Green PCR Master Mix (2X)	12.5 µL	0.02 U/µL
10 mM REV primer	1.25 µL	0.5 µM

10 mM FWD. primer	1.25 µL	0.5 µM
NFW	Up to 25 µL	

Visualization of the PCR products was carried out using the agarose gel electrophoresis as described in **Section 2.2.2.2** to identify positive transformants, and further confirmed using sequencing.

2.1.2.8 Purification of plasmid DNA

The plasmid miniprep purification was carried out using Qiagen Miniprep kit (QIA-prep Spin Miniprep Kit) according to the manufacturer's instructions. The overnight bacterial cultures were distributed into microcentrifuge tubes, and they were centrifuged at 6000 x g for 3 minutes. The supernatant was discarded, and the pellet was resuspended in 250 µL (P1) buffer with RNASe. Then the lysis buffer (P2) was added at 250 µL with gentle mixing by inverting the tube 4-6 times of the tube until the mixture appeared blue. Then the neutralization buffer (N3) at 350 µL was added with inverting the tubes 4-6 times until the mixture appeared white cloudy. To obtain the plasmid DNA, the mixture was centrifuged at 17,900 x g for 10 minutes and the supernatant was transferred to the spin column provided with collection tube. After centrifugation, the flow through was discarded. The column was washed twice with 500 µL PB buffer and followed by 750 µL of PE buffer with centrifugation after each washing step. Centrifugation of the spin column without any buffer was carried out to ensure dryness of the column with discarding the flow through after each centrifugation step. The DNA spin column was placed in a microfuge tube and the DNA was eluted in prewarmed 30-50 µL of elution buffer. The column was incubated for 5 minutes at room temperature and centrifuged for 2 minutes at 17,900 x g. The DNA concentration was measured using the Nano-drop machine and then stored at -20 °C.

2.1.2.9 Confirmation of the recombinant plasmids by Sanger sequencing

Plasmid DNA extracts or PCR products of positive clones were further verified by sanger sequencing. The concentration of primers and plasmids were prepared according to the sequencing company specifications. A 20 µL of either the DNA plasmid (100 ng/µL), or purified PCR products (10 ng/µL), and target-specific primers (3.2 pmol) were prepared in separate microfuge tubes and sent for sequencing at source bioscience Ltd

(Cambridge, UK). Sequence contigs were analysed using the NCBI BLAST tool and SnapGene.

2.1.2.10 Viral RNA extraction

Viral RNA extraction from the rescued VSV -G-GFP was performed according to the using QIA-amp Viral RNA Mini Kit (QIAGEN) kit manufacturer's instructions. For each sample BHK cell culture supernatant, (140 µL), a lysis buffer AVL (560 µL) and carrier RNA (5.6 µL) were added and mixed with pulse vortex for 15 s. The mixture was incubated at RT for 10 min and briefly centrifuged to remove drops from the inside lid. Absolute ethanol at 560 µL was added to the mixture and mixed by pulse-vertexing and brief centrifugation to remove drops from the lid. A 630 µL of lysate was then transferred into the QIAamp Mini column and centrifuged at 6000 x g for 1 min. The collection tube was discarded, and the column was placed in a new collection tube. The previous step was repeated until the sample was fully loaded. The column was washed twice once with 500 µL AW1 Buffer and the next wash with 500 µL of Buffer AW2. After each wash, the column was centrifuged at 6000 x g for 1 min in first wash and for 3 min at 20,000 x g in the second wash and placed into clean collection tube. To get rid of any residual washing buffer, the spin column was centrifuged for 1 min at full speed. A volume of 30 µL of AVE buffer was added to the centre of the membrane to elute the viral RNA after setting in a sterile microfuge tube. After incubation for 5 min at RT, centrifugation of the tubes at 6000 x g for 1 min was carried out. The extracted viral RNA was quantified and ready for cDNA synthesis or stored at -80 °C until use.

2.1.2.11 Reverse transcription polymerase chain reaction (RT-PCR)

The extracted viral RNA served as a template for RT-PCR. The cDNA synthesis mixture was prepared into a 0.2 mL thin-walled PCR tube for each sample. A 20 µL reaction included the following components in two steps:

The cDNA reaction mixture (step 1) was set as follows:

Component	Volume
2 µM gene-specific reverse primer	1 µL
10 mM dNTP mix (10 mM each)	1 µL

Template RNA (100 ng RNA) up to	8 µL
DEPC-treated water up to	3 µL

The reaction components were mixed followed by heating the template RNA primer mixture at 65 °C for 5 minutes and incubating on ice for 1 minute. The following components were added to each tube.

The cDNA reaction mixture (step 2) was set as follows:

Component	**Volume**
5× SSIV Buffer	4 µL
100 mM DTT	1 µL
RNase-OUT™ Recombinant RNase Inhibitor	1 µL
Super-Script® IV Reverse Transcriptase (200 U/µL)	1 µL

The contents of both reactions were mixed and incubated at 55 °C for 10 minutes, followed by inactivation the reaction at 80 °C for 10 minutes.

Component	**Amount (25 µL)**	**Final concentration**
DNA template	1 µL	100 ng
Dream-Taq Green PCR Master Mix (2X)	12.5 µL	0.02 U/µL
10 mM VSV-UP primer	0.625 µL	0.5 µM
10 mM VSV-Down primer	0.625 µL	0.5 µM
NFW	up to 25 µL	

2.1.2.12 Quantitative One step RT-qPCR (TaqMan™)

Quantification of viral RNA was quantified using the SuperScript™ III Platinum™ One-Step RT-qPCR Kit according to manufacturer's instructions.

Reactions were set up on ice, a master mix was prepared, followed by addition in plate wells on ice, then finally the template RNA was added separately to each well.

Reaction was set as follows.

Component	Volume	Final concentration
SuperScript™III	1 µL	
RT/Platinum™ *Taq Mix*		
2X Reaction Mix	25 µL	
FWD primer	1 µL	10 µM
REV primer	1 µL	10 µM
Fluorogenic probe	0.5 µL	10 µM
RNaseOUT™	1 µL	
Template	10 µL	1 pg to 1 µg total RNA
DEPC-treated water	Up to 50 µL	

2.1.2.13 CRISPR/Cas9 genome editing technique.

2.1.2.13.1 Design and cloning of the sgRNA in the PX459 V 2.0 plasmid.

In this study, we used CRISPR/Cas 9 technology to perform genomic knockout of DNA using Cas9 as described **(Figure 2.1).** The design of guide RNA (gRNA) targeting specific exons of the human ITGB1, mGluR2 and nAChR was carried out using the online Benchling web tool to minimize the off-target cleavage. For the FWD gRNA oligo sequence, an overhang of the (CACCG) was added at the 5' end. The extra G added after the restriction site to ensure efficient transcription initiation from the U6 promoter. While an overhang of (AAAC) was added at the 3' end of the reverse complement of the gRNA oligo sequence.

2.1.2.13.1.1 Annealing of the gRNA oligos

Component	Volume (20 µL)
Forward Oligo (100 µM)	2 µL
Reverse Oligo (100 µM)	2 µL
Annealing buffer*	2 µL
NFW	14 µL

***Annealing buffer composition: 10 mM Tris, 1 mM EDTA, 50 mM NaCl

The oligos were annealed at 90 °C for 3 min and then kept at 37 °C for 1 hr. The annealed oligos were diluted 1/50 (4 µL of the reaction /196 µL NFW).

2.1.2.13.1.2 CRISPR/Cas 9 plasmid restriction digestion reaction.

Component	Volume (25 µL)
Plasmid	1-2 µg
rCutSmart buffer	2.5 µL
BbsI-HF®	1 µL
NFW	up to 25 µL

The (pSpCas9(BB)-2A-Puro (PX459) V2.0 plasmid was digested at 37 °C overnight, followed by heat-inactivation at 80 °C for 20 min. The concentration of purified linearized plasmid was measured by nanodrop and used for ligation with the annealed oligos.

The annealed oligos were cloned into linearized plasmids with the following conditions:

2.1.2.13.1.3 Ligation of the gRNA oligos into (PX459) V 2.0 plasmid.

Component	Volume
Linearized Plasmid	100 ng
10 X T4 DNA ligase buffer	1 µL
Diluted annealed oligos 1/50	1 µL
T4 DNA Ligase®	1 µL
NFW	up to 20 µL

The ligation mixture was kept at 16 °C overnight., followed by transformation of the ligation mixture as described in section (2.2.1.6). Verification of the positive colonies was further assessed using colony PCR and sequencing using the FWD U6 promoter specific prime.

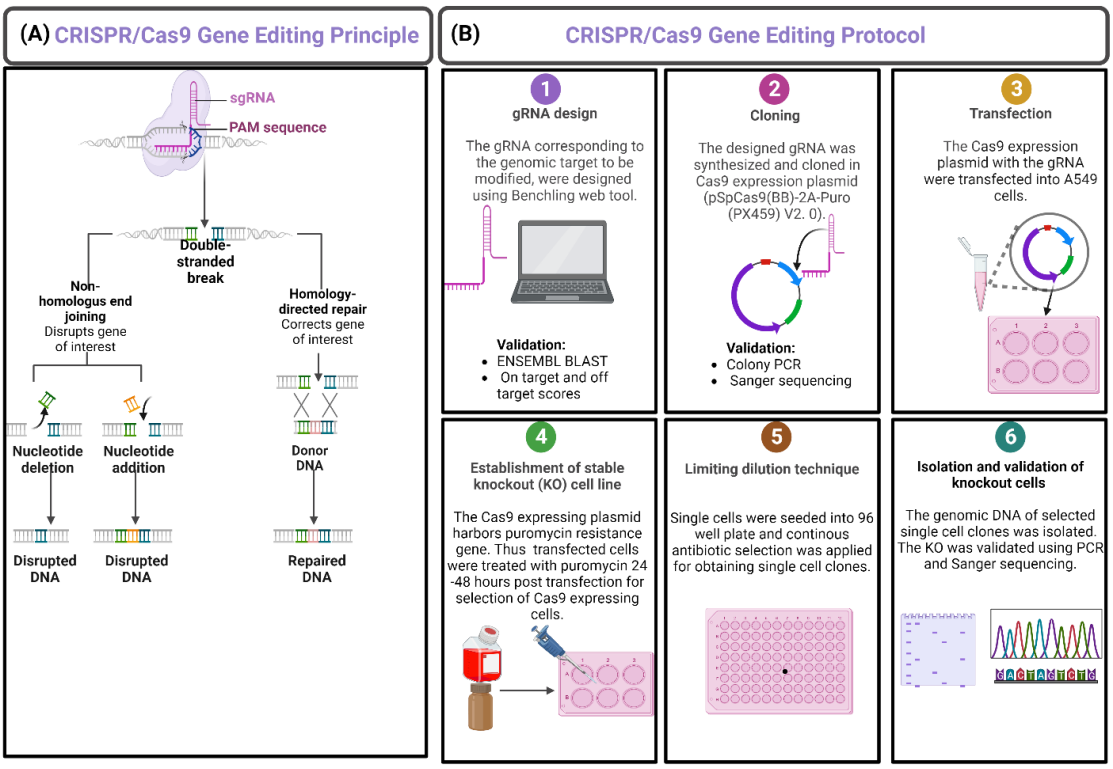

Figure 2.1 CRISPR/Cas9 principle and workflow.

(A). *The CRISPR/Cas9 consists of the Cas9 enzyme and the guide RNA. The gRNA is a short synthetic RNA composed of a scaffold sequence for Cas 9 binding, along with a 20-nucleotide spacer corresponding to the target genome to be modified. Upon recognition of the target site, the Cas 9- gRNA complex binds the DNA target, and the CRISPR/Cas 9 protein modifies the target region by inducing double-strand breaks (DSB). These DNA break sites are repaired by either insertion or deletion into the cut site (NHEJ, left). Or through homology-directed repair If a donor sequence is provided (HDR, right).* ***(B)*** *CRISPR/Cas9 workflow:* ***Step 1****: Initially the gRNA sequence corresponding to the genomic target to be modified is designed using the Benchling web tool. Suitable gRNAs were chosen based on two main parameters: on-target activity (cleavage specificity) and off-target scores (total number of mismatches). The best gRNA was chosen with the highest off-target and on-target scores. To ensure no off-target effects in the designed gRNA, the gRNA sequence is blasted in the Ensemble database against the genome of the target species. The small number of hits indicated promising activity for the gRNA.* ***Step 2****: The designed gRNA was synthesized and cloned into the PX 459 V 2.0 vector expressing the Cas9 and puromycin resistance gene. The cloning of the gRNA in the Cas9 expression plasmids was verified by colony PCR and sanger sequencing.* ***Step 3:*** *The PX459 V 2 .0 expressing the gRNA, Cas9 and the puromycin resistance gene was transfected into the A549 cells.* ***Step 4****: After 24 hrs post-transfection, transfected cells were treated with growth media containing puromycin 2 µg/mL to allow the selection of the cells only expressing the gRNA and Cas9.* ***Step 5:*** *Following the antibiotic selection, single-cell clones were isolated in 96-well plates by a limited dilution technique to allow the isolation of the single-cell clones and generate stable cell lines.* ***Step 6*** *Upon isolation and expanding the single-cell clones, the genomic DNA was extracted from the single cells to detect and*

characterize the introduced indels using PCR and Sanger sequencing in the target exons. Abbreviations NHEJ; non-homologous end joining; DSB, double-strand breaks; HDR, Homologous directed repair; KO knockout. This figure is adapted and modified from Biorender.com.

2.1.2.14 Total cellular RNA extraction

The procedure of extraction of the cellular RNA was performed as previously described (Rio et al., 2010). For quantification the endogenous receptor genes, total RNA from the cells were collected. The cells were centrifuged for 5 min at 300 x g. Then the cell pellet was resuspended in 200 µL of NFW. One mL of TRIzol was added to the suspended cells and mixed by inverting the tube. After incubation at RT for 20 min., 200 µL of chloroform was added to the mixture mixed by inverting the tube and incubated for 2 min at RT. The samples were centrifuged at 14,000 x g for 15 min 4 °C. After separation of the mixture, the colourless upper phase was aspirated and transferred to clean microfuge tube. For RNA precipitation, 2 volumes of isopropanol were added to the upper phase and kept at -80 °C., overnight. The following day, the mixture was centrifuged at maximum speed for 30 min at 4 °C., then the supernatant was discarded. For washing the RNA pellet, 1 mL of ethanol was added to the pellet and mixed. The microfuge tube was centrifuged at maximum speed for 5 min. at 4 °C. After centrifugation, removal of the ethanol with the pipette and the RNA pellet was left to air dry for approximately 15 min. When the pellet is completely dry with no visible ethanol, the RNA was resuspended by adding 30 µL of RNase free water by pipetting up and down. Quantification of the RNA concentration was carried out using Nanodrop.

2.1.2.15 Total DNA extraction

The genomic DNA of the A549 cells transfected with CRISPR/Cas9 plasmids was extracted for verification of the knockout. The DNA extraction was carried out performed using the DNeasy® Blood & Tissue. Qiagen kit and performed according to the manufacturer's instruction. Firstly, the knockout A549 cells were trypsinized, followed by addition of the growth medium and centrifugation at 300 x g for 5 min. The pellet was then resuspended in 200 µL PBS, followed by adding of 20 µL Proteinase K. A 200 µL Buffer AL was added to the sample, mixed, and incubated at 56 °C for 10 min.

Followed by the addition of 200 µL ethanol (96–100%) to the sample and mixed thoroughly by vortexing. Then the mixture was added to the DNeasy Mini spin column

placed in a 2 mL collection tube and centrifuged at ≥6000 x g) for 1 min. Upon centrifugation, the flowthrough was discarded. Followed by washing once with 500 µL Buffer AW1, followed by centrifugation for 1 min at 6000 x g. and discarding the flow through. Another wash step was performed by adding 500 µL Buffer AW2, followed by centrifugation for 3 min at 20,000 x g to ensure the absence of any residual ethanol. Finally for DNA elution, the DNeasy Mini spin column was placed in in a clean 1.5 mL, and 50 µL Buffer AE were added directly onto the DNeasy membrane, incubated at RT for 1 min. and followed by centrifugation at 6000 x g. Quantification of the DNA concentration was carried out using Nanodrop.

2.1.2.16 Quantitative real-time PCR (RT-qPCR)

The RT-qPCR was used to measure the fold change in the expression of the receptor genes in different cell lines in response to the rVSV-dG-RV-G-GFP compared with mock cell lines. The primer pairs were designed for the corresponding genes and synthesized by Invitrogen by Life Technologies, UK.

Component	Volume
2X SYBR® Green Reaction Mix	12.5 µL
Forward primer (10 µM each)	0.5 µL
Reserve primer (10 µM each)	0.5 µL
Mg SO_4 Enhancer	0.5 µL
SuperScript® III RT/Platinum® Taq Mix	0.5 µL
Template (1 pg to 1 µg total RNA)	<10 µL
Nuclease free water	Up to 25 µL

The reaction mixture was spun down for 10-20 seconds to remove drops from inside of the lid. The tubes were placed in the CFX96 real-time PCR system for detection and amplification of the target sequences.

The relative mRNA expression for the cellular genes were quantified compared to the housekeeping loading controls. The fold change in relative cellular expression levels was calculated using the following equation:

Fold Change = $2^{-\Delta\Delta Ct}$ = - (Δ*CT* of infected cells – Δ*CT* of mock-cells). The delta *CT* values refer to the difference in CT values between the gene of interest and the reference gene

(housekeeping gene) employed (beta-actin or 18S) for a given sample. Upon normalizing the *CT* values of each sample, the delta delta *CT* values were calculated to show the difference in *CT* values between infected and mock cells (Rao et al., 2013).

2.1.3 Cell Culture Methods

All cell culture techniques were performed in a class II cabinet.

2.1.3.1 General cell culture protocol

Human keratinocytes (HaCaT), A549, Human embryonic kidney cells (HEK 293), (Lung carcinoma cells (A549) Chicken embryonic fibroblast (CEF), chicken origin DF-1 cells (DF-1), and Canine Madin-Darby Canine kidney cell (MDCK) were maintained in DMEM (high glucose, GlutaMAX Supplement, pyruvate), supplemented with 5% foetal bovine serum (FBS) and 1X antibiotic antimycotic solution. The *P.alecto* brain cell (Pa-Br) was maintained in DMEM (F-12/HAM) supplemented with 10 % FBS and 1X antibiotic antimycotic solution All cell lines were cultured at 37 °C and 5% CO2. Cell lines were routinely passaged 2-3 times/week: cells were washed once with PBS and dissociated from the flask using a 0.25% trypsin-EDTA solution (Life Technologies). Cells were resuspended in complete DMEM (Thermo Scientific, USA) and typically split 1 in 3.

2.1.3.2 DNA Transfection of cell cultures

Transfection of the plasmid DNA was carried out using lipofectamine 2000 reagent (Invitrogen) following the manufacturer's instructions. All The DNA: Lipofectamine ratio and volumes were scaled accordingly (1 µL lipofectamine: 3 µg DNA) and the DNA: Lipofectamine complexes were diluted in Opti-MEM reduced serum medium (Gibco). The transfection mixture was incubated for 25 min at room temperature (RT) before being added dropwise onto the cell monolayer.

2.1.3.3 Generation of rVSV-dG-RV-G-GFP with reverse genetics system

For the recovery of the infectious virus from the pVSV-dG-RV-G-GFP, simultaneous transfection of the pVSV-dG-RV-G-GFP along with the VSV helper plasmids was carried out as previously described (Whitt, 2010). The BHK-21 cells were seeded in a 6 well plate for 70-90% confluency in the next day. The growth medium was aspirated, cells were washed with PBS. The cells were infected with recombinant fowl pox virus (rFPV),

MOI=2 as a source of T7 promoter for 2 hrs, then the inoculum was removed, and the infected cells were washed 3X with PBS. Followed by the co-transfection of BHK-21 cells with the pVSV-dG-RV-G-GFP, pBS-N-ΦT, pBS-P-ΦT, pBS-L-ΦT Plasmid, pBS-G-ΦT Plasmids. The transfection mixture was prepared by mixing the 2.5 µg of pVSV-dG-RV-G-GFP, 0.75 µg of pBS-N-ΦT, 1.25 µg of pBS-P-ΦT, 0.5 µg of pBS-L-ΦT and 2.5 µg of pBS-G-ΦT with 22.5 µL of turbofect transfection reagent, diluted in 500 µL Opti-MEM and incubated at RT for 25 min, followed by dropwise addition of transfection mixture to the cells and incubation at 37 °C and 5% CO2 overnight. After 72 hrs, freezing and thawing 3 times was performed the plate was frozen and thawed 3 times and harvested. The recovered virus was centrifuged at 300 x g, aliquoted stored at -80 °C.

2.1.3.4 . Freezing and thawing of cell lines.

For preservation of cell lines, cell lines were frozen using the following procedure. The cells were detached from the culture flask using trypsin, resuspended with growth medium and then centrifuged for 5 min at 300 x g. The ice-cold freezing medium (10% DMSO in FBS) was used to resuspend the pellet in cryovials and kept for -20 °C for one hour, then for -80 °C overnight and then transferred to liquid nitrogen.

For reuse the frozen cell, cells were removed form liquid nitrogen and incubated at 37 until completely thawed. The thawed cells were resuspended in 10 mL growth medium slowly to avoid osmotic shock. Followed by centrifugation at 300 x g for 5 min, then the pellet was resuspended in growth medium to be cultured in cell culture vessel. And kept overnight at 37 °C, 5% CO_2. The following day, the cells were inspected for attachment and the growth medium was changed to remove any residual DMSO.

2.1.3.5 Generation of KO cell lines using the single cell cloning dilution

For the generation of KO ITGB1, mGluR2 and nAChR A549 cell lines. A kill curve of the different puromycin concentrations (0-5 µg/mL) was carried out to determine the optimum puromycin concentration. The optimal concentration was determined at 2 µg/mL for A549 cell line. Cells were seeded in 6 well plate and the next day was transfected with the recombinant Cas9 plasmids with either ITGB1, mGluR2 or nAChR gene-specific gRNA using lipofectamine. The cells were incubated for 24 h prior to addition of the selective antibiotic medium containing the puromycin, after addition of

the antibiotic selection medium, the growth media was replaced every 48 hrs for removal of non-transfected cells. Then the cell clones were isolated in 96 well plates for generation of single cell clones. The antibiotic-resistant polyclonal cell populations were trypsinized and resuspended to 10,000 cells/mL. A 100 µL of antibiotic selection culture media was pipetted to all wells of the 96-well plate except the first well. Then, 200 µL of the cell suspension was added to the first well. A 100 µL from the first well containing the cells was transferred to the next well and mixed with the previously added culture media, resulting in a 2-fold serially diluted along the 96 well plate. The plate was then incubated at 37 °C. The single-cell clones were visible by microscopy within 10-14 days, which were expanded and transferred into a larger plate until enough cells were obtained for harvesting. Then, the harvested single cells were further screened using PCR and sequence analysis to detect and characterize the indels in the gene of interest (Giuliano et al., 2019a). The sanger sequences were analysed using the Tracking of Indels by Decomposition (TIDE)(Brinkman et al., 2014).

2.1.3.6 Treatment the Pa-Br cells with hepran sulphate/gangliosides

To evaluate the effect of the hepran sulphate and the ganglioside on the RV replication on Pa-Br cells. The cells were seeded in 12 well plates, when reaching confluency, the cells were incubated with the HS for 1 hr at 37 °C or incubated with the gangliosides for 20 min .at 37 °C. Following the incubation, cells were infected with rVSV-dG-RV-G-GFP at MOI of 5. In case of assessing the role of the HS and gangliosides on transfected cells. The Pa-Br cells were transfected with the *P.alecto* receptors, forty-eight hrs post transfection, cells were washed and incubated with the HS or gangliosides as described above and followed by rVSV-dG-RV-G-GFP (Sasaki et al., 2018).

2.1.4 Virological assays

2.1.4.1 Virus infection

Routinely, cells were seeded at 80-90% 24 h prior to infection. Once the cells are confluent, cells were washed once with sterile PBS to remove any residual serum. Cells were incubated at 37 °C and 5% CO_2 for 1 hour, shaking every 20 minutes. The virus was removed by washing the monolayer twice with sterile PBS. An appropriate volume of maintenance media was added to the cells and infection was left for the time indicated.

2.1.4.2 Virus quantification by plaque assay

Virus supernatant was collected, and 10-fold serial dilutions were prepared in serum free medium (DMEM). Virus dilutions were used to infect BHK-21 cells in 6-well plate. The Plates were incubated for 2 hrs at 37 °C with shaking every 20 minutes to ensure uniform distribution of the virus dilutions. Cells were washed twice with PBS following the removal of the virus inoculum and the cells were overlaid with 4 mL of the overlay methyl cellulose medium. The Plates were kept at 37 °C for 72 hrs, then cells were fixed with 4% paraformaldehyde (in PBS) (PFA) for 1 hr on a shaker at room temperature. The overlay medium was aspirated after fixing the plates and stained with 0.5% crystal violet for 1 hr. The plates were washed with water and the number and size of formed plaques were counted and measured and the plaque forming units (PFU) was determined accordingly.

2.1.4.3 Flow cytometry for quantification of labelled virus replication (GFP%)

Flow cytometry (FC) analysis was conducted to determine the percentage of labelled virus replication. Cells were seeded in 6-well plate. Upon reaching 70% confluency, cells were infected with rVSV-dG-RV-G-GFP or VSV GFP WT at MOI 1. After 30 hrs, following infection, cells were detached, then neutralized with DMEM containing 10% FBS and centrifuged at 300 x g for 5 min. The pellet was washed once with PBS, centrifuged, and then kept stained with live dead marker for 20 minutes on ice and in a dark place. Then the cells were washed, centrifuged, and resuspended in 1 X permeabilization buffer for 15 min. Subsequently, cells were washed with PBS, centrifuged and the pellet was resuspended in 100 µL PBS for flow cytometry analysis.

2.1.4.3.1 Gating strategy for the virus infected cells

The live, singlet cell populations were gated through forward and side scatters and PB450-A. from the live singlet cells, the infected positive cells with green fluorescent protein (GFP), were gated in the FITC channel compared to the uninfected cell control. The FC data were represented by plots or histograms generated from analysis using CytExpert and FC express software, respectively.

2.1.4.4 Flow cytometric cell analysis for quantification of GFP% from RFP positive cells

To quantify virus labelled infected cells, (infected, transfected cells) flow cytometry analysis was carried out as follows. For internalization/infection experiments, the Cells were transfected with the plasmid expressing receptor of interest. After 48 hr. Cells were infected with rVSV-dG-RV-G-GFP MOI=5. Thirty hours post infection, cells were detached, and centrifuged at 300 x g for 5 min. The pellet was washed once with PBS, centrifuged, and then stained and incubated with live/dead marker in dark, on ice for 20 minutes to allow gating the live cells population. Then upon centrifugation, cells were resuspended in 1 X permeabilization buffer for 15 min, then washed and resuspended in PBS with 2% FBS for 30 min for blocking. The cells were stained with anti-FLAG only targeting the receptors. For entry experiments and HaCaT receptor preference experiments, cells were transfected with the plasmid expressing receptor of interest. After 48 hr. Cells were infected with rVSV-dG-RV-G-GFP MOI=5 for 2 hrs, then cells were washed with PBS. Cells were prepared as described above. Cells were stained with anti-FLAG, targeting the receptors and anti RV-G targeting the viral surface protein. in both the infection and entry assay, for antibody staining equal volume of the antibody mix was prepared and added equally to each sample. The concentration of the antibodies was used at 1.5 µg/mL and then samples were incubated in cold room for 1 hr. The cells were washed 3 times with PBS (2% FBS), followed by incubating the cells with Alexa-Fluor antibody 568 (RFP signal) and Alexa Fluor antibody 468 (GFP signal in entry experiments and HaCaT cells experiments). After 1 hr, cells were washed 3 times with PBS (2 %FBS), centrifuged and resuspended in 100 µL PBS with 2% FBS for flow cytometry analysis. All FC experiments were carried out in tube mode, only the HaCaT cells experiments were carried out in plate mode in flow cytometry.

2.1.4.4.1 Gating strategy for the transfected/infected cells and entry experiments

The cells were gated against the forward and side scatter, and PB450-A to allow the selection of the live, singlet cell populations. The percentage of RFP positive cells populations corresponding to cells expressing the receptors was calculated. From the RFP positive cell populations, the GFP positive cells were gated. For the infection experiments, the GFP positive cell populations were referred to as GFP% of transfected

cells. For the entry experiments, the GFP positive was referred to as entry GFP % of transfected cells. In all experiments, uninfected cell control was used along as negative control for gating the GFP percentage.

The compensations of the samples were carried out with the negative cell control (uninfected, non-transfected), FITC positive sample (infected only; GFP positive only) only and RFP positive sample only (transfected only; RFP positive only). The analysis of data was conducted by FCS express software, upon compensation, data were plotted in representative histograms, along with empty vector (EV) control which served as infected, transfected empty vector control as well as the cell control (uninfected, non-transfected cells) which served as negative control.

2.1.5 Immunological assays

2.1.5.1 Western Blot

The expression of cellular receptors in pCAGG-FLAG plasmids was detected using rabbit anti-FLAG as primary antibody through western blot analysis. The HEK293 cells were washed with ice cold PBS 48 h post transfection. Followed by cells centrifugation and resuspension of cell pellet with 100 µL ice cold lysis buffer composed of NP-40 lysis buffer (10mL) with 1 tablet of pierce protease inhibitor and kept on ice rocker for 30 minutes. For removal of cell pellet, the mixture was centrifuged at 14,000 x g for 5 minutes. Then cell lysate was mixed with 2X of the NuPAGE™ LDS Sample Buffer 4 X with addition of 10% β- mercapto-ethanol for 5 min at 98 °C. Samples were run in 10% resolving gel composed of (4 mL dH_2O, 3.3 mL of 30% w/v Acrylamide with Bis (Bio-Rad), 2.5 mL 1.5 M Tris-HCl (pH 8.8), 100 µL 10% w/v SDS solution, 100 µL of 10% ammonium persulphate (APS) and 4 µL TEMED. The 4% stacking gel composed of: (2.7 mL dH_2O, 670 µ l 30% w/v Acrylamide with Bis, 500 µL 0.5 M Tris-HCl (pH 6.8), 40 µL 10% w/v/ SDS solution, 40 µL APS and 4 µL TEMED). Subsequently, after gel solidification, they were loaded into Bio-Rad Mini-PROTEAN Tetra System and filled with 1X SDS running buffer (6.04 gm tris base, 28.8 gm glycine and 2 gm of 0.1% SDS in 1.8 L dH_2O). Gels run for 30 minutes at 50 voltages(V) then for 2 hours at 100 V. To prepare for the blotting of the gel, the PVDF membrane (Thermo Scientific™), was activated with methanol (Fisher Chemical). In addition, the filter paper was immersed in transfer buffer,

prepared by adding 20 mL of Invitrogen™ Bolt™ Transfer Buffer (20 X) into 400 mL dH_2O. The arrangement of the gel in the transfer system (Bio-Rad) for blotting was in the following order: three layers of filter paper followed by the PVDF membrane then the gel followed by other 3 layers of filter paper. Transfer conditions were set as follows: 1.3 A, 25 V for 30 minutes for the mini gel. After membrane blotting, the membrane was blocked in 5% non-fat dry milk in PBST (0.5% tween-20 in PBS) for 1 hour in a falcon tube on the roller. Afterwards, the membrane was washed once with (0.5% tween 20 in PBS). Consequently, the membrane was incubated with M2 anti-FLAG® primary antibody produced in rabbit (SIGMA Aldrich) with dilution 1:2000 at 4° C overnight on the roller. Then the membrane was washed 3 times in PBST (0.5% tween 20 in PBS), 5 min/wash. Followed by incubation with the secondary antibody Goat pAb to Rb IgG (HRP) (Abcam,) at dilution 1:3000 for 2 hours at room temperature. Thereafter, the membrane was washed 3 times with PBST (0.5% tween 20 in PBS). Eventually, the membrane was incubated for 1 minute with Pierce ECL Western Blotting Substrate (Thermo Fisher) added 1:1 of detection reagent 1 and detection reagent 2. Visualization of membranes was performed by ChemiDoc™ MP imaging System (Bio-Rad Chemidoc, Hercules, CA, USA) using the following protocols: chemi hi sensitivity, chemi hi-resolution and multichannel protocols. As loading controls, identical protein lysate aliquots were incubated with mouse monoclonal anti-alpha tubulin antibody (Abcam,) with secondary antibody rabbit anti-Mouse IgG H&L (Abcam) (Mahmood and Yang 2012).

2.1.5.2 Immunofluorescence staining assay.

BHK-21 cells were cultured on cover slips, upon reaching 70% confluency, cells were infected with rVSV-dG-RV-G-GFP and VSV GFP WT at MOI 1. Twenty-four hrs post infections, cells were washed once with 200 µL PBS, then fixed for 1 hour with 200 µL 4% paraformaldehyde at room temperature, then washed with PBS. Afterwards, cells were permeabilized with 200 µL 0.1% Triton X-100 for 10 minutes, then the cells were washed once with PBS and blocked with 200 µL 0.5% bovine serum albumin (BSA) for 1 hour. After blocking, BSA was aspirated, and cells were incubated overnight at 4° C with the indicated concentration of RV-G primary antibody in 200 µL 0.5% BSA/ well on shaker. Next day, cells were washed 3X with PBS, followed by incubation with goat anti

mouse IgG H& L (Alexa Fluor® 468) (Thermo Fischer) the cells were incubated with the indicated concentration in 200 µL 0.5% BSA/well for 1 hour at room temperature on shaker. Then cells were washed 3 x with PBS, 5 min/wash, and a final wash with dH_2O was carried out. Thereafter, nuclei were stained with 200 µL 4',6-diamidino-2-phenylindole (DAPI) (Thermo Fischer) for 30 minutes (1:10,000). After nuclei staining, coverslips were prepared for mounting over microscopic slides using VECTASHIELD as the mounting medium (LS-BIO, LS-J1033) and fixed with clear nail varnish. Images were acquired with laser confocal microscope, (LSM880). Analysis and data processing were executed using Zeiss software (Flanagan, Middeldorp, and Sculley 2003).

2.1.5.3 Immunoprecipitation (IP)

Since in the current study, the *P.alecto* receptors have not been studied previously. Thus, Immunoprecipitation was performed to identify the potential interaction between the RV-G and the *P.alecto* receptors. The HEK 293 was transiently transfected with each of the *P.alecto* -FLAG tagged plasmids and the pCAGG-RV-G-HA vector. The cells were incubated for 36 hrs. then the HEK 293 cells were lysed for protein isolation. Firstly, a proportion of the lysate were used for western blot analysis to ensure the expression of each of the FLAG-tagged and HA tagged proteins. Then the lysates were incubated with FLAG-antibody bounded to protein G Sepharose beads for 4 hrs at 4° C. After incubation with the antibody bounded to the beads, samples were washed 4X with cell lysis buffer, followed by elution for western blot analysis (Bonifacino et al., 2016).

2.1.6 Electron Microscopy

Electron microscopy was conducted at Open University, UK using established protocols. Briefly, cell culture grown recombinant viruses were first separated by pelleting cell debris at 15000 x g for 15 min. The viruses were quantified using plague assay, real-time PCR and were processed for imaging under electron microscope. For preparation of samples, recombinant viruses were adsorbed for at least 5 minutes on pre-carbon coated grids. These grids were then blocked using 1% BSA for at least 10 minutes at 25 °C. The staining of the adsorbed and blocked virus particles was performed using 2% phosphotungstic acid at stable near-neutral pH of 7.5. After removing excessive

straining, the grids were dried in the air. Finally, virus images were captured with a Zeiss EM910 electron microscope and images were edited and labelled before presentation.

2.1.7 Statistical analysis

The statistical analysis was conducted using GraphPad Prism 9 and Microsoft Excel. The significance testing was carried out using a student t-test, in case only two groups were compared. Experimental means were compared using one-way ANOVA (analysis of variance) when multiple comparisons were required for a single factor. The presented data usually represents three biological replicates. with the Standards Error of Means (SEM). p-values: ns: non-significant; $p>0.05$, *$p < 0.05$, **$p < 0.01$, ***$p < 0.001$, ****$p < 0.0001$.

3 Chapter 3 Genetics and Diversity of Rabies Virus Receptors in Mammals

3.1 Introduction

Rabies is one of the viral zoonotic diseases causing approximately 60,000 human deaths each year as estimated by the WHO (Hampson et al., 2015). The rabies virion is made up of the helical ribonucleoprotein (RNP) core surrounded by the outer envelope (Jackson, 2013). The RNP is constituted by the viral nucleoprotein (N) which surrounds the negative sense viral RNA genome together with the virion associated RNA polymerase (L)and the polymerase co-factor phosphoprotein (P). The Matrix protein is located between the RNP coil and the viral envelope (Ng et al., 2022). On the viral surface, the G protein forms trimeric spikes like projections, mediating the attachment and fusion of the virus to host cell membranes due to its surface distribution (Yang et al., 2020). Excluding the signal peptide, the total length of the RV-G protein is 505 amino acids (a.a), consists of large ectodomain (1-439 a.a), transmembrane (440-462 a.a) and cytoplasmic domains (463-505 a.a) (Yang et al., 2020). The ectodomain is known to play the key role in the attachment with the host cellular receptors and virus entry (Ng et al., 2022).

The interaction of the viral surface protein with the host cellular receptors determines the host range, viral tropism, and viral pathogenesis (Maginnis, 2018b). Previous studies have identified the binding of the RV-G to multiple cellular receptors. Among those, the acetylcholine receptor subunit alpha (nAChR) (Lentz, 1990), metabotropic glutamate receptor subtype 2 (mGluR2) (Wang et al., 2018), integrin β1 (ITGB1) (Shuai et al., 2020), neural cell adhesion molecule (NCAM), and low-affinity nerve-growth factor receptor (p75 NTR) (Tuffereau et al., 1998b)**(Chapter 1, Figure 1.8)**. However, a previous study has shown that the p75 is not essential for RV infection (Tuffereau et al., 2007). None of those receptors have been identified as indispensable for RV infection.

RV can infect all mammalian species, posing a significant risk to humans. Human rabies is mostly acquired by contact with domestic dogs which is considered the primary reservoir (Jackson, 2013). Nevertheless, multiple bat species have been reported to maintain RV in the United States and Canada (Liu et al., 2021). The most common bat species to transmit RV are the Big brown bat, little brown bats, Mexican free-tailed bats, and the silver-haired bat. However, no studies have explored the possibility of RV infection in black fruit bats *(P.alecto).*

Unlike other members of Lyssaviruses, RV host shift events are common (Cho and Seok, 2020). The binding of host cell receptors is the most common trait rendering the virus to successfully infect the new host species (Longdon et al., 2014). From this perspective, the current chapter aims to map the differences in the rabies viral receptors among some RV susceptible hosts including human, bat, and dog. Additionally, identifying the differences in interaction sites among human, dog and bats is essential to understand the possibility for cross species transmission and the reasons for host shifting events of RV.

3.1.1 Aims:

1. Mapping the amino acid differences of the potential RV cellular receptors (ITGB1, mGluR2, nAChR and NCAM) among human, bats, and dogs.
2. Prediction of the 3D structures of the RV receptors (ITGB1, mGluR2, nAChR and NCAM) among human, bats, and dogs.
3. Protein-protein molecular docking for simulating the interaction between the predicted 3D structure of the RV-G and each of the following receptors: ITGB1, mGluR2, nAChR and NCAM in human dogs and bats.
4. Construction of pCAGG plasmids encoding the *P alecto* receptors (ITGB1, mGluR2, nAChR. NCAM and p75NTR) with FLAG tag at the C-terminus and their expression and cellular localization using Western blot and IFA assays, respectively.
5. Quantification of the endogenous expression of the ITGB1, mGluR2, nAChR, NCAM and p75 in *P. Alecto* brain (Pa-Br) cell line.

3.2 Results

3.2.1 Absence of Integrin Plexin domain in black fruit bat ITGB1

The domain organization of human ITGB1 revealed six distinct domains **(Figure 3.1 A).** A short disulphide rich domain (a.a. from 25 to 76) located at the N-terminus of integrin beta chains was named the Integrin plexin domain. In contrast to dog and human ITGB1, the Integrin plexin domain was missing in the black fruit bat **(Figure 3.1 B).** The von Willebrand A (VWA) domain is the longest domain within the ITGB1 encompassing the region from a.a. 36 to 464 **(Figure 3.1 A)** which showed high sequence variability among human, dog, and bats. Difference in 15 a.a. in the dog VWA protein sequence was

observed compared to the human and 18 a.a were variable between black fruit bat and human sequences. However, the area of greatest homology among the ITGB1 protein was the EGF-1 domain (a.a. 466–495) **(Figure 3.1 A)**, in which only one a.a. varied between the species **(Figure 3.1 B).** In the (EGF)-like domain 2 (a.a. 599–630), four and five a.a. residues showed differences in black fruit bat and dog, compared with human; respectively **(Figure 3.1 B).** Both dog and black fruit bat showed nine a.a. residue difference in the integrin beta tail domain (a.a. 640–728) relative to human. The most distal domain was the cytoplasmic domain (a.a. 752– 798). Nine different residues were different in the dog ITGB1 cytoplasmic domain compared to human and bats **(Figure 3.1 B)**.

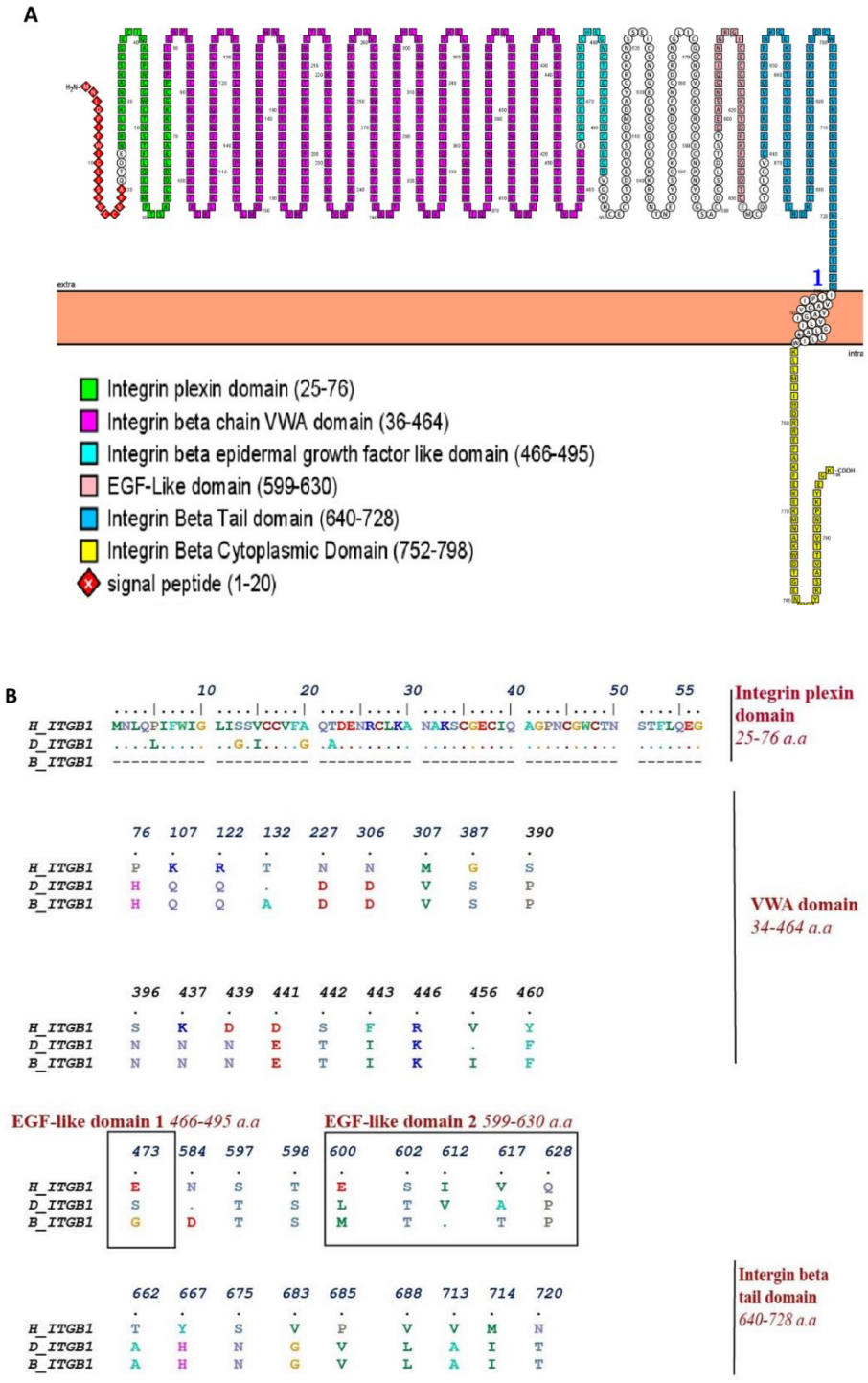

Figure 3.1 ITGB1 domains and sequence alignment.

(A). *General representation of human ITGB1. The graph was generated using PROTTER v1.0* ***(B).*** *Multiple protein sequence alignment of ITGB1, highlighting the different residues in integrin plexin domain, VWA domain, EGF-like domain (1 and 2), and integrin beta tail domain between human (H), dog (D), and black fruit bat (B).*

3.2.2 Binding mode analysis of ITGB1-RV-G docking complex

To elucidate the mechanism by which the RV-G protein interacts with the ITGB1 in distinct species, protein-protein docking was performed using GRAMMX for the 3D structures predicted by I-TASSER. Consequently, the docking complexes obtained from GRAMM-X were uploaded to PDBsum and PDBePISA servers for analysis of the protein-protein interactions and identification of the hydrogen bonds, the interacting interfaces, nonbonded contacts, salt bridges and the Gibb' free energy of binding (Δ G ^{int}, kcal/mol), in the protein complexes. Subsequently, mapping of the docking complexes was performed using PYMOL software. The ΔG^{int} value refers to the solvation free energy gain upon assembly formation (total solvation energies of assembled structures-solvation energies of isolated structures) (Pantsar and Poso, 2018). The RV-modelled 3D structure of Egyptian strain G protein was utilized to undertake the docking against different receptors. Analysis of the docking complex of human ITGB1 and Egyptian RV-G protein showed five interactions mediated by hydrogen bonds in the ITGB1 VWA and EGF-1-like domains with the RV-G protein **(Figure 3.2 A).** In addition to the formation of one salt bridge between Glu340 of human ITGB1 and His438 of the RV-G protein **(Figure 3.2 A).** A more stable docking complex between the dog ITGB1 and RV-G protein of ΔG^{int} −20.8 kcal/mol was mapped **(Figure 3.2 B).** The stability of the docking complex resulted from the formation of four hydrogen bonds and four salt bridges between the dog ITGB1 (Lus156, Asp287, Glu340, and Glu347) and the RV-G (Asp429, His105, His438, and Arg103). Three hydrogen bonds were mapped to mediate the interaction of the bat ITGB1 tail domain and the RV-G docking complex **(Figure 3.2 C).** Our results showed that the G protein ectodomain is responsible for binding to ITGB1 in different hosts **(Figures 3.2 A–C).**

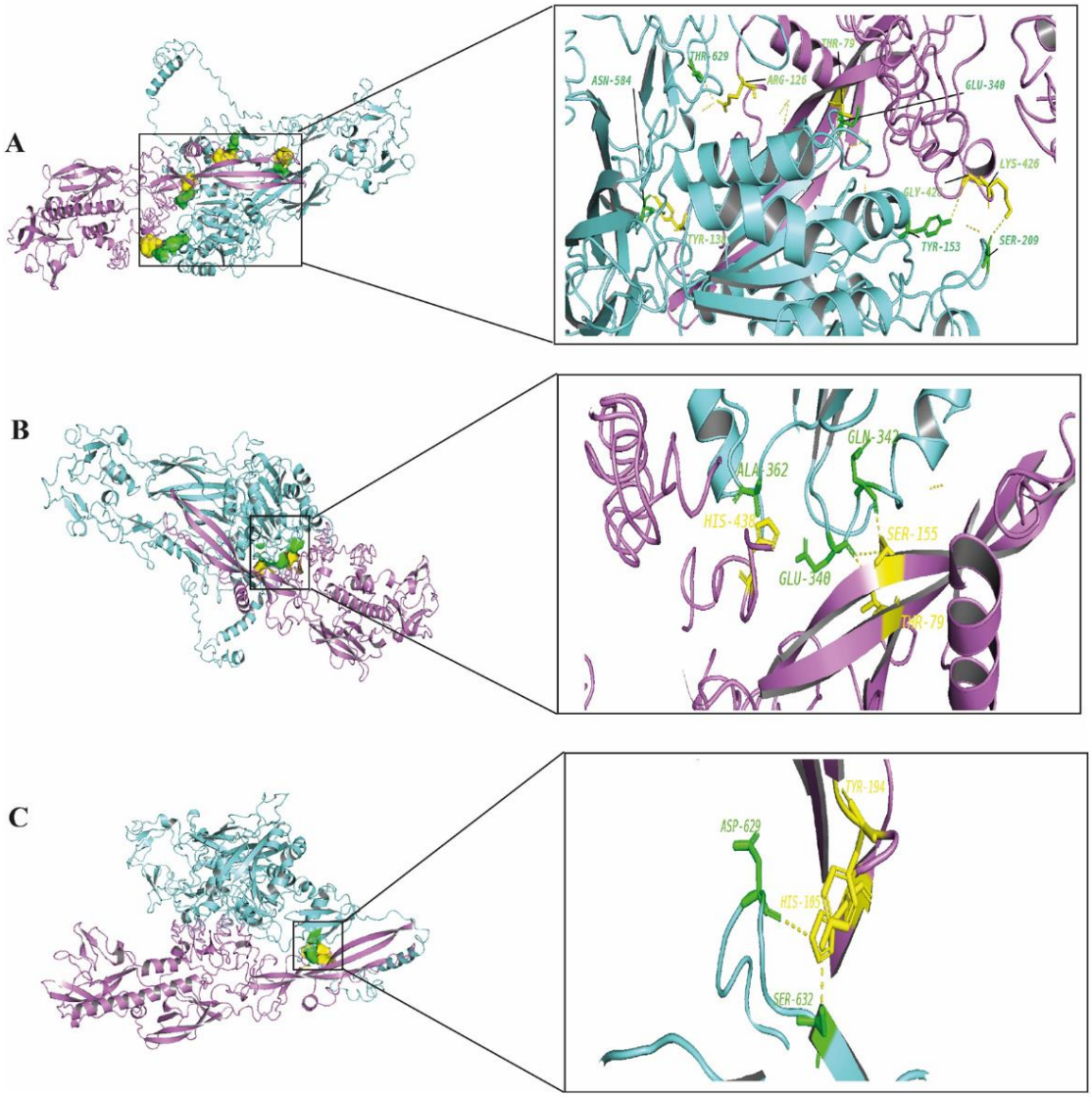

Figure 3.2. RV-G protein binding with ITGB1 in human, dog, and bats.

***(A)**. Residues involved in hydrogen bonds within the docking complex of human ITGB1 with RV-G protein, Egyptian strain (QEU57979.1). (**B).** Residues involved in hydrogen bonds within the docking complex dog ITGB1-RV-G protein, Egyptian strain (QEU57979.1). **(C).** Residues involved in hydrogen bonds within the docking complex black fruit bat ITGB1-RV-G protein, Egyptian strain (QEU57979.1). Docking complex (ITGB1-RV-G Egyptian strain); ITGB1 coloured in cyan, interacting a.a residues coloured in green, RV-G protein coloured in violet, interacting a.a residues coloured in yellow.*

3.2.3 CRD is the most conserved region in mGluR2.

The mGluR2 is structurally divided into three domains **(Figure 3.3 A).** Our sequence alignment results highlighted the sequence homology within the mGluR2 protein alignment among the distinct species **(Figure 3.3 B).** The large extracellular region which was identified as the ligand binding domain (LBD) showed the least sequence similarity among human, dog, and bats **(Figure 3.3 B).** The second domain is a highly conserved cysteine-rich domain (CRD) (a.a. 469–546) in which three different a.a. residues were mapped among human, dog, and bat. Linked to the CRD domain is a transmembrane domain composed of seven transmembrane helices (7 TMD) (a.a. 567–833). Only four residues were different in the transmembrane domain between human, dog, and bat **(Figure 3.3 B).**

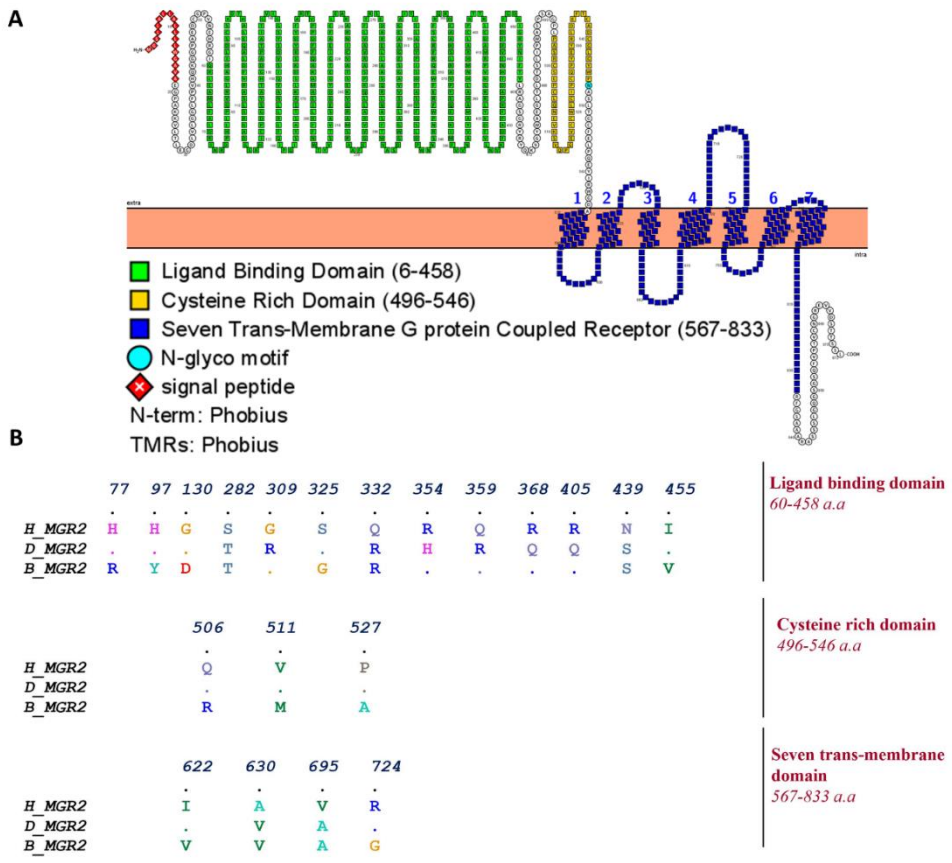

Figure 3.3 . mGluR2 domains and multiple sequence alignment

(A). *General representation of human mGluR2, highlighting different domains and most relevant features. The graphs were generated using PROTTER v1.0.* ***(B).*** *Multiple protein sequence alignment of mGluR2, highlighting the different residues in ligand-binding domain, cysteine-rich domain, and seven transmembrane domains between Human(H), Dog(D) and black fruit bat(B).*

3.2.4 The 7TM mediates the interaction of human and dog mGluR2-RV-G docking complexes.

Modelling of the interaction between mGluR2 in human and dog with RV-G protein showed that the interactions were only mediated by the hydrogen bonds in the seven-transmembrane domain of mGluR2 **(Figures 3.4 A-B).** Intriguingly, 10 hydrogen bonds were at the interface between the ligand-binding domain of mGluR2 from black fruit bat and the RV-G protein **(Figure 3.4 C),** along with formation of four salt bridges between Lys24, Arg107, and His129 in black fruit bat mGluR2 and Glu430, Asp427, and Asp420 in the RV-G protein. Interestingly, the G protein ectodomain, transmembrane, and cytoplasmic domains all play a role in interactions of G protein with mGluR2 in different hosts **(Figures 3.4 A–C).**

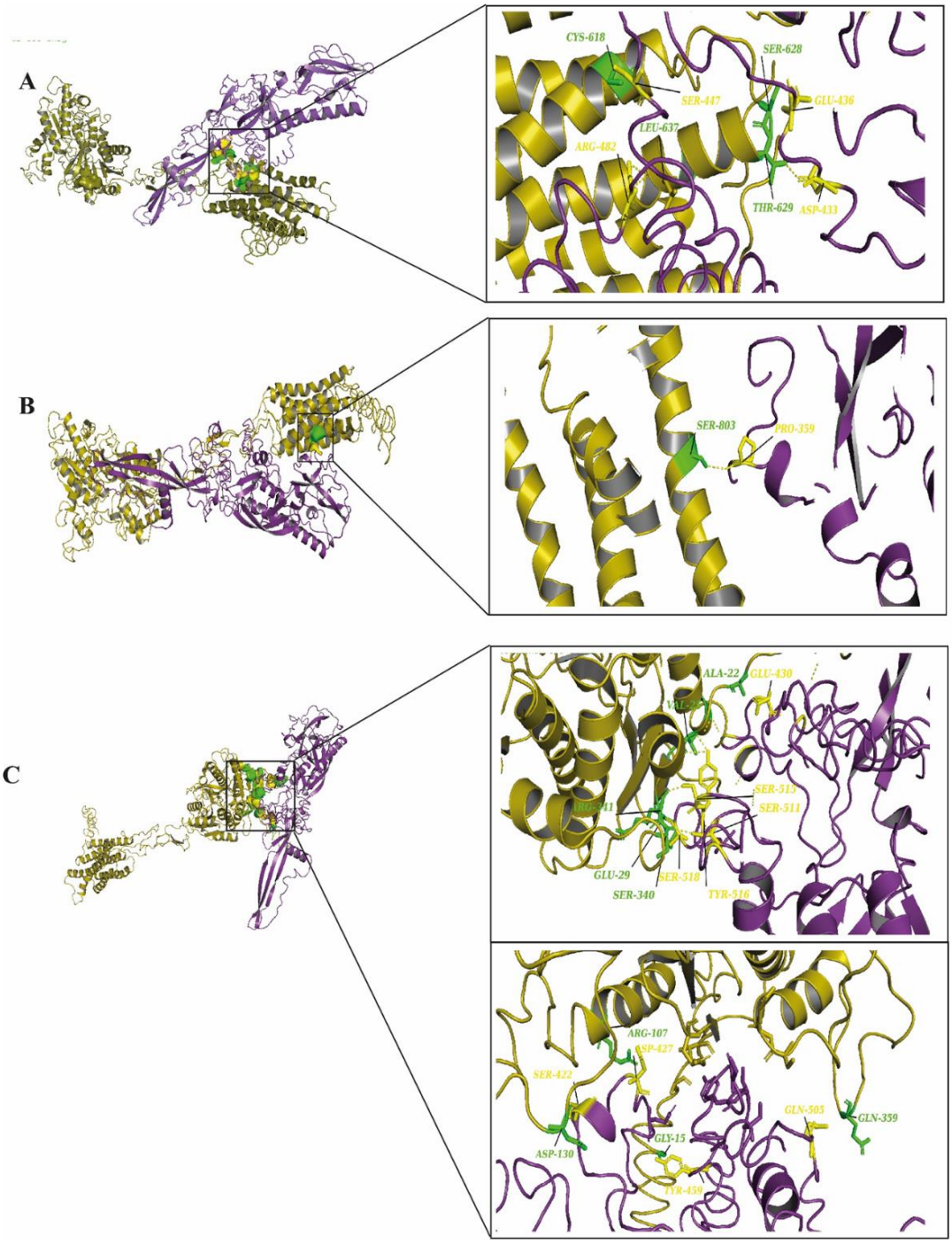

Figure 3.4 RV-G protein binding with mGluR2 in human, dog, and bats

(A). *Residues involved in hydrogen bonds within the docking complex human mGluR2-RV-G protein, Egyptian strain (QEU57979.1).* ***(B).*** *Residues involved in hydrogen bonds within the docking complex dog mGluR2-RV-G protein, Egyptian strain (QEU57979.1).* ***(C).*** *Residues involved in hydrogen bonds within the docking complex black fruit bat mGluR2-RV-G protein, Egyptian strain (QEU57979.1). Docking complex (mGluR2-RV-G protein, Egyptian strain); mGluR2 coloured in golden yellow, interacting a.a residues coloured in green, RV-G protein coloured in violet, interacting a.a residues coloured in yellow.*

3.2.5 Conserved interaction site of nAChR

The analysis of the structural organization of the nicotinic acetyl-choline receptor nAChR **(Figure 3.5 A)** demonstrated a large conserved extracellular domain (a.a. 22–256). Previously the nAChR interaction site with RV-G has been mapped to be in the region encompassing the173 and 204 a.a in the large extracellular domain (Lafon, 2005). Comparative sequence analysis in this region revealed its high conservation among dog and bats compared to the difference in four a.a. residues in the human nAChR interaction site **(Figure 3.5 B).** The existence of four transmembrane regions named neurotransmitter gated ion channel (a.a. 263–468) has been identified which was followed by a cytoplasmic loop in the distal part (Albuquerque et al., 2009).

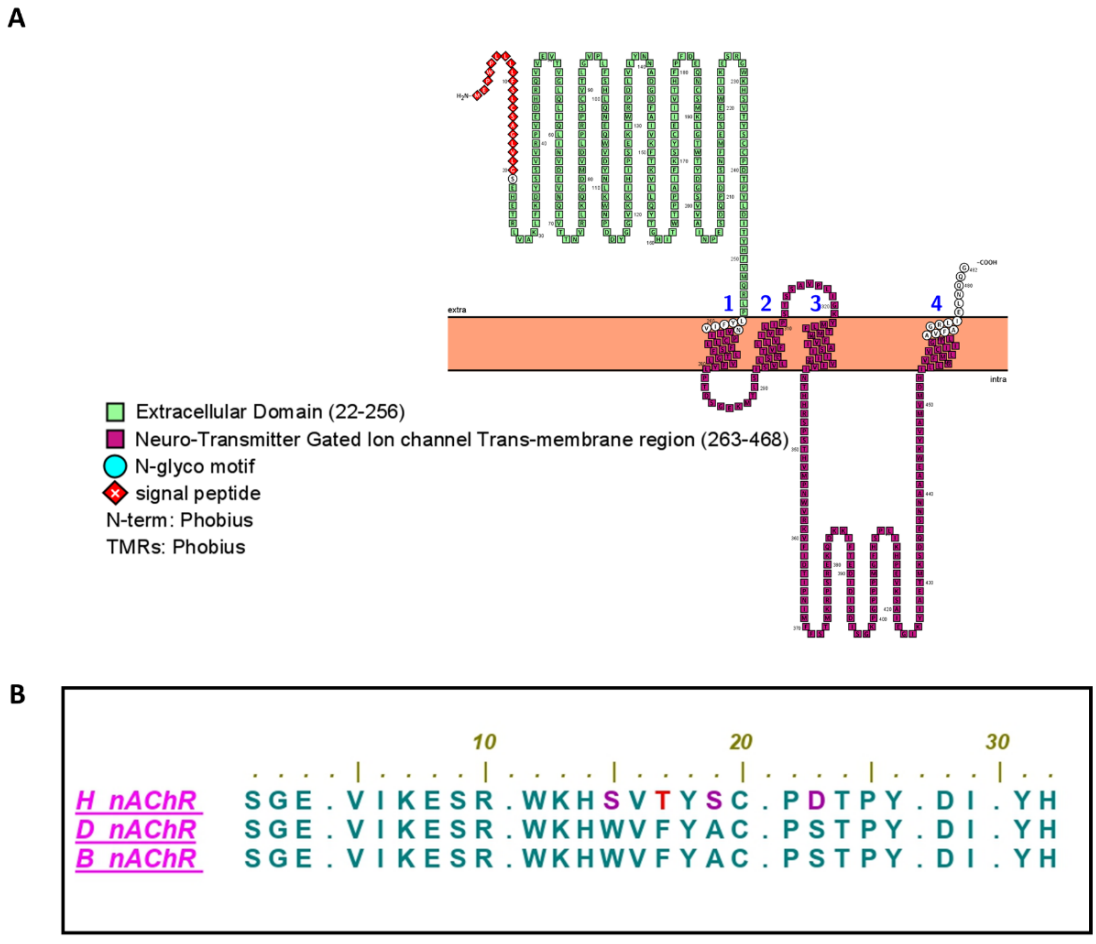

Figure 3.5 . nAChR domains and multiple sequence alignment.

(A). *General representation of human nAChR, highlighting different domains and most relevant features. The graphs were generated using PROTTER v1.0.* ***(B).*** *Multiple protein sequence alignment of nAChR, highlighting the nAChR interaction site with RV-G among human(H), dog(D), and black fruit bat (B).*

3.2.6 nAChR extracellular domain can mediate the interaction with the RV-G Ectodomain in human and bat.

The results obtained from the analysis of the human and bat nAChR -RV-G docking complex, showed that the extracellular domain of nAChR interacted with the RV-G ectodomain forming three hydrogen bonds **(Figures 3.6 A-B).** Surprisingly, the docking complex with dog nAChR showed neither hydrogen bonds nor any salt bridges with the RV-G protein which needs further investigation.

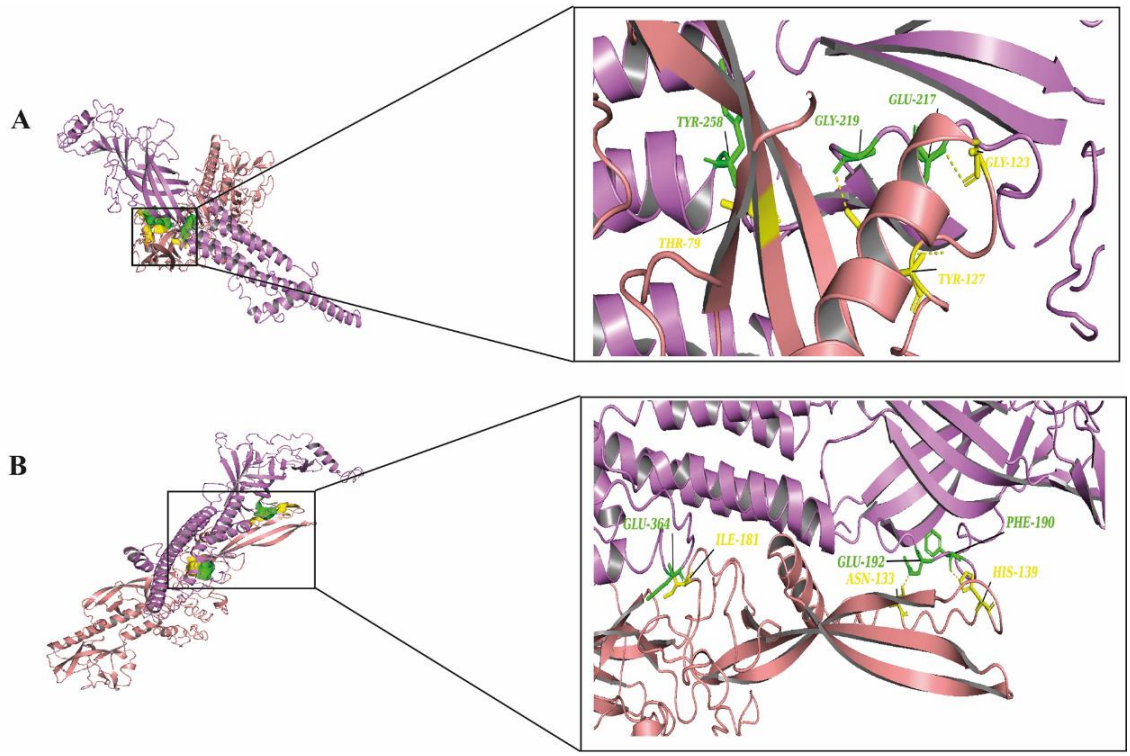

Figure 3.6 . RV-G protein binding with nAChR human and bats.

(A). *Residues involved in hydrogen bonds within the docking complex human nAChR-RV-G Egyptian strain (QEU57979.1).* (***B***). *Residues involved in hydrogen bonds within the docking complex black fruit bat nAChR RV-G Egyptian strain (QEU57979.1). Docking complex (nAChR-RV-G Egyptian strain); nAChR coloured in magenta, interacting a.a residues coloured in green, RV-G protein coloured in salmon, interacting a.a residues coloured in yellow.*

3.2.7 The Fibronectin III domain is highly variable in bat NCAM.

The neural cell adhesion molecule (NCAM) domain architecture is divided into an extracellular region, consists of five N-terminal Ig-like domains and two fibronectin type III domains. The analysis of the sequence alignment among human, dog and bats showed, that the first immunoglobulin domain and second and third immunoglobulin I-set domains were the most conserved regions **(Figure 3.7 B).** On the other hand, the first immunoglobulin I-set domain showed the most variable region among the three species where eight and ten a.a. residues differ in bat and dog, respectively, compared with human. The bat NCAM sequence showed the highest variability in its fibronectin type III domain in which 26 residues were variable, while only one residue differed in dog with respect to human **(Figure 3.7 B).**

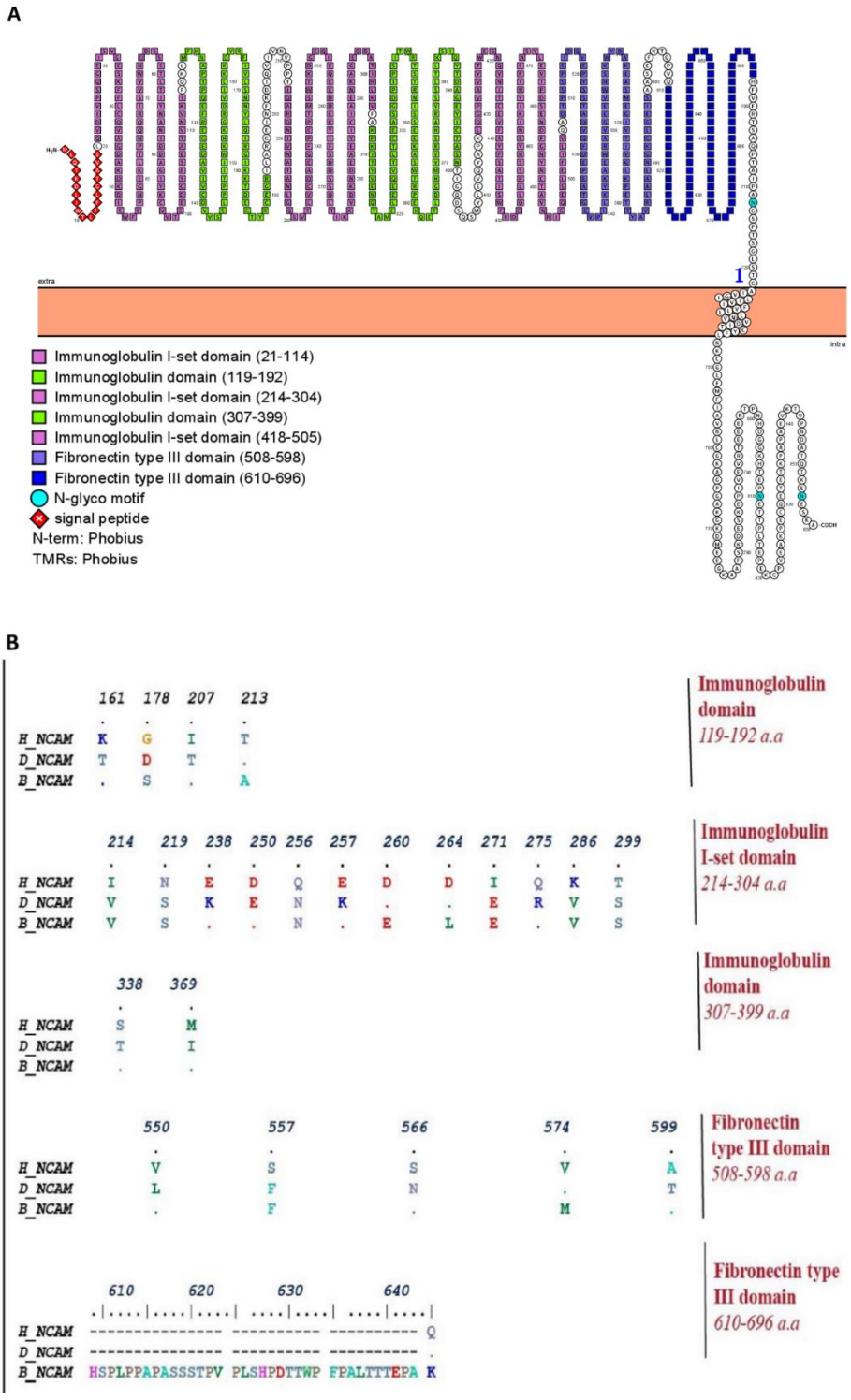

Figure 3.7 NCAM domains and multiple sequence alignment.

***(A)**. General representation of human NCAM highlighting different domains and most relevant features. The graphs were generated using PROTTER v1.0. **(B).** Multiple protein sequence alignment of NCAM, highlighting the different residues in immunoglobulin and fibronectin domains between human(H), dog(D), and black fruit bat (B).*

3.2.8 Involvement of Ig-like domain and Fibronectin III like domain in NCAM interaction to RV-G

The interaction pattern of the human NCAM and dog NCAM with the RV-G docking complex showed the involvement of the Ig-like domain in the binding interface. Two hydrogen bonds were mapped to the interaction between human NCAM and RV-G in the docking complex **(Figure 3.8 A).** A salt bridge was observed between residues Arg177 in human NCAM and Asp429 within the RV-G protein. Compared to the human NCAM-RV-G docking complex, modelling of the dog NCAM-RV-G docking complex demonstrated the formation of nine hydrogen bonds in the Ig-like domain **(Figure 3.8 B)**. **The** bat NCAM-RV-G docking interface displayed hydrogen bonds in both the Ig-like domain and Fibronectin III domains with the RV-G **(Figure 3.8 C)**. The RV-G ectodomain was the interacting part with human and dog NCAM, while both the RV-G ectodomain and cytoplasmic domains formed the hydrogen bonds with the bat NCAM.

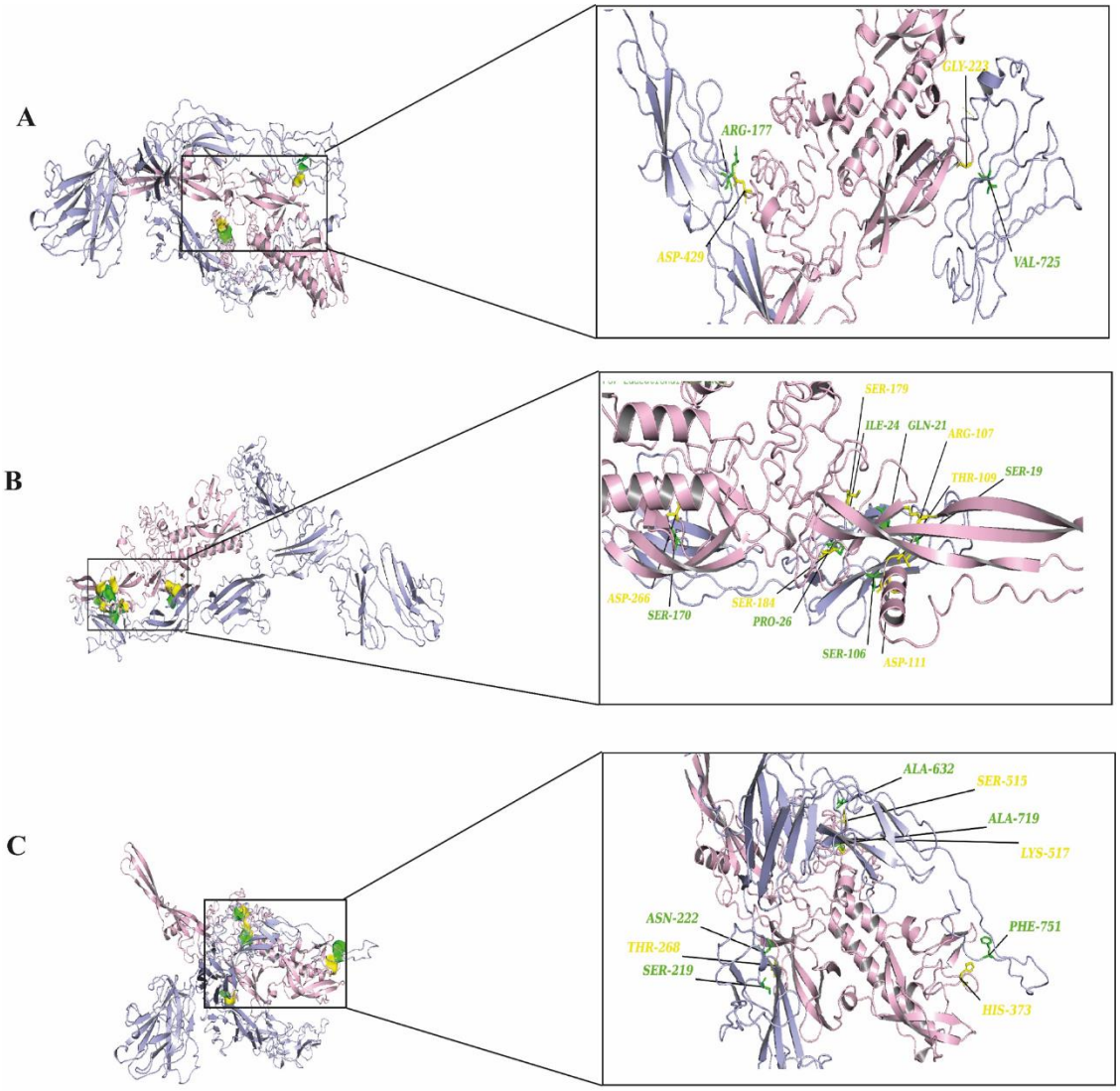

Figure 3.8 RV-G protein binding with NCAM human, dogs, and bats

(A). *Residues involved in hydrogen bonds within the docking complex human NCAM-RV-G Egyptian strain (QEU57979.1). (**B**). Residues involved in hydrogen bonds within the docking complex dog NCAM-RV-G Egyptian strain (QEU57979.1). (C) Residues involved in hydrogen bonds within the docking complex black fruit bat NCAM-RV-G Egyptian strain (QEU57979.1). Docking complex (NCAM-RV-G Egyptian strain); mGluR2 coloured in light blue, interacting a.a residues coloured in green, RV-G protein coloured in light pink, interacting a.a residues coloured in yellow.*

3.2.9 Expression and localization of *P. alecto* RV receptors on HEK293 cells

Given the role of bats in maintaining and transmitting the RV, we codon-optimized, fused with FLAG-tag at C-terminus and subcloned full-length ORF of ITG1B1 (XM_006903843.3), mGluR2(XM_006909150.1), nAChR (XM_006921218), NCAM (XM_006912806), and p75 (XM_006924778.1), of *P.alecto* in pCAGG plasmids with FLAG tag. To investigate the localization of *P.alecto* RV receptors in HEK293 cells, the constructed plasmids were used to transfect HEK293 cells. Using anti-FLAG as the primary antibody, an immunofluorescence assay was carried out to compare the cellular localization of receptors at 24 h post-transfection. As anticipated, ITGB1, mGluR2, nAChR, NCAM and p75 receptors showed perinuclear localization **(Figure 3.9 A).**

To further verify the expression of the *P.alecto* receptors, HEK293 cells were transfected with the plasmids encoding *P.alecto* receptors, 36 h post transfection, cell lysates were collected for testing the expression. HEK293 cell lysates were analysed with western blot analysis labelled with anti-FLAG antibodies. Our results showed the successful expression of the *P. alecto* cellular receptors at expected sizes as follows: ITGB1 (app. size 88 kDa), mGluR2 (app. size 180-200 kDa), NCAM (app. size 120 kDa), nAChR (app. size 45 kDa) and p75NTR (app. size 60-75 kDa) cellular receptors. To ensure uniform loading of samples, western blot analysis has been conducted against alpha-tubulin which revealed similar band intensities of tested plasmid proteins **(Figure 3.9 B).**

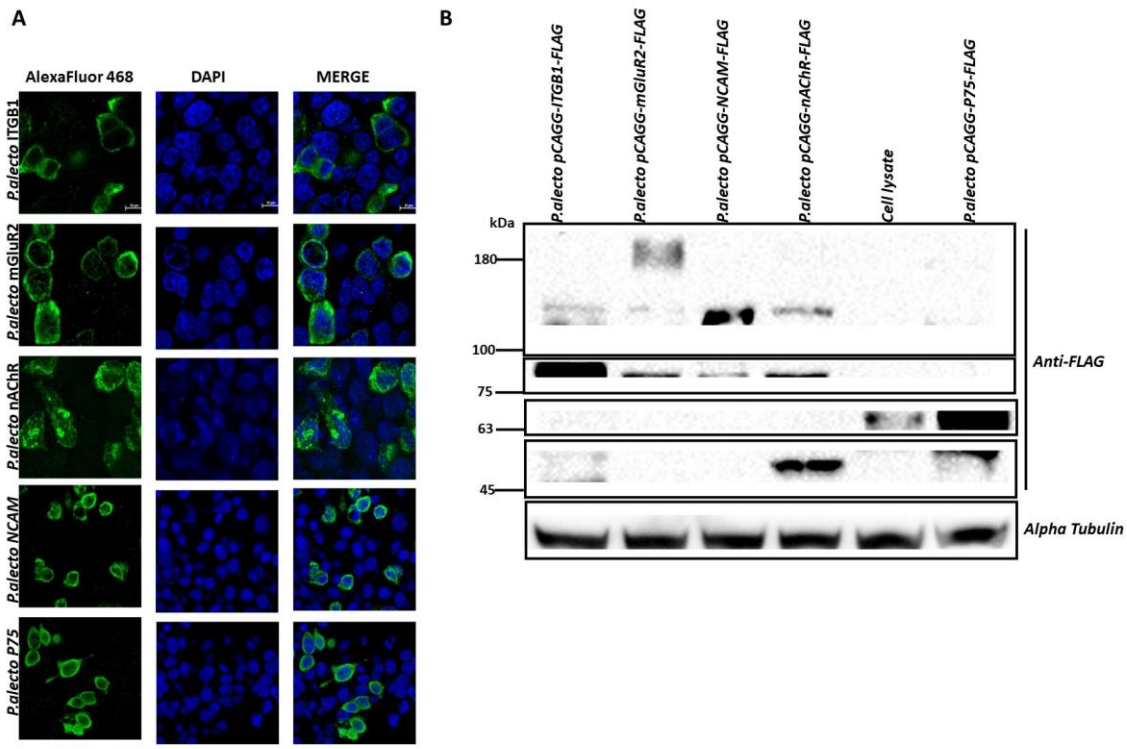

Figure 3.9 The P.alecto genes are functional receptors for RV.

***(A)**. Localization of the P.alecto receptors. HEK cells were transfected with plasmids encoding ITGB1-FLAG, mGluR2-FLAG; nAChR-FLAG; NCAM-FLAG and p75 for 24 h, After 24 hpi, cells were fixed and stained with Anti-FLAG antibody and FITC conjugated secondary antibody (Green). Cell nuclei were stained by DAPI (Blue). Fluorescence signals were visualized by confocal immunofluorescence microscopy. Scale bars are 20 µm. Images were analysed using the ZenCore 3.4 software. **(B).** Western Blot analysis of P.alecto receptors. HEK293 were transiently transfected with P.alecto receptor plasmids. Thirty-six hours post-transfection, cells were lysed, and total proteins were extracted. The cell lysates were then subjected to SDS-PAGE and Western blot analysis. The FLAG-tagged cellular proteins: pCAGG P.alecto ITGB1 (expected size: 88 kDa), pCAGG P.alecto mGluR2 (expected size 190 kDa), pCAGG P.alecto nAChR (expected size 45 kDa) pCAGG P.alecto NCAM (expected size 120 kDa) and pCAGG P.alecto p75 NTR (expected size 60-75 kDa) were detected using Rabbit Anti-FLAG as primary antibody and Goat anti-Rabbit HRP as secondary antibody. The experiments were performed two times independently (n=2). The uncropped images of the blot are shown in Chapter 9, Supplementary Figure 5.*

3.3 Discussion

The RV glycoprotein is classified as transmembrane III fusion protein, which mediates the binding to wide range of receptor (Jackson, 2013). Since it is proposed that virus adaptation from a reservoir to new species could occur if the potential host show high sequence similarity in the receptor proteins, which could enable the virus to cross the

species barrier (Cho and Seok, 2020). From this perspective, to gain more understanding of the wide host range of RV we compared the amino acid sequences of the RV cellular receptors in humans, dog, and black fruit bats. Interestingly, our comparative genomic analysis has shown that the integrin plexin domain and signal peptide are absent from the ITGB1 black fruit bat sequence. Signal peptides have a key role in protein sorting and localization and its absence is a matter of interest and requires further investigation. Thus, the absence of an N-terminal signal peptide among orthologous proteins might be linked to the absence of the integrin plexin domain (N-terminal domain) in ITGB1 from black fruit bats in comparison with ITGB1 in other species (Honigschmid et al., 2018).

For cellular entry, RV to binds to the nAChR in the region from 173-204 a.a (Lentz, 1990; Sajjanar et al., 2016). The high sequence conservation of the interaction site in nAChR among the dog and bats, suggests that changes in RV infectivity across species is unlikely due to the structural differences in nAChR.

On the molecular level, molecular modelling and mapping the protein interactions through docking can improve our understanding of the interactions occurring *in vivo*, though with less accuracy (Tovchigrechko et al., 2002). In the current study, we analysed the protein-protein interactions between the RV-G protein and ITGB1 in different species. Consistent with previous studies, mapping the RV-G ITGB1 interaction site that the interaction site between ITGB1 and RV-G protein within residues 1–728 a.a (ITGB1 ectodomain) (Shuai et al., 2020).

The interaction site of mGluR2 with the RV-G has not been identified yet. Our analysis for the docking results showed the involvement of different domains upon interacting with the RV-G. The transmembrane domain specifically in humans and dogs mGluR2 interacted with RV-G. In contrast, in black fruit bat mGluR2, the hydrogen bond with RV-G protein was in the ligand binding domain. This could be explained as despite the sequence similarity shared by proteins, divergent functions and interactions are commonly observed (Theobald and Wuttke, 2007) .

Our results showed different interacting residues between nAChR -RV-G docking complex than the previously identified interaction site. However, the interacting

residues within the same domain. This highlights the importance of future *in vitro* and studies to gain further molecular mechanistic insights.

The interaction site of NCAM with the RV-G protein has not been determined in previous studies. Our results demonstrated that hydrogen bonds bonded within immunoglobulin-like domains and fibronectin III-like domain which may define the interaction between the virus and cell receptor. Our focus in hydrogen bond mapping within interaction complexes was primarily due to their known roles in improving the stability of the interacting protein complexes (Nilofer et al., 2017).

All predicted protein-protein interactions in the current study were performed with Gramm-X software which is based on rigid body docking utilizing the Fast Fourier transform (FFT) algorithm (Tovchigrechko and Vakser, 2006b). The FFT algorithm relies on shape complementarity for the determination of the best surface match between molecules (Honigschmid et al., 2018). Implying this method has clear limitations represented in the possibility of large movements during binding which might result in weak binding and reduced accuracy (Pons et al., 2010). In addition, the possibility of large movements during binding which may result in transient or weak binding Moreover, the reliability of docking on structural models of proteins generated by computational analysis renders them more prone to errors (Szilagyi and Zhang, 2014). Besides the mentioned limitations, Gramm-X software does not allow for the selection of specific glycosylation sites in modulating the interactions between RV-G and receptors. Thus, the stability of the generated docking complex might have been affected. Since, anticipating the glycosylated sites might have resulted in higher free energy which is known to affect the stability of the docking complex (Shental-Bechor and Levy, 2008).

RV has the potential to be transmitted and maintained in several bat species that belong to microbats. In the current study, we attempted to explore the possibility that the RV receptors of other bat reservoirs belonging to the megabats as black fruit bats *(P. alecto*) could be studied. Analysis of the *in silico* identified that *P.alecto* RV receptors sequences showed their expression in cellular membranes.

However, further functional and receptor preference analysis are still required. This will require establishing a reverse genetics system encoding the RV-G protein, besides

comparative receptor preference studies in human and dogs. This will allow the understanding of the preference and mutual importance of each of these receptors for the entry mechanisms of RV.

4 Chapter 4 Development of Rabies Virus Entry Model for Functional analysis of RV-G

4.1 Introduction

4.1.1 Recovery of rVSV from Plasmids

Viruses initiate the entry into the host cellular compartments through the attachment with the cellular receptors which mediate viral entry. Some viruses rely on a sole receptor for host cell entry, while other viruses utilize multiple receptors for complete entry (Tani et al., 2012).

RV encodes the G protein which mediates viral entry through binding to multiple cellular receptors (Lafon, 2005; Wang et al., 2023). More understanding of the receptor mediated preference by RV-G is required for future development of entry inhibitors. Owing to the neurotropism nature of the RV surface glycoprotein (Morimoto et al., 2000), a reliable cell culture model is required to facilitate the understanding of the RV-G receptor preference.

In this chapter, we describe the production of a reverse genetics system based on the generation of vesicular stomatitis virus (VSV) in which the VSV (G) gene is replaced by a reporter gene, green fluorescent protein (GFP) together with the heterologous RV-G gene. This will allow studying the role of the RV-G in RV entry and its interaction with the cellular receptors.

Similar to the RV, the VSV is a non-segmented, negative strand RNA virus which belongs to the family *Rhabdoviridae*. The VSV possess 11-kb genome which encodes five structural genes: nucleoprotein (N) phosphoprotein (P) matrix (M) glycoprotein (G) and large polymerase (L). VSV has shown an efficient system for generating VSV recombinants with heterologous genes since it is capable of stably maintaining and expressing additional genes throughout several passages (Schnell et al., 1996; Wertz et al., 2002; Hastie et al., 2013).

This system is based on the recovery of the pVSV-dG-GFP using reverse genetics system **(Figure 4.1 A).** Prior to the rescue process, the antigenomic cDNA was manipulated to generate the desired modification. In the current study, we inserted the full-length open reading frame (ORF) of the RV-G, derived from the Egyptian strain isolate (GenBank accession number MK760770.1). The RV-G was inserted into the multiple cloning sites

of pVSV-dG-GFP between the matrix (M) and the GFP genes that include *MluI* and *NheI* restriction sites.

Consecutively, the recovery of the rVSV involved the co-transfection of the full length antigenomic viral RNA of the VSV (pVSV-dG-RV-G-GFP) along with the plasmids encoding the viral ribonucleoprotein complex (RNP). The RNP is formed by the phosphoprotein (P), large polymerase (L) along with the nucleoprotein (N). Upon co-transfecting the RNP complex along with the antigenome viral RNA, the RNA is transcribed, and translation of encoded proteins occurs allowing the assembly of nucleoprotein around the antigenomic RNA and polymerase to replicate forming RNP containing the genomic RNA. The assembly of the infectious virus occurs following the transcription of the mRNA from the genomic RNP and its translation (Roberts and Rose, 1998; Munis et al., 2020) **(Figure 4.1 B).**

The M protein required for assembly and budding was not provided *in trans* as it is produced from the virally encoded M gene released from the generated infectious viral particles (Lawson et al., 1995; Perez et al., 2007). Since all the DNA constructs are under the control of the T7 RNA polymerase promoter, the recombinant fowl pox virus (rFPV) was utilised to infect cells as a source of T7 polymerase *in trans*. The efficiency of T7 infection was assessed by transfecting the BHK-21 cells with pCITE GFP plasmid, which encodes GFP under the control of T7 promotor (Lawson et al., 1995). The rVSV can be easily propagated on BHK-21 cell, generating high virus titres (Abdelmmageed and Ferran, 2020).

4.1.2 Implications of reverse genetics

Previous study demonstrated the successful generation of rVSV incorporating the RV-G protein. This allowed the utilization of the generated recombinant virus as a retrograde transsynaptic tracer, for tracing the neuronal connections and studying the structure and function of the nervous system (Beier et al., 2013). However, no previous studies have utilised the generated rVSV encoding the RV-G protein for studying the RV tropism and its mediated cell entry in human, dog, and bat cell lines.

Reverse genetic manipulation technology has been extensively employed for studying the phenotypic effects of viral structural genes and for vaccine production. Notably, the

development of a SARS vaccine based on VSV expressing the SARS CoV spike protein has served as a potent vaccine(Kapadia et al., 2008). Furthermore, significant implications were demonstrated with the approval of the rVSV-dG-ZEBOV-GP vaccine, which has reduced infection risk associated with the Ebola virus. This vaccine represents the first approved vaccine in African countries that utilizes the VSV system specifically designed for EBOV (Tell et al., 2020).

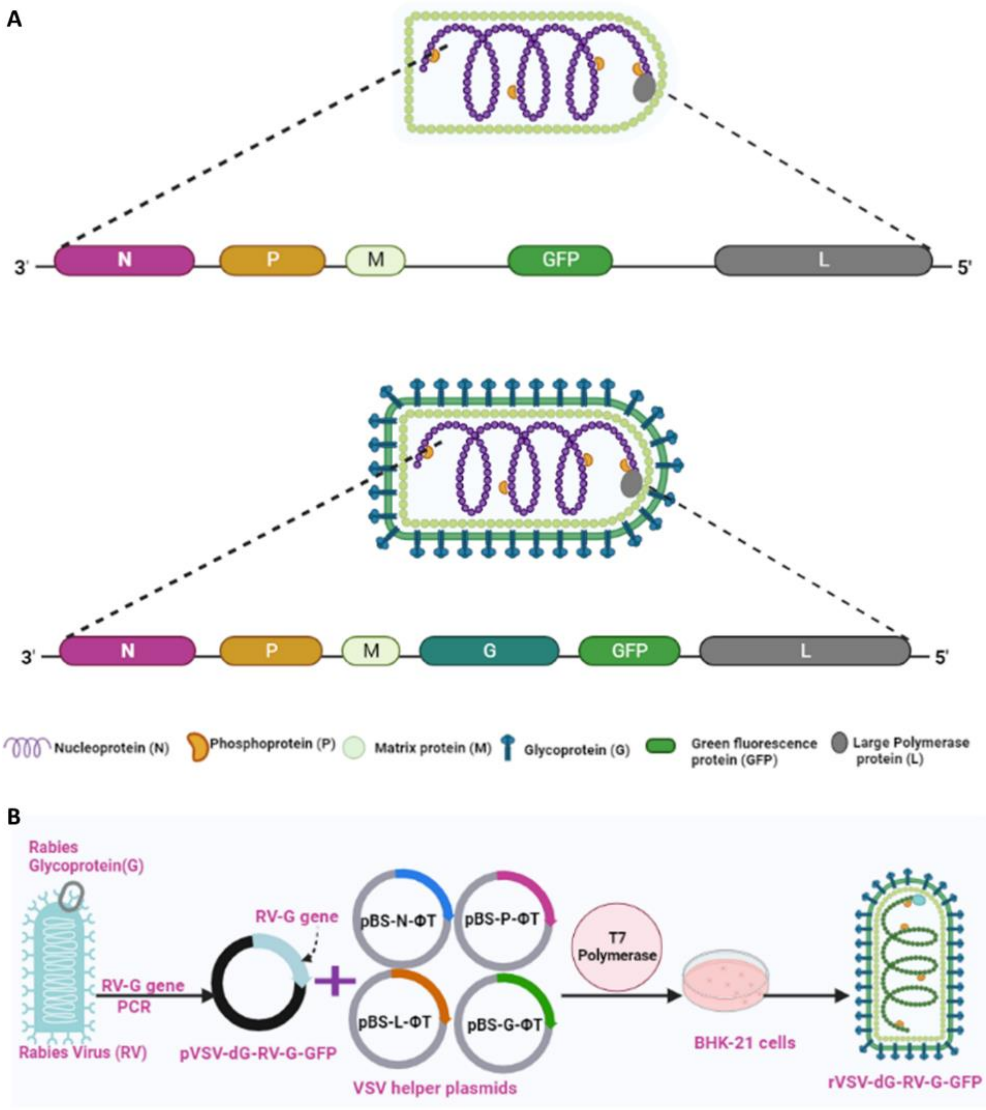

Figure 4.1. Schematic diagrams demonstrating the rVSV plasmids and generation process of rVSV-dG-RV-G-GFP from the pVSV-dG-RV-G-GFP.

(A) *Schematic diagram of the genomic organization of the pVSV-dG-GFP (top diagram) and rVSV-dG-RV-G-GFP (bottom diagram). Abbreviations: N; nucleoprotein, P; phosphoprotein, M; matrix, G; glycoprotein, GFP, green fluorescent protein, L large polymerase****. (B).*** *Schematic representation of the generation process of rVSV-dG-RV-G-GFP. Cloning of the RV-G gene from pCAGG RV-G-GHA plasmid into the pVSV-dG-GFP plasmid. BHK-21 cells were infected with rFPV-T7, followed by co transfection with pVSV-dG-RV-G-*

GFP, and VSV-system helper plasmids: pBS-N-ΦT, pBS-P-ΦT, pBS-L-ΦT and pBS-G-ΦT, resulted in generation of the rVSV-dG-RV-G-GFP.

4.1.3 Aims

In this chapter, we aim to generate a recombinant VSV expressing the RV-G protein instead of the VSV-G along with the GFP. Upon characterization of the replication competent virus, we will investigate the potential utilisation of the rVSV-dG-RV-G-GFP in the functional analysis of the RV-G for receptor binding through the following objectives:

1. To incorporate the RV-G gene into pVSV-dG-GFP expression vector using the standard cloning method.
2. To rescue the rVSV-dG-RV-GFP from artificially manipulated cDNA genome and evaluating its replication in BHK-21 cells.
3. To verify the expression of the RV surface G protein in the rVSV-dG-RV-G-GFP and to confirm the budding of viral particles through the expression of the VSV-M protein.
4. To compare the biological properties the rVSV expressing surface G protein to the rVSV-GFP-WT through:

a) Immunological assay: Western blot and IFA assays

b) Functional assay: Replication kinetics on BHK-21 cells

c) Structural evaluation by Electron microscopy

d) Molecular evaluation by RT-PCR and Sanger sequencing analysis

4.2 Results

4.2.1 Construction of pVSV-dG-RV-G-GFP into pVSV-dG-GFP 2.6 expression vector

The pVSV-dG-GFP encodes the positive antigenomic sense RNA of VSV in which the VSV G gene was replaced with GFP. To study the receptor preference of RV and cell tropism, the full codon optimized sequence of RV-G was inserted in the multiple cloning site flanking the region between M and GFP genes in the pVSV-dG-GFP vector using two restriction sites *MluI* and *NheI* **(Figure 4.2 A)**. The 1.5 kb RV-G coding sequence was

amplified from the pCAGG-RV-G-HA plasmid **(Figure 4.2 B)** using the forward and reverse primers **(Chapter 9)**. The forward primer contains *MluI* site (underlined, italic letters) and the first 20 nucleotides of the coding region of the G gene (bold letters), nucleotides before the restriction sites represented the complementary bases to the vector sequence. The reverse primer contains the last 27 nucleotides of the G gene (bold letters) followed by *NheI* site (underlined italic letters). Upon amplification, the pVSV-dG-GFP vector and the RV-G were subjected to restriction digestion with *MluI* and *NheI* enzymes **(Figure 4.2. C- D).** A standard cloning procedure was applied, through which the RV-G gene was introduced into the pVSV-dG-GFP vector.

Consequently, the RV-G gene fragment was ligated into the linearized vector using 3:1 ratio inserts to vector, which resulted in number of colonies on LB agar plates upon transformation into DH5-alpha competent cells. Three colonies were picked and screened for validation of the insert. Colony PCR using the insert specific primers, showed successful amplification in two colonies **(Figure 4.2 E)**. Consequently, diagnostic restriction digestion using *MluI* and *NheI* enzymes was employed to the positive colonies which showed two expected bands corresponding to the vector (13.4 kb) and the insert (1.5 kb) (RV-G) confirmed the presence of the correct insert in the vector backbone **(Figure 4.2 F).**

Based on Sanger's sequence analysis utilizing forward (VSV UP) and reverse primers (VSV down) flanking the RV-G region in the pVSV-dG-GFP vector specific for the vector, clearly showed the presence of start codon ATG flanking the VSV M and GFP genes. The resulting plasmid was designated as pVSV- dG-RV-G-GFP.

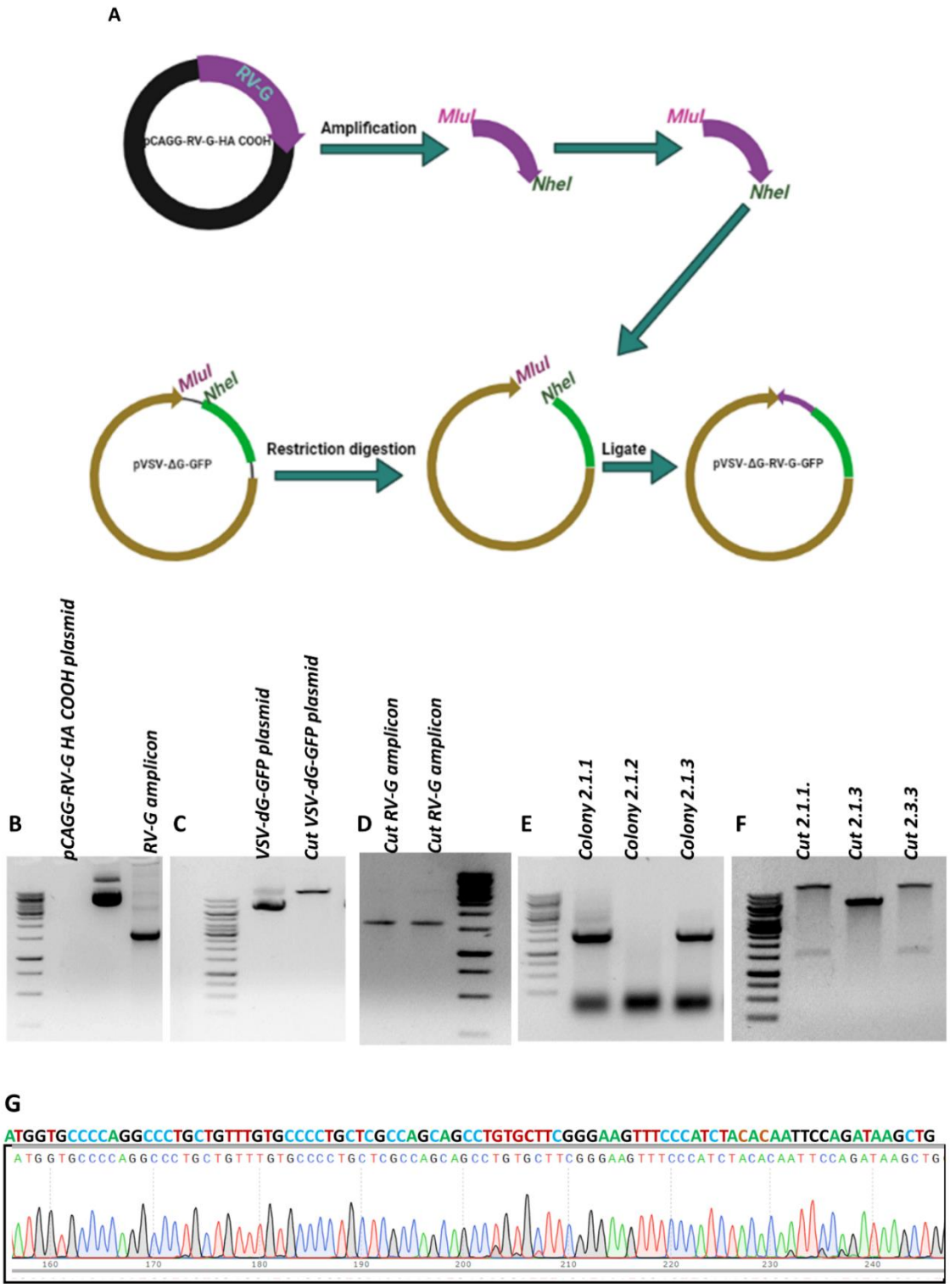

Figure 4.2. Cloning of the RV-G in to the pVSV-dG-GFP backbone

(A) *Schematic diagram representation of the of the RV-G cloning into pVSV-dG-GFP; Firstly, the RV-G was amplified from the pCAGG-RV-G-HA-COOH vector, followed by restriction digestion of the RV-G amplicon and the pVSV-dG-GFP with MluI-HF and NheI-HF restrictions enzymes. Once the ends are compatible, the digested amplicon (RV-G) was ligated into the pVSV-dG-GFP.* ***(B****). Amplification of RV-G from pCAGG RV-G HA plasmid using primers with MluI and NheI restriction sites, Agarose gel electrophoresis showing the*

pCAGG-RV-G-HA-vector (left) and the PCR product of the RV-G ~ 1.5 kb (Right) ***(C****). Restriction digestion of the pVSV-dG-GFP with MluI-HF and NheI-HF enzymes; Agarose gel showing the uncut pVSV-dG-GFP (uncut vector, ~ 13.4 kb, left side) and the linearized vector; ~ 13.4 kb, right side).* ***(D).*** *Restriction digestion of the RV-G PCR amplicon with MluI-HF and NheI-HF restriction enzymes, Agarose gel showing the linearized RV-G amplicon 1.5 kb.* ***(E).*** *Agarose gel electrophoresis of colony PCR products upon ligation and transformation****.*** *Three colonies were analysed for the presence of the 1.5 kb insert corresponding to the RV-G. Positive colonies were shown in colonies 2.1.1 and 2.1.3* ***(F).*** *Diagnostic restriction digestion to purified pVSV-dG-RV-G-GFP plasmid with MluI and NheI enzymes, to confirm the presence of the RV-G insert in the pVSV-dG-GFP backbone, the cloned plasmid from positive colonies, was purified and digested with MluI and NheI enzymes as demonstrated in agarose gel :pVSV-dG-GFP backbone. (13.4 kb) and the RV-G insert (1500 bp,) shown in the cut colonies 2.1.1 and 2.1.3****, while the colony 2.1.2 showed no insert****.*** ***(G).*** *Sanger sequencing of the amplified RV-G from the pVSV-dG-RV-G-GFP vector to confirm successful cloning and orientation of the RV-G insert in the pVSV-dG-GFP backbone.*

4.2.2 Recovery of rVSV-dG-RV-G-GFP from BHK-21 cells

The recovery of infectious virus from the pVSV-dG-RV-G-GFP required the simultaneous transfection of the pVSV-dG-RV-G-GFP which encodes the rabies surface glycoprotein and the VSV antigenomic RNA along with the N, P, L and G proteins expressed from the corresponding VSV helper plasmids as described in a previous study (Garbutt et al., 2004). The GFP in the pVSV-dG-RV-G-GFP served as the marker of infection.

The expression of VSV antigenomic cDNA and N, P, L and G helper plasmids were under the control of T7 polymerase promotor. Consequently, to ensure efficient transcription of the plasmids in the cellular cytoplasm, BHK-21 cells were primarily infected with recombinant fowl pox virus (rFPV) which encodes the T7 polymerase. To verify the function of T7 polymerase from (rFPV), a control plasmid pCITE-GFP was transfected into BHK-21 cells after infecting with rFPV. Hence, the pCITE-GFP encodes the GFP under control of the T7 promoter, the observation of GFP signal indicated the efficiency of the rFPV used as a source of T7 polymerase **(Figure 4.3 A).** To assess the transfection efficacy, pCAGG-GFP plasmid was transfected into BHK-21 cells, and the GFP was observed 3 days post transfection **(Figure 4.3 B).** Two sequential filtration steps were applied for the recovered reporter virus for the removal of the residual rFPV.

To assess the recovery of the pVSV-dG-RV-G-GFP, we compared the GFP observed from transfecting either the pVSV-dG-RV-G-GFP or pVSV-dG-GFP WT along with the VSV

helper plasmids on BHK-21 cells. Successful recovery was observed for the pVSV-dG-RV-G-GFP, evidenced by the GFP observed in transfected BHK-21 cells. However, earlier GFP signal was observed in the pVSV-dG-GFP WT (24 hours post transfection (hpt) **(Figure 4.3 C).** While in the pVSV-dG-RV-G-GFP, the GFP was observed 72 hpt.

Consequently, the supernatant containing the rVSV-dG-RV-G-GFP was collected, centrifuged, and used for further passaging on BHK-21 cells until passage 4. To determine if the recovered VSV with heterologous RV G protein could produce syncytia, the GFP signal and syncytia formation were observed 72 hours post infection (hpi) in the second passage. Notably, subsequent virus passaging resulted in increasing the GFP signal and syncytia formation which appeared 48 hpi **(Figure 4.3 E).**

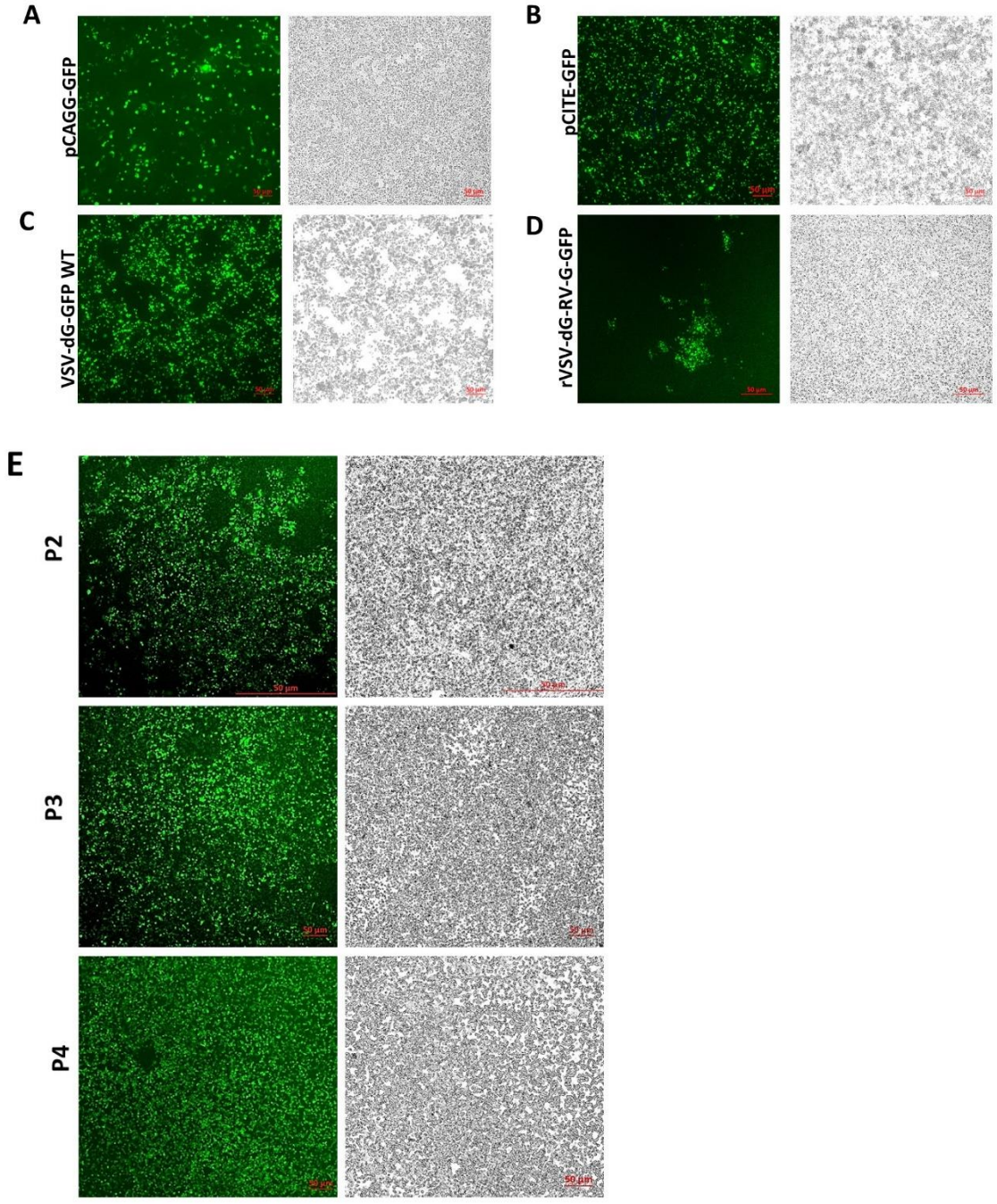

Figure 4.3 Transfection and rFPV-T7 infection efficiencies

Representative microscopic fluorescent. (left) and bright (right) fields of BHK-21 cells ***(A****). transfected with pCAGG-GFP (upper panel),* ***(B).*** *infected with rFPV-T7 and transfected with pCITE-GFP (lower panel) are illustrated as transfection controls. Constitutive GFP expression driven by pCAGGS is an indicator of transfection efficiency, whereas T7 promoter driven GFP expression by pCITE is a control for rFPV infection and T7 polymerase activity****. (C).*** *Representative microscopic fluorescent (left) and bright (right) fields of the BHK-21 cells 24 hours post transfection with the helper plasmids and pVSV-dG-GFP.* ***(D****). Representative microscopic fluorescent (left) and bright (right) of the BHK-21 cells 72 hours post transfection with the helper plasmids and rVSV-dG-RV-G-GFP (P1).* ***(E).*** *Microscopic fluorescent (left) and bright (right) of the*

BHK-21 cells cytopathic effects appeared 72 hrs following the inoculation of the BHK-21 cells with the subsequent passages of the recovered VSV-dG-RV-G-GFP. Images representing the subsequent passages of rVSV-dG-RV-G-GFP; P2, P3 and P4. Scale bars 50 µm.

4.2.3 Characterization of the recovered rVSV-dG-RV-G-GFP

4.2.3.1 Verification of the genetic stability of rVSV-dG-RV-G-GFP (Molecular Assay)

To validate the stability of the introduced RV-G in the rVSV genome, specific primers were designed, flanking the RV-G in the VSV genome. The forward primer encoded the last 20 bp of VSV M gene and reverse primer encoded the first 38 nucleotides of GFP gene **(Chapter 9, section 9.1.4), (Figure 4.4 A).** The fourth passage of the recovered viral supernatant was collected and analysed. As a control, the viral RNA of the rVSV-GFP WT was collected. The viral RNA was extracted and subsequently reverse transcribed to cDNA for verifying the stability of RV-G insert by PCR. The findings confirmed the presence of insert 1.9 kb in the cDNA of rVSV-dG-RV-G-GFP, corresponding to the RV-G, while as expected the cDNA of rVSV-dG-GFP failed to produce any product **(Figure 4.4 B).** These results suggested the stability of the RV-G insert which was intactly retained in the VSV genome during four consecutive passages. To further verify that no mutations were introduced in the RV-G coding sequence during the propagation, genomic nucleotide sequence analysis of the RV-G insert using primers specific for the VSV backbone and flanking the RV-G insert was conducted. Sequencing results showed no deletions or insertions in the RV-G gene confirming the stability and proper orientation of the introduced insert during virus propagation **(Figure 4.4 C).**

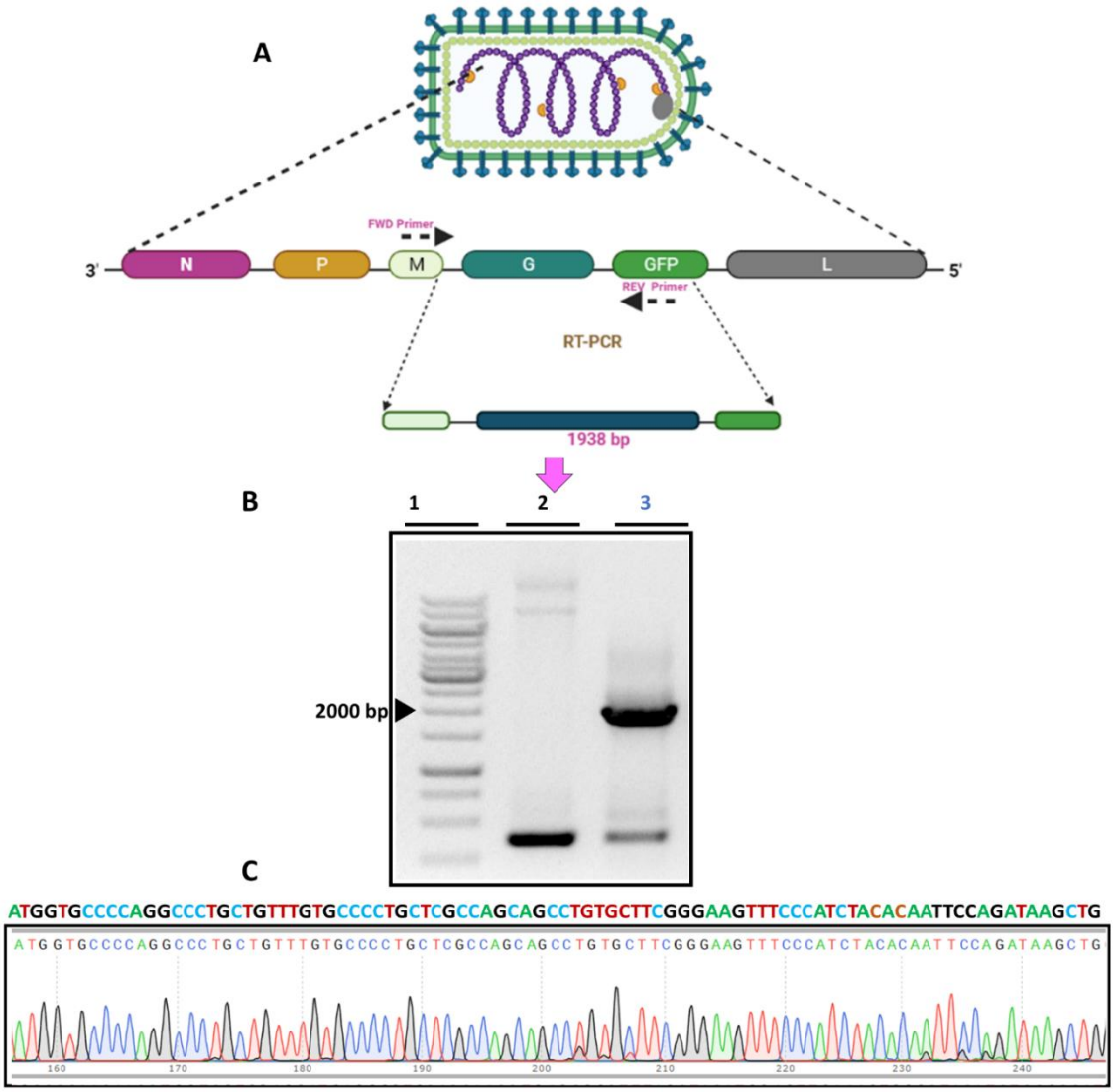

Figure 4.4 Genetic stability of RV-G insert in rVSV-dG-RV-G-GFP.

(A). *Schematic diagram representing the rVSV-dG-RV-G-GFP viral genome organization: 3'-N, P, M, G, GFP and L 5', the FWD (VSV-Up) and REV primers (VSV down) designed to target the vector DNA flanking the RV-G insert.* ***(B).*** *RT-PCR analysis of RNA extracted from rVSV. Upon the passaging of the rVSV-dG-RV-G-GFP, the viral supernatant was collected and reverse transcribed, followed by amplification with the VSV UP and VSV down primers. Agarose gel electrophoresis showing the Lane 1, DNA ladder (1 Kb); Lane 2, rVSV-GFP WT and Lane 3, rVSV-dG-RV-G-GFP (P4) RV-G insert (1.9 Kb)* ***(C).*** *Forward Sanger sequencing for RV-G amplicon, amplified from the rVSV-dG-RV-G-GFP using the VSV up primer, indicating the start codon of RV-G with no deletions or insertions in the RV-G- gene.*

4.2.3.2 Determine the expression of VSV-M and RV-G proteins (Expression Assay)

To assess the incorporation of the RV-G during replication of rVSV-dG-RV-G-GFP in infected cells, the localization and expression of VSV-M and RV-G proteins were identified upon infecting BHK-21 cells with VSV-dG-RV-G-GFP and VSV- dG-GFP WT at an

MOI of 1.0. After 24 hpi, cells were fixed with 4% PFA, followed by incubation with VSV-M and RV-G antibodies then subsequently, incubated with Alexa Fluor 468 secondary antibody. The surface distribution of the RV-G protein was only observed in rVSV-dG-RV-G-GFP infected cells which confirmed the stable insertion and surface expression of RV glycoprotein surface protein **(Figure 4.5 A)**. Since VSV budding is dictated by the M protein, the BHK-21 infected cells were stained against the VSV M monoclonal antibody (mAb) to assess the budding of rVSV. Intracellular localization of the VSV M protein was observed similarly in both protein in both rVSV-dG-RV-G-GFP and VSV-dG-GFP WT infected cells confirming efficient particle release **(Figure 4.5 A).**

Further expression of the RV-G and VSV-M proteins was analysed in the recovered VSV-dG-RV-G-GFP or VSV-GFP WT. The BHK-21 cells were infected with VSV-dG-RV-G-GFP or VSV-dG-GFP WT at an MOI of 1.0. Twenty-four hpi, lysates of infected cells were collected and then subjected to SDS-PAGE and immunoblotting. Using mAb specific for RV-G, a band migrated at 60 kDa corresponding to the RV-G protein in the cell lysates infected with rVSV-dG-RV-G-GFP but not in the rVSV-dG-GFP WT, indicating the expression and incorporation of the RV surface glycoprotein in rVSV particles **(Figure 4.5 B).**

The same lysates were incubated with mAb against VSV M protein to verify the assembly and budding of the rVSV particles from BHK-21 cell lysates. The expression of VSV M protein was assessed through incubating the membranes with VSV-M antibody. Notably, both the lysates from infected BHK-21 cells with rVSV-dG-RV-G-GFP and VSV-dG-GFP WT showed a band of approximately 25-35 kDa corresponding to VSV M protein **(Figure 4.5 B).**

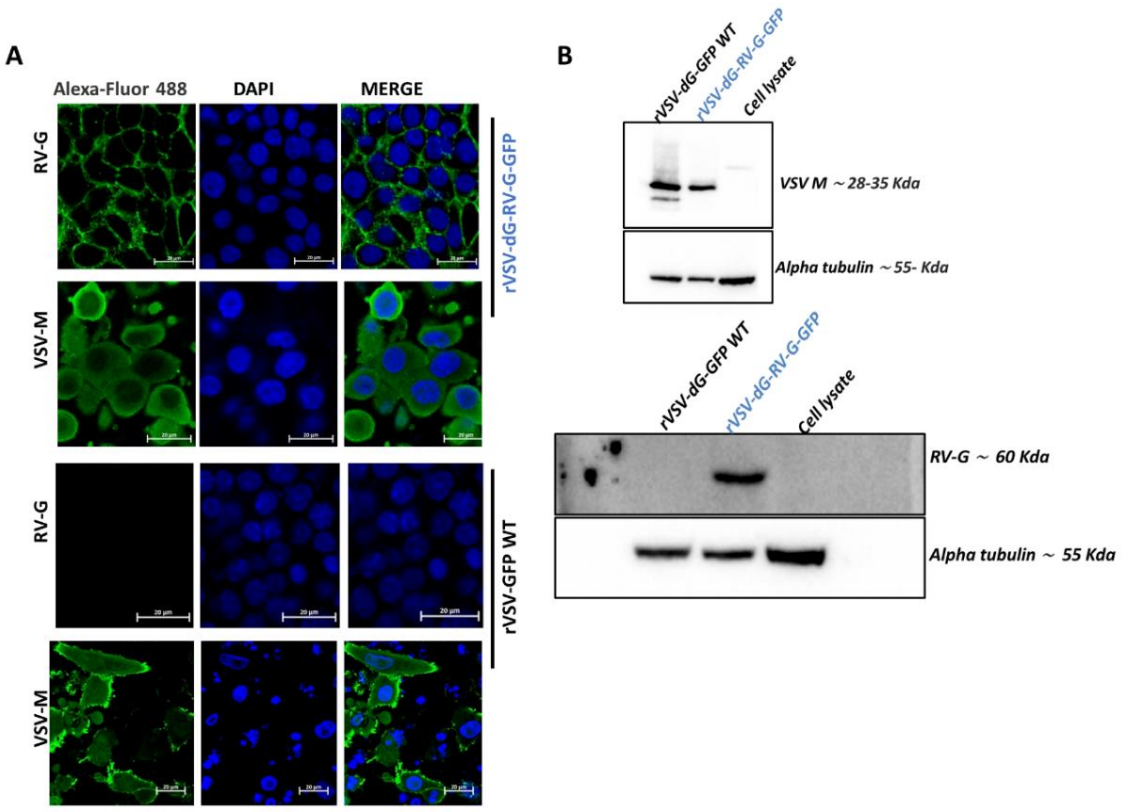

Figure 4.5 RV-G and VSV M proteins expression in BHK infected cells.

(A). *Immunofluorescence of the BHK-21 infected cells. BHK cells were infected with the rVSV-dG-RV-G-GFP and rVSV-GFP WT at MOI of 1. Twenty-four hours post infections, cells were fixed and stained with RV-G and VSV-M antibodies to detect the RV-G and VSV M proteins; respectively by immunofluorescence, followed by incubation with FITC conjugated antibodies (green), indicating the surface expression of the RV-G in rVSV-dG-RV-G-GFP infected cells and the Intracellular localization of VSV M in the rVSV-dG-RV-G-GFP and rVSV-GFP WT infected cells was indicated. Nucleus (blue) labelled with DAPI, the VSV-M and RV-G (green), Scale bars are 20 µm. Fluorescence signals were visualized by confocal immunofluorescence microscopy. Images analysed using the ZenCore 3.4 software. (**B).** Immunoblot analysis of the BHK-21 cell lysates. BHK-21 cells infected with VSV-GFP WT and rVSV-dG-RV-G-GFP at MOI =1, after 24hpi, the cell lysates were collected, and blots were stained using antibodies against VSV M (upper panel) and RV-G (lower panel) on 8% non-reducing SDS-PAGA gel. Alpha tubulin was used as a loading control. The experiments were performed two times independently (n=2). Images were analysed using Image Lab software. Images of uncropped blots are shown in Chapter 9, Supplementary figure 6.*

4.2.3.3 Electron Microscopy (Structural Analysis)

To compare the ultrastructure of recovered rVSV-dG-RV-G-GFP and VSV WT, we performed electron microscopy. The classical bullet shaped virions were observed in both VSV-dG-WT and rVSV-dG-RV-G-GFP. The VSV-dG-WT showed densely packed nucleocapsids in the interior **(Figure 4.6 A).** Notably, the rVSV-dG-RV-G-GFP showed

clear protruded spikes on the outer surface of the virion **(Figure 4.6 B),** indicating the expression of the Rabies surface glycoprotein which has remarkably differentiated the recombinant VSV than the WT with deleted G. These data confirm the successful incorporation of the RV surface glycoprotein into the VSV.

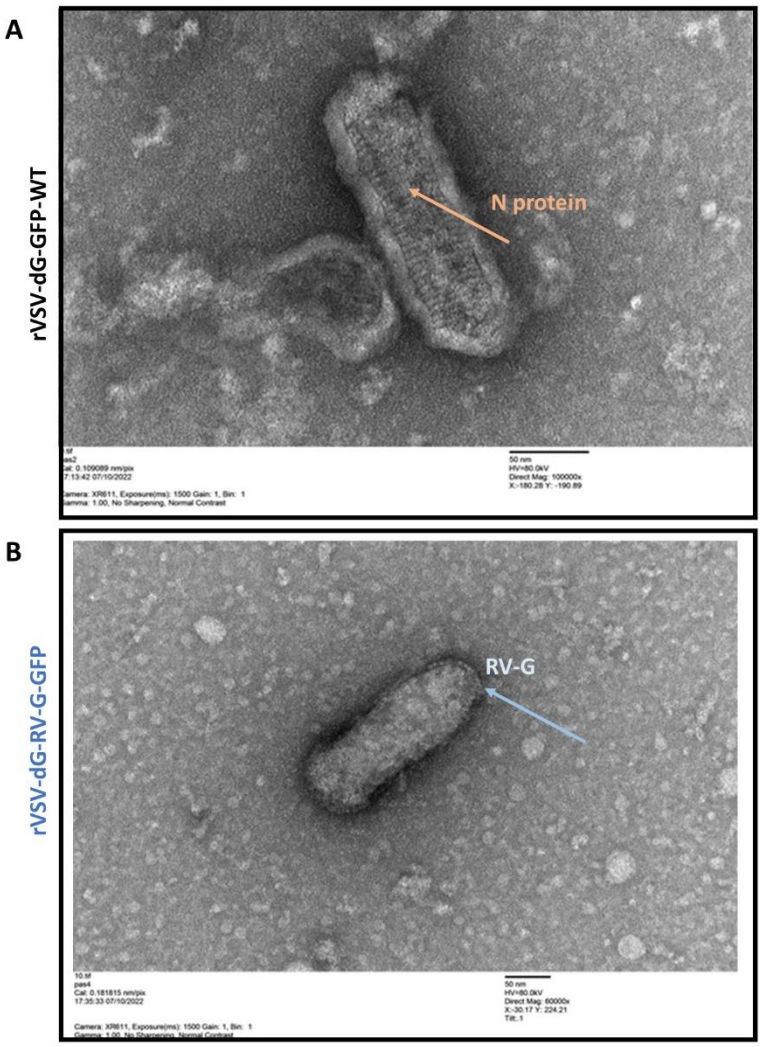

Figure 4.6 Electron microscopy of rVSV-dG-RV-G-GFP and VSV WT.

Transmission electron micrographs of rVSV-dG-GFP (top panel) compared to rVSV-dG-RV-G-GFP (bottom panel). ***(A****) Purified VSV-WT showing the helical nucleoprotein (upper panel)* ***(B)*** *Purified rVSV-dG-RV-G GFP (lower panel) showing the spike glycoprotein on the surface.*

4.2.3.4 Reduced RNA viral copies in rVSV-dG-RV-G-GFP compared to WT VSV.

To assess the growth kinetics of the generated rVSV-dG-RV-G-GFP relative to the rVSV-GFP WT, we employed the relative qPCR method in which the viral RNA copies of both rVSV-dG-RV-G-GFP and rVSV-GFP-WT were compared. The VSV N protein was targeted to quantify the genomic viral RNA, since the VSV genome RNA replication is proportional to the amount of N protein synthesized (Hanke et al., 2017). For initial assessment, the BHK-21 cells were infected with both rVSV-dG-RV-G-GFP and rVSV-GFP-WT at MOI of 1. Subsequently, a tenfold serial dilution series of the viral RNA extracted from the infected cells were plotted as a standard curve. Five different concentrations of the viral RNA were used which ranged from 1000, 100, 10, 1 and 0.1 ng/µL. BHK-21 cells were infected at MOI 1, the viral supernatants were collected in time time-dependent manner and the viral copies of the rVSV-GFP-WT and rVSV-dG-RV-G-GFP were generated based on the standard curves. The WT VSV cultures showed progeny virus at the initial stages of infection starting at 6 hpi (2.8±0.26) which were significantly higher than the viral RNA detected from rVSV-dG-RV-G-GFP viral supernatants at this time point (0.65±0.13). Followed by the gradual increase in the viral RNA in both WT and replication competent virus to reach the peak levels 24 hpi in cells infected with WT VSV (4.55±0.33) which was followed by a gradual decline in the genomic viral RNA levels. In contrast, the N-protein viral mRNA transcripts levels in rVSV-dG-RV-G-GFP peaked at 30 hpi (3.59±0.10) and plateaued afterwards (**Figure 4.7 A).**

By comparing the replication curves using a plaque assay, we observed distinct patterns in viral replication. The rVSV-GFP-WT reached its peak levels at 18 hpi with peak titres (7 x10^{10} PFU/mL), which then maintained plateau levels before a decrease in the release of virus progeny was observed at 36 hpi, reaching its lowest levels at 42 hpi. On the other hand, rVSV-dG-RV-G-FP showed the highest levels of released virus at 24 hpi (8 x10^{10} PFU/mL). Likewise, in rVSV-dG-GFP WT, a decrease in virus progeny levels was observed at 36 hpi, eventually reaching the lowest levels at 42 hpi **(Figure 4.7 B-C).** Taken together, these results suggested slower replication profiles of the rVSV-dG-RV-G-GFP compared to the VSV-WT which is presumably associated with the insertion of the RV-G gene.

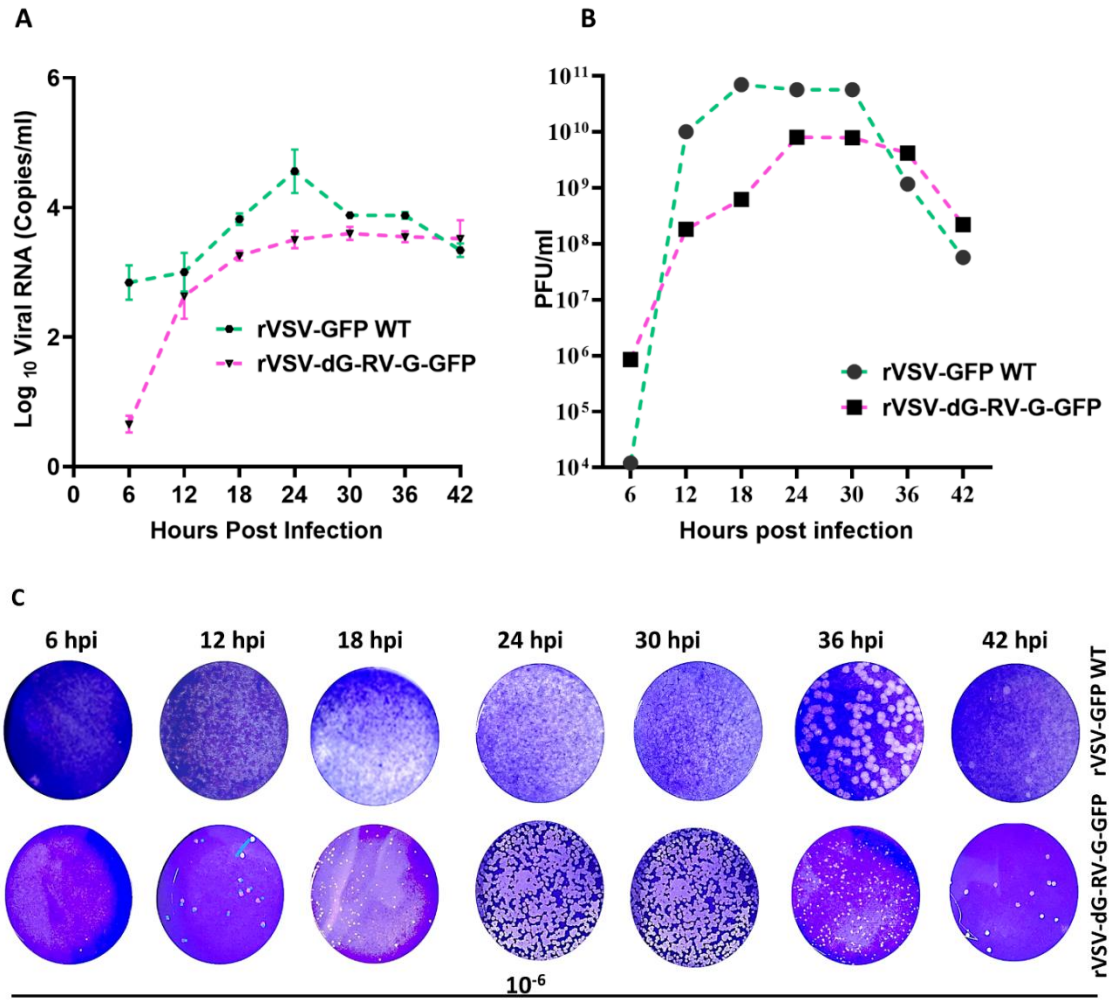

Figure 4.7 Growth kinetics of rVSV-dG-GFP and rVSV-RV-G-GFP in BHK-21 cells.

(A). *Absolute quantification of the viral RNA copies by qRT-PCR. BHK cells infected with either rVSV-dG-RV-G-GFP and rVSV-dG-GFP at MOI =1. Viral supernatants were collected at different time points: 6 hrs, 12 hrs, 18 hrs. 24 hrs, 30 hrs, 36 hrs, and 42 hrs post infection. Viral RNA was extracted and assessed for the absolute quantities of the genomic RNA by qRT-PCR targeting the VSV N gene, the data represented the mean values of three biological replicates. Error bars represent the SEM.* ***(B)*** *Plaque assay-based quantifications of the progeny virus released from the BHK-21 cells infected with either the rVSV-dG-RV-G-GFP and rVSV-dG-GFP at MOI =1., in the viral supernatants were collected in a time-dependent manner (6 hpi -42 hpi). The data represented the mean of three biological replicates and the error bars represent the SEM.* ***(C).*** *Representative plaque counts of each of the BHK-21 cells infected with either rVSV-dG-RV-G-GFP and rVSV-dG-GFP at MOI =1. The plaques shown represent rVSV-GFP WT (upper panel) and rVSV-dG-RV-G-GFP (lower panel) replication in virus dilution in a time-dependent manner The progeny viruses were quantified on BHK-21 cells and stained with 0.5% crystal violet after 72 hpi. These experiments were performed three times independently (n=3).*

4.2.3.5 Ability of rVSV to replicate in the BHK-21 cells.

Further analysis to demonstrate the replication competence of the rVSV-dG-RV-GFP compared to the rVSV-GFP WT in BHK cells were assessed by plaque assay. The collected virus was serially diluted and infected the BHK-21 cells for 2 hrs with shaking. Semi solid medium of 3% CMC was added to the plates after removal of the inoculum and cells were washed with PBS. After 72 hrs, cells were fixed and stained with 0.5% crystal violet and the formed plaques were counted. Plaque assay based viral counts showed higher viral titres in cells infected with the rVSV GFP WT virus which reached 5 x 10^{10} PFU/mL whereas the rVSV-dG-RV-GFP titres 1.4 x 10^{8} PFU/mL were 2 log and significantly lower compared to the WT virus (**Figure 4.8 A-B).** Interestingly, despite the ability of the rVSV-GFP WT and the rVSV-dG-RV-GFP to form plaques in BHK-21 cells, comparison of the size of plaques showed clearly formed significantly larger plaques by the rVSV-GFP WT compared to the rVSV-dG-RV-G-GFP **(Figure 4.8 C).**

Since the rVSV-GFP WT and the rVSV rVSV-dG-RV-GFP carry GFP as reporter gene, the quantity of the GFP positive percentage was directly correlated with the quantity of virus released in infected cells. The GFP percentage was quantified for the BHK-21 cells infected at MOI of 1.0 with the rVSV-GFP-WT and the rVSV-dG-RV-G-GFP. Twenty-four hours following the infection, the cells were incubated with live dead marker followed by permeabilization of cells prior to the flow cytometry analysis. The flow cytometry analysis showed that significantly higher GFP % observed in BHK-21 cells infected with the rVSV-GFP WT (81.4%) compared to the cells infected with the rVSV-dG-RV-G-GFP (69.4%). These findings suggests that the inserted RV-G might influence protein expression in rVSV-dG-RV-GFP. The non-infected cell BHK-21 cell control was used along which showed no GFP **(Figure 4.8 D).** Overall, the rVSV-GFP-WT showed enhanced replication in BHK-21 cells than the rVSV-dG-RV-GFP.

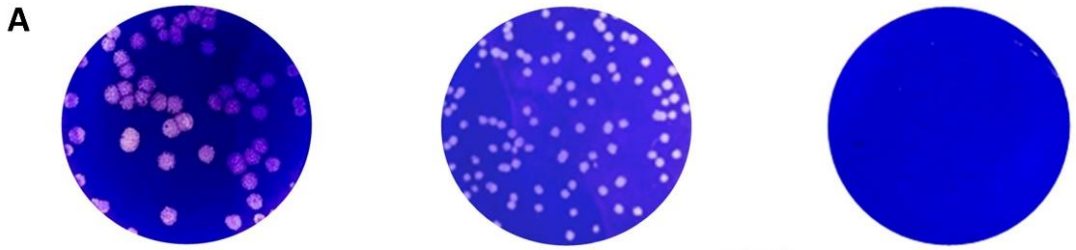
A

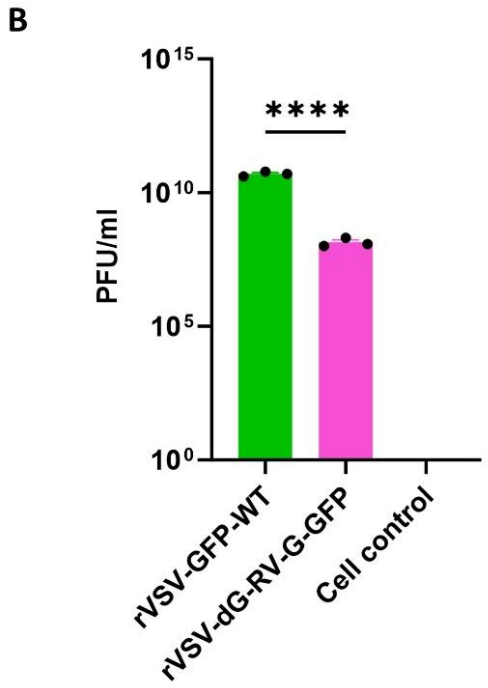
B
PFU/ml
10^{15}
10^{10}
10^{5}
10^{0}
****
rVSV-GFP-WT
rVSV-dG-RV-G-GFP
Cell control

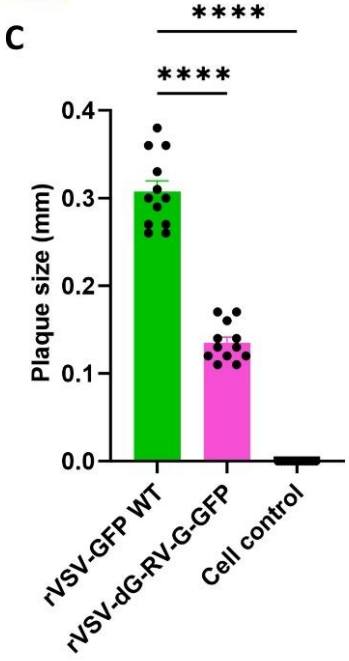
C
****
****
Plaque size (mm)
0.4
0.3
0.2
0.1
0.0
rVSV-GFP WT
rVSV-dG-RV-G-GFP
Cell control

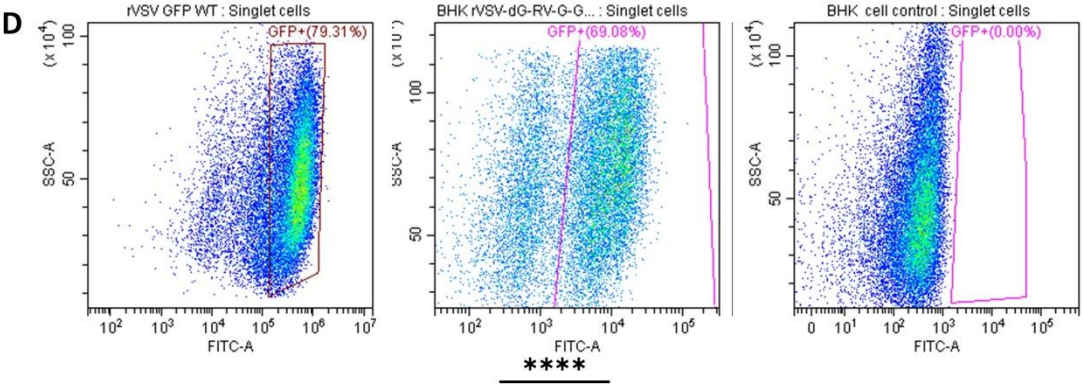
D
rVSV GFP WT : Singlet cells
GFP+(79.31%)
BHK rVSV-dG-RV-G-G... : Singlet cells
GFP+(69.08%)
BHK cell control : Singlet cells
GFP+(0.00%)
SSC-A
FITC-A

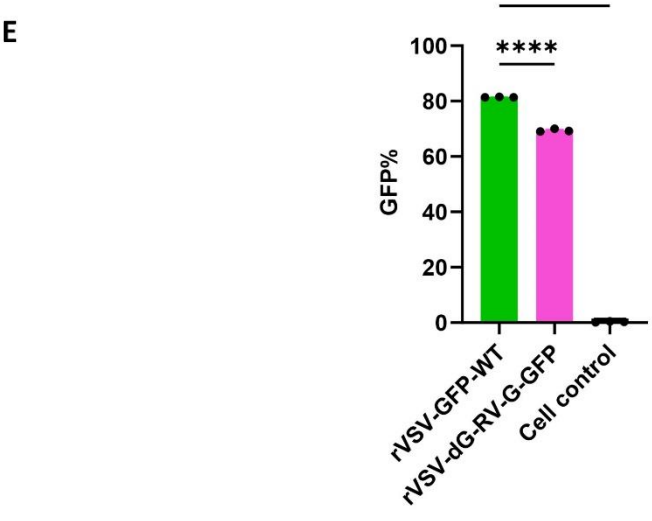
E
****
GFP%
100
80
60
40
20
0
rVSV-GFP-WT
rVSV-dG-RV-G-GFP
Cell control

Figure 4.8 Replication of rVSV-dG-RV-G-GFP and VSV-GFP-WT on BHK-21 cells

(A). *Representative plaque counts. BHK cells were infected with the rVSV-GFP-WT or rVSV-dG-RV-G-GFP (MOI 1). Twenty-four hpi, the viral supernatants were collected for plaque assay. The progeny viruses were quantified on BHK-21 cells and stained with 0.5% crystal violet 72 hours post-infection.* ***(B).*** *Plaque assay-based quantification comparing the released virus progeny from BHK-21 cells infected with rVSV-GFP -WTand rVSV-dG-RV-G-GFP (MOI 1) after 30 hpi. These data represent the average of three biological replicates with S.E.M. indicated, the non-infected BHK-21 cell was used as control.****(C)*** *Comparison of the plaque size between rVSV-dG-GFP and rVSV-dG-RV-G-GFP, the plaques were measured using ImageJ software.* ***(D).*** *Representative plots for the GFP percentage in BHK cell line. Cells were infected with GFP expressing viruses; rVSV-GFP-WT and rVSV-dG-RV-G-GFP (MOI 1), and the non-infected cell control was used, after 30 hpi, the cells were collected for GFP-positive cells were collected for flow cytometry.* ***(E).*** *Mean fluorescence intensities of the BHK-21 cell population infected with rVSV-GFP-WT and rVSV-dG-RV-G-GFP MOI of 1 in comparison with the control cells. These experiments were performed three times independently (n=3). These data represent the average of three biological replicates with S.E.M. indicated. ****p < 0.0001 using one-way ANOVA and student's t-test.*

4.2.4 Permissive and non-permissive cell lines to RV replication

To test the cellular tropism of RV, we tested the susceptibility of diverse range of cell types including epithelial cells (Caco-2, MDCK, VERO), fibroblast (CEF, DF-1), neuroblastoma (PA-BR) and keratinocytes (HaCaT) cell lines derived from different host species including human, canine, bats, and chicken were infected with rVSV-dG-RV-G-GFP. Cells were infected at MOI of 1.0 with rVSV-dG-RV-G-GFP. The GFP signal was observed under fluorescence microscope for infected cell lines 24 hpi. Of the ten tested cell lines, nine appeared to be susceptible to RV infection. Susceptible cell lines (BHK-21, HEK293, Vero, CEF, DF-1 Caco-2 and Pa-Br) showed variable signals of GFP upon infection **(Figure 4.9-41.0)**. Further quantification for the GFP expression percentage in infected cells compared to the cell uninfected control was carried out using flow cytometry. The GFP percentage among cell lines showed significant differences compared to their corresponding non infected controls, demonstrating productive infection with rVSV-dG-RV-G-GFP **(Figure 4.9-4.10).** The highest GFP percentage was shown in infected BHK cells (86.3%), while the lowest percentage was observed in infected Pa-Br cells (21%). Interestingly CEF and DF-1 cells showed GFP upon infection with rVSV-dG-RV-G-GFP. The GFP percentage was significantly higher from uninfected

controls reaching 62% and 54% in infected DF-1 and CEF, respectively. In contrast, HaCaT cell showed no GFP upon infection with similar MOI of rVSV-dG-RV-G-GFP.

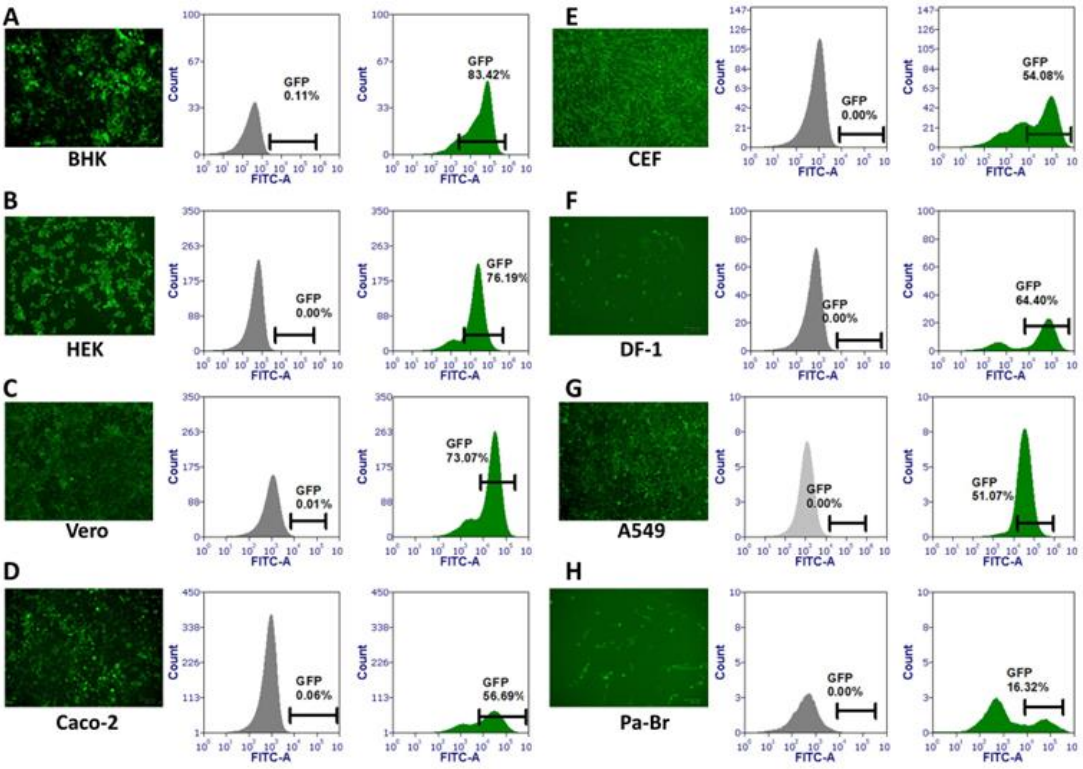

Figure 4.9 Susceptibility to rVSV-dG-RV-G-GFP infection.

Microscopic images of the fluorescence of cell monolayers of ***(A)*** *BHK-21,* ***(B)*** *HEK293, (C) Vero,* ***(D)*** *Caco-2,* ***(E)*** *CEF,* ***(F)*** *DF-1,* ***(G)*** *A549 and* ***(H)*** *Pa-Br cells were infected with rVSVS-dG-RV-G-GFP (MOI =1) and incubated at 37 °C for 30 h. After 30 hpi, the cells were then permeabilized and undergone flow cytometry analysis. Representative histograms of cells indicating the shift in green fluorescence intensity corresponding to the virus replication in each of the infected cells with rVSV-dG-RV-G-GFP and the non-infected cell control. Data were analysed by FCS Express software.*

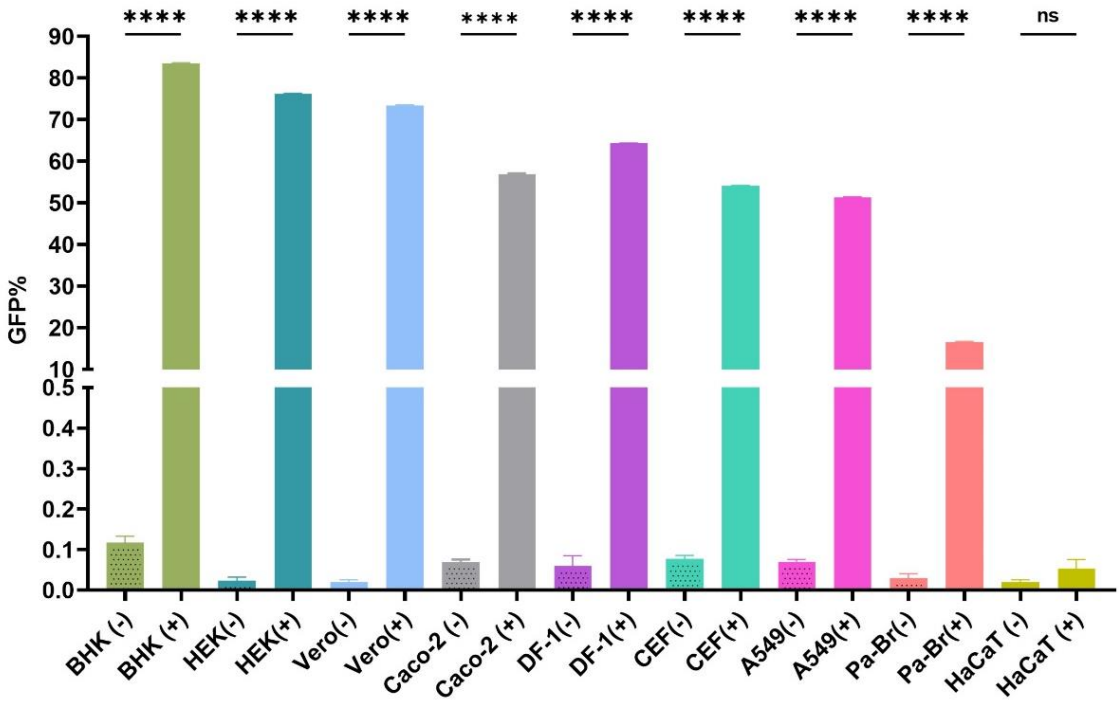

Figure 4.10 Susceptibility of different cell lines to rVSV-dG-RV-G-GFP infection.

*The mean GFP fluorescence of the infected cells with rVSV-dG-RV-G-GFP (MOI=1), after 30 hpi, measured by flow cytometry analysis. The non-infected cells were used as control. Error bars represent the SEM from three separate experiments (n = 3); ****, p < 0.0001, ns; non-significant, p >0.05 by Student's t test.*

4.2.5 HaCaT cells are infected with rVSV-GFP WT but not rVSV-dG-RV-G-GFP

The susceptibility of the RV demonstrated wide cellular tropism, identifying a resistant cell line would provide a controlled experimental system to investigate viral interactions with specific host species or cell types, aiding in the identification of host-specific factors, viral entry mechanisms, immune responses, and guiding the development of antiviral drugs. To exclude the possibility that HaCaT cells are resistant to infection with all members of *Rhabdoviridae*. We tested the ability of HaCat cells to be infected with rVSV-GFP WT at MOI of 1.0 and rVSV-dG-RV-G-GFP as a negative control. Virus replication was first assessed by the microscopic observation of GFP. At 24 hpi, GFP was clearly observed on rVSV-GFP WT infected HaCaT cells **(Figure 4.11 A).** Unlike the uninfected cell control and HaCaT cells infected with rVSV-dG-RV-G-GFP which did not show any GFP signal. Next, the percentage of GFP expression of HaCaT infected cells was quantified with flow cytometry. A significant increase in the GFP % (50.62%) of the rVSV-GFP WT infected HaCaT cells compared to non-infected cell control and cells infected with rVSV-dG-RV-GFP which showed no GFP signal **(Figure 4.11 B-C).** These results

clearly indicate the ability of HaCaT cells to support the VSV-GFP WT infection, but not rVSV-dG-RV-G-GFP.

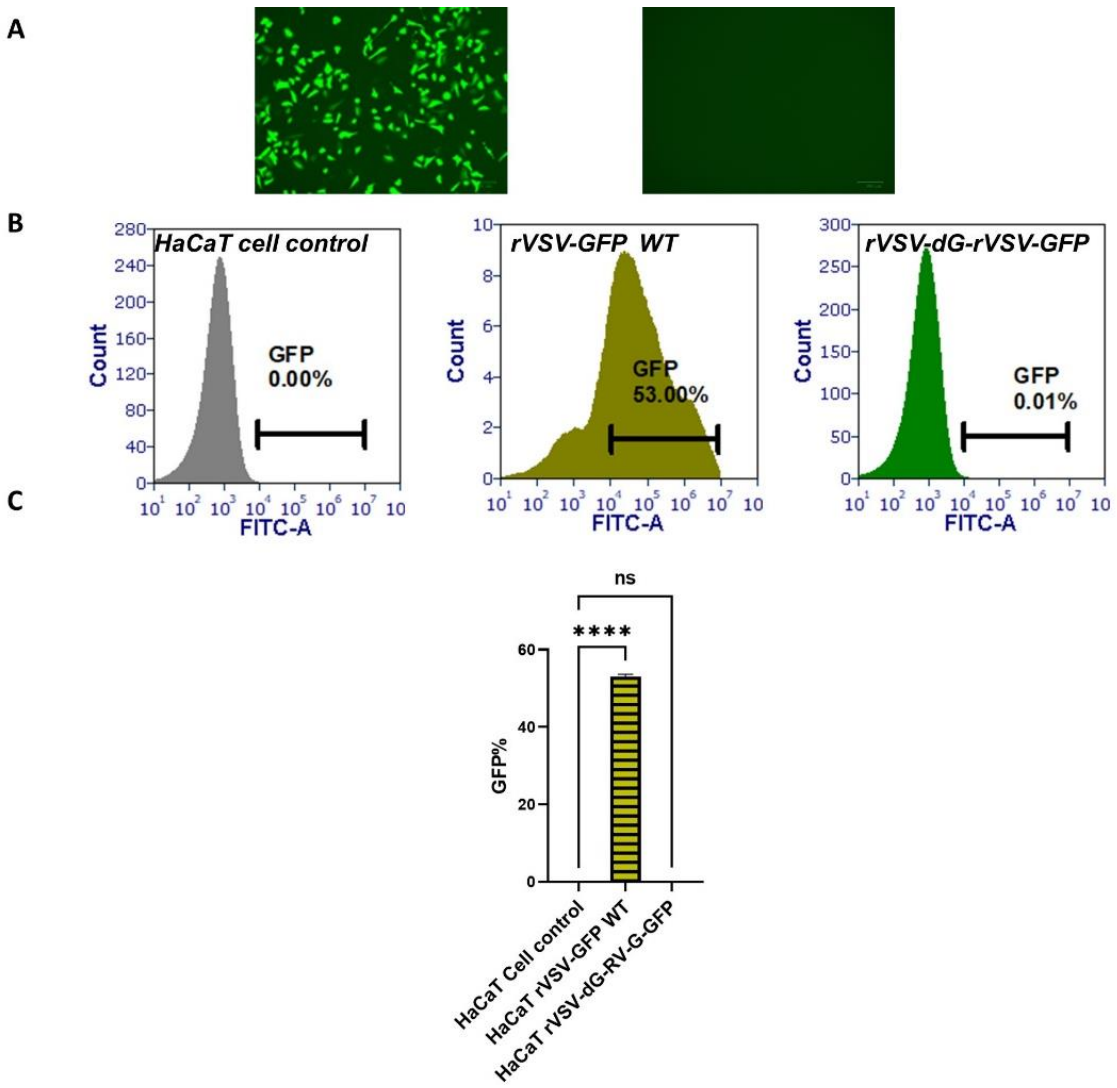

Figure 4.11. HaCaT cells are permissive to rVSV-WT virus infection. but not rVSV-dG-RV-G-GFP

(A). Representative *microscopic green fluorescence of the HaCaT cells infected with VSV-WT (left) and rVSV-dG-RV-G-GFP (right).* ***(B).*** *Representative histograms showing the percentage of infected cells as quantified by flow cytometry at 30 h post infection with HaCaT cell control, HaCat cells infected with rVSV-dG-GFP WT and HaCaT cells infected with rVSV-dG-RV-G GFP (MOI=1).* ***(C).*** *Graph showing the mean GFP% as quantified by the flow cytometry in HaCaT cells infected with VSV-GFP WT and rVSV-dG-RV-G-GFP. Error bars represented the SEM from three biological replicates (n = 3); ns; non-significant p>0.05, ****, p < 0.0001, by one-way ANOVA.*

4.3 Discussion

To allow studying the RV tropism, we developed the rVSV in which the VSV G was swapped with a reporter GFP gene along with the insertion of the surface glycoprotein

of RV. Replacing the VSV G protein would attribute the attachment and host cellular tropism of the recovered virus to the Rabies surface glycoprotein (Tani et al., 2012). VSV has shown an enormous potential over other virus expression systems. Since it does not require the insertion of proteolytic cleavage sites on the proteins to be expressed as proteins are readily expressed from newly synthesized mRNA (Schnell et al., 1996). In addition to its high viral yield, allowing high and efficient protein expression (Majid and Barber, 2006). As well as, preventing genomic reassortment which is observed in segmented viruses (Majid and Barber, 2006). Moreover, since VSV and RV belong to *Rhabdoviridae*, they exhibit significant resemblances in their replication cycle (Beier et al., 2013). The pseudo-type and recombinant viral systems represent reliable tools for studying viral entry through heterologous expression of foreign glycoproteins. However, the recombinant virus system sets a more powerful tool as it allows the production of multiple infectious cycles and producing infectious progeny virus. Unlike the pseudo-type virus system which is only restricted to single round of infection (Garbutt et al., 2004; Whitt, 2010)

Hence the expression level of foreign genes is affected by their site of insertion in the negative strand RNA virus's genome (Wertz et al., 2002). The foreign rabies glycoprotein gene was inserted between the M and L genes junction, as insertions away from the N/P junction of the VSV genome were proven to enhance the expression of heterologous proteins (Wertz et al., 2002). In our study, we confirmed the surface expression of the rabies glycoprotein by western blot and immunofluorescence assay using monoclonal antibodies against the rabies glycoprotein. Moreover, the clear spikes distribution observed on the surface of the rVSV-dG-RV-G-GFP which we have verified through electron microscopy. Taken together, these findings indicate that the substitution of the VSV-G gene did not affect the particle structure formation.

The recovery of the rVSV from plasmids using reverse genetics system involves the co-transfection of the VSV antigenome RNA along with the cDNA for the VSV proteins (N, P, G and L) except the M protein. Since VSV M protein is not provided *in trans,* its presence is only dependent on the production of the genomic RNA through the VSV polymerase complex which act on the encapsulated anti-genome, and lead to mRNA synthesis and virus production and expression of the viral structural proteins (Whitt,

2010). Therefore, our results of the VSV M expression profiles in rVSV-dG-RV-G-GFP cell lysates besides its intracellular localization remarkably indicates the successful viral budding and assembly from the VSV genome which requires the interaction of the VSV M protein and the nucleocapsid complex.

The replicative fitness of the recovered VSV displaying the surface RV-G was characterized in comparison to the VSV-GFP WT by qRT-PCR and plaque assays. The obtained results indicate relatively less viral titres in the recombinant virus in respect to the VSV WT virus. The resulting recombinant virus attenuation could be attributed to the delayed processing and reduced expression rate of the foreign glycoprotein (Garbutt et al., 2004). In addition to the possible role of the length of the foreign gene insert to affect the replication efficiency (Roberts and Rose, 1998).

To demonstrate if the reporter genes expressed by recombinant viruses might be lost during virus passaging, we tested the GFP expression profiles by flow cytometry of the BHK infected cells with the VSV GFP WT and rVSV-dG-RV-G-GFP. Nevertheless, our findings indicated the GFP expression in the rVSV-dG-RV-G-GFP infected cells, indicating its ability to retain the reporter gene in the fourth passage of virus. Ultimately, the generated virus will serve as a potential tool to monitor the spread of the virus *in vitro* (Shen et al., 2009).

To demonstrate the host cellular tropism of the generated rVSV-dG-RV-G-GFP, infection on various cell lines was carried out. The demonstrated ability of the rVSV-dG-RV-G-GFP to replicate in various cell lines indicated the wide host range of the RV-G. Whereas, clear change in cell tropism was evidenced between the VSV-GFP WT and the rVSV-dG-RV-G-GFP in which HaCaT cells were refractory to the recombinant virus displaying the RV-G compared to the rVSV WT-GFP.

To this end, our results, indicate the successful recovery of VSV carrying the RV-G on their surface. Thereby, serves as cellular model which will allow mechanistic study of rabies virus replication and host interaction mediated by the surface rabies glycoprotein **(Figure 4.12)**. Besides providing efficient and safe handling in tissue culture facilities. In addition, screening a wide variety of cell lines has identified that HaCaT cells were refractory to rVSV-dG-RV-G-GFP. Transfection of these cells with individual RV receptors

will allow understanding the potential role of these receptors in the entry of rVSV-dG-RV-G-GFP.

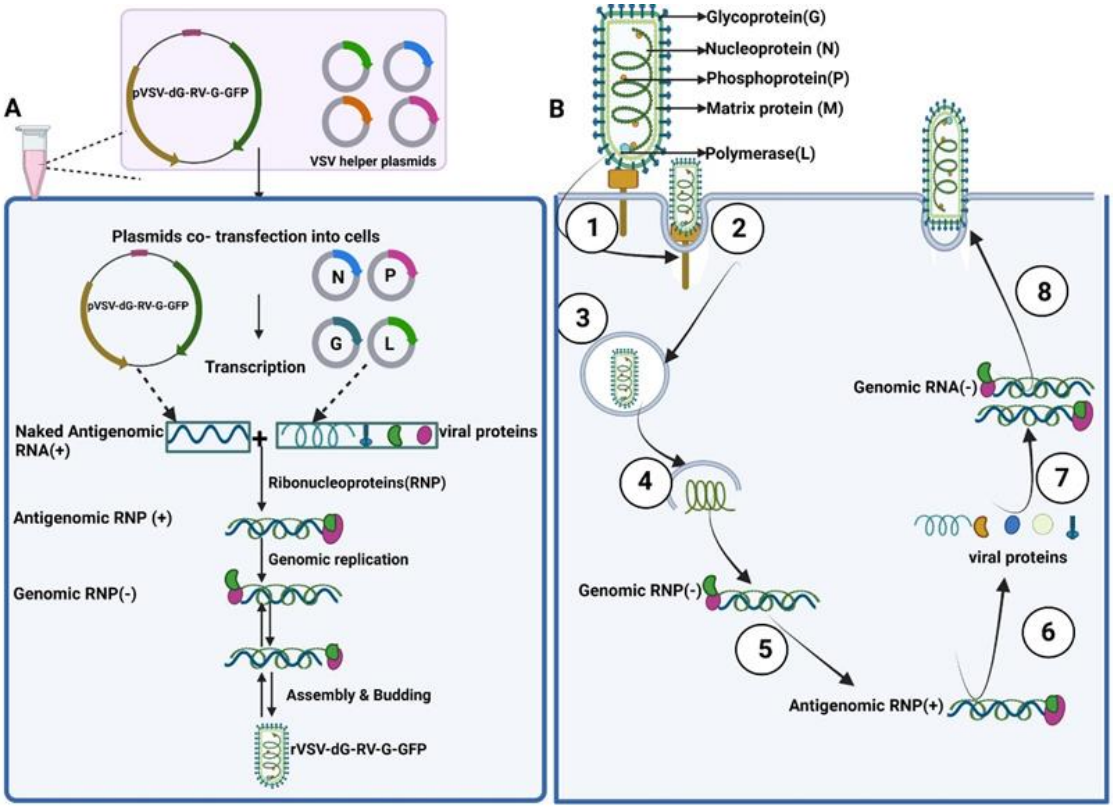

Figure 4.12 Replication of the rVSV-dG-RV-G-GFP and rabies virus.

(A) *Cycle during the rescue process of rVSV-dG-RV-G-GFP. The rescue process of the rVSV-dG-RV-G-GFP required the co-transfection of the pVSV-dG-RV-FG-GFP plasmid encoding the antigenome of the VSV after modification (incorporation of the rabies glycoprotein and GFP marker gene) along with the VSV helper plasmids (pBS-N, pBS-P, pBS-L& pBS-G). Upon co-transfection, the pVSV-dG-RV-FG-GFP was transcribed into the modified naked antigenome of VSV, and the helper plasmids were transcribed into the corresponding VSV viral proteins (N, P, L and G). Subsequently, the ribonucleoprotein complex formed of the nucleoprotein (N) along with the viral polymerase complex (Phosphoprotein (P) and polymerase (L)) together encapsulate the antigenomic RNA. The reconstituted encapsulated antigenome RNPs, acts as a template for the generation of the complementary RNA genome (negative strand), which is subsequently encapsulated in the RNP complex. Consequently, the normal replication cycle takes place in the cytoplasm of infected cells, resulting in the assembly and budding of the recombinant virions encapsulating the modified genomes of the VSV.* ***(B)*** *Natural replication cycle of rabies virus (1) Virus binding to the cellular receptors (2) Upon the binding of the virus surface G protein to the cellular receptors, the virus is internalized via receptor mediated endocytosis (3) Upon internalization into the endosomal compartments, the endosome low pH allows the fusion of the viral membrane into endosomal membrane*

(4) Subsequently, uncoating and release of viral RNA (-) occurs (5) Transcription of the genomic RNP into the antigenomic RNA (positive strand) (6) Translation of the viral proteins occurs in the (7) Genome replication, the antigenomic RNP acts as a template for replicating the RNA genomes which are encapsulated by the nucleoprotein (8) Assembly of the viral proteins and the RNA genome subsequently the release of the virus occurs by budding.

5 Chapter 5 Understanding Rabies Virus Receptors Preference in Mediating Virus Entry

5.1 Introduction

Virus entry into host cellular compartments is determined by the interaction between the surface viral glycoprotein and surface cellular receptors which act as the key to unlock the cell for viral infection (Grove and Marsh, 2011). Some viruses rely on one single receptor for entry into cellular compartments such as poliovirus. However, other viruses use multiple cell surface molecules as potential receptors to gain its cellular entry (Blanco, 2013). Rabies recognizes different cellular receptors and enter host cells through receptor mediated endocytosis. Following the virus-receptor interaction, low pH induces the fusion of the viral and cellular membranes which triggers the release of the viral genome into cytoplasm for transcription and replication of viruses (Yang et al., 2020). While six different receptors have been identified historically for RV, it is not known which of these receptors are essential for RV entry into the cells (Lafon,2005). Moreover, it has not been identified if RV utilizes those receptors in series or in parallel.

5.1.1 Viruses binding to receptors.

Rabies can access the host cellular compartment through its interaction with the receptors which is primarily facilitated by the electrostatic binding to the attachment factors **(Chapter 7).**

Following the binding of the virus to the receptor, the next step is to enter the host cell in which viruses use two different strategies:

- Receptor mediated endocytosis: upon the virus interaction with the surface cellular receptor, the endocytic cellular machinery uptake the virus into the host cellular compartment. It is exploited that the virus particles internalization is triggered through signalling pathways induced by the virus-receptor interactions. While other studies supported that the virus-receptor does not usually lead to virus uptake, and that virus uptake occur through uptake by the host cell rather than depending on signal induction.
- Endocytosis independent receptor mediated entry: the virus binding to the cellular receptor results in direct virus penetration from the plasma membrane, bypassing the endocytic cellular machinery.

  Studying the mechanism by which the virus particles land on host cells will open new insights into the receptors involved in the primary attachment of the virus to host cell.

Three proposed scenarios for the movement of the virus in the host cells include:

- **Random motion:** viruses display directional displacement followed by virus confinement in specific microdomain in the plasma membrane. The virus initially binds to its primary cellular receptor followed by their movements to plasma membrane where they interact with high affinity to their secondary receptor allowing the virus to be internalized. The Influenza and polyomaviruses are examples for this type of movement (Boulant et al., 2015).
- **Constrained diffusion:** viruses remain confined after their attachment to primary cellular receptor, awaiting binding to secondary receptor or to be endocytosed as is observed in in VSV and Reoviruses (Cureton et al., 2009)
- **Directional movement:** following the virus receptor attachment on the cell surface, it diffuses to the cell surface and shortly after it interacts with the clathrin-coated pits as shown by canine parvovirus (Thwaites et al., 2020).

  It is important to note that however virus-receptor binding is crucial for virus endocytosis. The binding of multiple receptors to the virus particle might slow its diffusion rate to the plasma membrane which affects the virus internalization (Boulant et al., 2015). More studies are required to evaluate if slower or higher diffusion rates would enhance or inhibit virus endocytosis.

  To this aim in this chapter, we attempted to test which virus receptors played critical role in the primary virus/receptor interaction and which is mostly required in the internalization process.

5.1.2 Genomic approaches to identify the role virus receptors.

The identification of host receptors involved in virus attachment and entry into host cells is pivotal to understand virus pathogenesis and tissue and species tropism (Coffin, 2013).

Recent advancement in genomic approaches to study virus receptors can be categorized into either study involving loss or gain of function. Both strategies allow understanding of the functional role of host protein in virus replication (Barrass and Butcher, 2020).

5.1.2.1 Loss of function strategy

The loss of the host factors known to facilitate virus replication, allows studying its effect on viral replication. The genetic knockout is one of the approaches which allow studying the role of certain protein through its complete deletion. In this chapter, we performed genomic deletion using the Clustered Regularly Interspaced Short Palindromic Repeats (CRISPR/Cas9) technology. Primarily, the CRISPR/Cas9 system has evolved as an adaptive immune response within bacteria which target and destroy the pathogenic DNA through the dual trans-activating CRISPR RNA tracrRNA:crRNA duplex which is known as single guide RNA in performing the knockout experiments (Doudna and Charpentier, 2014). The CRISPR/Cas9 knockout experiments are performed through the generation of guide-RNA (gRNA) targeting specific coding region within the gene of interest, which consequently result in targeted double strand DNA breaks resulting in non-homologous end joining and consequently the generation of null phenotype. Comparing the genomic knockout generated from RNAi to the CRISPR/Cas9, the knockout generated through the CRSIPR/Cas9 showed fewer off targets effects **(Chapter 2, Figure 2.1)** (Barrass and Butcher, 2020).

5.1.2.2 Gain of function strategy

It allows the introduction of new functional receptors through the ectopic expression of proteins which render non permissive cells susceptible to certain virus infection. To introduce new functionality to permissive cell lines, cDNA is synthesized from mRNA using reverse transcription followed by cloning in expression vector. Aspects need to be considered for implementing this strategy which is the challenge of obtaining non permissive cell line to infection. Along with the effect of the mRNA expression levels of certain gene in the tested cell line (Barrass and Butcher, 2020).

5.1.3 Aims:

In the previous chapter, we demonstrated the ability of various cell lines to sustain the rVSV-dG-RV-G-GFP replication. We identified that HaCaT cell line was refractory to infection. In this chapter, using HaCaT cell line, we aim to identify the receptor preference of RV based on the following approaches:

1. Assess the entry and replication of the rVSV-dG-RV-G-GFP in HaCaT cells overexpressing the RV receptors individually and in combination **(Figure 5.1).**

- Evaluate the endogenous expression levels of the RV receptor genes on HaCaT cells.

2. Generate and characterize three different knockout cell lines devoid of endogenous ITGB1, mGluR2 and nAChR receptors.

- Assess the entry and replication of the rVSV-dG-RV-G-GFP on each of the generated KO cell lines to identify the functional role of these receptors in RV replication.

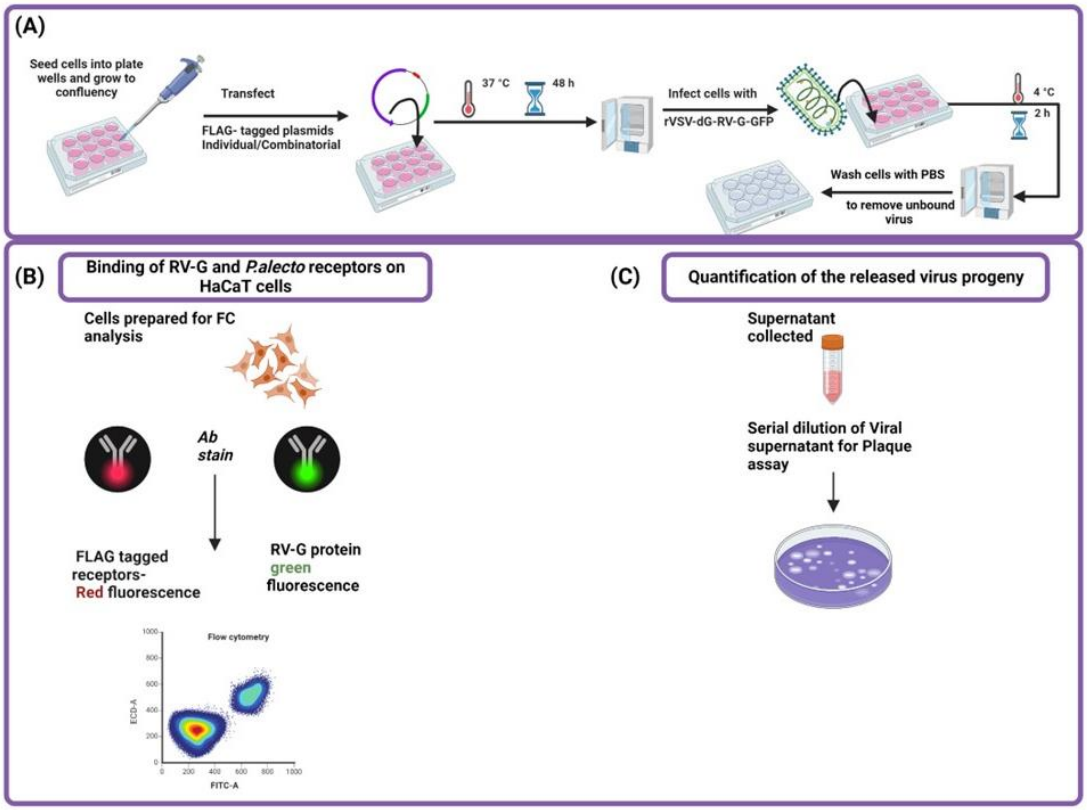

Figure 5.1. Schematic diagram illustrating the workflow for quantification the RV-G binding and released virus progeny on HaCaT cells.

(A). *Into a 70-80% confluent HaCaT cells in a 96 well plate, cells were transfected with P.alecto receptors with Flag tag at the C-terminus, and incubated for 48 hrs. After 48h, cells were infected with rVSV-dG-RV-G-GFP(MOI=5) for 2 hrs with shaking. Followed by, washing the cells with PBS for the removal of unbound virus. (**B**). For quantification of the bound G protein to the infected cells, cells were detached and prepared for flow cytometry analysis. Cells were stained with anti-FLAG (targeting the FLAG-tagged receptor) and RV-G antibodies (targeting the virus RV-G), followed by staining with Alexa Fluor 568 and Alexa Fluor 468 antibodies; respectively, then the percentage of bound virus (GFP +ve) was quantified from the transfected (RFP +ve) cell population **(C).** For quantification of the released virus progeny, cells were incubated for 30 hrs at 37 °C, followed by collecting the virus supernatant for virus quantification by plaque assay performed on BHK-21 cells.*

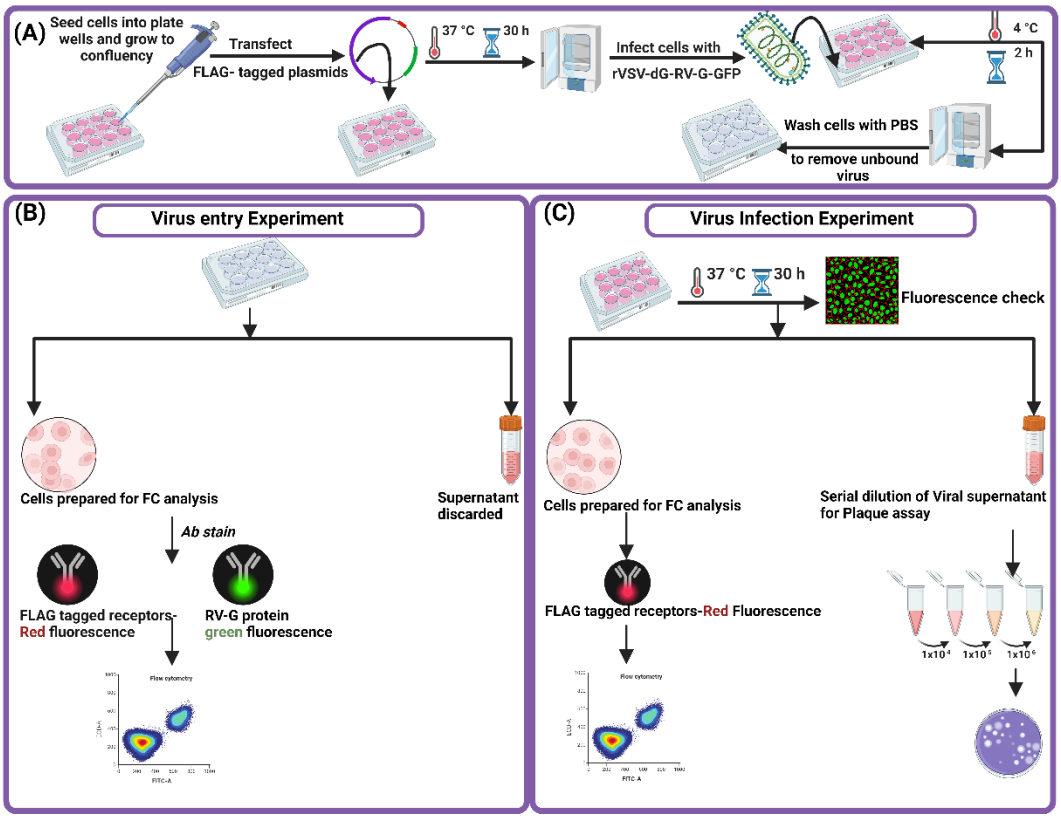

Figure 5.2 Schematic diagram illustrating the workflow for the virus infection and virus entry assays in all cell lines.

(A). *Into confluent cells in a 24 well plate, cells were transfected with respective receptors with Flag tag at the C-terminus, followed by incubating the transfected cells for 48 hrs 37 °C. After 48h, cells were infected with rVSV-dG-RV-G-GFP MOI=5 for 2 hrs with shaking. Followed by, washing the cells with PBS for removal of unbound virus. (**B).** For virus entry experiment, (quantification of the bound virus), cells were detached and prepared for flow cytometry analysis in which cells were stained with then cells were collected and stained with anti-FLAG (targeting the FLAG-tagged receptor) and RV-G antibodies(targeting the virus RV-G), followed by staining with Alexa Fluor 568 and Alexa Fluor 468 antibodies: respectively. The percentage of bound virus (GFP +ve) was quantified from the transfected (RFP +ve) cell population (**C.)** For virus infection experiments after removal the unbound virus, cells were incubated for 30 hrs, then the GFP was visualized, followed by collecting the virus supernatant for virus quantification by plaque assay performed on BHK-21 cells. Then cells were detached, collected, and prepared for flow cytometry analysis by staining with anti-FLAG (targeting the FLAG-tagged receptor) followed by Alexa Fluor 568 antibodies. The GFP % represents the internalized virus from the transfected (RFP +ve) cell populations.*

5.2 Results

5.2.1 Receptor preference study on non-permissive cell line

5.2.1.1 HaCaT cells express the RV receptors genes.

To gain additional understanding of the resistance of the HaCaT cells to the rVSV-dG-RV-G-GFP infection, we studied the endogenous expression patterns of the RV surface receptors genes in non-infected HaCaT cell compared to their expression levels in response to the rVSV-dG-RV-G-GFP infection. The mRNA expression patterns of the RV receptor genes indicated the relative expression of the RV receptor genes in HaCaT cells. Comparing the expression of the mRNA levels in response to the rVSV-dG-RV-G-GFP indicated that only the mRNA levels of the nAChR and NCAM were down regulated by 5-fold and 4-fold, respectively 24 hr post rVSV-dG-RV-G-GFP infection. In contrast, the expression profiles of the ITGB1, mGluR2 and p75 genes remained unaffected **(Figure 5.3).** These findings indicate the possible utilization of the RV-G to the nAChR and NCAM as surface receptors which were not sufficient for establishing productive infection.

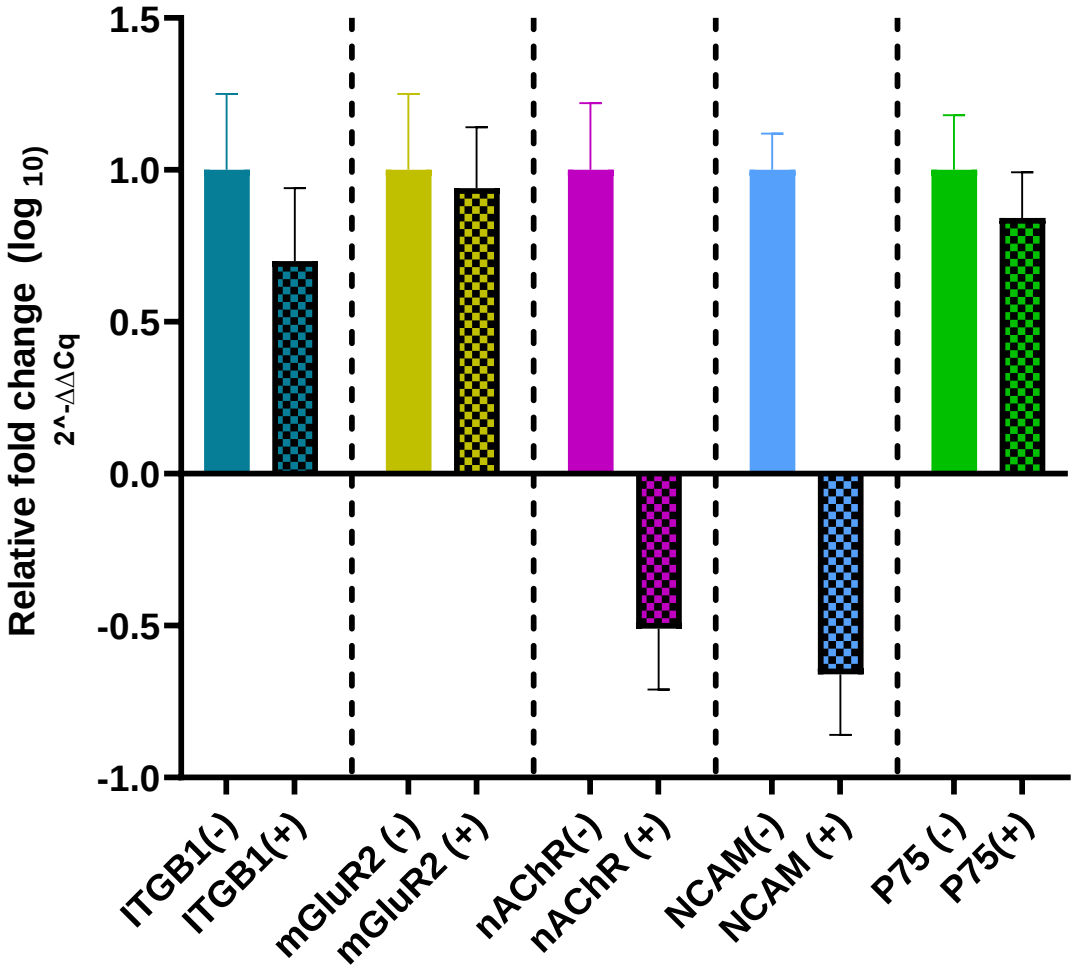

Figure 5.3 Relative expression (in fold change value) of RV cellular receptor genes in HaCaT cells.

The differential expression (in fold change) of the RV cellular genes were measured by qRT-PCR on HaCaT cells before (-) and after infection (+) with rVSV-dG-RV-G-GFP. Twenty-four hrs after infection, cellular RNA was extracted from infected and non-infected HaCaT cells. The relative RNA expression (mean ± SEM) of each of RV receptor gene were normalised to human beta-actin using the ΔΔCt method. The experiment was performed three times independently (n=3). Error bars represented the SEM from three biological replicates.

5.2.1.2 Individual receptor expression is not sufficient for rVSV-dG-RV-G-GFP infection on HaCaT cells.

The HaCaT cells are described as immortalized human keratinocyte cells. In the previous chapter, we showed the non-permissiveness of HaCaT cells to rVSV-dG-RV-G-GFP infection **(Chapter 4, section 4.2.5)**. Next, we sought to assess if the ectopic expression of each of the RV receptors individually would render HaCaT cells susceptible to infection. HaCat cells were transfected with plasmids encoding each of the RV receptors. At 48 hr post transfection, cells were infected with rVSV-dG-RV-G-GFP at MOI =5. Thirty

hrs post infection, we expected to observe GFP, but surprisingly, no GFP was observed. For this purpose, to quantify the binding efficiency of the RV-G with HaCaT cells expressing different receptors. The HaCaT cells were infected with rVSV-dG-RV-G-GFP following its transfection with the *P.alecto* receptors. Infected cells with rVSV-dG-RV-G-GFP (MOI =5) were incubated for 2 hr, then cells were dissociated and collected for flow cytometry (FC analysis) **(Figure 5.1).** Subsequently to allow gating the cell population bound to the RV-G (GFP+ve) from the cell population expressing the receptors (RFP+ve). The cells were stained against both the FLAG-tag (targeting the receptors) and the RV-G antibodies (targeting the bound RV-G protein), followed by staining cells with the conjugated secondary antibodies: Alexa fluor 568 for receptor staining and Alexa fluor 468 for staining the RV-G positive cells. For quantifying the released progeny virus, the transfected HacaT cells were infected with rVSV-dG-RV-G-GFP (MOI 5) and incubated for 30 h, followed by plaque assay analysis **(Figure 5.1)**.

The results obtained from the flow cytometry analysis, indicated significantly higher binding of the RV-G to HaCaT cell expressing ITGB1 **(Figure 5.4 A-B),** mGluR2 **(Figure 5.5 A-B),** nAChR **(Figure 5.6 A-B**), NCAM **(Figure 5.7 A-B**). While the lowest binding of the RV-G was shown in cells expressing the p75 expressing cells **(Figure 5.8 A-B)**.

Next, we assessed if this binding resulted in producing more infectious virus particles. The viral supernatants were collected to perform a plaque assay. Interestingly, despite no GFP was observed, significantly higher levels of the released virus resulted from HaCaT cells expressing the nAChR **(Figure 5.6 B-C),** mGluR2 **(Figure 5.5 B-C)** and NCAM **(Figure 5.7 C-D)**. However, the released virus observed in HaCaT cells ectopically expressing, ITGB1 **(Figure 5.5 C-D),** and p75, (**Figure 5.8 C-D)** showed no significant difference compared to the empty vector control. These results suggested the potential role of the ITGB1, nAChR and mGluR2 in promoting RV entry.

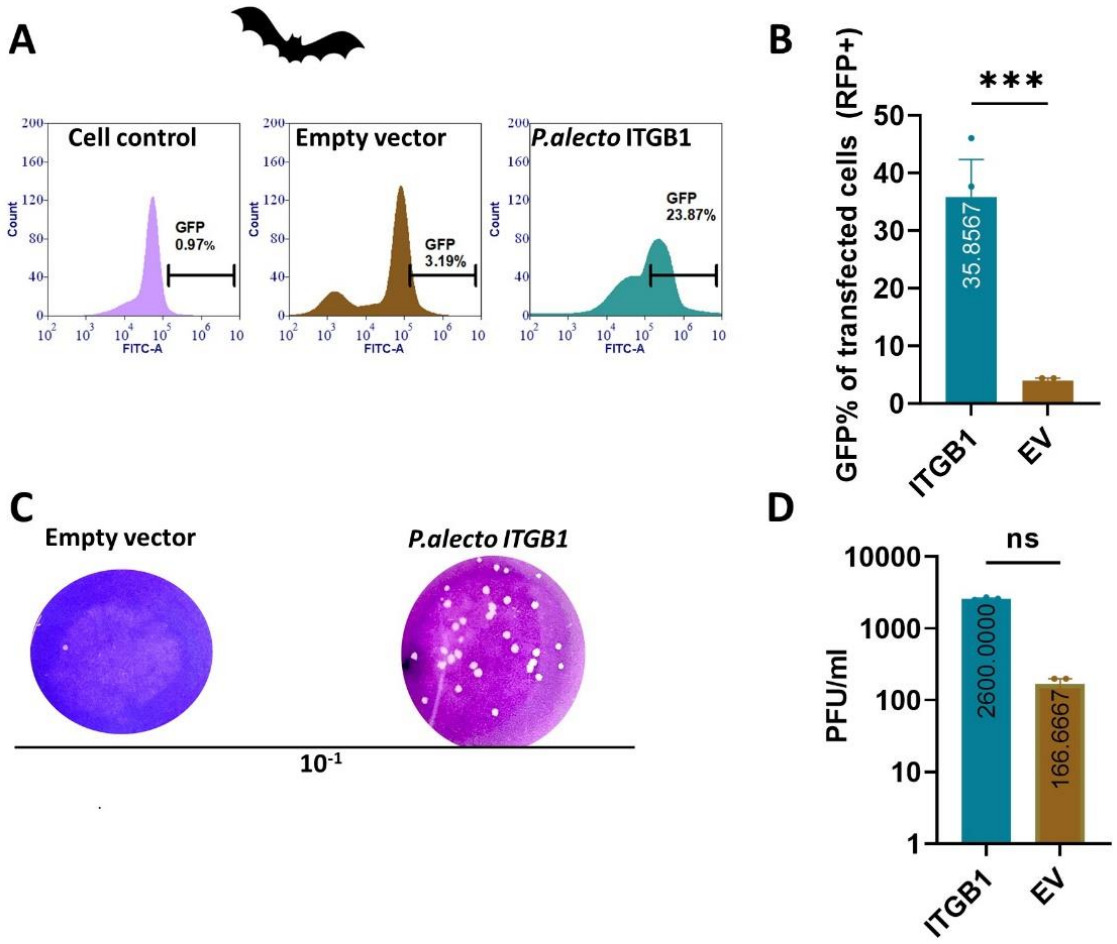

Figure 5.4 Infectivity of rVSV-dG-RV-G-GFP on HaCaT cells transiently transfected with P.alecto ITGB1.

(A). *Representative histograms showing the GFP % of rVSV-dG-RV-G-GFP infected HaCaT cells and transfected with P.alecto ITGB1 (Right) and HaCaT cells transfected with empty vector(left). HaCaT cells were transfected with the P.alecto ITGB1, 48 hpt, cells were infected with the rVSV-dG-RV-G-FP (MOI=5) for 2 hrs, then cells were collected and stained with anti-FLAG (targeting the FLAG-tagged receptor) and RV-G antibodies(targeting the virus RV-G), followed by staining with Alexa Fluor 568 and Alexa Fluor 468 antibodies; respectively for flow cytometry analysis. Flow cytometry data were analysed by FCS Express software. Cell control was used as non-infected control* ***(B.).*** *Graph showing the mean of the GFP% of HaCat cells infected and transfected with P.alecto ITGB1 compared to cells transfected with the empty vector., the GFP % corresponds to the RV-G bound to the transfected HaCaT cells.* ***(C).*** *Representative plaque morphology of infected HaCat cells expressing P.alecto ITGB1. HaCaT cells were transfected with the P.alecto ITGB1 and empty vector, 48 hpt, cells were infected with the rVSV-dG-RV-G-FP (MOI=5). Thirty hpi, the viral supernatants were collected for quantifying the released progeny virus. The released viruses were quantified using plaque assay on BHK-21 cells after 72 hrs.* ***(D).*** *Graph showing the difference of the mean PFU/mL of rVSV-dG-RV-G-GFP between HaCaT cells transfected with P.alecto ITGB1 and HaCat cells transfected with empty vector. All experiments were performed three times (n=3) independently. All the data represent the average of three biological replicates with S.E.M. using student's t-test. ns; non-significant; p>0.05, ****p < 0.0001.*

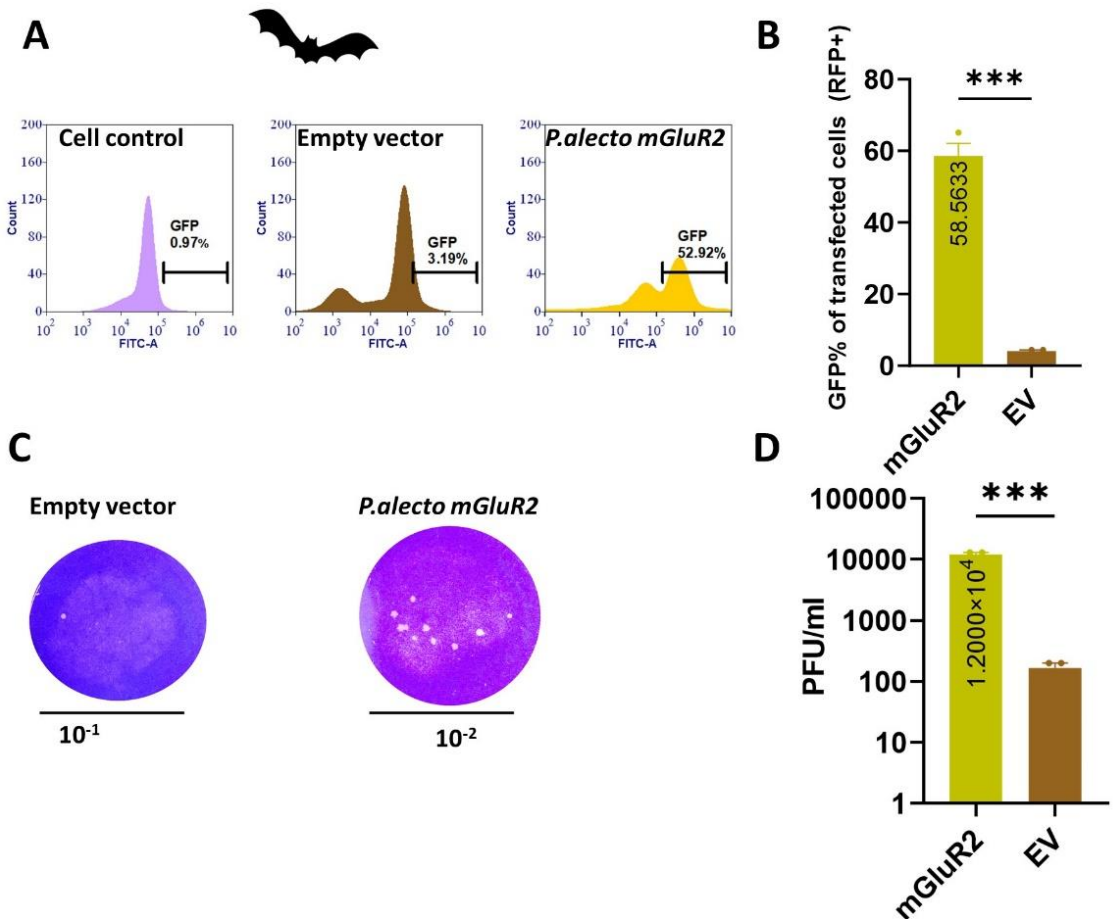

Figure 5.5 Infectivity of rVSV-dG-RV-G-GFP on HaCaT cells transiently transfected with P.alecto mGluR2.

(A). *Representative histograms showing the GFP % of rVSV-dG-RV-G-GFP infected HaCaT cells and transfected with P.alecto mGluR2 (Right) and HaCaT cells transfected with empty vector(left). HaCaT cells were transfected with the P.alecto mGluR2, 48 hpt, cells were infected with the rVSV-dG-RV-G-FP (MOI=5) for 2 hrs, then cells were collected and stained with anti-FLAG (targeting the FLAG-tagged receptor) and RV-G antibodies(targeting the virus RV-G), followed by staining with Alexa Fluor 568 and Alexa Fluor 468 antibodies, respectively for flow cytometry analysis. Flow cytometry data were analysed by FCS Express software. Cell control was used as non-infected control.* ***(B.).*** *Graph showing the mean of the GFP% of HaCat cells infected and transfected with P.alecto ITGB1 compared to cells transfected with the empty vector. The GFP % corresponds to the RV-G bound to the transfected HaCaT cells.* ***(C).*** *Representative plaque morphology of infected HaCat cells expressing P.alecto mGluR2. HaCaT cells were transfected with the P.alecto mGluR2 and empty vector, 48 hpt, cells were infected with the rVSV-dG-RV-G-FP (MOI=5). Thirty hpi, the viral supernatants were collected for quantifying the released progeny virus. The released viruses were quantified using plaque assay on BHK-21 cells after 72 hrs.* ***(D).*** *Graph showing the difference of the mean PFU/mL of rVSV-dG-RV-G-GFP between HaCaT cells transfected with P.alecto mGluR2 and HaCat cells transfected with empty vector. All experiments were performed three times (n=3) independently. All the data represent the average of three biological replicates with S.E.M. using student's t-test. ***p < 0.001.*

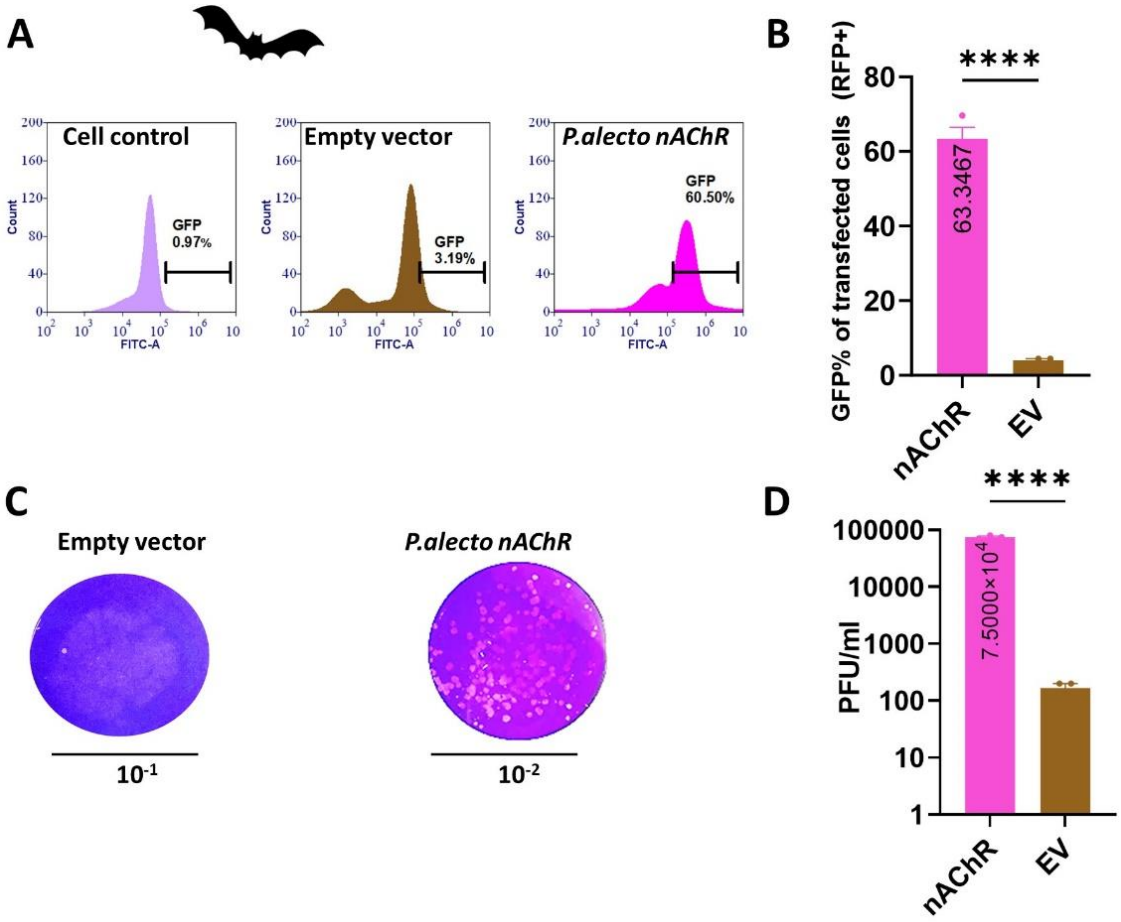

Figure 5.6 Infectivity of rVSV-dG-RV-G-GFP on HaCaT cells transiently transfected with P.alecto nAChR.

(A). *Representative histograms showing the GFP % of rVSV-dG-RV-G-GFP infected HaCaT cells and transfected with P.alecto nAChR (Right) and HaCaT cells transfected with empty vector(left). HaCaT cells were transfected with the P.alecto nAChR, 48 hpt, cells were infected with the rVSV-dG-RV-G-FP (MOI=5) for 2 hrs, then cells were collected and stained with anti-FLAG (targeting the FLAG-tagged receptor) and RV-G antibodies(targeting the virus RV-G), followed by staining with Alexa Fluor 568 and Alexa Fluor 468 antibodies, respectively for flow cytometry analysis. Flow cytometry data were analysed by FCS Express software. Cell control was used as non-infected control.* ***(B.).*** *Graph showing the mean of the GFP% of HaCat cells infected and transfected with P.alecto nAChR compared to cells transfected with the empty vector. The GFP % corresponds to the RV-G bound to the transfected HaCaT cells.* ***(C).*** *Representative plaque morphology of infected HaCat cells expressing P.alecto nAChR. HaCaT cells were transfected with the P.alecto nAChR and empty vector, 48 hpt, cells were infected with the rVSV-dG-RV-G-FP (MOI=5). Thirty hpi, the viral supernatants were collected for quantifying the released progeny virus. The released viruses were quantified using plaque assay on BHK-21 cells after 72 hrs.* ***(D).*** *Graph showing the difference of the mean PFU/mL of rVSV-dG-RV-G-GFP between HaCaT cells transfected with P.alecto nAChR and HaCat cells transfected with empty vector. All experiments were performed three times (n=3) independently. All the data represent the average of three biological replicates with S.E.M. using student's t-test. ****p < 0.0001.*

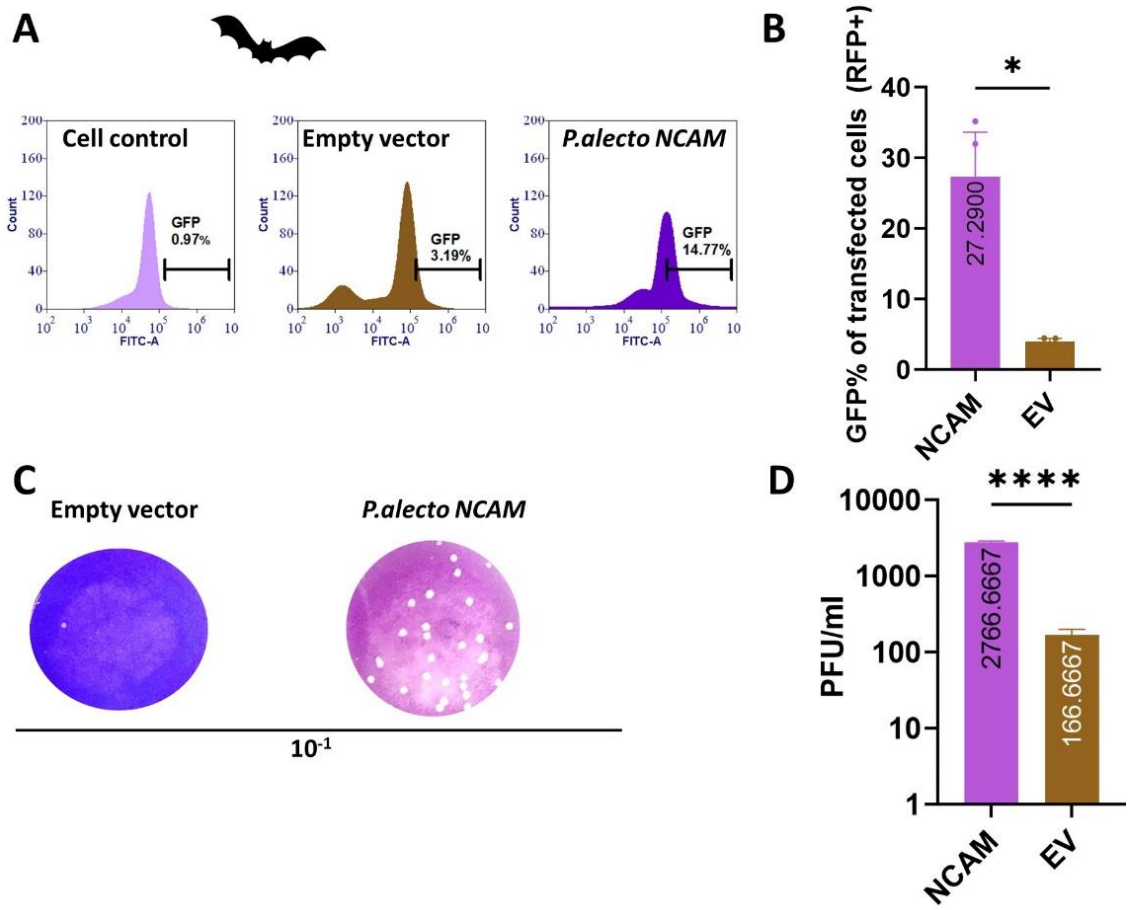

Figure 5.7 . Infectivity of rVSV-dG-RV-G-GFP on HaCaT cells transiently transfected with P.alecto NCAM.

(A). *Representative histograms showing the GFP % of rVSV-dG-RV-G-GFP infected HaCaT cells and transfected with P.alecto NCAM (Right) and HaCaT cells transfected with empty vector(left). HaCaT cells were transfected with the P.alecto NCAM, 48 hpt, cells were infected with the rVSV-dG-RV-G-FP (MOI=5) for 2 hrs, then cells were collected and stained with anti-FLAG (targeting the FLAG-tagged receptor) and RV-G antibodies(targeting the virus RV-G), followed by staining with Alexa Fluor 568 and Alexa Fluor 468 antibodies, respectively for flow cytometry analysis. Flow cytometry data were analysed by FCS Express software. Cell control was used as non-infected control.* ***(B).*** *Graph showing the mean of the GFP% of HaCat cells infected and transfected with P.alecto NCAM compared to cells transfected with the empty vector. The GFP % corresponds to the RV-G bound to the transfected HaCaT cells.* ***(C).*** *Representative plaque morphology of infected HaCat cells expressing P.alecto NCAM. HaCaT cells were transfected with the P.alecto NCAM and empty vector, 48 hpt, cells were infected with the rVSV-dG-RV-G-FP (MOI=5). Thirty hpi, the viral supernatants were collected for quantifying the released progeny virus. The released viruses were quantified using plaque assay on BHK-21 cells after 72 hrs.* ***(D).*** *Graph showing the difference of the mean PFU/mL of rVSV-dG-RV-G-GFP between HaCaT cells transfected with P.alecto NCAM and HaCat cells transfected with empty vector. All the data represent the average of three biological replicates with S.E.M. using student's t-test. ns; non-significant; p>0.05, **p < 0.01.*

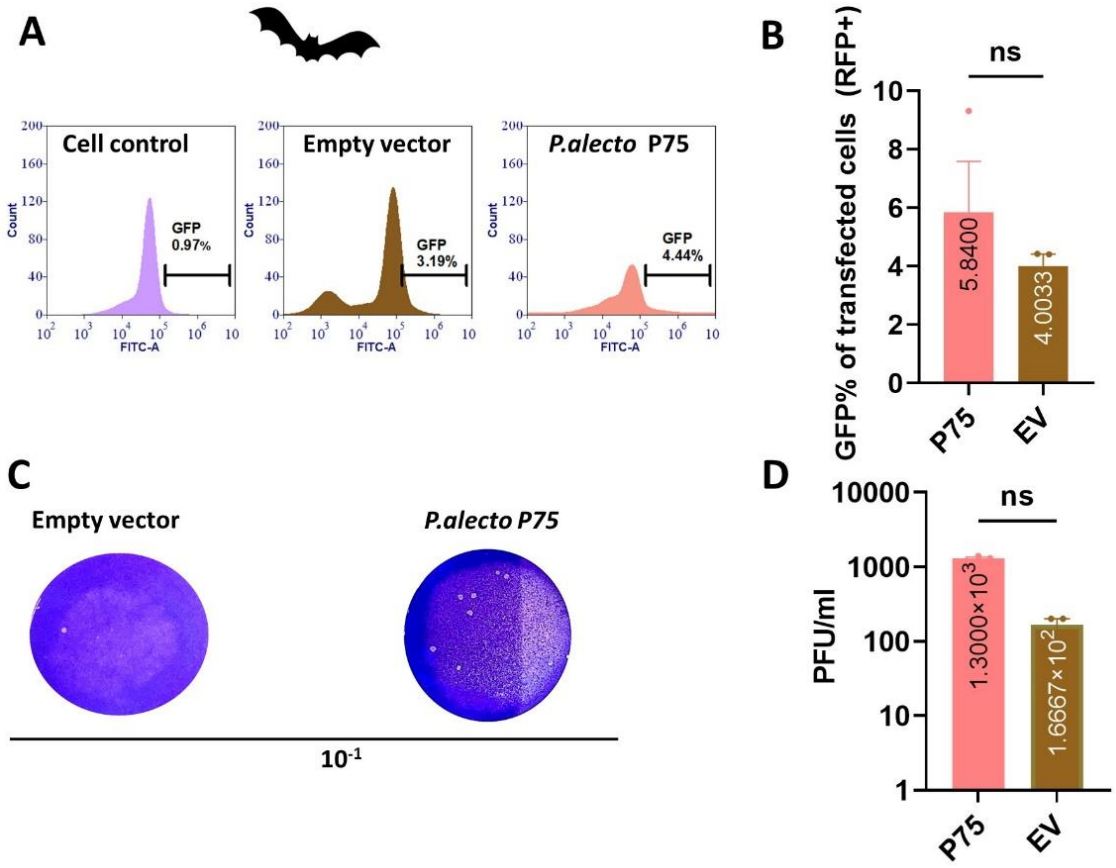

Figure 5.8 . Infectivity of rVSV-dG-RV-G-GFP on HaCaT cells transiently transfected with P.alecto p75.

(A). *Representative histograms showing the GFP % of rVSV-dG-RV-G-GFP infected HaCaT cells and transfected with P.alecto p75 (Right) and HaCaT cells transfected with empty vector(left). HaCaT cells were transfected with the P.alecto p75, 48 hpt, cells were infected with the rVSV-dG-RV-G-FP (MOI=5) for 2 hrs, then cells were collected and stained with anti-FLAG (targeting the FLAG-tagged receptor) and RV-G antibodies(targeting the virus RV-G), followed by staining with Alexa Fluor 568 and Alexa Fluor 468 antibodies, respectively for flow cytometry analysis. Flow cytometry data were analysed by FCS Express software. Cell control was used as non-infected control.* ***(B.).*** *Graph showing the mean of the GFP% of HaCat cells infected and transfected with P.alecto p75 compared to cells transfected with the empty vector. The GFP % corresponds to the RV-G bound to the transfected HaCaT cells.* ***(C).*** *Representative plaque morphology of infected HaCat cells expressing P.alecto p75. HaCaT cells were transfected with the P.alecto p75 and empty vector, 48 hpt, cells were infected with the rVSV-dG-RV-G-FP (MOI=5). Thirty hpi, the viral supernatants were collected for quantifying the released progeny virus. The released viruses were quantified using plaque assay on BHK-21 cells after 72 hrs.* ***(D).*** *Graph showing the difference of the mean PFU/mL of rVSV-dG-RV-G-GFP between HaCaT cells transfected with P.alecto p75 and HaCat cells transfected with empty vector. All experiments were performed three times (n=3) independently. All the data represent the average of three biological replicates with S.E.M. using student's t-test. ns; non-significant; p>0.05.*

5.2.1.3 Combinations of the mGluR2, ITGB1 and nAChR receptors enhanced binding to the RV-G and increased virus release.

Given that the overexpression of individual receptors in HaCaT cells did not lead to GFP observation upon infection with rVSV-dG-RV-G-GFP, which might indicate that their oover-expression were not sufficient. Thus, we further examined whether the simultaneous co-expression of two receptors would render HaCaT cells susceptible to infection by rVSV-dG-RV-G-GFP.

We introduced two receptors simultaneously into HaCaT cells at equal concentrations. Following a 48-hour post-transfection period, the cells were infected with rVSV-dG-RV-G-GFP at an MOI of 5. After 30 hours post-infection, no GFP expression was detected. Consequently, we employed a similar flow cytometry approach to quantify the binding of surface G protein to HaCaT cells expressing the combined receptors **(Figure 5.1).** The binding affinity of the RV-G was significantly higher in HaCaT cells ectopically expressing receptor combinations involving specifically mGluR2, ITGB1 and nAChR. receptors **(Figure 5.9-5.11 A-B**) compared to the empty vector negative control. While less binding was observed in combinations involving the ITGB1. similar enhanced viral release was demonstrated in the combinations with both the mGluR2 nAChR and ITGB1 **(Figures 5.9-5.11 C, D).** However, no significant difference from the empty vector control was observed. Likewise, the released virus progeny was significantly higher in HaCaT cells co-expressing mGluR2, nAChR and NCAM. The obtained findings supported that the enhanced virus entry and release are promoted when co-expressing receptors simultaneously, with ITGB1 playing a potential role in virus initial attachment.

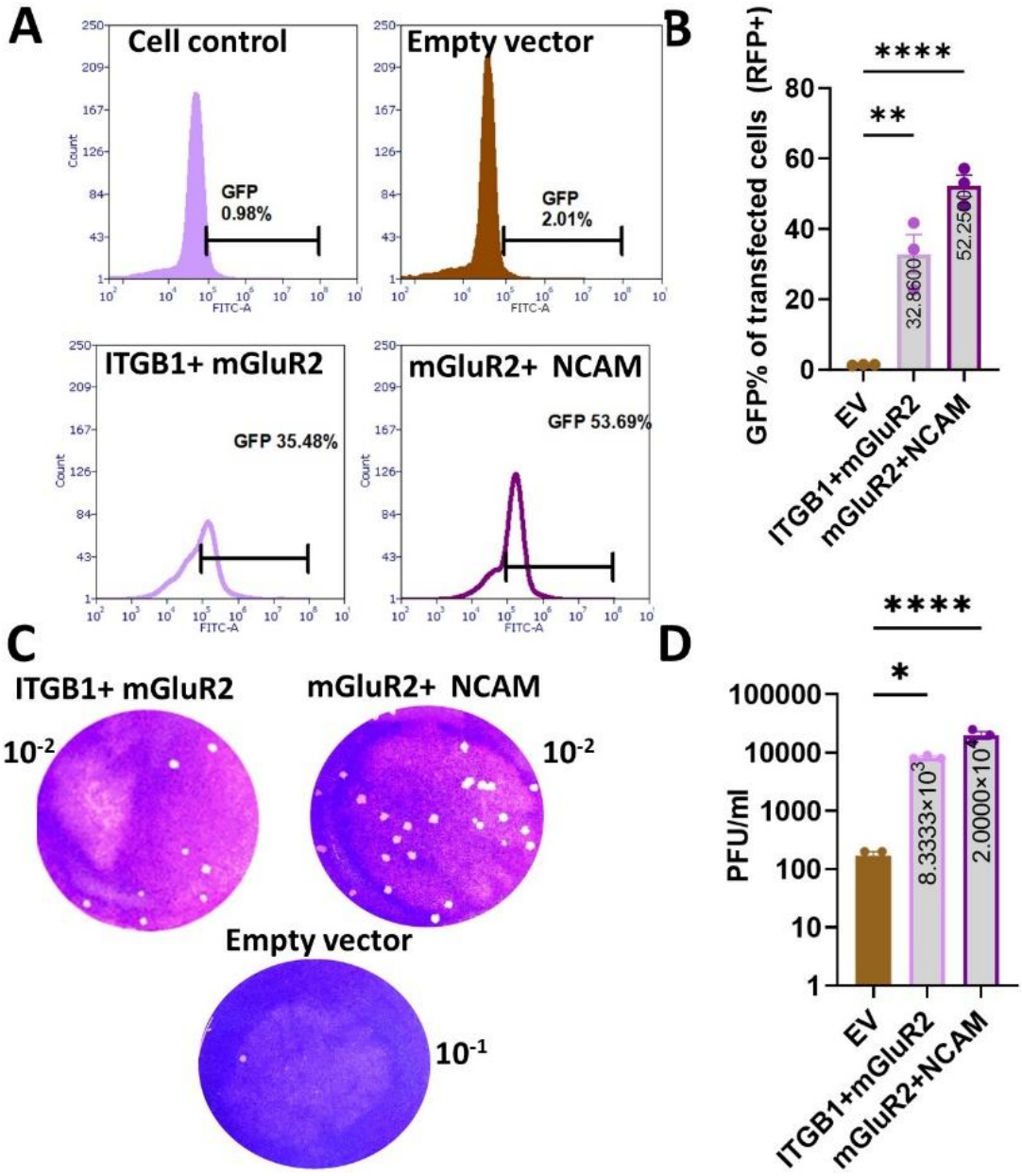

Figure 5.9 Infectivity of rVSV-dG-RV-G-GFP on HaCaT cells transiently transfected with P.alecto combined receptors (ITGB1+mGluR2) and (mGluR2+NCAM).

(A). *Representative histograms showing the GFP % of rVSV-dG-RV-G-GFP infected HaCaT cells and transfected with P.alecto (ITGB1+mGluR2) and (mGluR2+NCAM) (upper panel) and HaCaT cells transfected with empty vector (lower panel). HaCaT cells were transfected with the P.alecto (ITGB1+mGluR2) and (mGluR2+NCAM), 48 hpt, cells were infected with the rVSV-dG-RV-G-FP (MOI=5) for 2 hrs, then cells were collected and stained with anti-FLAG (targeting the FLAG-tagged receptor) and RV-G antibodies(targeting the virus RV-G), followed by staining with Alexa Fluor 568 and Alexa Fluor 468 antibodies, respectively for flow cytometry analysis. Flow cytometry data were analysed by FCS Express software. Cell control was used as non-infected control.* ***(B).*** *Graph showing the mean of the GFP% of HaCat cells infected and transfected with P.alecto (ITGB1+mGluR2) and (mGluR2+NCAM) compared to cells transfected with the empty vector. The GFP % corresponds to the RV-G bound to the transfected*

HaCaT cells. ***(C).*** *Representative plaque morphology of infected HaCat cells expressing P.alecto (ITGB1+mGluR2) and (mGluR2+NCAM). HaCaT cells were transfected with the P.alecto (ITGB1+mGluR2) and (mGluR2+NCAM) and empty vector, 48 hpt, cells were infected with the rVSV-dG-RV-G-FP (MOI=5). Thirty hpi, the viral supernatants were collected for quantifying the released progeny virus. The released viruses were quantified using plaque assay on BHK-21 cells after 72 hrs.* ***(D).*** *Graph showing the difference of the mean PFU/mL of rVSV-dG-RV-G-GFP between HaCaT cells transfected with P.alecto (ITGB1+mGluR2) and (mGluR2+NCAM) and HaCat cells transfected with empty vector. All experiments were performed three times (n=3) independently. All the data represent the average of three biological replicates with S.E.M. using one-way ANOVA. *P ≤ 0.05, **P ≤ 0.01, **** P ≤ 0.0001.*

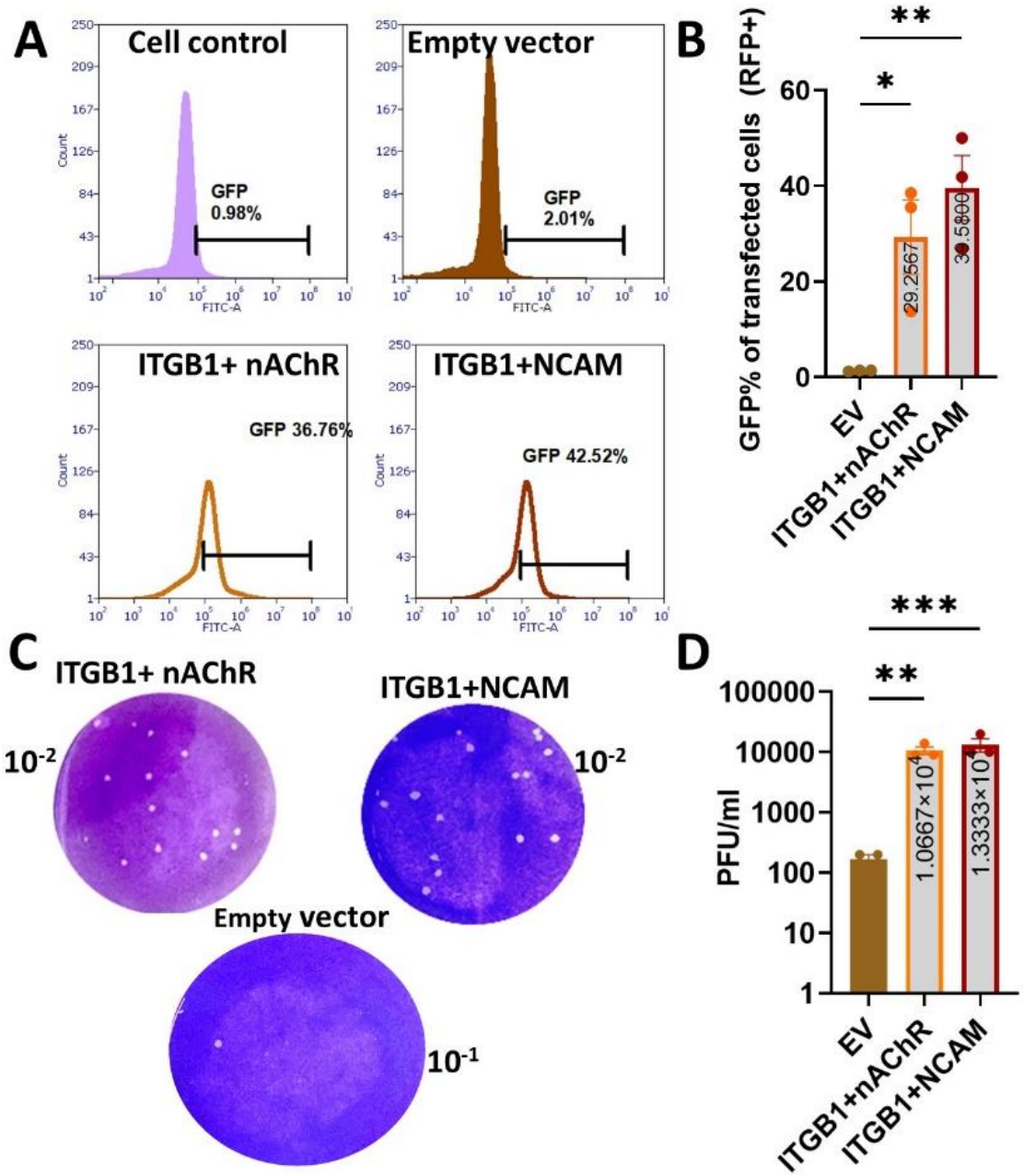

Figure 5.10 Infectivity of rVSV-dG-RV-G-GFP on HaCaT cells transiently transfected with P.alecto combined receptors (ITGB1+nAChR) and (ITGB1+NCAM)

(A). Representative *histograms showing the GFP % of rVSV-dG-RV-G-GFP infected HaCaT cells and transfected with P.alecto (ITGB1+nAChR) and (ITGB1+NCAM) (upper panel) and HaCaT cells transfected with empty vector (lower panel). HaCaT cells were transfected with the P.alecto (ITGB1+nAChR) and (ITGB1+NCAM), 48 hpt, cells were infected with the rVSV-dG-RV-G-FP (MOI=5) for 2 hrs, then cells were collected and stained with anti-FLAG (targeting the FLAG-tagged receptor) and RV-G antibodies(targeting the virus RV-G), followed by staining with Alexa Fluor 568 and Alexa Fluor 468 antibodies, respectively for flow cytometry analysis. Flow cytometry data were analysed by FCS Express software. Cell control was used as non-infected control* ***(B).*** *Graph showing the mean of the GFP% of HaCat cells infected and transfected with P.alecto (ITGB1+nAChR) and (ITGB1+NCAM) compared to cells transfected with the empty vector. The GFP % corresponds to the RV-G bound to the transfected HaCaT cells.* ***(C).*** *Representative plaque morphology of infected HaCat cells expressing P.alecto (ITGB1+nAChR) and (ITGB1+NCAM). HaCaT cells were transfected with the P.alecto (ITGB1+nAChR) and (ITGB1+NCAM) and empty vector, 48 hpt, cells were infected with the rVSV-dG-RV-G-FP (MOI=5). Thirty hpi, the viral supernatants were collected for quantifying the released progeny virus.The released viruses were quantified using plaque assay on BHK-21 cells after 72 hrs.* ***(D).*** *Graph showing the difference of the mean PFU/mL of rVSV-dG-RV-G-GFP between HaCaT cells transfected with P.alecto (ITGB1+nAChR) and (ITGB1+NCAM) and HaCat cells transfected with empty vector. All experiments were performed three times (n=3) independently. All the data represent the average of three biological replicates with S.E.M. using one-way ANOVA. *P ≤ 0.05, **P ≤ 0.01, *** P ≤ 0.001.*

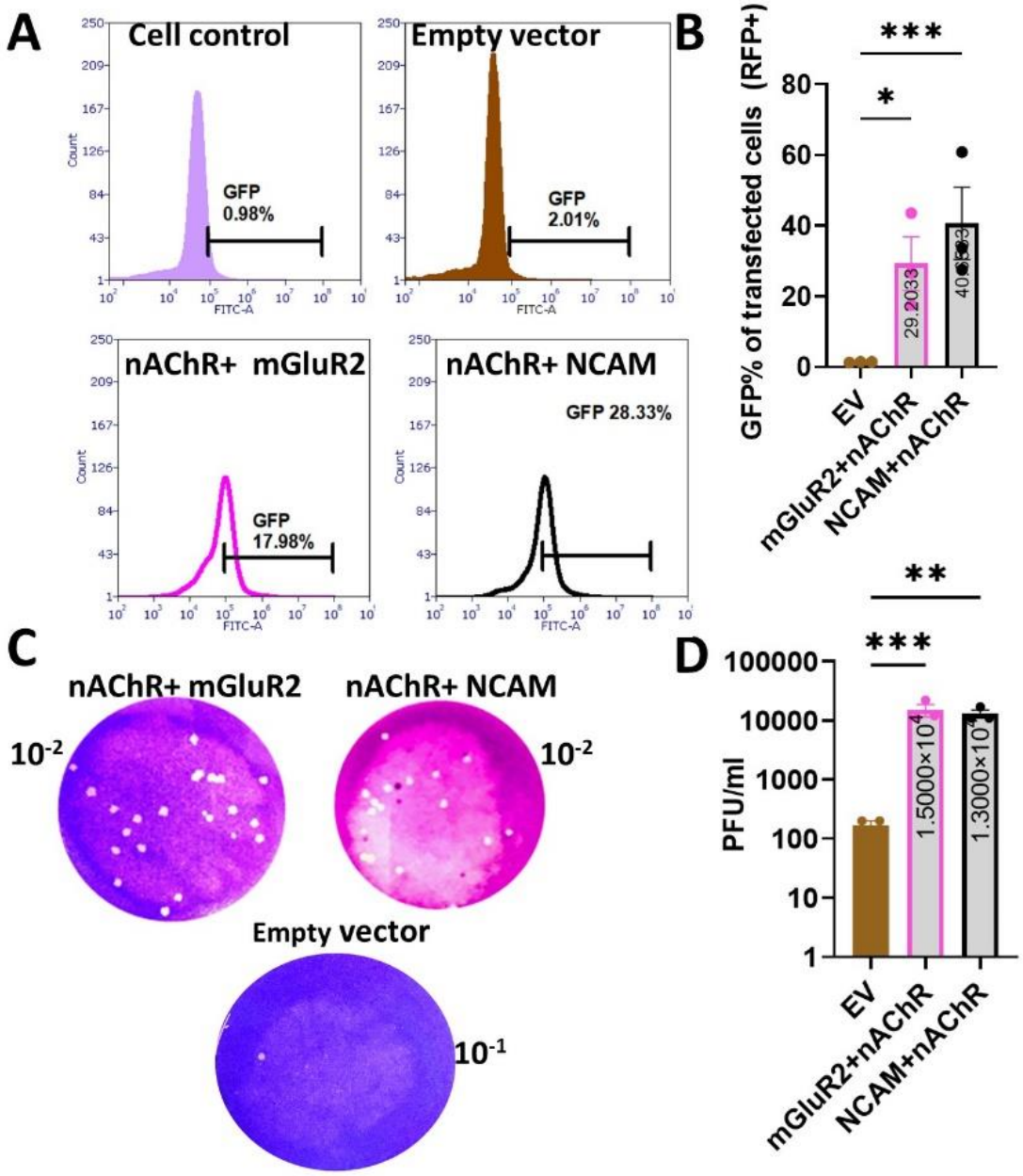

Figure 5.11 Infectivity of rVSV-dG-RV-G-GFP on HaCaT cells transiently transfected with P.alecto combined receptors (nAChR+mGluR2) and (nAChR+NCAM)

(A). *Representative histograms showing the GFP % of rVSV-dG-RV-G-GFP infected HaCaT cells and transfected with P.alecto (nAChR+mGluR2) and (nAChR+NCAM) (upper panel) and HaCaT cells transfected with empty vector (lower panel). HaCaT cells were transfected with the P.alecto (nAChR+mGluR2) and (nAChR+NCAM), 48 hpt, cells were infected with the rVSV-dG-RV-G-FP (MOI=5) for 2 hrs, then cells were collected and stained with anti-FLAG (targeting the FLAG-tagged receptor) and RV-G antibodies(targeting the virus RV-G), followed by staining with Alexa Fluor 568 and Alexa Fluor 468 antibodies, respectively for flow cytometry analysis. Flow cytometry data were analysed by FCS Express software. Cell control was used as non-infected control.* ***(B).*** *Graph showing the mean of the GFP% of HaCat cells infected and transfected with P.alecto (nAChR+mGluR2) and (nAChR+NCAM) compared to cells transfected with the*

empty vector. The GFP % corresponds to the RV-G bound to the transfected HaCaT cells. ***(C).*** *Representative plaque morphology of infected HaCat cells expressing P.alecto (nAChR+mGluR2) and (nAChR+NCAM). HaCaT cells were transfected with the P.alecto (nAChR+mGluR2) and (nAChR+NCAM) and empty vector, 48 hpt, cells were infected with the rVSV-dG-RV-G-FP (MOI=5). Thirty hpi, the viral supernatants were collected for quantifying the released progeny virus The released viruses were quantified using plaque assay on BHK-21 cells after 72 hrs.* ***(D).*** *Graph showing the difference of the mean PFU/mL of rVSV-dG-RV-G-GFP between HaCaT cells transfected with P.alecto (nAChR+mGluR2) and (nAChR+NCAM) and HaCat cells transfected with empty vector. All experiments were performed three times (n=3) independently. All the data represent the average of three biological replicates with S.E.M. using one-way ANOVA. *P ≤ 0.05, **P ≤ 0.01, *** P ≤ 0.001.*

5.2.1.4 Combinations with the p75 reduced the produced virus and RV-G binding to the cells compared to other combinations.

Co-expressing the RV receptors resulted in significantly enhanced virus binding and release on HaCaT cells. Nevertheless, when combined with p75, the receptor combinations exhibited non-significant binding affinity and released virus compared to the empty vector control **(Figure 5.12-5.13)**. These findings align with previous study which reported that the role of p75 in RV entry is non-essential (Tuffereau et al., 2007). However, it is worth noting that HaCaT cells co-expressing p75 with either mGluR2 or ITGB1 showed significantly higher binding affinity.

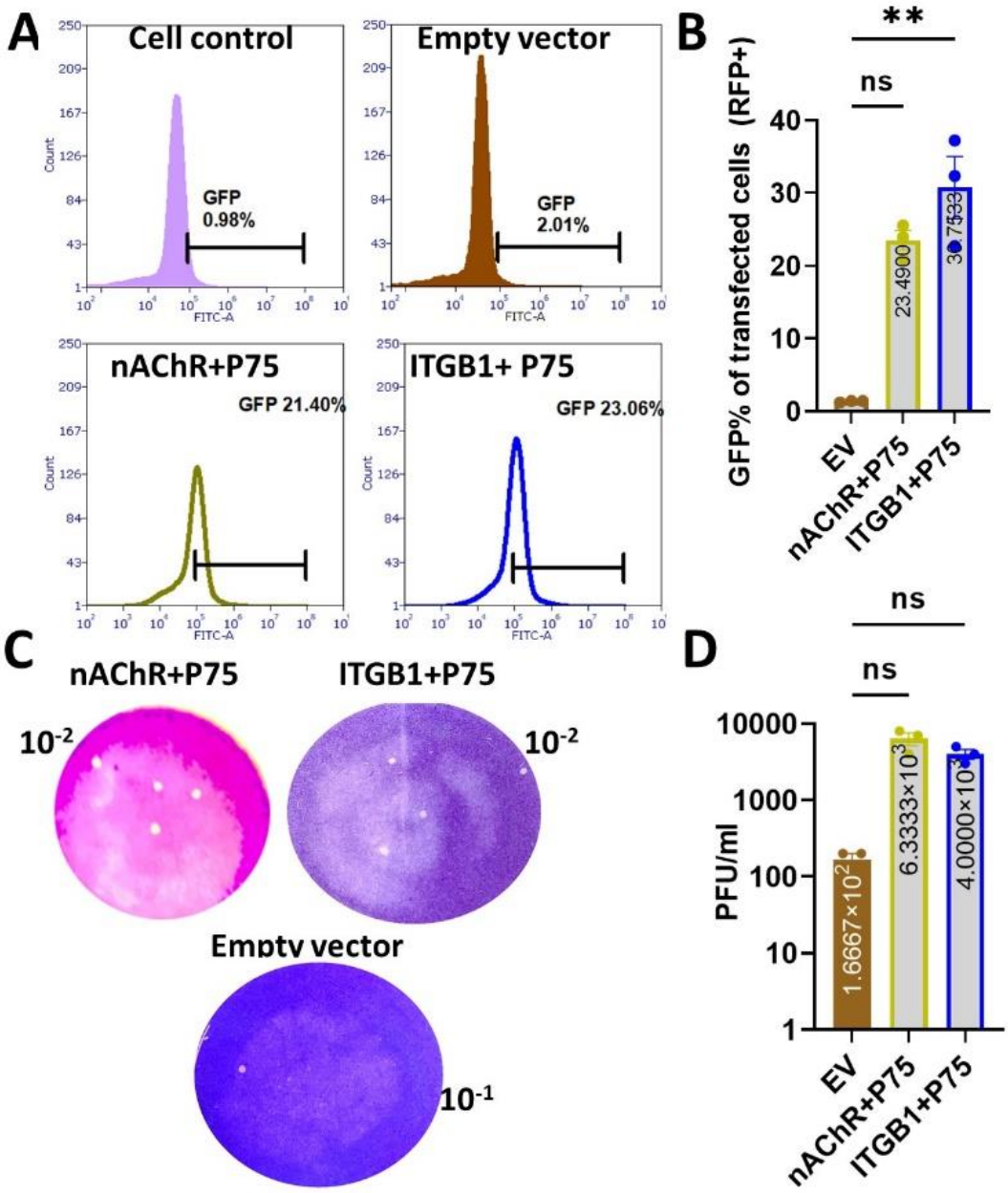

Figure 5.12 Infectivity of rVSV-dG-RV-G-GFP on HaCaT cells transiently transfected with P.alecto combined receptors (nAChR+p75) and (ITGB1+p75)

(A). *Representative histograms showing the GFP % of rVSV-dG-RV-G-GFP infected HaCaT cells and transfected with P.alecto (nAChR+p75) and (ITGB1+p75) (upper panel) and HaCaT cells transfected with empty vector (lower panel). HaCaT cells were transfected with the P.alecto (nAChR+p75) and (ITGB1+p75), 48 hpt, cells were infected with the rVSV-dG-RV-G-FP (MOI=5) for 2 hrs, then cells were collected and stained with anti-FLAG (targeting the FLAG-tagged receptor) and RV-G antibodies(targeting the virus RV-G), followed by staining with Alexa Fluor 568 and Alexa Fluor 468 antibodies, respectively for flow cytometry analysis. Flow cytometry data were analysed by FCS Express software. Cell control was used as non-infected control.* ***(B).*** *Graph showing the mean of the GFP% of HaCat cells infected and transfected with P.alecto (nAChR+p75) and (ITGB1+p75) compared to cells transfected with the empty vector. The GFP*

% corresponds to the RV-G bound to the transfected HaCaT cells. ***(C).*** *Representative plaque morphology of infected HaCat cells expressing P.alecto (nAChR+p75) and (ITGB1+p75). HaCaT cells were transfected with the P.alecto (nAChR+p75) and (ITGB1+p75) and empty vector, 48hpt, cells were infected with the rVSV-dG-RV-G-FP (MOI=5). Thirty hpi, the viral supernatants were collected for quantifying the released progeny virus The released viruses were quantified using plaque assay on BHK-21 cells after 72 hrs.* ***(D).*** *Graph showing the difference of the mean PFU/mL of rVSV-dG-RV-G-GFP between HaCaT cells transfected with P.alecto (nAChR+p75) and (ITGB1+p75) and HaCat cells transfected with empty vector. All experiments were performed three times (n=3) independently. All the data represent the average of three biological replicates with S.E.M. using one-way ANOVA. ns; non-significant; p>0.05, **P ≤ 0.01.*

.

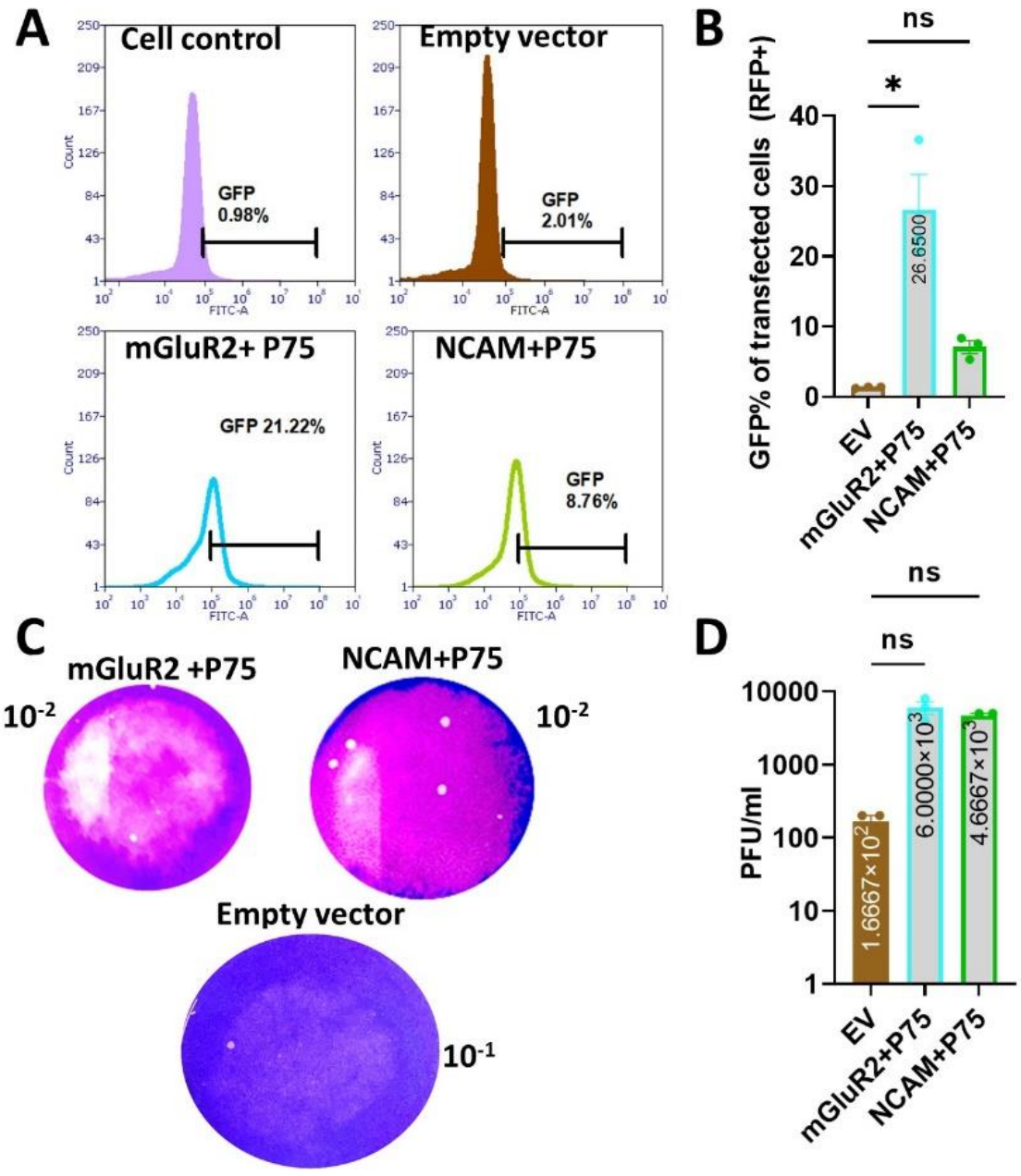

Figure 5.13 Infectivity of rVSV-dG-RV-G-GFP on HaCaT cells transiently transfected with P.alecto combined receptors (mGluR2+p75) and (NCAM+p75)

(A). *Representative histograms showing the GFP % of rVSV-dG-RV-G-GFP infected HaCaT cells and transfected with P.alecto (mGluR2+p75) and (NCAM+p75) (upper panel) and HaCaT cells transfected with empty vector (lower panel). HaCaT cells were transfected with the (mGluR2+p75) and (NCAM+p75), 48 hpt, cells were infected with the rVSV-dG-RV-G-FP (MOI=5) for 2 hrs, then cells were collected and stained with anti-FLAG (targeting the FLAG-tagged receptor) and RV-G antibodies(targeting the virus RV-G), followed by staining with Alexa Fluor 568 and Alexa Fluor 468 antibodies, respectively for flow cytometry analysis. Flow cytometry data were analysed by FCS Express software. Cell control was used as non-infected control.* ***(B).*** *Graph showing the mean of the GFP% of HaCat cells infected and transfected with P.alecto (mGluR2+p75) and (NCAM+p75) compared to cells transfected with the empty vector. The GFP % corresponds to the RV-G bound to the transfected HaCaT cells.* ***(C).*** *Representative plaque morphology of infected HaCat cells expressing P.alecto (mGluR2+p75) and (NCAM+p75). HaCaT cells were transfected with the P.alecto (mGluR2+p75) and (NCAM+p75) and empty vector, 48hpt, cells were infected with the rVSV-dG-RV-G-FP (MOI=5). Thirty hpi, the viral supernatants were collected for quantifying the released progeny virus The released viruses were quantified using plaque assay on BHK-21 cells after 72 hrs.* ***(D).*** *Graph showing the difference of the mean PFU/mL of rVSV-dG-RV-G-GFP between HaCaT cells transfected with P.alecto (mGluR2+p75) and (NCAM+p75) and HaCat cells transfected with empty vector. All experiments were performed three times (n=3) independently. All the data represent the average of three biological replicates with S.E.M. using one-way ANOVA. ns; non-significant; p>0.05, *P ≤ 0.05.*

5.2.1.5 Combinations with ITGB1, mGluR2 enhanced viral replication.

The findings from the expression of individual and combined RV receptors in HaCaT cells were summarized using a heat map **(Figure 5.14 A-B).** The combinations involving mGluR2, ITGB1, and nAChR exhibited increased binding with the RV surface glycoprotein. While combinations with the p75 receptor resulted in reduced production of viral particles and demonstrated the lowest binding to RV-G. Additionally, the significant increase in the progeny virus was achieved through combinations involving the mGluR2, nAChR and NCAM. The ectopic expression of either the nAChR or mGluR2 receptors individually, significantly enhanced the binding capacity with the RV-G, even exceeding the affinity observed in the co-expression of receptors. However, none of these receptors were able to render HaCaT cells susceptible to infection through observation of a GFP signal.

Considering that our study primarily focuses on RV entry, the selection of ITGB1, mGluR2, and nAChR receptors for further studies was based on their potential role for

promoting RV-G entry. Further investigation into their specific roles in RV entry will be conducted through knockout studies.

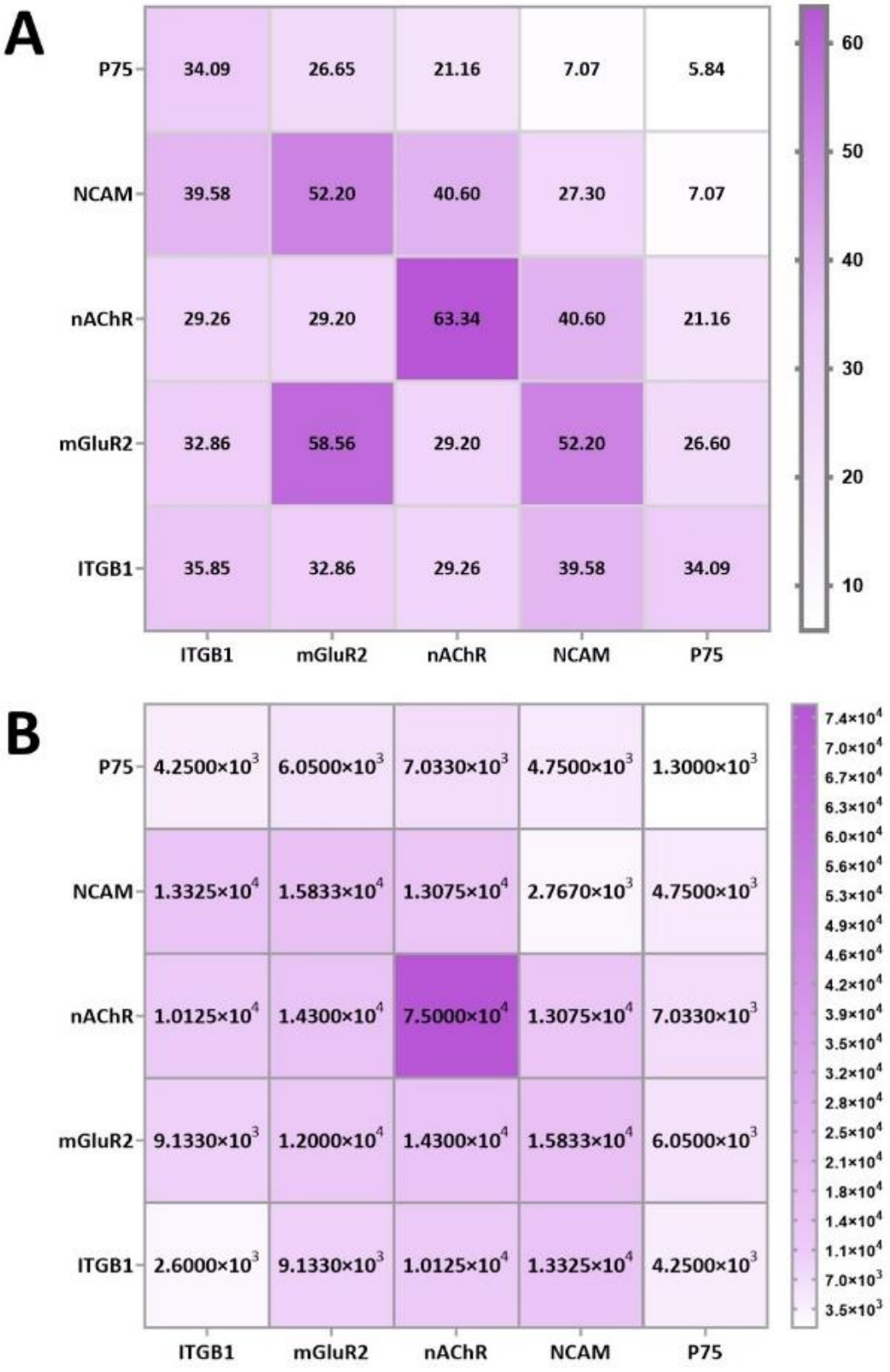

Figure 5.14 Heat maps summarizing the plaque assay and RV-G binding to HacaT cells expressing P.alecto receptors.

(A) *The Mean RV-G binding percentage of the rVSV-dG-RV-G-GFP to HaCaT cells transiently expressing individual or combined P.alecto receptors.* ***(B).*** *The mean PFU/mL of rVSV-dG-RV-G-GFP upon expressing individual and combinatorial P.alecto receptors on HaCaT cells.*

5.2.2 Knockout the RV receptor genes

5.2.2.1 The human A549 cell line selected for knockout studies.

The second approach we employed for elucidating the exact role of each of the RV receptors in RV replication was to generate KO cell line devoid of each of the ITGB1, mGluR2 and nAChR receptors. The choice to knockout those three receptors was based on the results obtained from the receptor preference experiments on HaCaT cells **(Section 5.2.1)**. In which the ectopic expression of those three receptors showed the significantly highest binding affinity to the RV-G and resulted in more virus release compared to the cells expressing NCAM and p75 receptors. Prior to performing the knockout strategy, we tested the levels of the endogenous expression of the RV receptor genes in A549 cells which was susceptible to rVSV-dG-RV-G-GFP infection **(Figure 5.15. A)**. We assessed the transcription profiles of the RV receptor genes in infected and non-infected A549 cell line. Down modulation of the mRNA levels corresponding to ITGB1, mGluR2, nAChR and p75 genes was observed 24 hrs post infection with the rVSV-dG-RV-GFP. However, the mRNA levels of NCAM remained unchanged. These results suggested the susceptibility of the A549 human cells to RV infection which renders it an ideal cell line to study the functional effect of knocking out of ITGB1, mGluR2 and nAChR receptors on the susceptibility to RV infection.

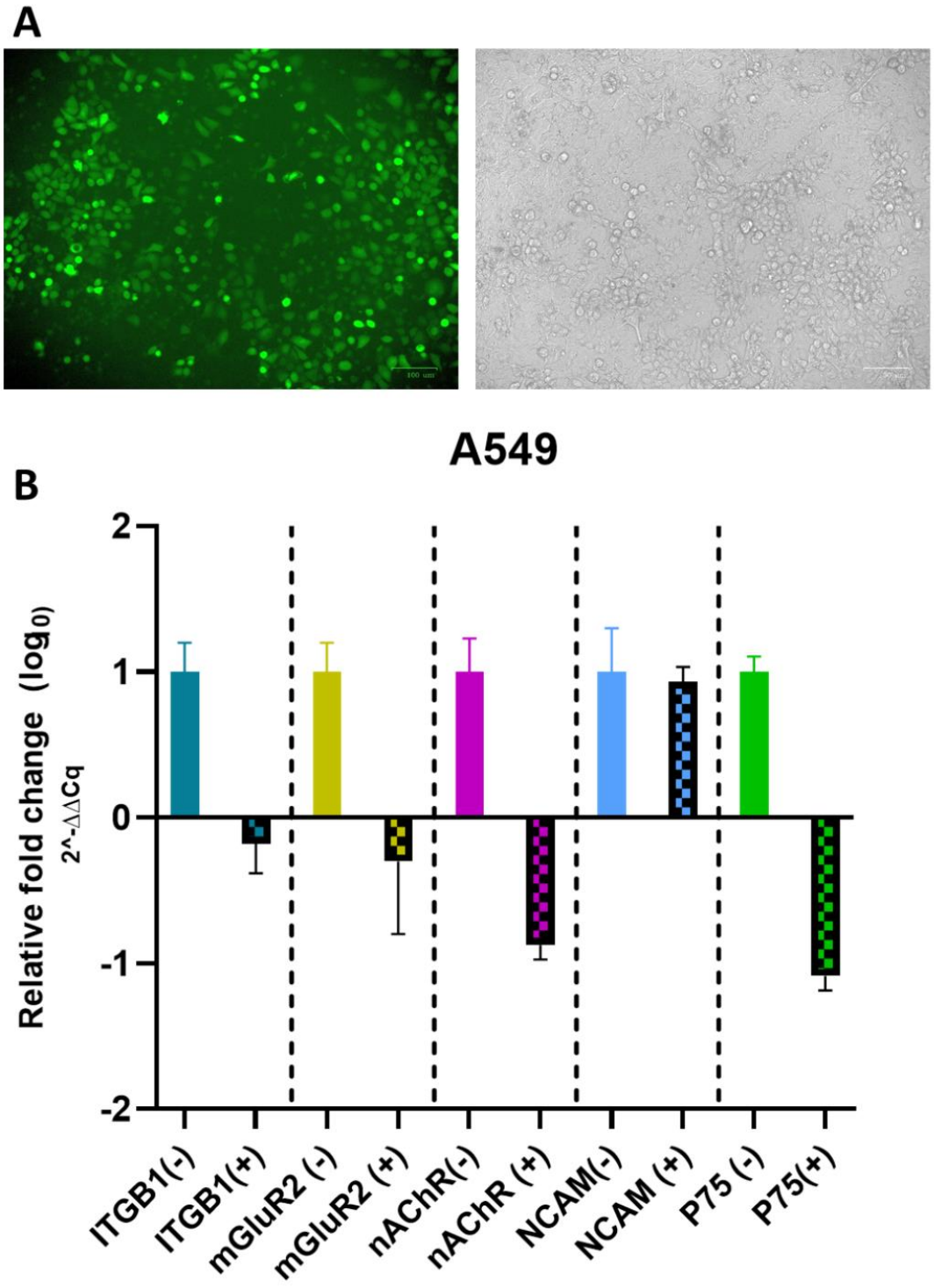

Figure 5.15. Relative expression (in fold change value) of RV cellular receptor genes on A549 cells

(A). *Microscopic images of infected A549 cells green (left), bright (right). A549 cells were infected with rVSV-dG-RV-G-GFP (MOI 5), 24 hpi, cells were imaged for the GFP expression corresponding to virus replication.* ***(B).*** *The differential expression (in fold change) of the RV cellular genes were measured by qRT-PCR on A549 cells before (-) and after infection (+) with rVSV-dG-RV-G-GFP. Twenty-four hrs after infection, cellular RNA was extracted from infected and non-infected A549 cells. The relative RNA*

expression (mean ± SEM) of each of RV receptor gene were normalised to human beta actin using ΔΔCt method. The experiment was performed three times (n=3) independently. Error bars represented the SEM from three biological replicates.

5.2.2.2 Generation of mGluR2 KO cell line

Recent study has reported the effect of the knocking down the mRNA levels of mGluR2 in reducing the ERA-GFP strain replication levels (Wang et al., 2018). Herein, we attempt to investigate if complete deletion of the mGluR2 gene would still allow the rVSV-dG-RV-G-GFP replication in A549 cells, adopting the CRISPR/Cas9 mediated knockout strategy. To this aim, we designed a single guide RNA (sgRNA) targeting the second exon of the mGluR2 **(Figure 5.16.)**. The cloning of the sgRNA in the PX459 V2.0 vector allowed simultaneous expression of the Cas9 endonuclease and the sgRNA upon transfection in the in A549 cells **(Chapter 9, Supplementary Figure 18).** Analysis of the generated mGluR2 KO and WT A549 genomic DNA from cells clones was carried out initially by amplifying the genomic sequence flanking 200 bases upstream and 200 bases downstream the designed sgRNA. A difference in the band size was observed between the amplified genomic DNA of KO cells (clone 3.2) compared to the WT cell clones (482 bp) **(Figure 5.16 A).** Owing to the unavailability of the commercial antibodies specific to the mGluR2 protein, validation of the KO cells was carried out through sequence analysis. Subsequently, we sequenced the PCR products to compare the sequence difference between the KO cell clone and WT cells. Analysis of the sanger sequence revealed that various indels events occurred in exon 2 downstream the PAM (Protospacer Adjacent Motif) sequence **(Figure 5.16 C).** The resulted indels included clones with deleted nucleotides and other clones showed inserted nucleotides compared to the WT sequence with a score of 31% indels as determined by TIDE analysis. Among the introduced indels was the deletion of one nucleotide, which resulted in six amino acids substitution in the KO compared to the WT cells **(Figure 5.16 D-E).**

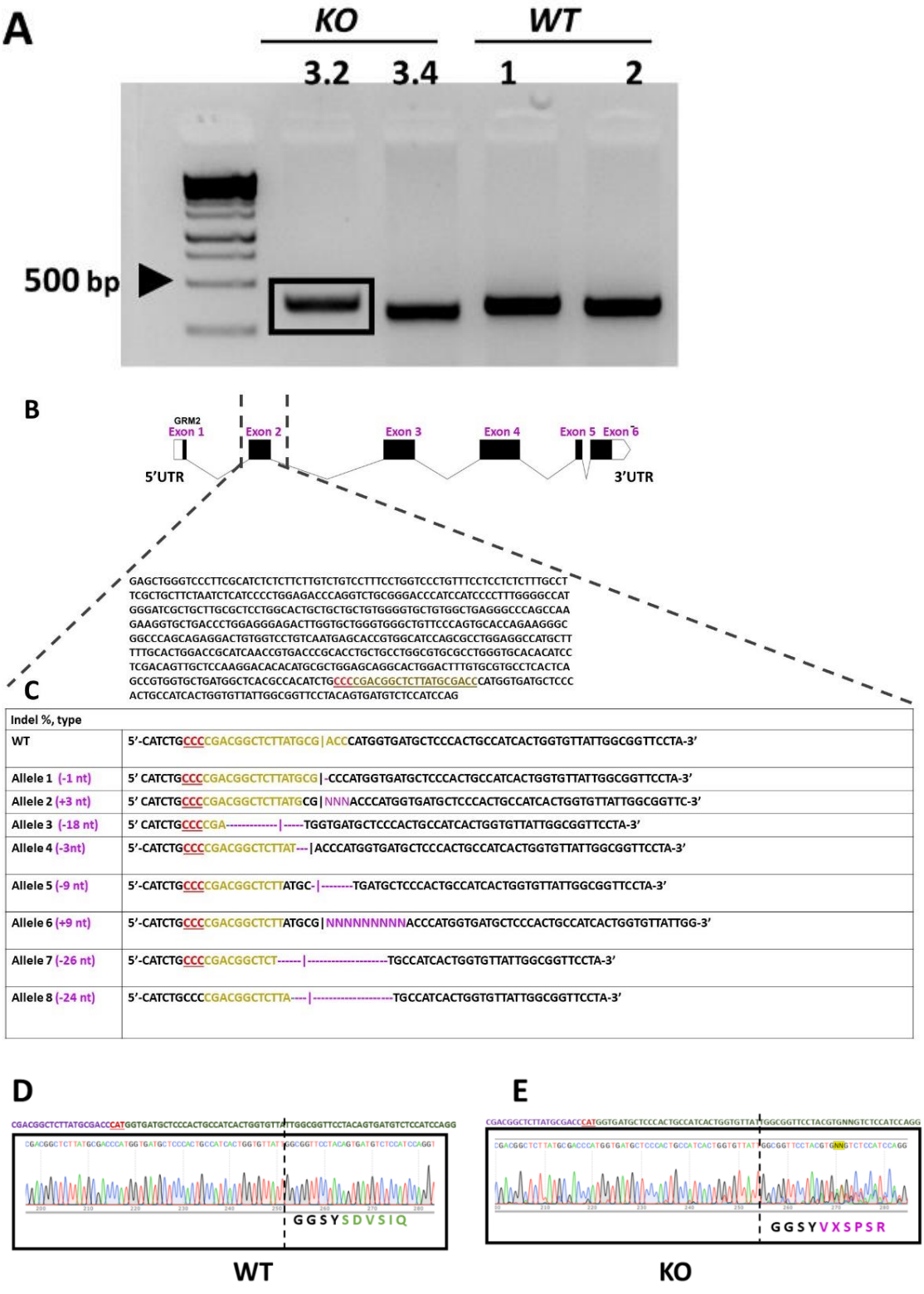

Figure 5.16 Generation and validation of the A549 mGluR2 KO through CRISPR/Cas9 targeting exon 2 mGluR2.

(A). *Agarose gel electrophoresis showing the PCR products amplified by primers encompassing the CRISPR gRNA target in exon 2 of human mGluR2. The genomic DNA from the single-cell clones of A549 KO mGluR2 cells (clone 3.2, clone 3.4) and WT cells (clone 1, clone 2) was extracted and amplified with primers flanking*

the region of the gRNA sequence. The PCR products were shown on the gel electrophoresis, indicating a difference in band size of the KO cell clone 3.2 compared to the WT cell .1 kb DNA ladder (left). ***(B).*** *Schematic diagram showing the genomic organization of human mGluR2 intron-exon.* ***(C)****. A table summarizing the number of alleles resulting from the introduced indels in mGluR2 exon 2 regions obtained from the sequence analysis of the amplicons corresponding to clone 3.4(KO) and WT (clone 1). The underlined sequence corresponds to the sequence in which indels were introduced. Amino acid difference between* ***(D).*** *WT allele and* ***(E).*** *The KO cell (clone 3.4) was highlighted. The alleles resulted from the introduced indels in mGluR2 exon 2 regions. The PAM site is indicated in red letters, the gRNA sequence is represented in yellow letters, and Magenta represents the indels introduced (deletions or insertion of bases). Validation of cloning ghumGluR2 in PX459 V2.0 is shown in Chapter 9, Supplementary Figure 18.*

5.2.2.3 A549 KO mGluR2 cell reduced the rVSV-dG-RV-G-GFP entry.

To determine to which extent the mGluR2 KO cells would support rVSV-dG-RV-G-GFP infection, mGluR2 KO, mGluR2 KO cells over expressing the human mGluR2 or empty vector and WT A549 cells were infected with rVSV-dG-RV-G-GFP at MOI of 5, KO uninfected cell control was employed. After 30 hr, GFP was observed in both KO and WT cells, however less signal was clearly observed in KO cells **(Figure 5.17 A)**. The percentage of the internalized virus was measured by flow cytometry analysis which showed significantly lower GFP percentage in KO cells compared to the WT. The ectopic expression of humGluR2 in mGluR2 KO resulted in significantly higher levels of the internalized virus compared to the KO infected cells **(Figure 5.17 B-C).** Comparing the levels of the released virus particles, indicated the significant inhibition of the rVSV-dG-RV-G-GFP replication in KO cells by 5-fold compared to the WT cells **(Figure 5.18 A-B).** Interestingly, the expression of humGluR2 in KO cells was capable of restoring the viral replication as the WT cells with significantly increased levels compared to the KO cells (**Figure 5.18 A-B).** To dissect at which stage of RV replication the mGluR2 is required, an entry assay was performed to compare the entry of rVSV-dG-RV-G-GFP on mGluR2 KO cells and mGluR2 KO cells ectopically expressing the human mGluR2 protein. Employing flow cytometry analysis in which the binding of RV-G was compared, it was observed that KO cells allowed initial binding of the RV-G which was significantly less in KO cells compared to KO cells expressing humGluR2. (**Figure 5.18 C-D).** Overall, the depletion of the mGluR2 levels from the A549 cell significantly reduced the replication and attachment ability of the virus glycoprotein to the cells. These results indicate the

potential role of the mGluR2 in rVSV-dG-RV-G-GFP entry and replication, yet its absence did not result in complete inhibition of virus replication.

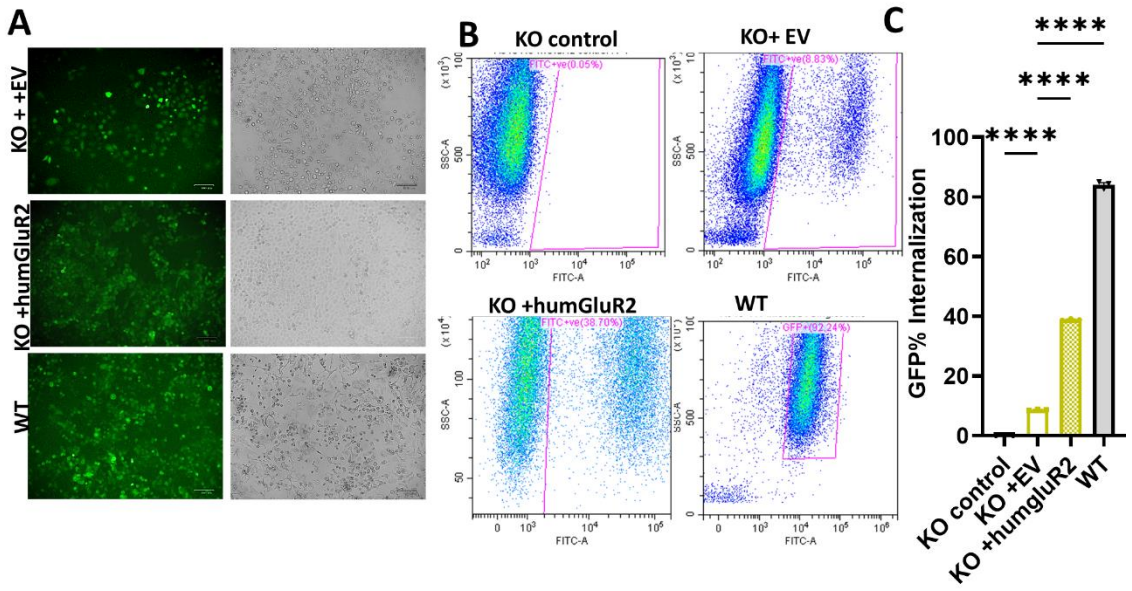

Figure 5.17 Replication of rVSV-dG-RV-G-GFP on mGluR2 KO cells.

(A). *Representative microscopic fields green (left), bright (right) for A549 KO mGluR2 cells infected with rVSV-dG-RV-G-GFP MOI=5. A549 KO mGluR2 cells, were transfected with empty vector and human mGluR2 FLAG vector; respectively, after 48h, cells were infected with rVSV-dG-RV-G-GFP (MOI=5). Thirty hpi, the GFP percentage corresponding to virus replication were imaged, The WT A549 cells were used as infection control* ***(B).*** *Representative flow cytometry plots of the mGluR2 KO cells transiently transfected with empty vector and human mGluR2 FLAG vectors; respectively. Forty-eight hrs post transfections, cells were infected with rVSV-dG-RV-G-GFP at MOI=5. Thirty hpi, the cells were collected and analysed for GFP percentage using flow cytometry analysis, the KO control cells were used as non-infected control, and the WT A549 cells were used as infection control.* ***(C).*** *Graph showing the mean of the GFP% of mGluR2 KO cells transiently transfected with empty vector and human mGluR2 FLAG vectors; respectively. The KO control cells were used as, non-infected control and the WT A549 cells were used as infection control. The GFP% corresponds to the internalized virus. All experiments were performed three times (n=3) independently. Error bars represent the SEM of three biological replicate samples. using one-way ANOVA. **** $P \leq 0.0001$.*

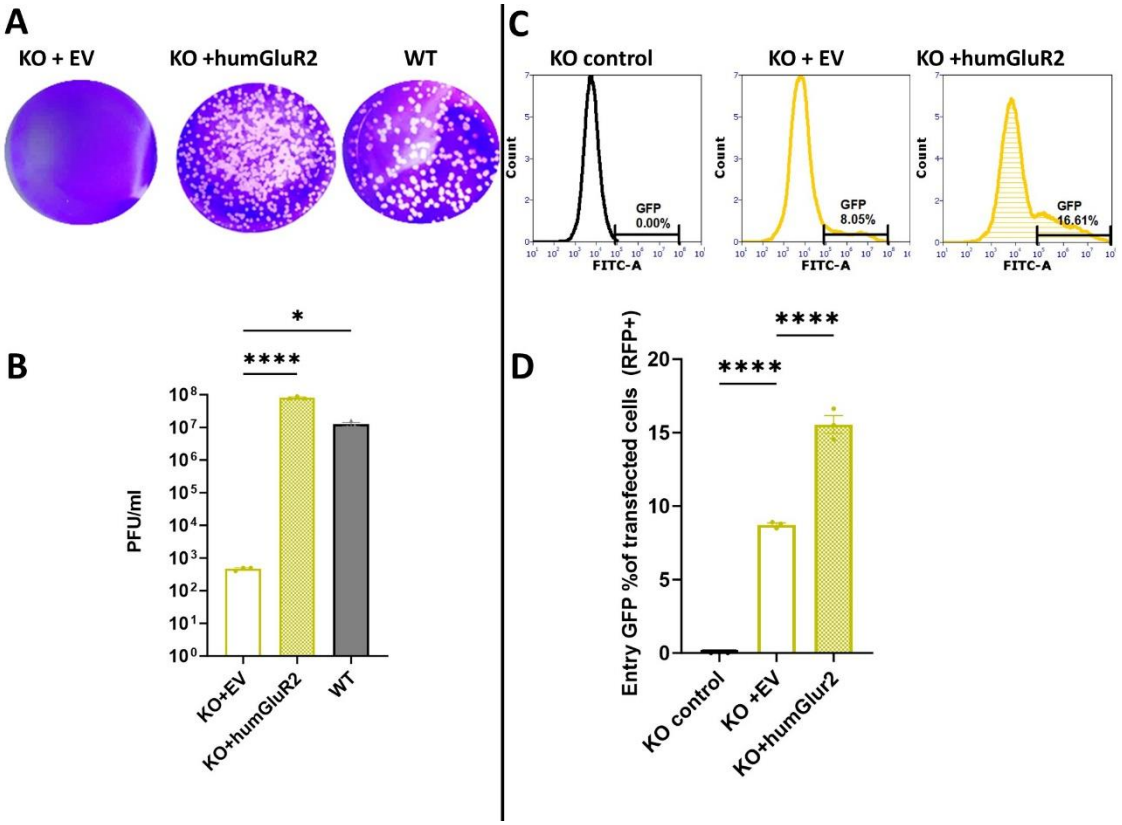

Figure 5.18 Replication and entry of rVSV-dG-RV-G-GFP on mGluR2 KO cells.

(A). *Representative plaque morphology of the A549 KO mGluR2 cells infected with rVSV-dG-RV-G-GFP. The A549 KO mGluR2 cells were transiently transfected with the empty vector and human mGluR2 FLAG, respectively. Forty-eight hr post-transfection, cells were infected with the rVSV-dG-RV-G-GFP MOI=5. Thirty hpi, the viral supernatants were collected for quantifying the released progeny virus. The released viruses were quantified using plaque assay on BHK-21 cells after 72 hrs.* ***(B).*** *Graph showing the difference of the mean PFU/mL of rVSV-dG-RV-G-GFP between A549 mGluR2 KO cells transfected with either EV or human mGluR2 FLAG, the WT A549 cells were used as infection control.* ***(C).*** *Representative histograms showing the GFP % of rVSV-dG-RV-G-GFP infected A549 KO mGluR2 cells. The A549 KO mGluR2 cells were transiently transfected with the empty vector and human mGluR2 FLAG; respectively. Forty-eight hr post-transfection, cells were infected with the rVSV-dG-RV-G-GFP MOI=5 for 2 hrs. After washing with PBS, for removal of unbound virus, cells were collected and stained with anti-FLAG (targeting the FLAG-tagged receptor) and RV-G antibodies (targeting the virus RV-G), followed by staining with Alexa Fluor 568 and Alexa Fluor 468 conjugated antibodies, respectively for flow cytometry analysis. Flow cytometry data were analysed by FCS Express software****. (D.).*** *Graph showing the mean of the GFP% of A549 KO mGluR2 cells infected and transfected with EV and human mGluR2 vector, KO control was used as non-infected control The entry GFP % corresponds to the RV-G bound to the transfected A549 KO mGluR2 cells. All experiments were performed three times (n=3) independently. Data represent the average of three biological replicates with S.E.M. using one-way ANOVA. *, P ≤ 0.05, ****, P ≤ 0.0001.*

5.2.2.4 Generation of ITGB1 KO cells

ITGB1 is known to be a crucial cellular factor for RV peripheral entry (Shuai et al., 2020). To evaluate the function of ITGB1 during RV replication, we adopted the CRISPR/Cas9 mediated knockout technology. A sgRNA targeting the fourth exon of ITGB1 gene was designed **(Figure 5.19)** and cloned in the PX459 V2.0 vector to allow the delivery of both the sgRNA and Cas9 into the A549 cells **(Chapter 9, Supplementary Figure 19)**. Single cell colonies were obtained through the dilution technique and characterized. Upon extraction of the genomic DNA of the single cell KO clone and WT cells, the region encompassing the sgRNA was amplified and run on agarose gel. A smaller band of the KO single cell clone compared to the WT (513 bp) was observed **(Figure 5.19 A).** Further PCR sequencing of the ITGB1 single cell clones originated from KO A549 cells analysis showed the derivation of two CRISPR indels in the KO single cell clones. The deletion generated two different alleles with deletion of either three bases or twenty bases induced in the targeted fourth exon of ITGB1. Subsequently, the introduced deletions resulted in thirteen amino acids different from the WT allele. The resulted indels included clones with deleted nucleotides compared to the WT sequence with a score of 54.5% indels as determined by TIDE analysis **(Figure 5.19 B-E).**

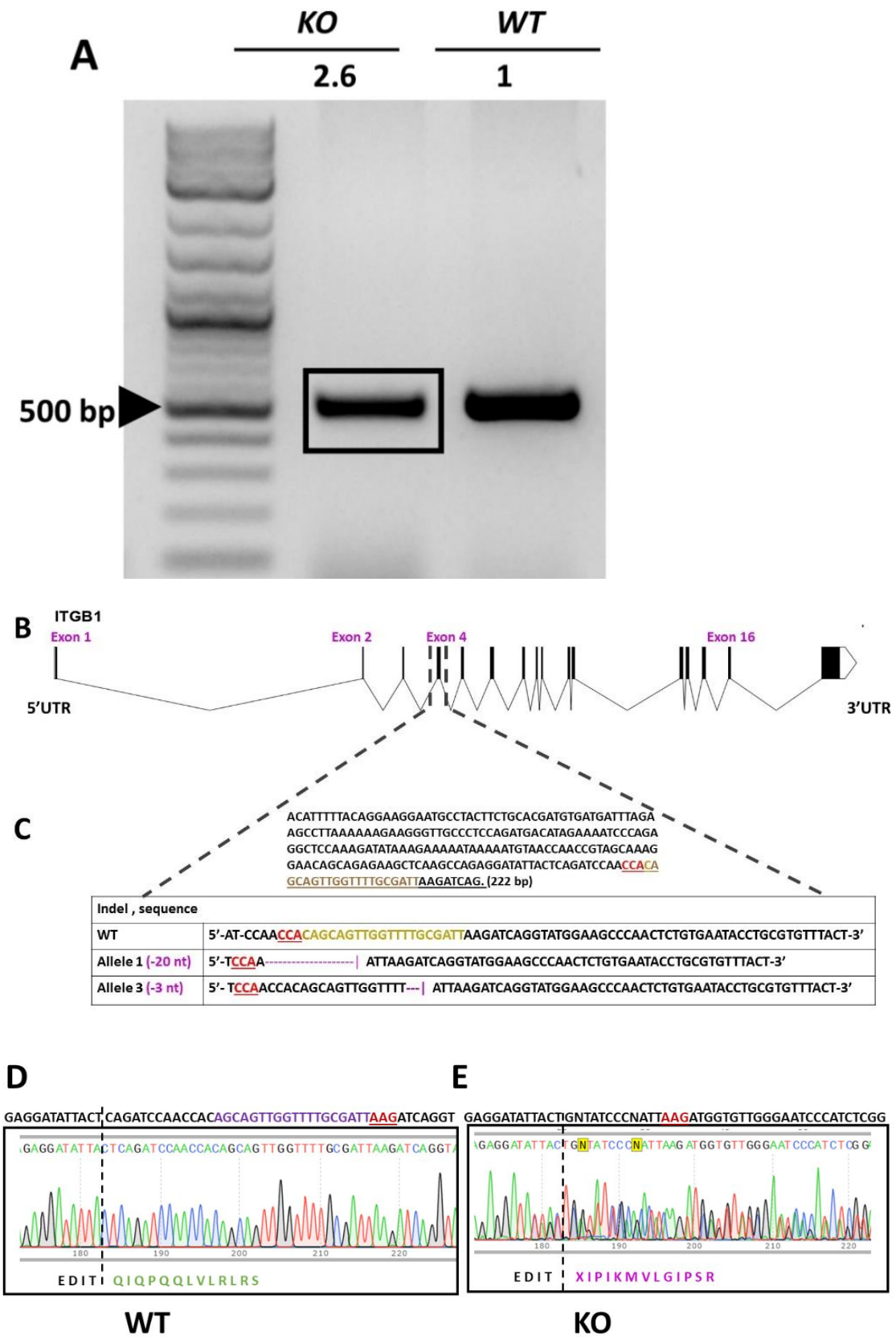

Figure 5.19 Generation and validation of the A549 ITGB1 KO through CRISPR/Cas9 targeting exon 4 ITGB1.

(A) *Agarose gel electrophoresis showing the PCR products amplified by primers encompassing the CRISPR gRNA target in exon 4 of human ITGB1. The genomic DNA from the single cell clones of A549 KO ITGB1 cells (clone 2.6) and WT cells (clone 1) was extracted and amplified with primers flanking the region of the gRNA sequence. The PCR products were shown on the gel electrophoresis, indicating a smaller band in KO cell clone 2.6 compared to WT cell clone, 1 kb DNA plus ladder (left)* ***(B).*** *Schematic diagram showing the genomic organization of human ITGB1 intron-exon.* ***(C).*** *A table summarizing the number of alleles resulting from the introduced indels in ITGB1 exon 4 regions obtained from the sequencing analysis of the amplicons corresponding to clone 2.6(KO) and WT (clone 1). The underlined sequence corresponds to the sequence in which indels were introduced. Amino acid difference between* ***(D).*** *WT allele and* ***(E).*** *The KO cell clone (2.6) was highlighted. The alleles resulted from the introduced indels in ITGB1 exon 4 regions. The PAM site is indicated in red letters, the gRNA sequence is represented in yellow letters, and the Magenta represents the indels introduced (deletions or insertion of bases). Validation of cloning the ghuITGB1 in PX459 V2.0 is shown in Chapter 9, Supplementary Figure 19.*

5.2.2.5 Entry of the of rVSV-dG-RV-G-GFP on ITGBI KO cells was impaired.

Functional studies were carried out to further elucidate the potential impact of the ITGB1 absence in rVSV-dG-RV-G-GFP replication on A549 KO ITGB1 cells. The ITGB1 KO cell, ITGB1 KO cells over expressing the human ITGB1 cDNA together with the WT A549 cells were infected with rVSV-dG-RV-G-GFP (MOI 5) for 24 hr, KO uninfected cell control was employed. Next, we evaluated the rVSV-dG-RV-G-GFP infectivity on the cells through visualizing and measuring the GFP percentage. A significant reduction in the GFP percentage was shown in infected KO cells compared to the WT cells. Also, GFP levels were non significantly different from the uninfected KO control. Over expressing the human ITGB1 in KO cells showed increase in the GFP levels, however, the GFP expression levels remained non significantly different from the infected KO cells not expressing the ITGB1 **(Figure 5.20 A-C).** Three-fold reduction in the released progeny virus was observed in KO cells, which was significantly less compared to WT cells However, the over expression of huITGB1 was capable of recapitulating the rVSV-dG-RV-G-GFP replication as in the WT cells **(Figure 5.21 A-B).** To test if the KO of ITGB1 affect the attachment of the rVSV-dG-RV-G-GFP to the cells, we infected ITGB1 KO and ITGB1 KO cells expressing huITGB1 with rVSV-dG-RV-G-GFP MOI=5 for 1 hr to allow attachment of RV-G to the susceptible cells followed by evaluating the binding percentage. The RV-G binding to the KO ITGB1 cells was not significantly different from the KO uninfected control. However, significantly enhanced virus binding was observed

in KO cells transiently expressing the human ITGB1 receptor **(Figure 5.21 C-D). These** results showed the role of ITGB1 in promoting the virus entry.

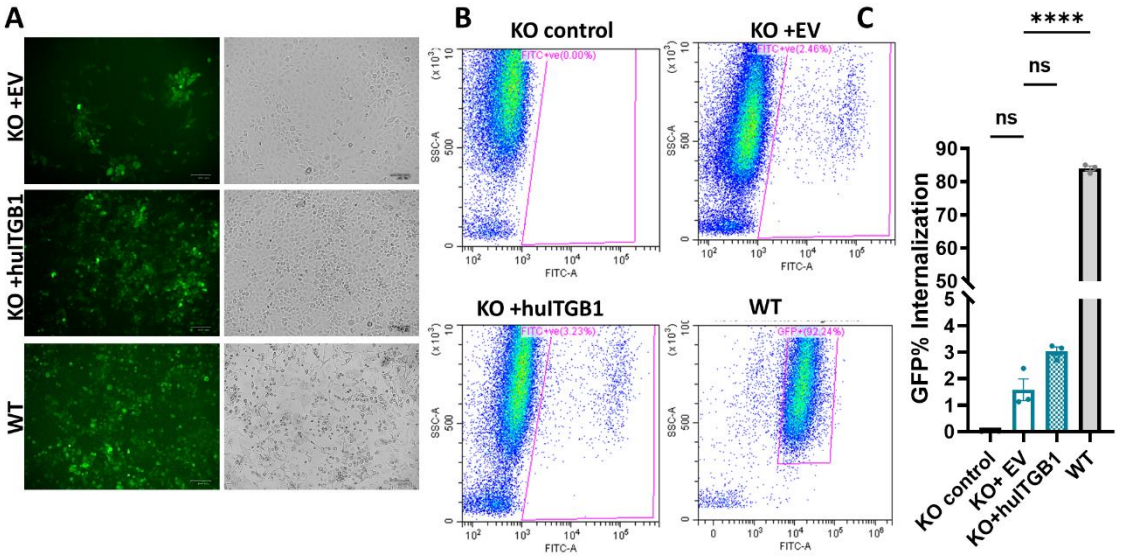

Figure 5.20 Replication of rVSV-dG-RV-G-GFP on ITGB1 KO cells.

(A). *Representative microscopic fields green (left), bright (right) for A549 KO ITGB1 cells infected with rVSV-dG-RV-G-GFP MOI=5. A549 KO ITGB1 cells, were transfected with empty vector and human ITGB1 FLAG vector; respectively, after 48h, cells were infected with rVSV-dG-RV-G-GFP (MOI=5). Thirty hpi, the GFP percentage corresponding to virus replication were imaged. The WT A549 cells were used as infection control* ***(B).*** *Representative flow cytometry plots of the ITGB1 KO cells transiently transfected with empty vector and human ITGB1 FLAG vectors; respectively. Forty-eight hrs post transfections, cells were infected with rVSV-dG-RV-G-GFP at MOI=5. Thirty hpi, the cells were collected and analysed for GFP percentage using flow cytometry analysis, the KO control cells were used as non-infected control, and the WT A549 cells were used as infection control.* ***(C).*** *Graph showing the mean of the GFP% of ITGB1 KO cells transiently transfected with empty vector and human ITGB1 FLAG vectors; respectively. The KO control cells were used as non-infected control and the WT A549 cells were used as infection control. The GFP% corresponds to the internalized virus. All experiments were performed three times (n=3) independently. Error bars represent the SEM of three biological replicate samples. using one-way ANOVA. ns, non-significant, P > 0.05., **** P ≤ 0.0001.*

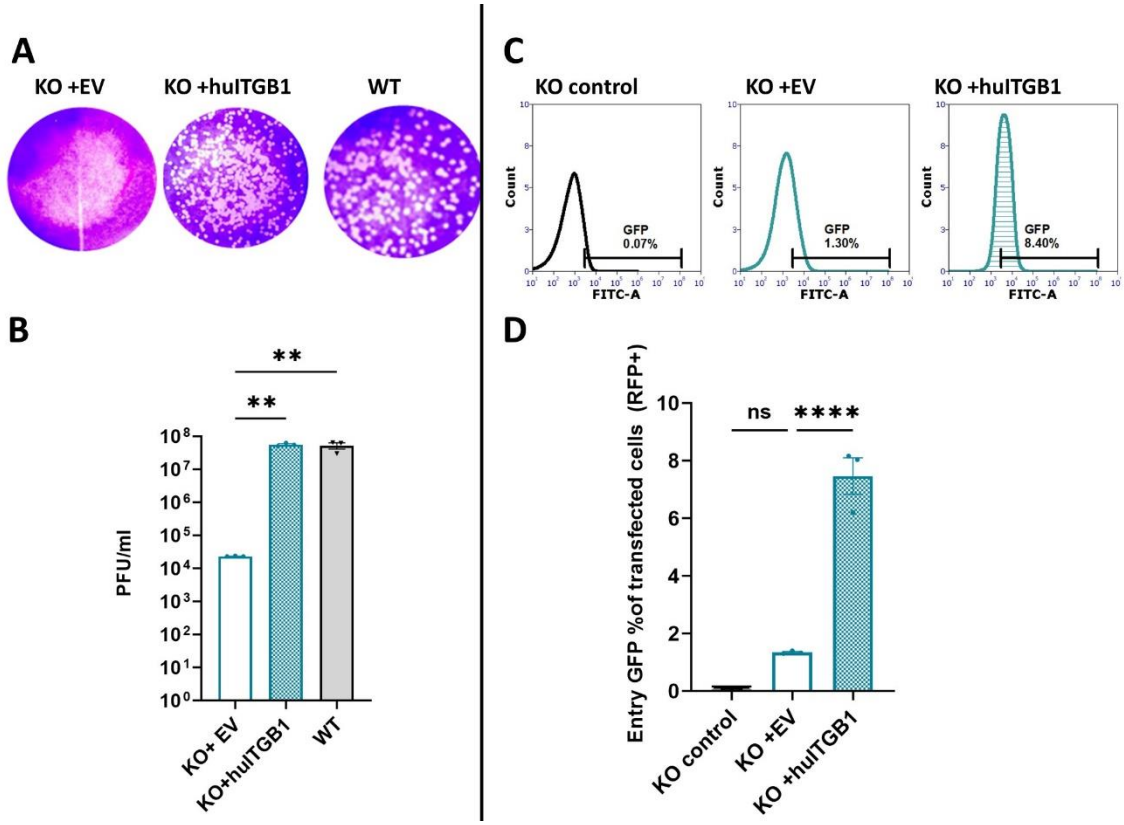

Figure 5.21 Replication and entry of rVSV-dG-RV-G-GFP on ITGB1 KO cells.

(A)*. Representative plaque morphology of the A549 KO ITGB1 cells infected with rVSV-dG-RV-G-GFP. The A549 KO ITGB1 cells were transiently transfected with the empty vector and human ITGB1 FLAG, respectively. Forty-eight hr post-transfection, cells were infected with the rVSV-dG-RV-G-GFP MOI=5. Thirty hpi, the viral supernatants were collected for quantifying the released progeny virus. The released viruses were quantified using plaque assay on BHK-21 cells after 72 hrs.* ***(B).*** *Graph showing the difference of the mean PFU/mL of rVSV-dG-RV-G-GFP between A549 ITGB1 KO cells transfected with either EV or human ITGB1 FLAG, the WT cells were used as infection control and KO cell used as non-infected control.* ***(C).*** *Representative histograms showing the GFP % of rVSV-dG-RV-G-GFP infected A549 KO ITGB1 cells. The A549 KO ITGB1 cells were transiently transfected with the empty vector and human ITGB1 FLAG, respectively. Forty-eight hr post-transfection, cells were infected with the rVSV-dG-RV-G-GFP MOI=5 for 2 hrs. Then cells were collected and stained with anti-FLAG (targeting the FLAG-tagged receptor) and RV-G antibodies (targeting the virus RV-G), followed by staining with Alexa Fluor 568 and Alexa-Fluor 468 conjugated antibodies, respectively for flow cytometry analysis. Flow cytometry data were analysed by FCS Express software****.*** ***(D)****. Graph showing the mean of the GFP% of A549 KO ITGB1 cells infected and transfected with EV and human ITGB1 vector, KO control was used as non-infected control The GFP % corresponds to the RV-G bound to the transfected A549 KO ITGB1 cells. All experiments were performed three times (n=3) independently. Data represent the average of three biological replicates with S.E.M. using one-way ANOVA. ns, non-significant, P > 0.05., ** P ≤ 0.01, **** P ≤ 0.0001.*

5.2.2.6 Generation of nAChR KO cells

Since nAChR has been the first identified cellular receptor for RV (Lafon, 2005). To evaluate the role of nAChR deficient cells on RV permissiveness, we introduced a sgRNA targeting the first exon of nAChR into the PX459 V2.0 vector through cloning. **(Chapter 9, Supplementary Figure 20)**. We attempted to delete the first coding exon within the human nAChR gene **(Figure 5. 22).** The KO cell genomic DNA and WT cells were compared for the band size following amplification of the targeted exon site. A 100 nucleotide bases less was observed in the KO PCR product compared to the WT cells PCR clone (**Figure 5.22).** Further sequence analysis showed that no indels were introduced in the exon region. For this purpose, subsequent validation through functional studies was crucial to confirm whether the absence of 100 nucleotides in the targeted region resulted in any mutations in the nAChR gene.

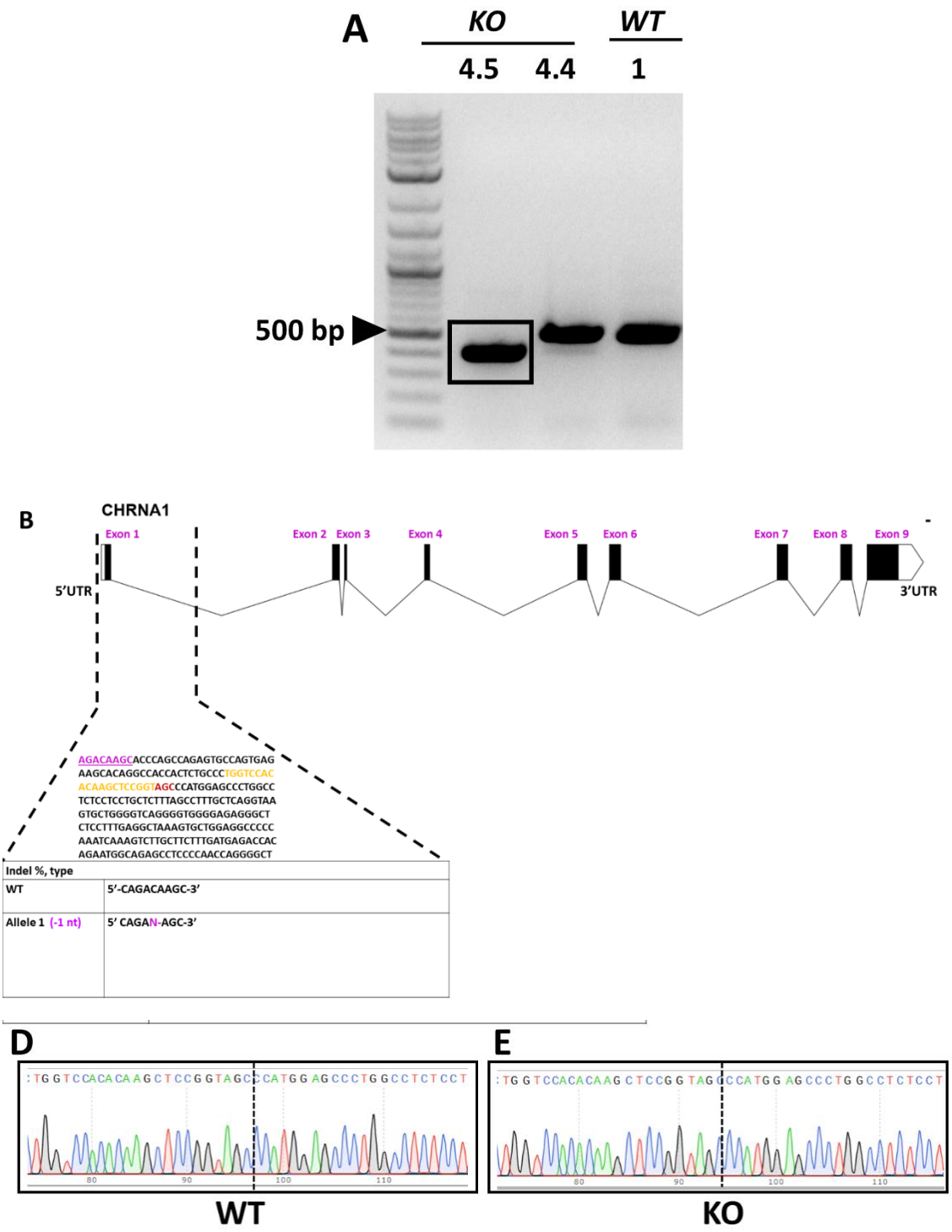

Figure 5.22 Generation and validation of the A549 nAChR KO through CRISPR/Cas9 targeting exon 1 nAChR.

(A) *Agarose gel electrophoresis showing the PCR products amplified by primers encompassing the CRISPR gRNA target in exon 1 of human nAChR. The genomic DNA from the single-cell clones of A549 KO nAChR cells (clone 4.4, 4.5) and WT cells (1) was extracted and amplified with primers flanking the region of the gRNA sequence. The PCR products were shown on the gel electrophoresis, indicating a smaller band in KO cell clone 4.5 compared to the WT cell.* ***(B).*** *Schematic diagram showing the genomic organization of*

human nAChR intron-exon. ***(C).*** *A table summarizing the number of alleles resulting from the introduced indels in nAChR exon 1 regions obtained from the sequencing analysis of the amplicons corresponding to clone 4.4(KO) and WT (1). The underlined sequence corresponds to the sequence in which indels were introduced. The amino acid comparison did not show any difference between* ***(D).*** *WT allele and* ***(E).*** *The KO cell clone 4.4 was highlighted. The alleles resulted from the introduced indels in nAChR exon 2 regions. The PAM site is indicated in red letters, the gRNA sequence is represented in yellow letters, and the Magenta represents the indels introduced (deletions or insertion of bases). Validation of cloning the ghunAChR in PX459 V2.0 is shown in Chapter 9, Supplementary Figure 20.*

5.2.2.7 nAChR is not essential for RV but enhances its entry.

To validate if the putative nAChR null cells could allow infectivity of rVSV-dG-RV-G-GFP. The nAChR KO cells, nAChR KO cells over expressing the human nAChR and WT A549 cells were infected with rVSV-dG-RV-G-GFP at MOI of 5, KO uninfected cell control was employed. Results showed there was no significance. Although, over expressing the human nAChR in KO cells were capable of significantly increasing the GFP expression levels compared to KO cells **(Figure 23 A-C).**

Plaque assay analysis was carried out to compare the released virus progeny from infected KO nAChR cells, KO nAChR cells ectopically expressing the human nAChR and WT. Significantly 4-fold reduction in the virus released from the nAChR KO cell was observed compared to the WT cells **(Figure 24 A-B).** Over expressing the human nAChR in KO cells restored virus replication despite the released virus progeny was non significantly different from the KO cells. The KO nAChR cells allowed initial virus binding which showed significantly higher levels compared to the KO uninfected cell control. Significantly enhanced virus binding was supported in nAChR KO cells expressing the human nAChR compared to the nAChR KO cell **(Figure 24 C-D).** These results might suggest that the role of the nAChR is potentially in promoting the virus replication rather than virus initial attachment to the cells.

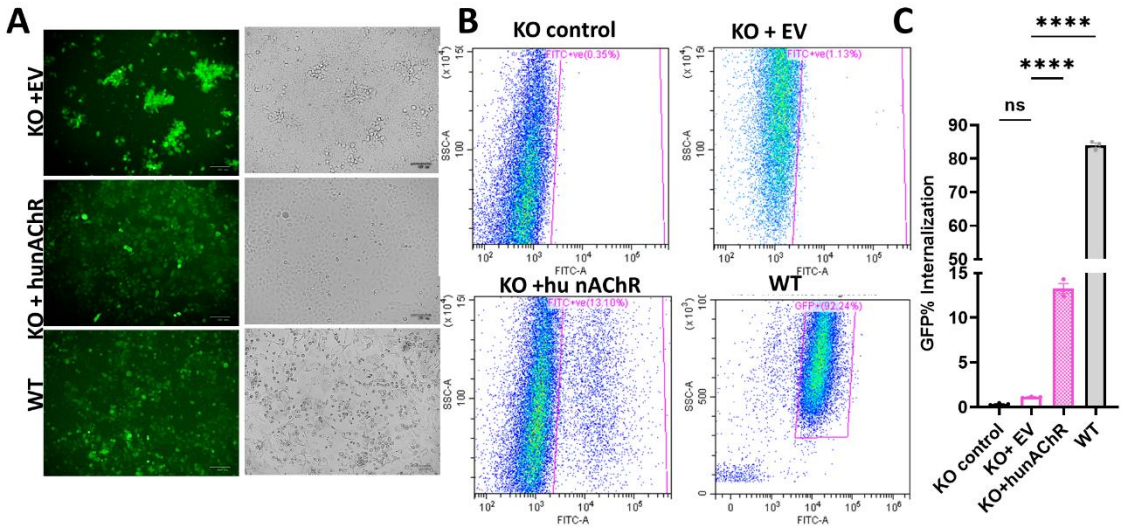

Figure 5.23 Replication of rVSV-dG-RV-G-GFP on nAChR KO cells.

(A). *Representative microscopic fields green (left), and bright (right) for A549 KO nAChR cells infected with rVSV-dG-RV-G-GFP MOI=5. A549 KO nAChR cells were transfected with an empty vector and human nAChR FLAG vector; respectively, after 48h, cells were infected with rVSV-dG-RV-G-GFP (MOI=5). Thirty hpi, the GFP percentage corresponding to virus replication was imaged, The WT A549 cells were used as infection control* ***(B).*** *Representative flow cytometry plots of the nAChR KO cells transiently transfected with empty vector and human nAChR FLAG vectors; respectively. Forty-eight hrs post transfections, cells were infected with rVSV-dG-RV-G-GFP at MOI=5. Thirty hpi, the cells were collected and analysed for GFP percentage using flow cytometry analysis, the KO control cells were used as non-infected control, and the WT A549 cells were used as infection control.* ***(C).*** *Graph showing the mean of the GFP% of nAChR KO cells transiently transfected with empty vector and human nAChR FLAG vectors; respectively. The KO control cells were used as non-infected control and the WT A549 cells were used as infection control. The GFP% corresponds to the internalized virus. All experiments were performed three times (n=3) independently Error bars represent the SEM of three biological replicate samples. using one-way ANOVA. ns, non-significant $P > 0.05$, **** $P \leq 0.0001$.*

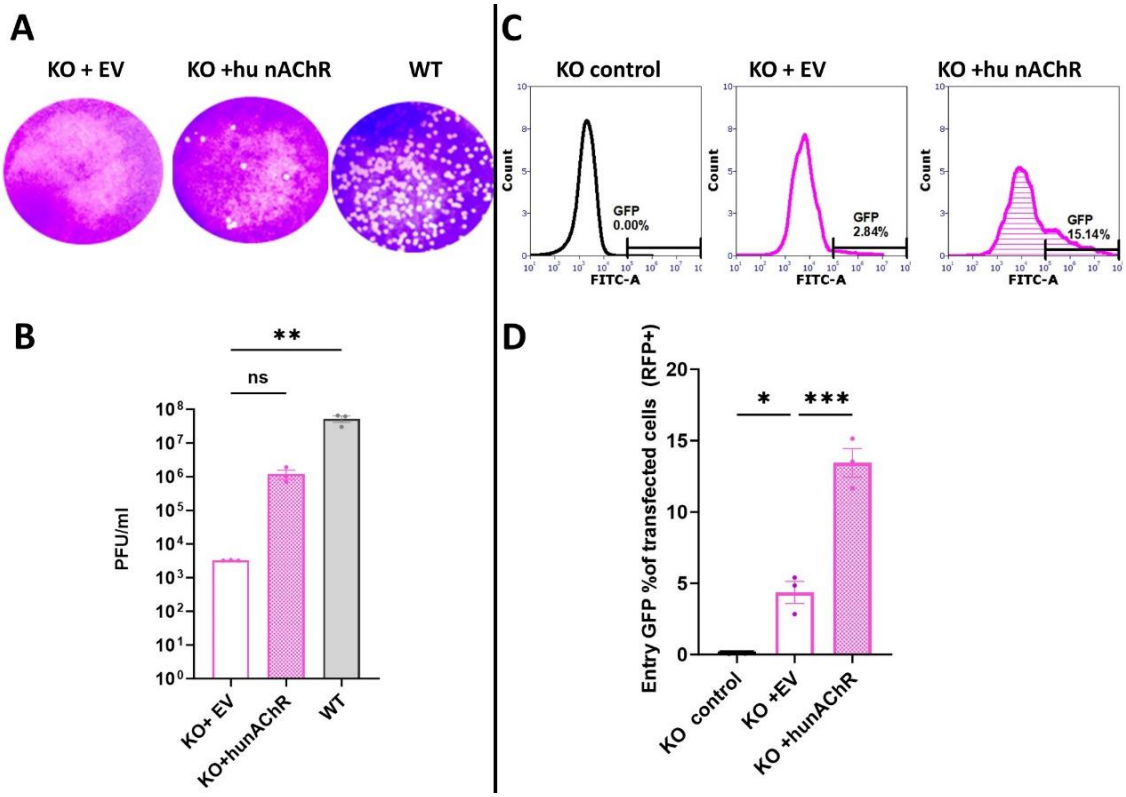

Figure 5.24 Replication and entry of rVSV-dG-RV-G-GFP on nAChR KO cells

(A). *Representative plaque morphology of the A549 KO nAChR cells infected with rVSV-dG-RV-G-GFP. The A549 KO nAChR cells were transiently transfected with the empty vector and human nAChR FLAG, respectively. Forty-eight hr post-transfection, cells were infected with the rVSV-dG-RV-G-GFP MOI=5. Thirty hpi, the viral supernatants were collected for quantifying the released progeny virus. The released viruses were quantified using plaque assay on BHK-21 cells after 72 hrs.* ***(B).*** *Graph showing the difference of the mean PFU/mL of rVSV-dG-RV-G-GFP between A549 nAChR KO cells transfected with either EV or human nAChR FLAG, the WT cells were used as infection control and KO cell used as non-infected control.* ***(C).*** *Representative histograms showing the GFP % of rVSV-dG-RV-G-GFP infected A549 KO nAChR cells. The A549 KO nAChR cells were transiently transfected with the empty vector and human nAChR FLAG, respectively. Forty-eight hr post-transfection, cells were infected with the rVSV-dG-RV-G-GFP MOI=5 for 2 hrs. Then cells were collected and stained with anti-FLAG (targeting the FLAG-tagged receptor) and RV-G antibodies (targeting the virus RV-G), followed by staining with Alexa Fluor 568 and Alexa Fluor 468 conjugated antibodies, respectively for flow cytometry analysis. Flow cytometry data were analysed by FCS Express software.* ***(D).*** *Graph showing the mean of the GFP% of A549 KO nAChR cells infected and transfected with EV and human nAChR vector, KO control was used as non-infected control The GFP % corresponds to the RV-G bound to the transfected A549 KO nAChR cells. All experiments were performed three times (n=3) independently. Error bars represent the SEM of three biological replicate samples. using one-way ANOVA. ns, non-significant, P > 0.05., ** P ≤ 0.01, **** P ≤ 0.0001.*

5.3 Discussion

Entry of RV into the cells is typically directed by the interactions of multiple cellular receptors with the surface glycoprotein (Lafon, 2005). With the advancement in high throughput technology and genetic screening methods, new proteins which act as receptor candidates for RV have been discovered (Wang et al., 2018, 2023; Shuai et al., 2020). However, this knowledge represents an enormous potential for designing new structural guided antiviral drugs. More understanding of the underlying molecular interactions involving the strategies by which the RV binds and internalizes to the cellular compartments is deemed essential.

The expression profiles of infected HaCaT cells showed down regulation of only nAChR and NCAM genes. This might explain the resistance of HaCaT cells to RV infections since the utilization of only the nAChR and NCAM were not sufficient for productive infection of the rVSV-dG-RV-G-GFP.

We opted to utilize HaCaT cells for our study due to their susceptibility to VSV, as previously demonstrated in **chapter 4**. We detected the endogenous expression of RV receptor genes in HaCaT cells; however, only 2 of these receptors exhibited downregulation in response to the rVSV-dG-RV-G-GFP. To establish a heterologous system focusing solely on receptor overexpression, we ectopically expressed the *P.alecto* receptors into HaCaT cells, disregarding other factors influencing rVSV-dG-RV-G-GFP interactions. To alleviate the cellular stress induced by transfection, we incorporated an empty vector control throughout the entire study as a means of normalization.

The individual and combined expression of the RV receptors on HaCaT cells showed neither distinguished cytopathic effect (CPE) nor any GFP upon infection with the rVSV-dG-RV-G-GFP. Thus, comparing the effect of receptors on the cell's permissiveness was based on the binding percentage to the RV-G and the virus release in the supernatants. Clearly more binding and production of virus progeny was observed on infected HaCaT cells individually expressing nAChR and mGluR2 receptors.

Similarly, the combining effect of expressing mGluR2, nAChR, ITGB1 and NCAM resulted in more enhanced viral replication than combinations involving the p75 receptor. This might be correlated with previous study which reported the possible transport of the

RV in p75 in-in-dependent pathway. Highlighting that the p75 role in RV infections is to accelerate its transport to the neuronal cell body (Gluska et al., 2014).

Interestingly, the higher levels of virus production obtained by co expressing the ITGB1 and nAChR receptors might be correlated with their interaction in CO-IP as established in previous study (Shuai et al., 2020). Notably, higher levels of virus release were detected in infected HaCaT cells expressing NCAM in combination with mGluR2 or ITGB1 or nAChR. This could be delineated to the role of NCAM in conferring resistant cells susceptible to RV infection (Hotta et al., 2006).

From HaCaT cell permissive studies, several conclusions can be drawn. The cells' susceptibility to virus infection is not solely governed by the expression of the entry receptors. Hence HaCaT cells showed endogenous expression of the known RV receptors but could not sustain the infection. This could be explained by the fact that accumulation or high binding between the surface glycoprotein and the receptor does not necessarily trigger the post-binding events that allow viral entry, due to the presence of restriction factors (Maginnis, 2018a). Another probable reason might be correlated with the innate immune response of the HaCaT cells to viral infection. As reported in previous studies, the absence of CPE in HaCaT cells infected with rhinovirus might be due to the conservation of the HaCaT cell integrity (Morgene et al., 2018).

The receptor preference results suggested enhanced binding and replication of RV upon interacting with nAChR, mGluR2 and ITGB1. Thus, more understanding to exploit in which stage of virus replication these receptors were required though the CRISPR/Cas9 mediated knockout was carried out. Implementing the CRISPR/Cas9 mediated knockout has been extensively used to study the distinct functions of specific genes for various in multiple areas among which is to address the role of proteins in virus replication. Herein, our goal was to disrupt the gene composition of each of the ITGB1, mGluR2 and nAChR to evaluate their exact role in the RV replication.

The selection to knockout the nAChR was based on the elicited high binding efficiency to the RV-G in HaCaT cells. Thus, more understanding of the role it plays during virus infection and entry was required. Additionally, selecting to knock out each of the ITGB1 and mGluR2 was attributed to the elevated levels of virus release and binding obtained

from expression of ITGB1 and mGluR2 individually or in combination in HaCaT cells which suggest their crucial role in RV replication.

Despite NCAM expressing cells showing prominent levels of replication, we did not attempt to genetically delete the NCAM genes. Since our results showed that its down regulation in HaCaT cells in response to rVSV-dG-RV-G-GFP infection did not contribute to cell permissiveness (GFP not observed). Additionally, previous studies have reported the influence of the NCAM deficient mice on RV invasion (Cremer et al., 1994; Hotta et al., 2006).

Disrupting the gene is initiated through delivery of sgRNA which is complementary to the target site in the gene of interest which when coupled with the Cas9 result in gene disruption (Giuliano et al., 2019b). To this aim we used the sgRNA approach targeting specific coding region in ITGB1, mGluR2 and nAChR genes individually. The genetic characterization of the clonal knockouts of the ITGB1 and mGluR2 cell lines was carried out. Multiple copies of alleles were obtained through disrupting the ITGB1 or mGluR2 which showed either deletion or insertion in the targeted exon regions predicted to cause frameshift mutations. As mentioned previously, due to unavailable commercial antibodies for the ITGB1, mGluR2 and nAChR receptors, further confirmation of the disrupted genes effect on RV replication was carried out using the functional studies.

A previous study demonstrated that the mGluR2 uses similar endocytic pathway as that of RV in which they showed co-internalization into the early and late endosomes highlighting the role of the mGluR2 in RV internalization (Wang et al., 2018). Besides, the results previously reported, that knockdown of the mGluR2 levels in mice resulted in more survival rates of mice against the challenge with RV street strain compared to mice without knock down of the mGluR2 (Wang et al., 2018). This strongly support our results obtained in which virus replication was more influenced with the genetic deletion of the mGluR2 rather than the virus binding to KO mGluR2. This might be concluded that however KO mGluR2 cells supported initial virus binding, the virus replication was substantially inhibited, highlighting the mGluR2 prevalent role in virus internalization.

In contrast, the deficient levels of ITGB1 in A549 cells resulted in significant reduction of G protein binding to cells (entry), however, it has shown higher levels of supporting the

RV replication compared to knockout mGluR2 cell line, suggesting its significant role in the initial cellular attachment to the RV-G. These results are contradicting the results from the recent study which suggested that ITGB1 is co localized with the RV in early and late endosomes, indicating its role in virus internalization (Shuai et al., 2020). Thus, more studies are required to elucidate in which step of virus replication the ITGB1 is involved.

Despite the nAChR receptor was the first known host cellular receptor for RV (Lentz, 1990; Lafon, 2005) there is lack of data in understanding its exact role in RV replication. The nAChR null cells allowed significantly less virus internalized in absence of nAChR than its effect on virus initial binding to the KO nAChR cells. Even though, the ectopic expression of the human nAChR in KO nAChR was not capable of allowing similar virus replication as in WT cells.

Taken together, from the obtained data, it is tempting to speculate that the mGluR2 is the cellular receptor which plays the most crucial role in RV infection since its depletion from cells resulted in the least virus replication, evidenced by less released virus progeny compared to other generated KO cells (KO ITGB1, KO nAChR cells) **(Figure 5.25)**. Additionally, RV internalization might be regulated by interactions between two receptors. Recent study reported that RV-mGluR2 complex internalization is dependent on interaction with the transferrin receptor protein which allows the uptake of the RV-mGluR2 complex in the clathrin coated pits (Wang et al., 2023). Further to these findings, another study outlined the potential role of an interaction between the ITGB1 and nAChR receptors in enhancing the peripheral entry of RV (Shuai et al., 2020).

In conclusion, we might have been able to answer one of the questions involving the RV receptor preference. Since these results indicated the independence of RV on the previously identified receptors and that it utilizes these receptors simultaneously rather than sequentially as the knockout of these receptors failed to abolish virus entry/replication (ITGB1, mGluR2 and nAChR). Answering this question led to another question which is whether the architecture of the target cells, and the species which the virus infects would allow similar receptor utilization/preference. This would shape the RV tropism **(chapter 6).**

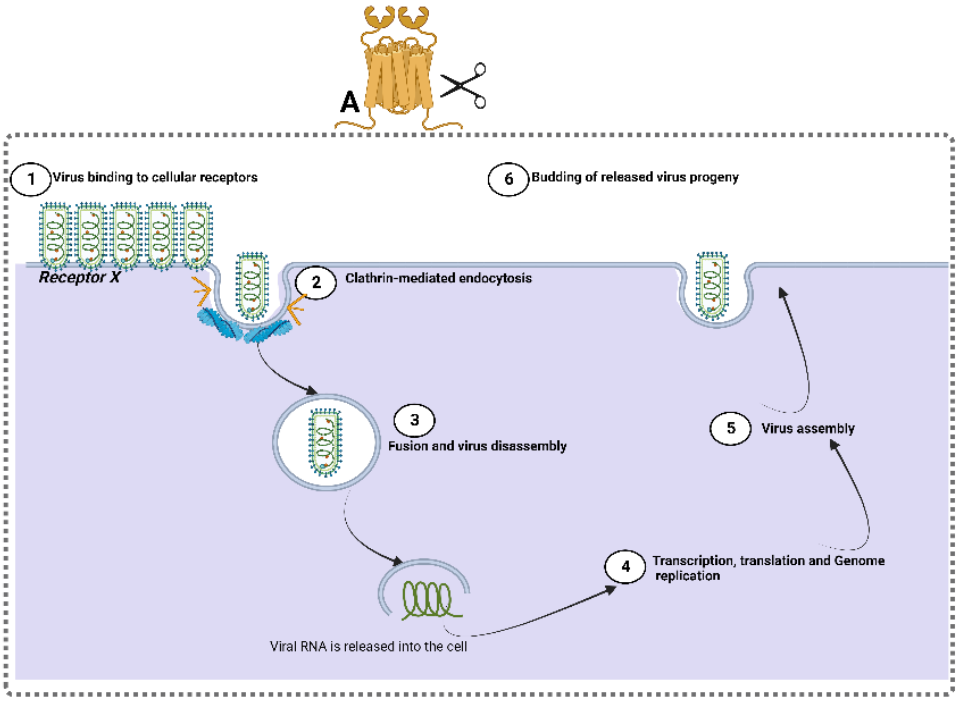
A
1 Virus binding to cellular receptors
6 Budding of released virus progeny
Receptor X
2 Clathrin-mediated endocytosis
3 Fusion and virus disassembly
5 Virus assembly
4 Transcription, translation and Genome replication
Viral RNA is released into the cell

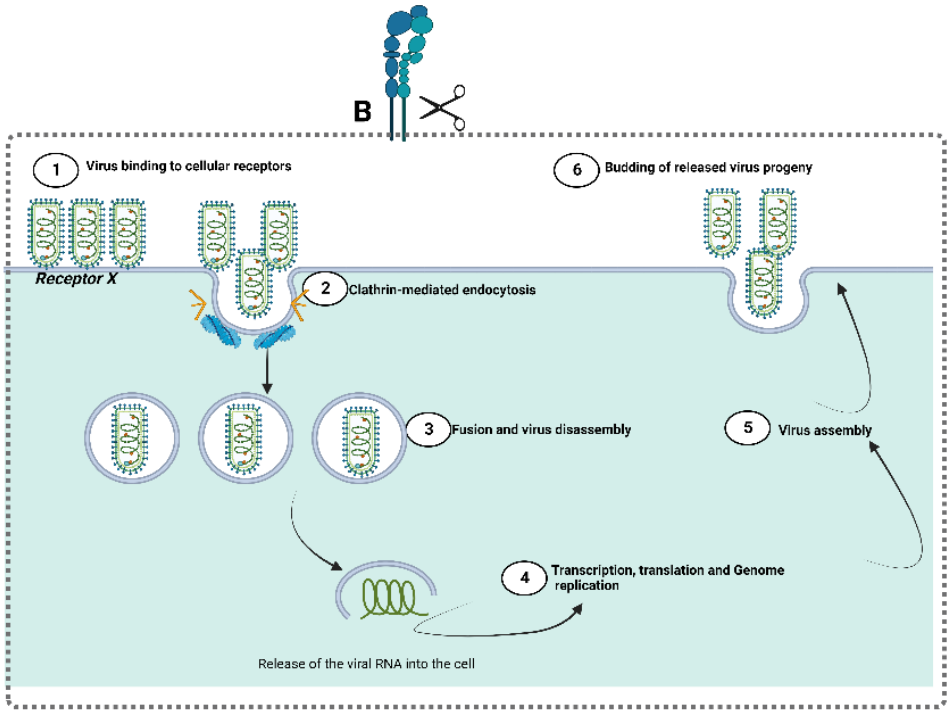
B
1 Virus binding to cellular receptors
6 Budding of released virus progeny
Receptor X
2 Clathrin-mediated endocytosis
3 Fusion and virus disassembly
5 Virus assembly
4 Transcription, translation and Genome replication
Release of the viral RNA into the cell

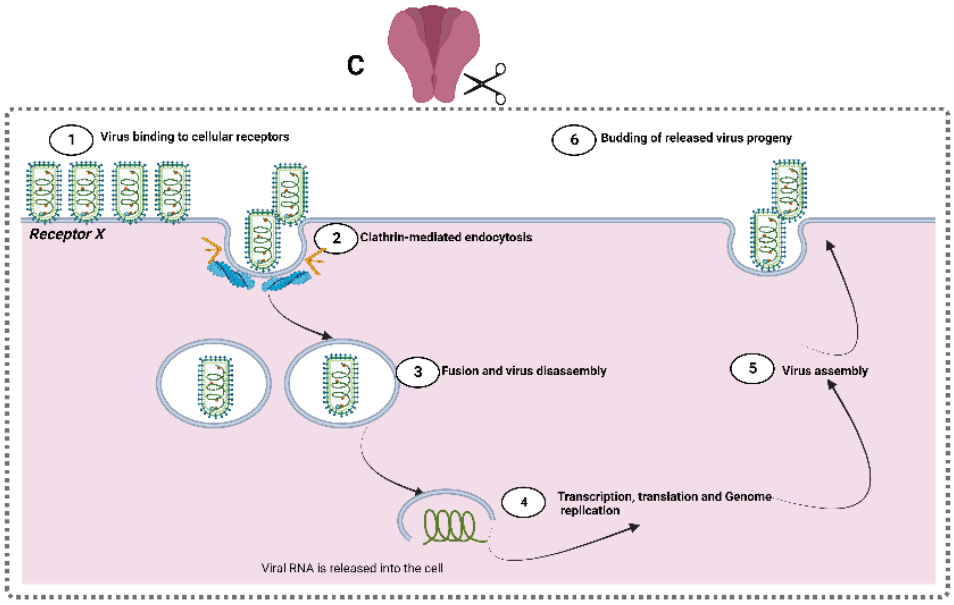

Figure 5.25 Entry and replication of rVSV-dG-RV-G-GFP on A549 KO cells

(A). *Schematic diagram showing the putative entry and replication of RV in A549 KO mGluR2 cells, many virus particles could bind and enter the cells, however only few virus particles were internalized, resulting in decrease in the released virus progeny. (**B).** Schematic diagram showing the putative entry and replication of RV in A549 KO ITGB1 cell, virus binding and entry was less compared to KO mGluR2 cells. However, all the bound viruses get internalized efficiently resulting in higher virus progeny, indicating that internalization of the bound virus was less affected **(C).** Schematic diagram showing the putative entry and replication of RV in A549 KO nAChR cells, virus binding decreased and subsequently virus entry decreased, however more released virus progeny was observed compared to the virus released on A549 KO mGluR2 cells.*

6 Chapter 6 Multi-receptor orthologs mediated Rabies Virus Entry in Susceptible Mammalian Hosts

6.1 Introduction

Rabies represents one of the most fatal zoonotic viral diseases which shows extensive ability to infect diverse mammalian hosts resulting in thousands of human deaths each year (Escobar et al., 2023). It is well established that RV belongs to lyssaviruses in which each species is permanently maintained in a bat species according to the geographical location (Begeman et al., 2018).

6.1.1 Tropism

Viral tropism is defined by the virus ability to cross and spread throughout different cell types and species. Tropism defines the virus ability to replicate and spread in discrete host species (Feige et al., 2021a). Multiple factors enable the virus tropism to productively infect certain cell types. Among which is the expression of the cellular receptors and the innate immune response which regulate the viral infection. Other factors could be related to the virus including viral evolution which would allow recognition of the cell surface receptors, availability of transcription factors involved in viral replication and its ability to evade the host innate immune response (McFadden et al., 2009).

Many viruses show narrow cellular tropism for example hepatitis C virus (HCV), which is restricted to hepatocytes with limited host range (Sato et al., 2012). Whereas other viruses display extraordinarily wide host range including mammals and mosquitos such as the mosquito vector born viruses including Flaviviruses such as Zika virus (Zhang et al., 2023).

Despite its neurotropic nature, rabies virus represents a historically broad host and cellular range with the ability to infect diverse cell types among multiple species (Feige et al., 2021a). Understanding the mechanism through which RV infects other species is important for preventing its spread.

6.1.2 RV Spillover events

Spillover transmission is referred to the viruses which could breach the species barrier to be transmitted from its original host to a new host (Escobar et al., 2023). Usually in spillover events, the virus is transmitted from wildlife virus reservoir into a new domestic

animal host which subsequently spread through intraspecies transmission. These events might be accompanied with secondary spillover events in which the viruses are transmitted from the domestic animals to humans (Escobar et al., 2023).

Many viruses impose a significant risk to human owing to their spillover capacity such as Zika virus, Ebola virus and the severe acute respiratory syndrome coronavirus (SARS-CoV). In a recent investigation using a web-based application, RV has been classified as one of the top 10 high-risk spillover viruses. This tool considers multiple factors, including host epidemiology, environmental conditions, genetic aspects, and virus distribution. By inputting these parameters into the tool to assess RV's risk, it was assigned an approximate risk score of 84.60% (Feng et al., 2021).

It is well established that the RV epidemiological cycles are maintained with the *Carnivore and* the *Chiropteran.* The bats belong to the order *Chiropteran*, which is classified into two suborders: the Megachiroptera (megabats) and the Microchiroptera (microbats). RV is maintained in *Chiropteran* in the Americas, while the global virus maintenance is through the *Carnivores.* Phylogenetic analysis based on glycoprotein nucleotide sequence classifies RV into two major groups: bat-related, and dog-related RV (Sadeuh-Mba et al., 2017)

6.1.2.1 Bat related RV

Given that canine rabies is mostly eliminated in the Americas, the bat born rabies is extensively emerging especially through the common vampire bats. The most common species contributing to bat rabies is *Desmodus rodontus* which are prevalent in South America to North Mexico (Johnson et al., 2010). Multiple factors contribute to the substantial risk imposed by the bats acting as RV reservoirs. One of the most crucial factors is their complete dependence on blood to survive which allows the virus transmission to their prey through feeding (Hayes and Piaggio, 2018). This results in primary and secondary spillover events. For example, the RV could be transmitted from the *D. rotundus* to cats (primary spillover) and from cats to humans (secondary spillover)(Escobar et al., 2023).

Only the microbats have been reported to act as RV reservoirs and none of the previous surveillance data have shown if any of the bat species belonging to the megabats could

serve as intermediate host for RV. The *P.alecto* a bat genus belongs to the megabats, and that has been previously reported to be associated with Lyssavirus infection but not with RV (Gould et al., 1998). Thus, in this chapter, we will investigate whether the *P.alecto* representing one of the mega bats could be susceptible to RV infection or not.

6.1.2.2 Dog related RV

Despite the decrease of human rabies in China from 2007-2020, the risk of dog rabies remains significant. According to the latest study of rabies cases over the period from 2010-2020, dogs were the main source of virus transmission which contributed to around 41% of the reported cases. Followed by other animals such as cattle, sheep, foxes, camels, badgers, racoon dog, horse, and donkey. Further observation, that the stray dogs in rural areas amplify the potential risk of multiple biting incidents by one animal which becomes more prevalent in spring and summer than autumn and winter (Feng et al., 2021). In addition, the first documented transmission of Irkut virus from bats was reported, raising the warning against bat bites **(Chapter 1, Figure 1.3).**

6.1.3 Aims

Briefly, the aims of this chapter are to:

- Codon optimize the ORF sequences of human and canine ITGB1, mGluR2 and nAChR and subclone in pCAGG plasmids with a FLAG tag at the C-terminus.
- Confirm the expression and localization of the human and dog receptor orthologs using IFA and WB.
- Investigate the role of the host cellular receptors in the entry of rVSV-dG-RV-G-GFP to human, bat, and canine cell lines.
- Comparatively assess the rVSV-dG-RV-G-GFP replication pattern on different cells overexpressing the RV orthologs receptors.
- Compare the replication and entry represented in the GFP percentage and the quantity of virus release from cells expressing the orthologs of RV receptors.
- Evaluate the endogenous expression levels of the host genes on human, bat, and dog cell lines before and in response to the rVSVS-dG-RV-G-GFP infection.

6.2 Results

6.2.1 rVSV-dG-RV-G-GFP infection mediated the down regulation of all RV receptor genes in Pa-Br bat cells except ITGB1 expressing gene.

Vampire bats have been considered the most common source of RV transmission through bites (Banyard et al., 2013). We tested the possibility of other bat species such as the Australian black flying fox (*P.alecto*) allowing the rVSV-dG-RV-G-GFP replication *in vitro*. First, we assessed if the RV infection could play a role in the regulation of putative receptor genes. The immortalized bat brain cell line (Pa-Br) was infected with the rVSV-dG-RV-G-GFP at MOI of 5. Twenty-four hours post-infection, GFP signal was observed indicating that the Pa-Br supports the rVSV-dG-RV-G-GFP infection. This provided the first demonstration of the susceptibility of the Pa-Br cell line to RV infection **(Figure 6.1 A).** Consequently, the cellular RNA was extracted for qRT-PCR analysis to determine the relative modulation of the cellular receptor genes induced by infection with the rVSV-dG-RV-G-GFP. The RV infection downregulated the p75 mRNA levels (2.5-fold). Further, the RV infection down-modulated the expression of the nAChR and NCAM genes at approximately 1-fold upon infection with rVSV-dG-RV-G-GFP. Likewise, the mGluR2 expression was downregulated but to a lesser extent compared to the p75, nAChR and NCAM genes. In contrast, the ITGB1 mRNA levels showed similar expression pattern among infected and non-infected Pa-Br cells. These results provide the first evidence of the ability of the rVSV-dG-RV-G-GFP encoding the G protein of dog related RV to infect the brain cell line belongs to the *P.alecto*. Further we provided evidence that the RV may have the ability to downmodulate all the host receptor genes except the ITGB1 at the mRNA levels **(Figure 6.1 A-B).**

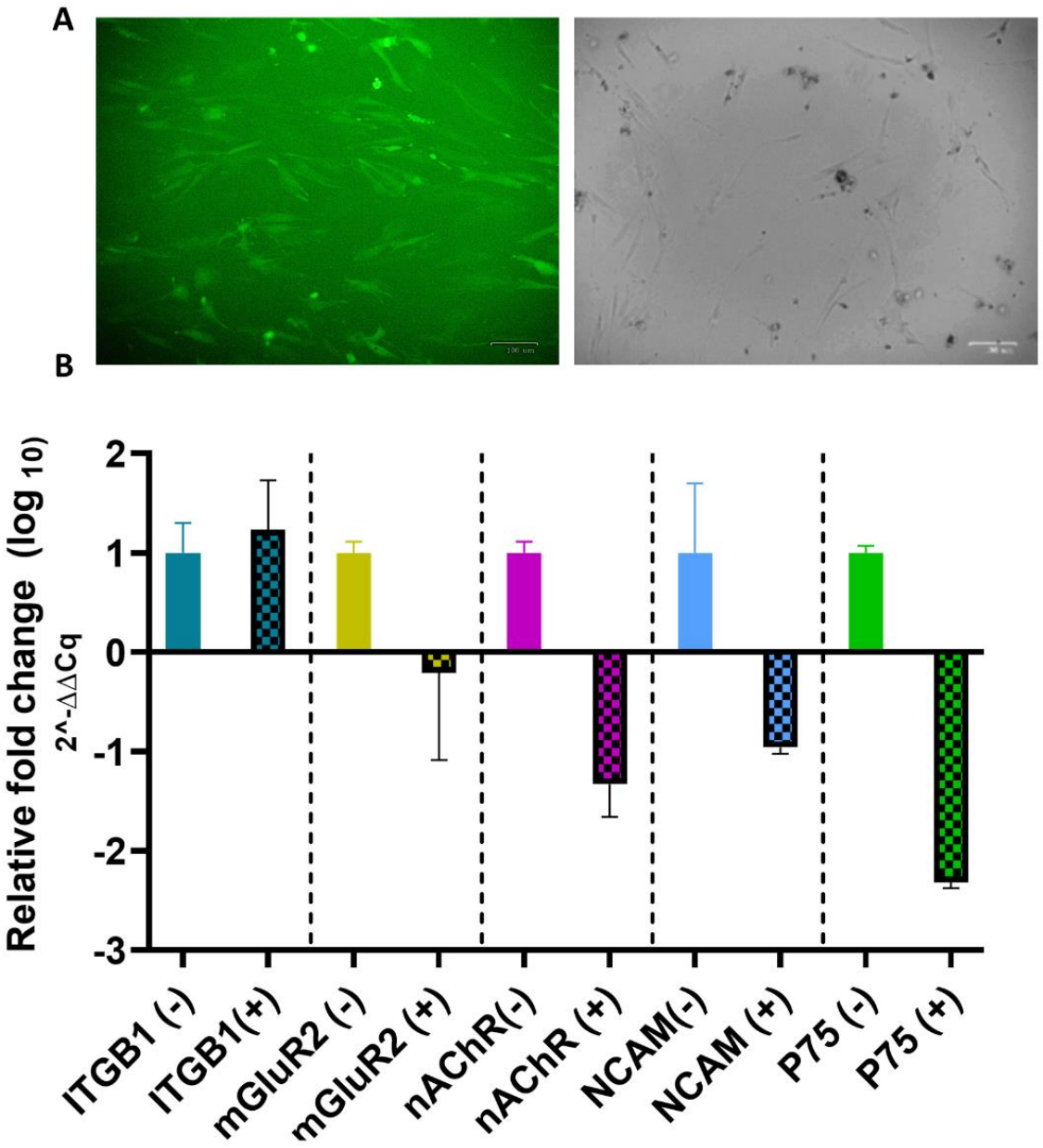

Figure 6.1 Relative expression (in fold change value) of RV cellular receptor genes on Pa-BR cells.

(A). *Microscopic fields of infected Pa-Br cells green (left), bright (right). Pa-Br cells were infected with rVSV-dG-RV-G-GFP (MOI 5), 24 hpi, cells were imaged for the GFP expression corresponding to virus replication.* ***(B).*** *The differential expression (in fold change) of the RV cellular genes were measured by qRT-PCR on Pa-Br cells before (-) and after infection (+) with rVSV-dG-RV-G-GFP. Twenty-four hrs after infection, cellular RNA was extracted from infected and non-infected Pa-Br cells. The relative RNA expression (mean ± SEM) of each of RV receptor gene were normalised to P.alecto 18S using ΔΔCt method. The experiment was performed three times (n=3) independently. Error bars represented the SEM from three biological replicates.*

6.2.2 The *P.alecto* p75 receptor enhances virus replication and internalization in Pa-BR cells.

To further demonstrate the role of the *P.alecto* RV receptors on the rVSV-dG-RV-G-GFP replication, the *P.alecto* ORF sequences corresponding to the RV receptors (ITGB1, mGluR2, nAChR, NCAM and p75) were retrieved from the NCBI. Sequences were then codon optimized and cloned into pCAGG plasmids with the FLAG tag at the C-terminus and expressed **(Chapter 3, section 3.2.9).** Each of the *P.alecto* receptors were ectopically expressed on the Pa-BR cells, followed by infecting with the rVSV-dG-RV-GFP (MOI 5) on the following day. The virus infected cells were analysed by flow cytometry for quantification of the GFP percentage, for plaque assay and for virus entry as previously described **(Chapter 5, Figure 5.2).**

As a negative control, an empty vector was utilized for cell transfection, followed by infection, along with cell control representing un-infected cells. Interestingly, our results demonstrated that the Pa-Br cells ectopically expressing the *P.alecto* receptors significantly increased the rVSV-dG-RV-G-GFP replication compared to the empty vector control. Over-expression of the *P.alecto* p75 enhanced the virus replication, compared to the *P.alecto* ITGB1 **(Figure 6.2 A-C).**

To demonstrate additional evidence of roles of receptors, quantification of the released virus was performed. The Pa-BR cells over expressing the *P.alecto* p75, NCAM and nAChR significantly increased the rVSV-dG-RV-G-GFP replication compared to the empty vector control. While the virus released from Pa-Br cells over expressing *P.alecto* mGluR2 or *P.alecto* ITGB1 receptors showed no significance difference compared to the empty vector control. **(Figure 6.3 A-B).**

To further asses the specificity of the rVSV-dG-RV-G-GFP in utilizing the *P.alecto* receptors for entry, the Pa-BR was transiently transfected with each of the *P.alecto* receptors, then infected for 1 hr, followed by the FC analysis with dual labelling infected transfected cells with the G protein and anti-FLAG antibodies to gate the cells binding to the RV-G (GFP+) cells from the transfected cells (RFP+). FC analysis suggested more efficient RV-G binding to the cells over expressing p75, and thus allowing more virus entry. Conversely, cells expressing the ITGB1 bat receptor allowed extremely limited viral

entry **(Figure 6.4 A-B).** Taken together, these results support that the rVSV-dG-RV-G-GFP efficiently bind to each of the p75, NCAM and nAChR *P.alecto* receptors, allowing enhanced virus entry, replication and release compared to the mGluR2 and ITGB1 receptors.

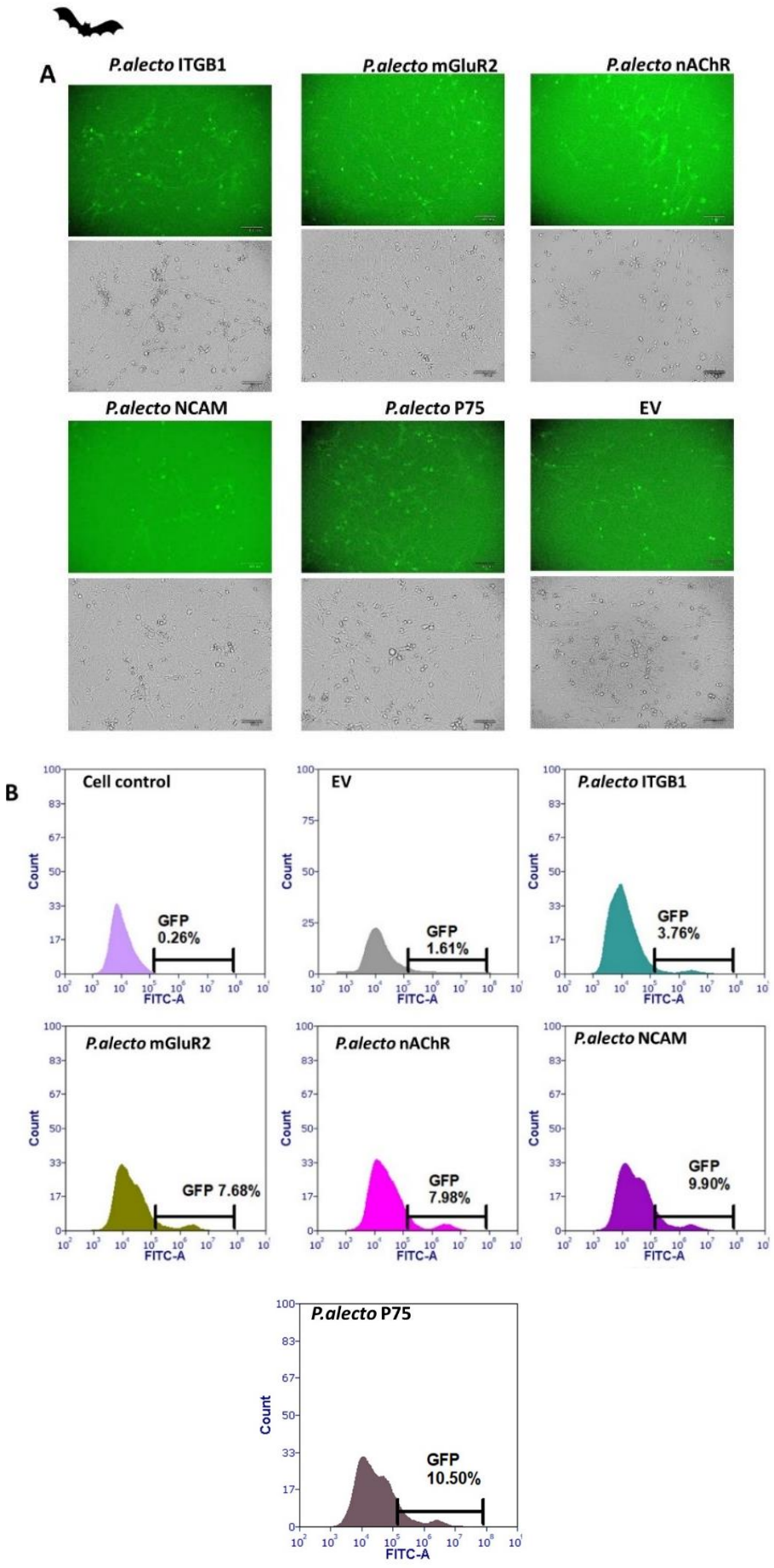
A
P.alecto ITGB1
P.alecto mGluR2
P.alecto nAChR
P.alecto NCAM
P.alecto P75
EV
B
Cell control
GFP 0.26%
EV
GFP 1.61%
P.alecto ITGB1
GFP 3.76%
P.alecto mGluR2
GFP 7.68%
P.alecto nAChR
GFP 7.98%
P.alecto NCAM
GFP 9.90%
P.alecto P75
GFP 10.50%
Count
FITC-A

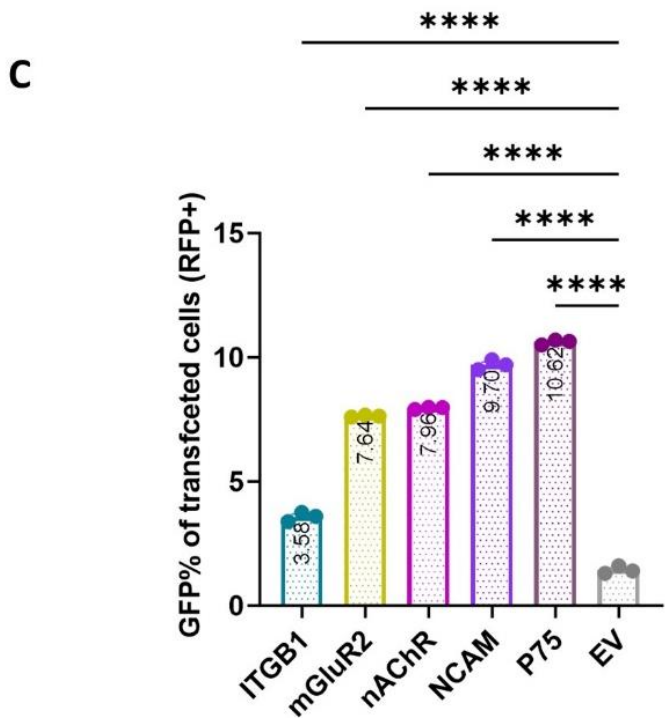

Figure 6.2 Replication of rVSV-dG-RV-G-GFP on Pa-Br cells overexpressing P.alecto receptors.

(A) *Representative Microscopic fields green, fluorescent (upper), bright (lower) of Pa-Br cells infected with rVSV-dG-RV-G-GFP. The Pa-Br cells were transiently transfected with the P.alecto receptors Forty-eight hrs post transfection, cells were infected with the rVSV-dG-RV-G-GFP, MOI=5. Thirty hpi, the cells were imaged for fluorescence.* ***(B).*** *Representative histograms showing the GFP % of rVSV-dG-RV-G-GFP infected Pa-Br cells. Pa-Br cells were transiently transfected with P.alecto receptors. Forty-eight hrs post transfection, cells were infected with rVSV-dG-RV-G-GFP, MOI=5. Thirty hpi, the cells collected and stained against the FLAG antibody (targeting the receptors) and followed by staining with Alexa Fluor 568 conjugated antibody for Flow cytometry analysis. GFP% was calculated from the receptor expressing cells, the empty vector transfected Pa-Br cells was used as control, cell control represents the un-infected cell control* ***(C).*** *Graph showing the mean of the GFP% of Pa-Br cells infected and transfected with P.alecto receptors compared to cells infected and transfected Pa-Br cells with the empty vector. The GFP % corresponds to the rVSV-dG-RV-G-GFP internalized to the transfected Pa-BR cells. The experiment was performed three times (n=3) independently. Data are representative of the mean and SEM of three biological replicates using one way ANOVA. ****, P < 0.0001. The experiment was performed three times (n=3) independently. The mean fluorescence intensity is shown in Chapter 9, Supplementary Table 1*

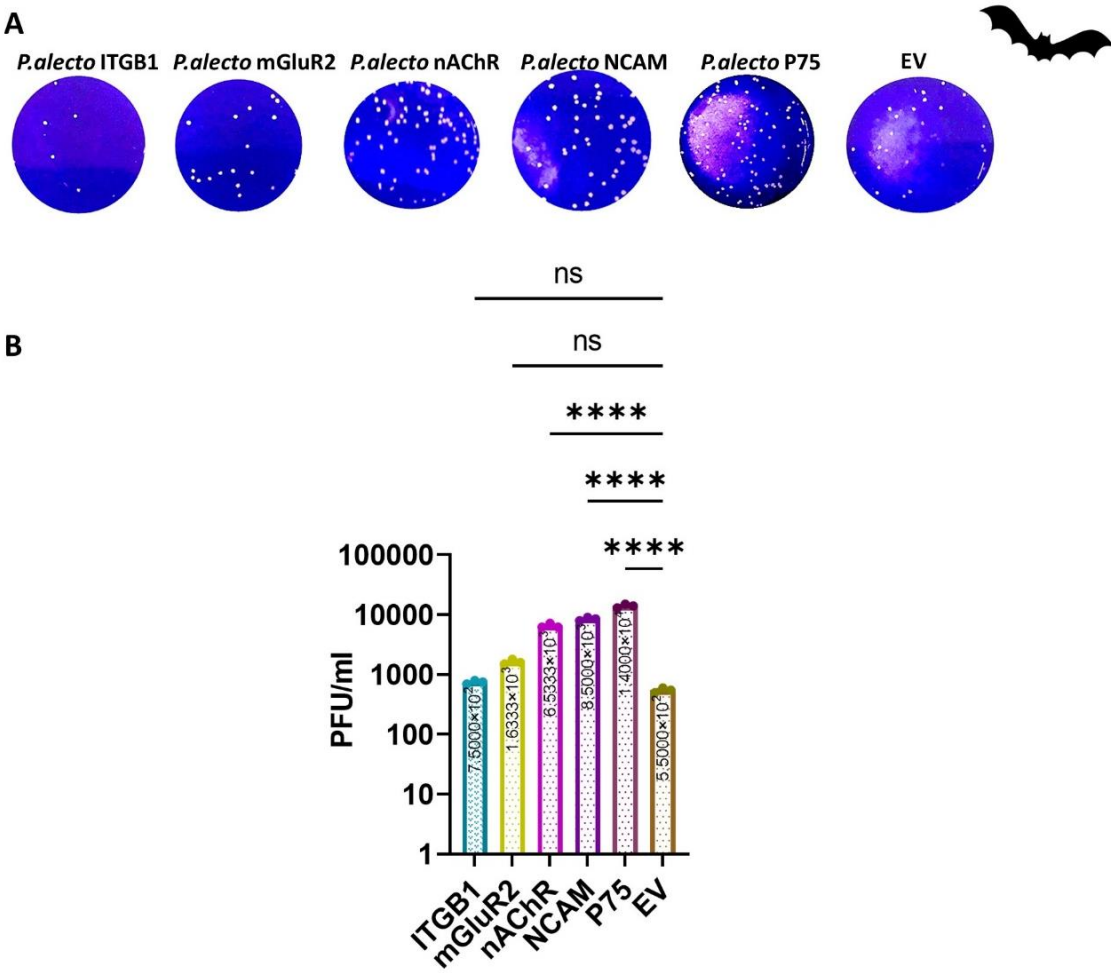

Figure 6.3 Replication of rVSV-dG-RV-G-GFP on Pa-Br cells overexpressing P.alecto receptors.

(A). *Representative plaque morphology of infected Pa-Br cells. Pa-Br cells transiently expressing the P.alecto receptors, were infected with the rVSV-dG-RV-G-GFP MOI=5. Thirty hpi, the viral supernatants were collected for quantifying the released progeny virus. The released viruses were quantified using plaque assay on BHK-21 cells after 72 hrs.* ***(B).*** *Graph showing the difference of the mean PFU/mL of rVSV-dG-RV-G-GFP between Pa-Br expressing P.alecto receptors and the Pa-Br cells infected and transfected with the empty vector. The experiment was performed three times (n=3) independently. Data are representative of the mean and SEM of three biological replicates using one-way ANOVA. ns, non-significant, P > 0.05, ****, P< 0.0001. `*

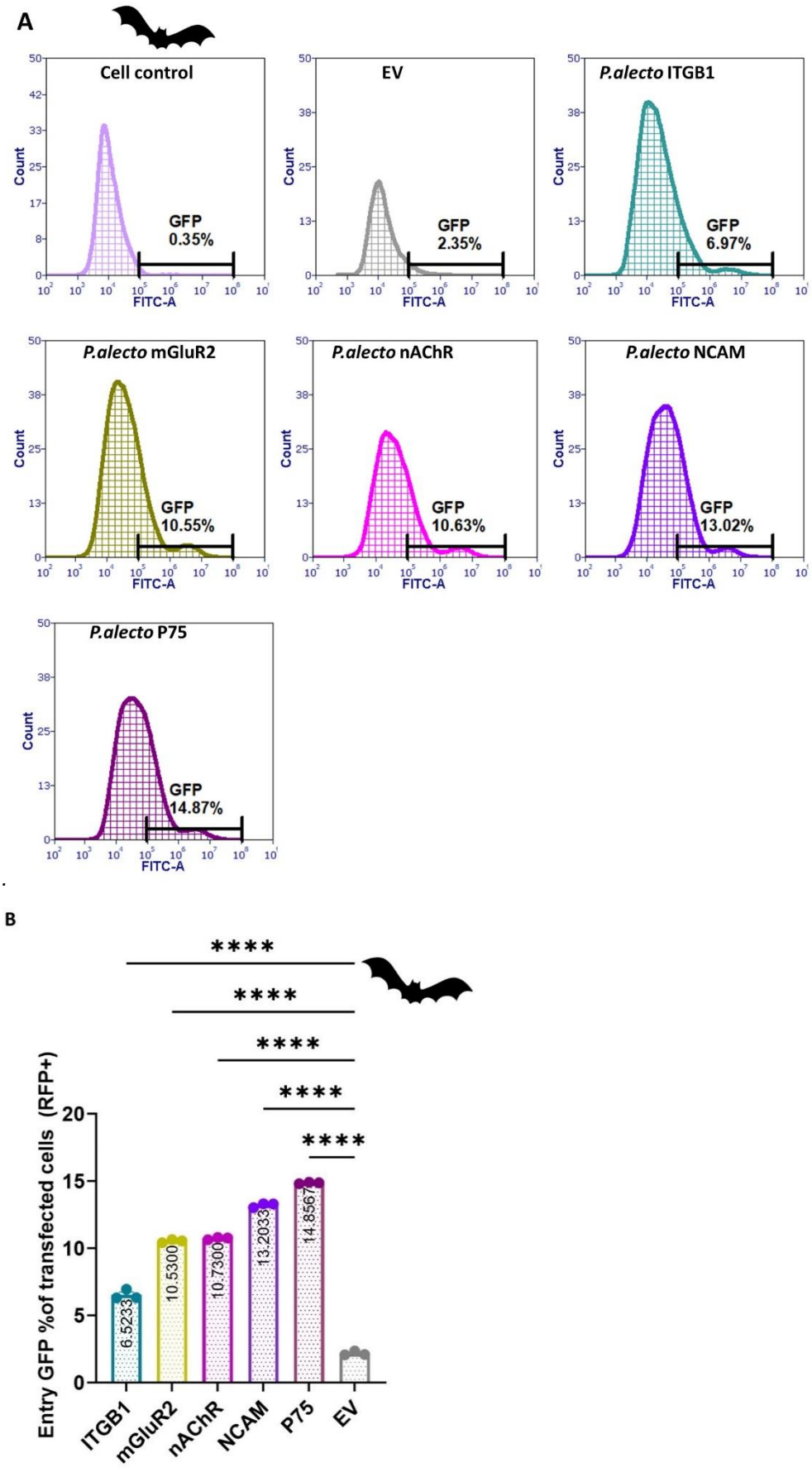

Figure 6.4 Entry of the rVSV-dG-RV-G-GFP in Pa-Br cells overexpressing P.alecto receptors.

(A). *Representative histograms showing the GFP % of rVSV-dG-RV-G-GFP infected Pa-Br cells. The Pa-Br cells were transiently transfected with the P.alecto receptors and empty vector. Fourty-eight hr post transfection, cells were infected with the rVSV-dG-RV-G-GFP MOI=5 for 2 hrs., then cells were washed, collected, and stained with anti-FLAG (targeting the FLAG-tagged receptor) and RV-G antibodies(targeting the virus RV-G), followed by staining with Alexa Fluor 568 and Alexa Fluor 468 conjugated antibodies, respectively for flow cytometry analysis. Flow cytometry data were analysed by FCS Express software. Cell control represents the un-infected cells.* ***(B.).*** *Graph showing the mean of the GFP% of Pa-Br cells infected and transfected with P.alecto receptors and EV. The GFP % corresponds to the RV-G bound to the transfected Pa-Br cells. The experiment was performed three times (n=3) independently. Data are representative of the mean and SEM of three biological replicates using one way ANOVA. ****, P < 0.0001.*

6.2.3 The rVSV-dG-RV-G-GFP down regulates human RV receptor genes on A549 cells.

As previously described **(Chapter 5, section 5.2.2.1, Figure 5.155)**, the rVSV-dG-RV-G-GFP infected A549 cells displayed down modulation of the mRNA levels corresponding to ITGB1, mGluR2, nAChR genes.

6.2.4 Expression of ITGB1, mGluR2 and nAChR orthologs in human A549 cells

To test the ability of the *H.sapiens* ITGB1 (NM_002211.4), mGluR2(NM_000839.5) and nAChR (NM_001039523.3) orthologs to mediate the rVSV-dG-RV-G-GFP entry and replication. We codon optimized and cloned each of the full length ORF of *H.Sapiens* ITGB1, mGluR2 and nAChR with FLAG tag at the C-terminus in pCAGG vector. The vectors were referred to as *H.sapiens* ITGB1 (huITGB1), *H.sapiens* mGluR2 (humGluR2) and *H.sapiens* nAChR (hunAChR), respectively. The expression of the plasmids was evaluated by the immunofluorescence analysis and western blot. Interestingly the *H.sapiens* ITGB1 and *H.sapiens* mGluR2 were expressed as perinuclear dots. While a distinct cytoplasmic accumulation was observed in the *H.sapiens* nAChR **(Figure 6.5 A-C).** Western blot analysis showed the specificity of expression of the expected sizes **(Figure 6.5 D).**

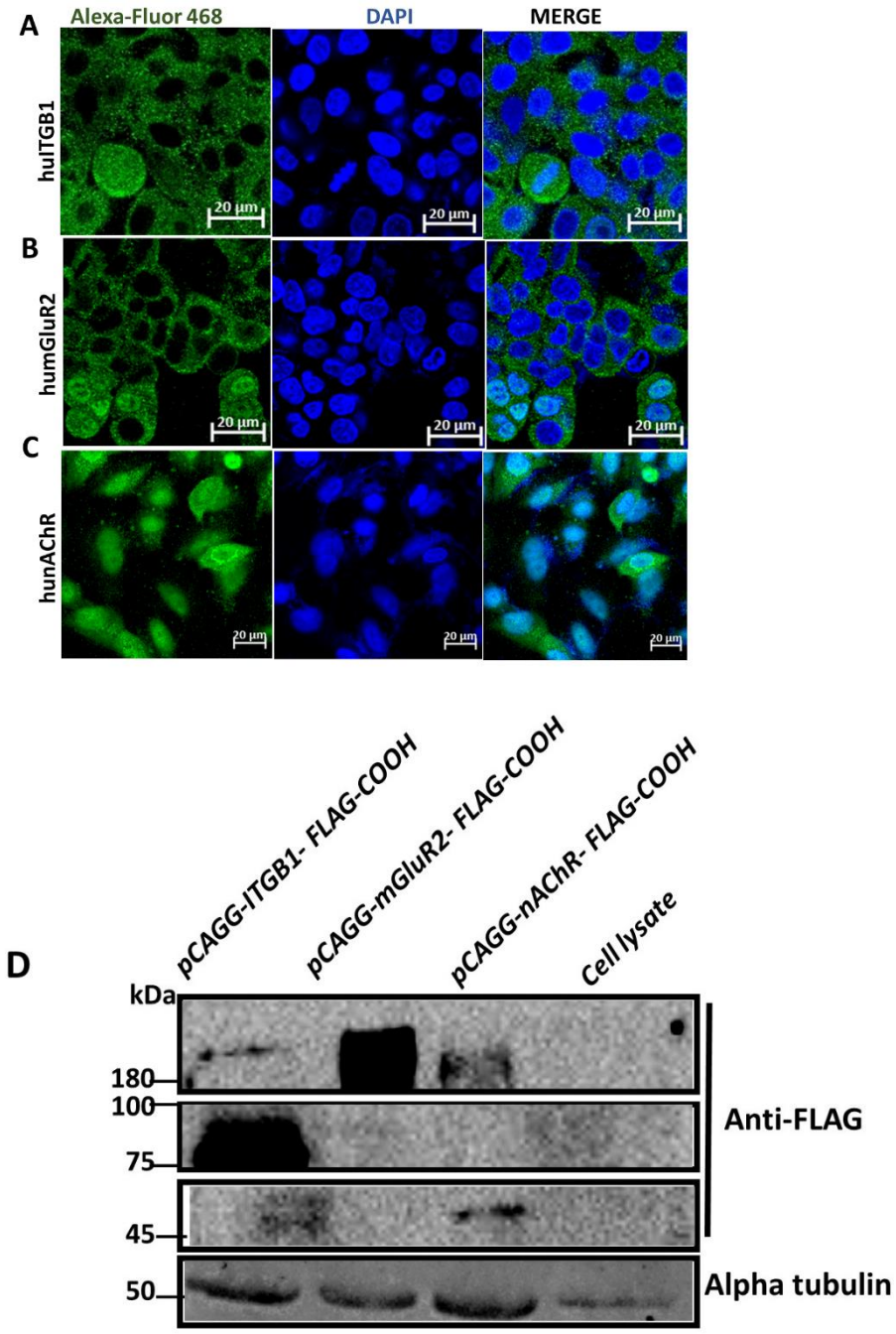

Figure 6.5 Expression of human RV cellular receptors in A549 cells.

*Validation and expressing the H.sapiens plasmids on A549 cells**. (A-C)** The A549 cells were transfected with plasmids encoding. H. Sapiens ITGB1-FLAG, mGluR2-FLAG, and nAChR-FLAG; respectively for 24 h. After 24 hpi, cells were fixed and stained with Anti-FLAG antibody and Alexa-Fluor 468 secondary antibody (Green). Cell nuclei were stained by DAPI (Blue). Fluorescence signals were visualized by confocal immunofluorescence microscopy. Scale bars size, 20 µm**, i**mages analysed using the ZenCore 3.4 software **(D).** Immunoblot analysis of human receptors. A549 were transiently transfected with H.sapiens receptor plasmids. Thirty-six hrs post-transfection, cell lysates were obtained and subjected to SDS-PAGE and Western blot analysis. The blots were stained against the FLAG tag. Alpha tubulin blot was used as a*

loading control. The FLAG-tagged cellular proteins showed the expected sizes pCAGG human ITGB1 (expected size: 88 kDa), pCAGG human mGluR2 (expected size 190-200 kDa), pCAGG human nAChR (expected size 45 kDa) The experiments were performed two times independently (n=2). Cell lysates served as negative control. Uncropped blots are shown in Chapter 9, Supplementary Figure 7

6.2.5 A549 cells expressing *H.sapiens* nAChR enhances viral replication and *H.sapiens* ITGB1 increased virus entry.

Next, we assessed the possibility of more efficient use of the human RV receptors by the rVSV-dG-RV-G-GFP. The A549 cells were overexpressed with the human vectors encoding each of the RV receptors (ITGB1, mGluR2 and nAChR) followed by infecting the cells 48 h later with the rVSV-dG-RV-G-GFP (MOI=5.0). Thirty hpi, revealed significantly high virus replication in A549 cells over expressing each of the human receptors. All receptors showed significantly higher levels of infection compared to the empty vector control **(Figure 6.6 A-C).** These findings were supported by further quantifying the released virus from cells by plaque assay. of the three tested receptors, all infected cells resulted in significantly higher release of the progeny virus compared to the empty vector**,** with the highest virus progeny release and GFP expression in human cells transfected with the *H.sapiens* nAChR **(Figure 6.7 A-B).**

To identify if the enhanced viral replication in cells ectopically expressing the *H.sapiens* nAChR, resulted from initial binding to the nAChR, we employed the entry assay as previously described **(Chapter 5, Figure 5.2)**. The results indicated that however enhanced virus replication was achieved in cells overexpressing the *H.sapiens* nAChR, the highest virus binding was exhibited in cells over expressing the *H.sapiens* ITGB1. The cells ectopically expressing the *H.sapiens* nAChR and *H.sapiens* mGluR2 allowed significantly higher virus entry compared to the empty vector control **(Figure 6.8 A-C).**

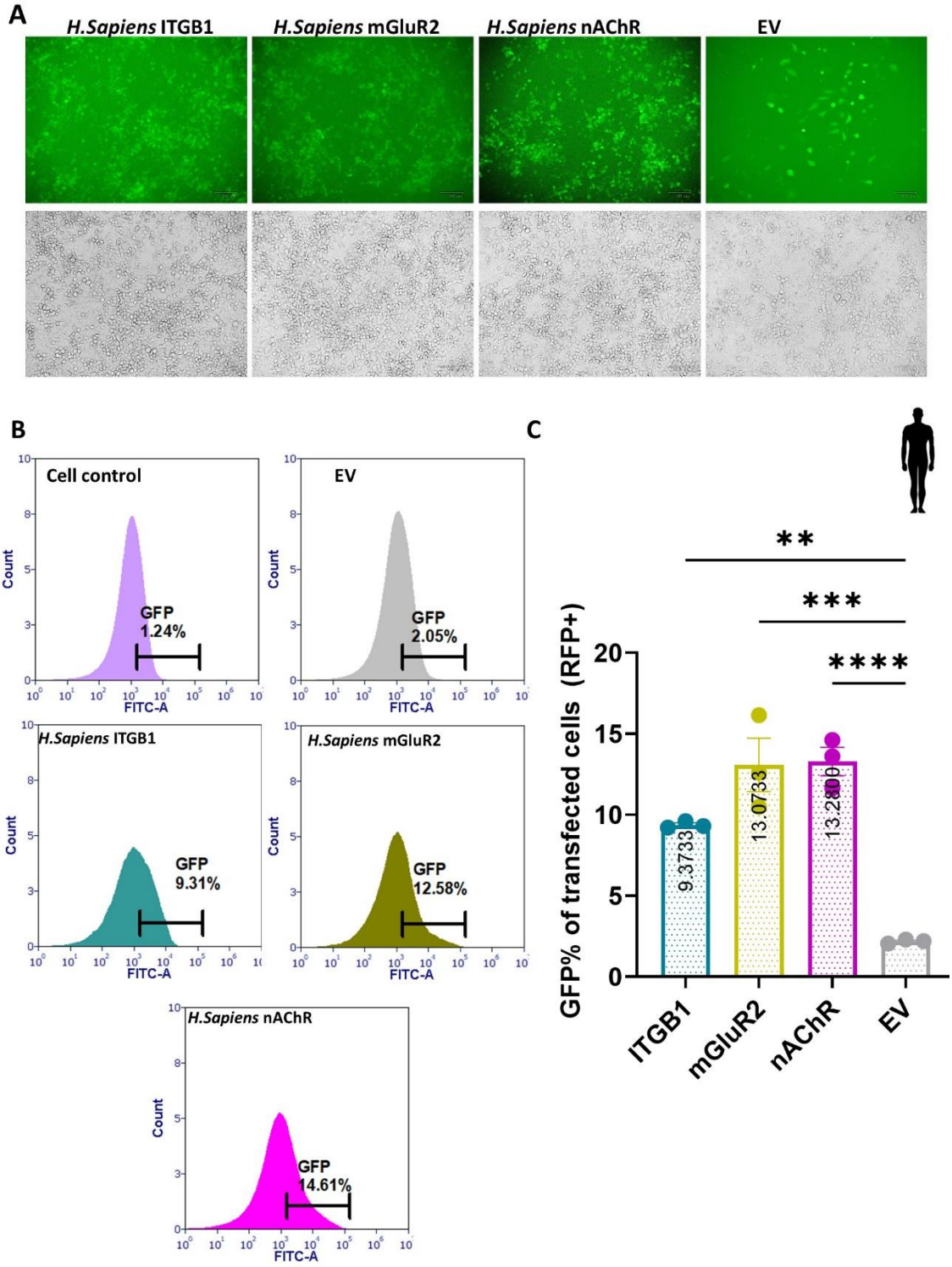

Figure 6.6 Ability of the human receptors to enhance the replication of the rVSV-dG-RV-G-GFP on A549 cells.

(A). *Representative Microscopic fields green, fluorescent (upper), bright (lower) fields of A549 cells infected with rVSV-dG-RV-G-GFP. The A549 cells were transiently transfected with the H.sapiens receptors. Forty-eight hrs post transfection, cells were infected with the rVSV-dG-RV-G-GFP, MOI=5. Thirty hpi, the cells were imaged for fluorescence.* ***(B).*** *Representative histograms showing the GFP % of rVSV-*

dG-RV-G-GFP infected Pa-Br cells. A549 cells were transiently transfected with H.sapiens receptors. Forty-eight hrs post transfection, cells were infected with rVSV-dG-RV-G-GFP, MOI=5. Thirty hpi, the cells collected and stained against the FLAG antibody (targeting the receptors) and followed by staining with Alexa Fluor 568 conjugated antibody for Flow cytometry analysis. GFP% was calculated from the receptor expressing cells, the empty vector transfected A549 cells was used as control, cell control represents the un-infected cells. ***(C).*** *Graph showing the mean of the GFP% of A549 cells infected and transfected with H.sapiens receptors compared to A549 cells infected and transfected with the empty vector. The GFP % corresponds to the rVSV-dG-RV-G-GFP internalized to the transfected A549 cells. The experiment was performed three times (n=3) independently. Data are representative of the mean and SEM of three biological replicates using one way ANOVA. **, P < 0.01, ****, P < 0.0001.*

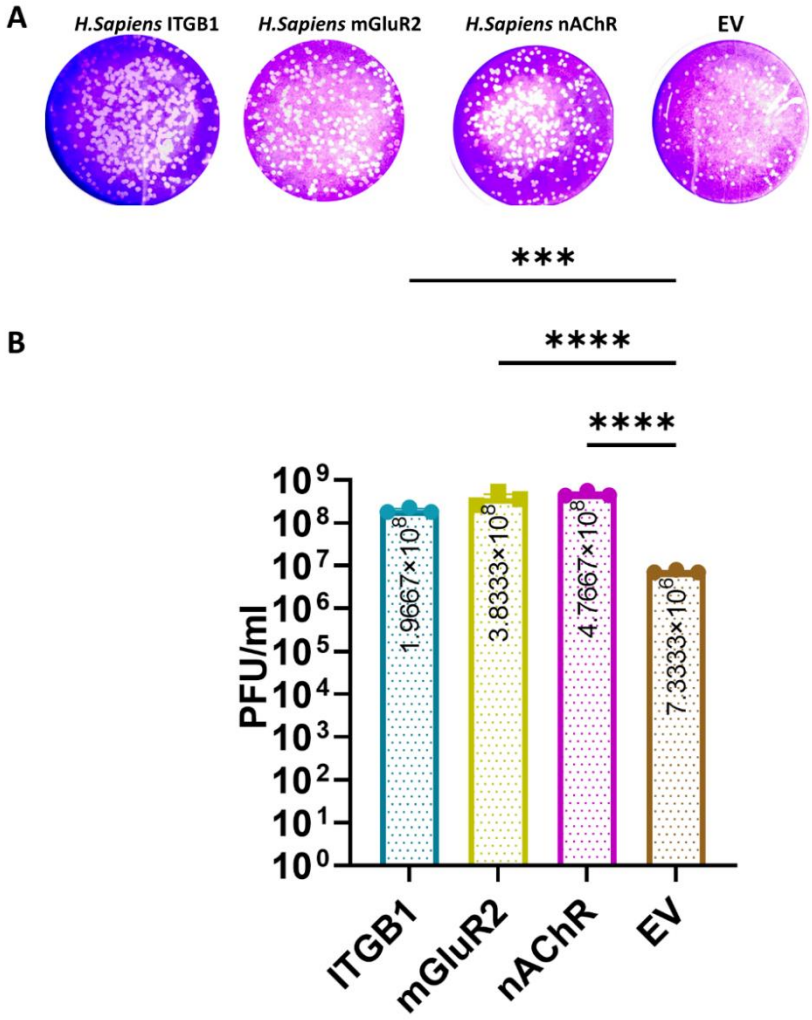

Figure 6.7 Replication of rVSV-dG-RV-G-GFP on A549 cells overexpressing human receptors.

(A). *Representative plaque morphology of infected A549 cells. A549 cells transiently expressing the H.sapiens receptors, were infected with the rVSV-dG-RV-G-GFP MOI=5. Thirty hpi, the viral supernatants were collected for quantifying the released progeny virus. The released viruses were quantified using plaque assay on BHK-21 cells after 72 hrs.* ***(B).*** *Graph showing the difference of the mean PFU/mL of rVSV-*

*dG-RV-G-GFP between A549 cells expressing H.sapiens receptors and the empty vector. The experiment was performed three times (n=3) independently. Data are representative of the mean and SEM of three biological replicates using one way ANOVA. ***, P < 0.001, ****, P <0.0001.*

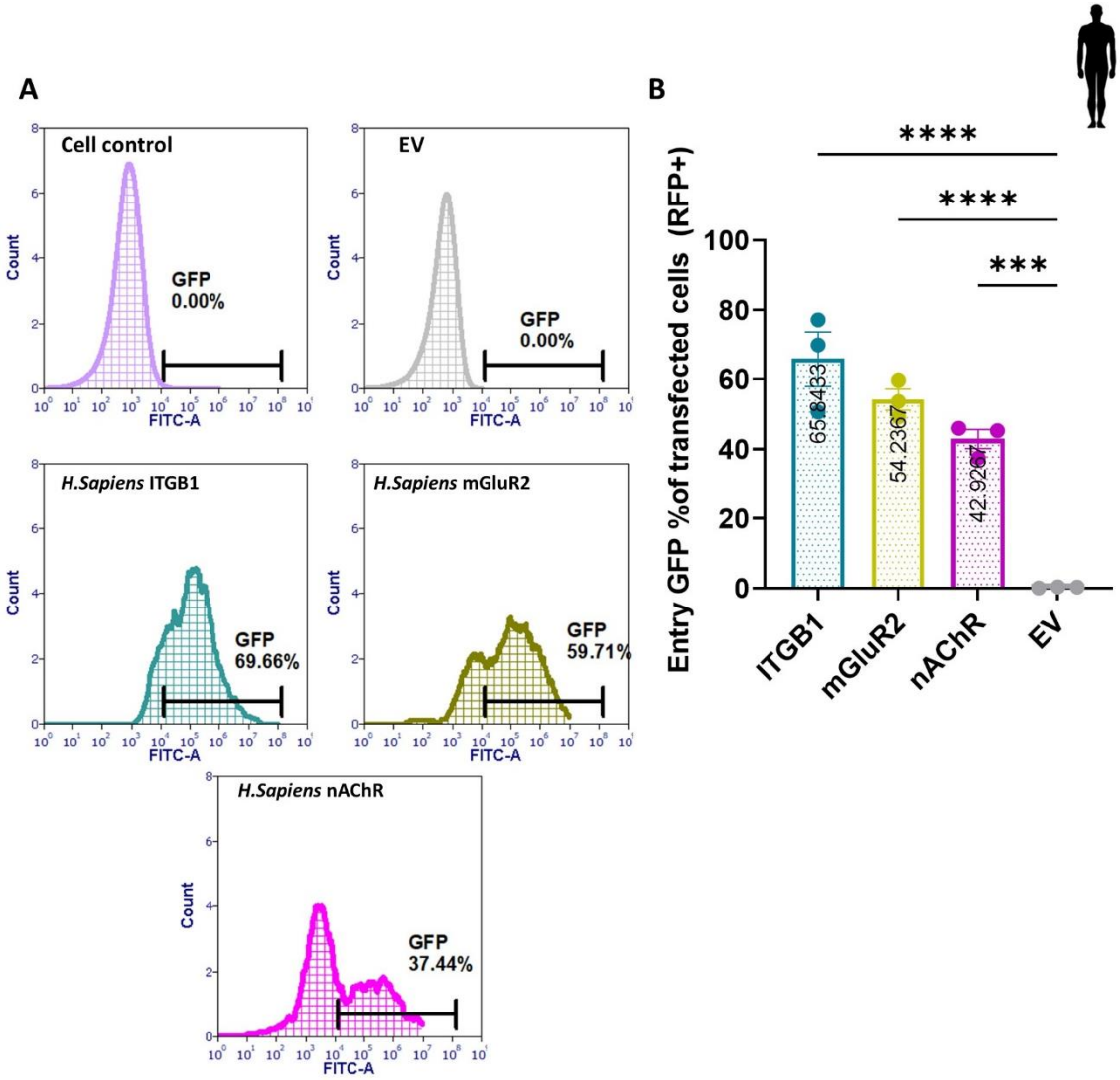

Figure 6.8 Entry of rVSV-dG-RV-G-GFP on A549 cells expressing human receptors.

(A). *Representative histograms showing the GFP % of rVSV-dG-RV-G-GFP infected A549 cells. The A549 cells were transiently transfected with the H.sapiens receptors and empty vector (as control). Forty-eight hr post transfection, cells were infected with the rVSV-dG-RV-G-GFP MOI=5 for 2 hrs., then cells were washed, collected, and stained with anti-FLAG (targeting the FLAG-tagged receptor) and RV-G antibodies(targeting the virus RV-G), followed by staining with Alexa Fluor 568 and Alexa Fluor 468 conjugated antibodies, respectively for flow cytometry analysis. Flow cytometry data were analysed by FCS Express software. Cell control represents the un-infected cells.* ***(B).*** *Graph showing the mean of the GFP% of A549 cells infected and transfected with H.sapiens receptors and EV. The GFP % corresponds to the RV-G bound to the transfected A549 cells. The experiment was performed three times (n=3) independently. Data are representative of the mean and SEM of three biological replicates using one way ANOVA. **, P < 0.01, ***, P < 0.001*

6.2.6 Down-regulated ITGB1, nAChR and NCAM receptor genes are sufficient for RV replication in MDCK cells.

To fully elucidate the role of the cellular genes involved in RV replication in MDCK cells, these cells were infected with the rVSV-dG-RV-G-GFP at MOI of 5. After 24h, the cellular RNA was extracted and the difference in the mRNA levels was compared in uninfected cells and in response to infection. The rVSV-dG-RV-G-GFP infection resulted in downregulation of the ITGB1, NCAM and nAChR to a similar extent, whereas the mRNA levels of the mGluR2 and p75 were less affected **(Figure 6.9 A-B).**

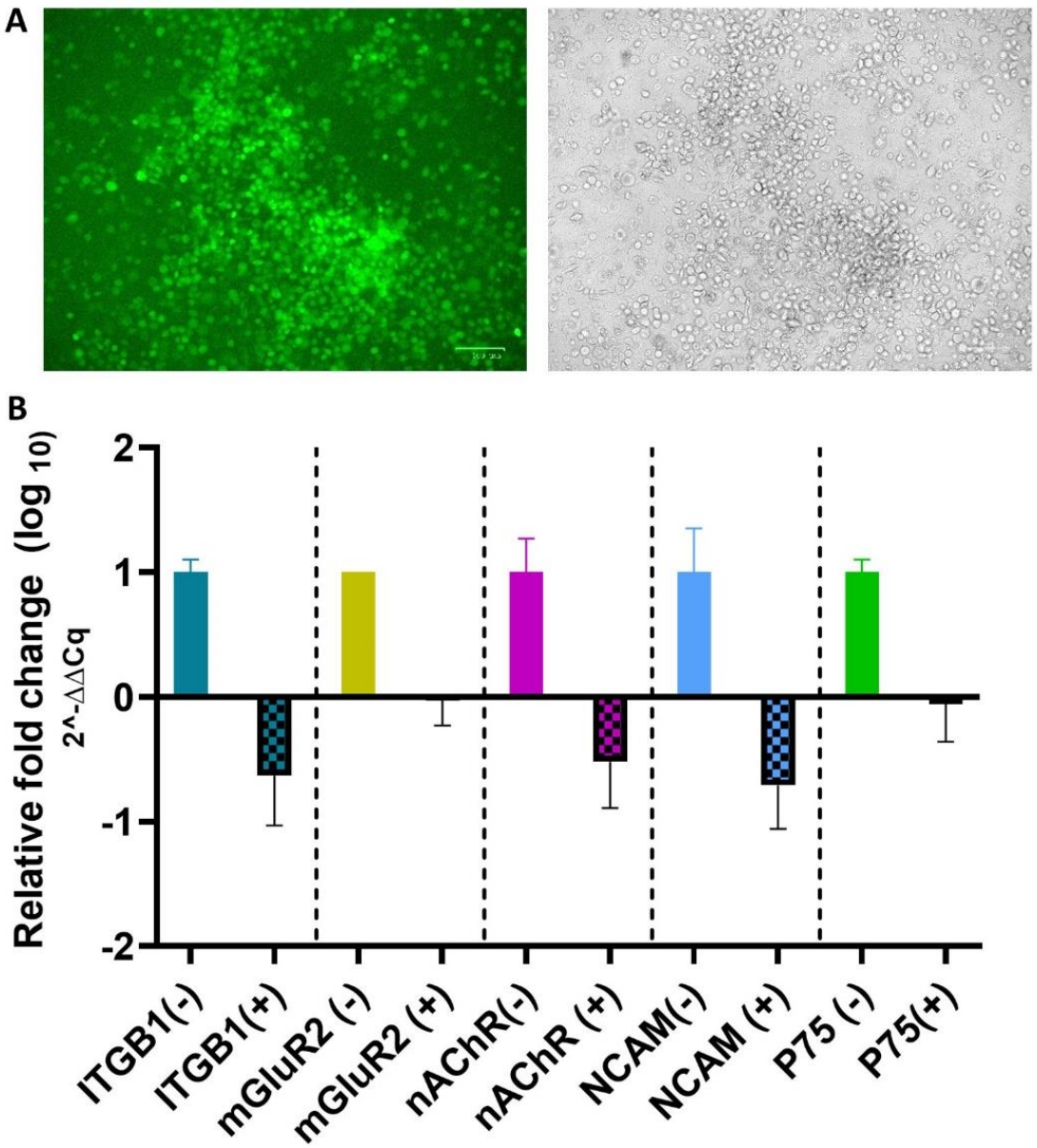

Figure 6.9 Relative expression (in fold change value) of RV cellular receptor genes on MDCK cells.

***(A**). Microscopic fields of infected MDCK cells green (left), bright (right). MDCK cells were infected with rVSV-dG-RV-G-GFP (MOI 5), 24 hpi, cells were imaged for the GFP expression corresponding to virus replication. **(B).** The differential expression (in fold change) of the RV cellular genes were measured by qRT-PCR on MDCK cells before (-) and after infection (+) with rVSV-dG-RV-G-GFP. Twenty-four hrs after infection, cellular RNA was extracted from infected and non-infected MDCK cells. The relative RNA expression (mean ± SEM) of each of RV receptor gene were normalised to dog beta actin using ΔΔCt method. The experiment was performed three times (n=3) independently. Error bars represented the SEM from three biological replicates.*

6.2.7 Expression of Canine ITGB1, mGluR2 and nAChR in MDCK cells

For demonstrating the replication of the rVSV-dG-RV-G-GFP in dogs, the Madin-Darby canine kidney (MDCK) cell line was selected since they represent the canine kidney cells, and they support the RV replication. To test the receptor preference of RV on MDCK cells, we cloned the full length ORF of *C.familiaris* ITGB1 (XM_038658027.1), mGluR2 (XM_038427610.1) and nAChR (NM_001003144.2) in pCAGG vector with a FLAG tag at the C-terminus, referred as *C.familiaris* ITGB1 (doITGB1), *C.familiaris* mGluR2 (domGluR2) and *C.familiaris* nAChR (donAChR), respectively. The localization of the canine receptors was tested with the immunofluorescence analysis revealing different localization patterns. The ITGB1 was localized on the cells in the form of perinuclear dots, distinct from the cytoplasmic localization displayed by the *C.familiaris* mGluR2 and *C.familiaris* nAChR proteins (**Figure 6.10 A-C)**. Further validation for the receptor's expression was carried out using the western blot which showed expression of the protein at bands corresponding to the expected molecular weight **(Figure 6.11 D).**

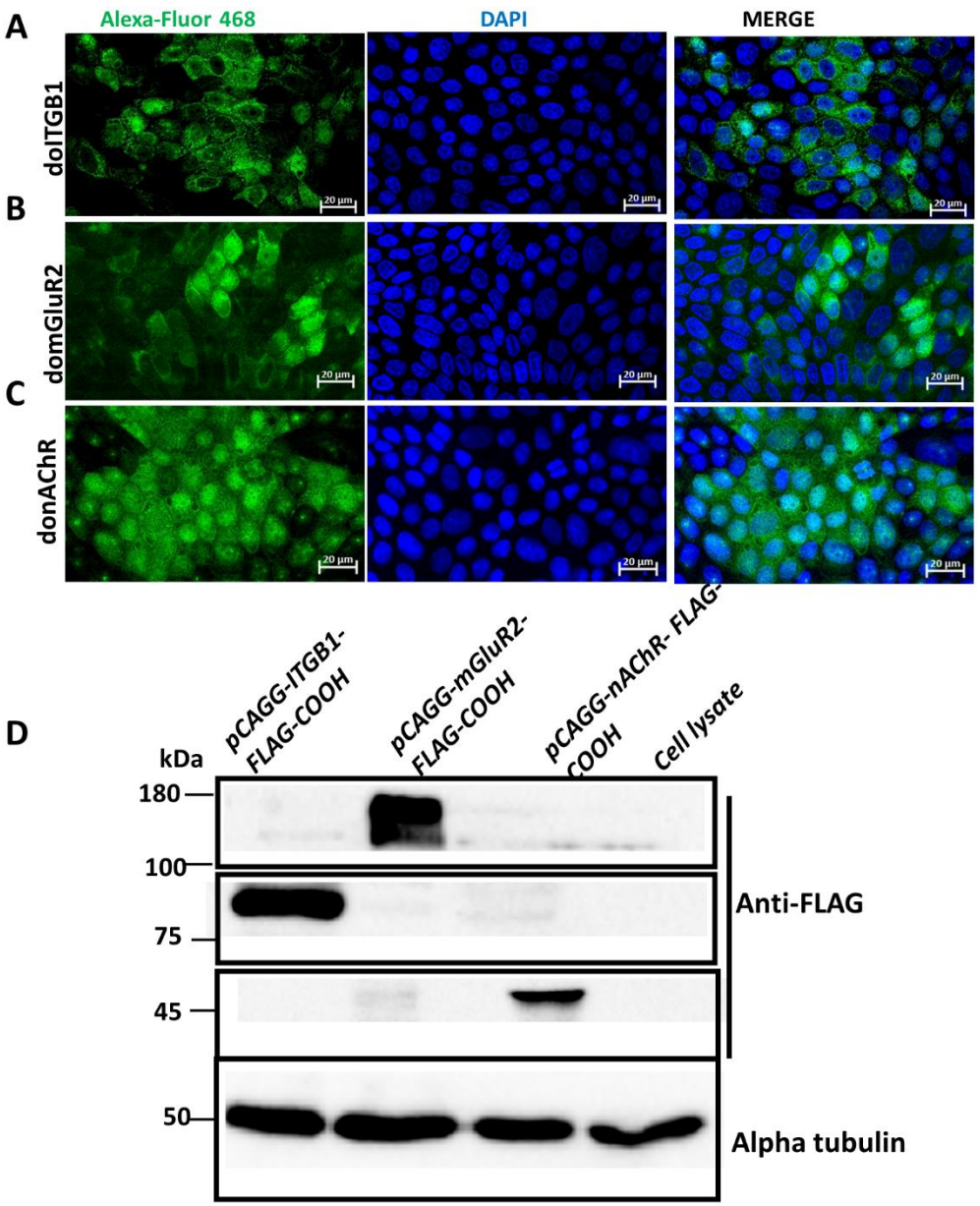

Figure 6.10 Expression of dog RV cellular receptors on MDCK cells.

Validation the expression and localization of C.familiaris plasmids on MDCK cells ***(A-C)*** *The MDCK cells were transfected with plasmids encoding. C.familiaris ITGB1-FLAG, mGluR2-FLAG, and nAchR-FLAG; respectively for 24 h. After 24 hpi, cells were fixed and stained with Anti-FLAG antibody and Alexa-Fluor 468 secondary antibody (Green). Cell nuclei were stained by DAPI (Blue). fluorescence signals were visualized by confocal immunofluorescence microscopy. Scale bars size, 20 µm Images analysed using the ZenCore 3.4 software.* ***(D).*** *Immunoblot analysis of dog receptors on MDCK cells. MDCK cells were transiently transfected with the C.familiaris receptor plasmids. Thirty-six hrs post-transfection, cell lysates were obtained and subjected to SDS-PAGE and Western blot analysis. The blots were stained against the FLAG tag. Alpha tubulin blot was used as a loading control. The FLAG-tagged cellular proteins showed the expected sizes pCAGG canine ITGB1 (expected size: 88 kDa), pCAGG canine mGluR2 (expected size 180-*

*200 kDa), pCAGG canine nAChR (expected size 45 kDa**).** Cell lysates served as the negative control. The experiment was performed two times independently (n=2). Uncropped blots are shown in Chapter 9, supplementary Figure 8*

6.2.8 ITGB1 enhances virus attachment and replication on MDCK cells.

Since dogs represent the main reservoir for RV, we tested the receptors preference enhancing the rVSV-dG-RV-G-GFP binding and replication on MDCK cells. To assess the rVSV-dG-RV-G-GFP replication and virus progeny release in respect to the canine receptors. The MDCK cells were transfected with the cDNA encoding the *C.familiaris* ITGB1, mGluR2 and nAChR. After 48 h, cells were infected with rVSV-dG-RV-G-GFP at an MOI of 5. Thirty hrs, post infection, the GFP percentage and the released virus progeny were compared. A significant increase in the GFP percentage was observed in the cells expressing the *C.familiaris* ITGB1 and *C.familiaris* nAChR and *C.familiaris* mGluR2 compared to the empty vector control **(Figure 6.11 A-C).** However, the plaque assay results showed no significant difference from the empty vector control **(Figure 6.12 A-B)**.

To compare the binding preference of the RV-G to the cells expressing the canine receptors, the entry assay was employed. The MDCK cells were transfected with the *C.familiaris* receptors. Forty-eight hours post-transfection, cells were infected with the rVSV-dG-RV-G-GFP at MOI=5 for 2 hrs, followed by washing and cells were prepared for FC analysis. A similar preference pattern was also illustrated, wherein a substantial increase in viral entry occurred in cells that were transiently expressing *C.familiaris* ITGB1 compared to the empty vector control. The less binding capacity of the RV to the MDCK cells ectopically expressing the *C.familiaris* nAChR compared to the *C.familiaris* ITGB1 was observed. Notably, the lowest RV-G binding was observed on MDCK cells overexpressing the *C.familiaris* mGluR2. Collectively, the obtained results indicatethat ITGB1 play a significant role in the entry and replication of rVSV-dG-RV-G-GFP on MDCK cells **(Figure 6.13 A-C).**

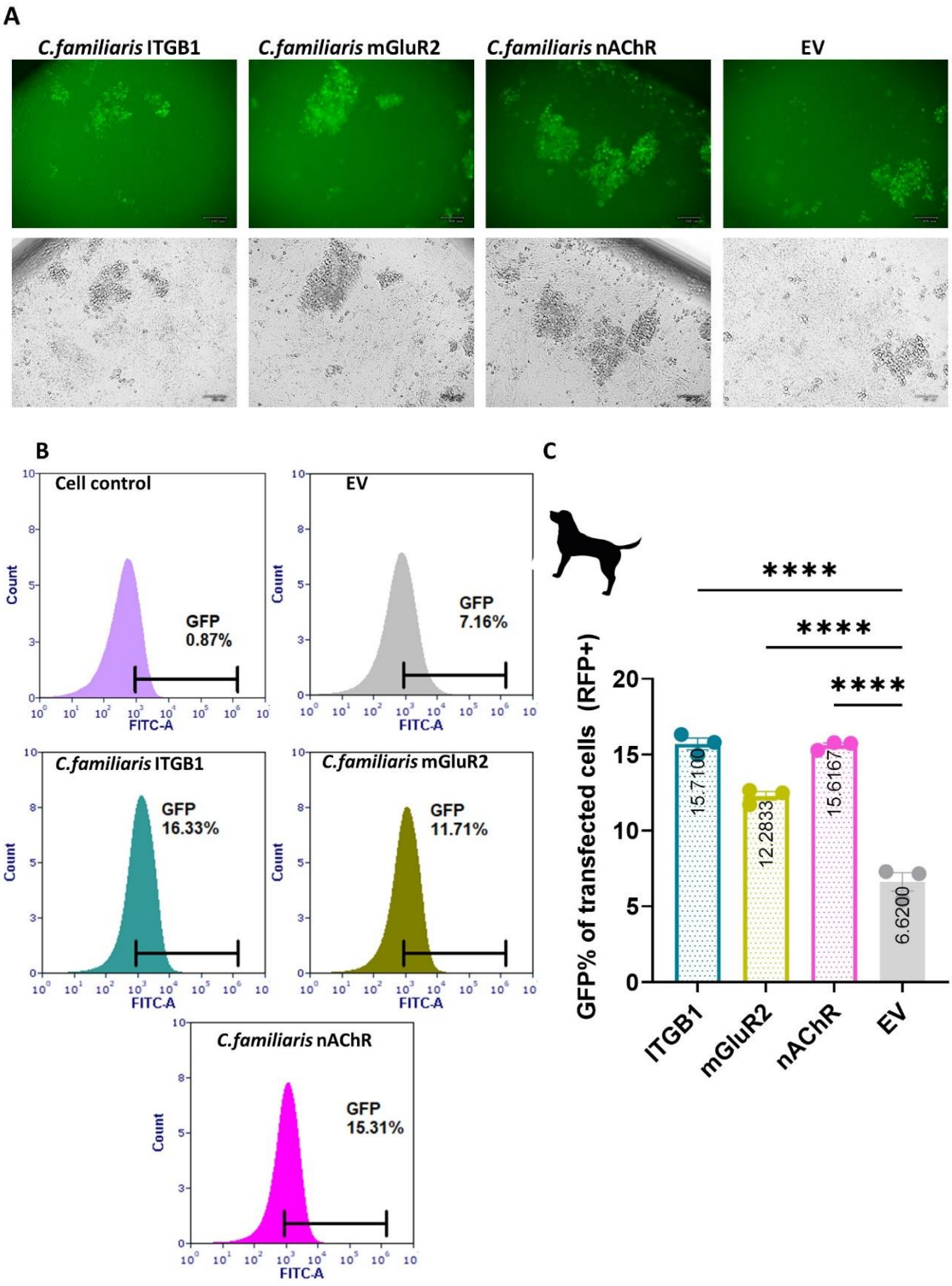

Figure 6.11 Replication of rVSV-dG-RV-G-GFP on MDCK cells overexpressing C.familiaris receptors

(A) *Representative Microscopic fields green, fluorescent (upper), bright (lower) of MDCK cells infected with rVSV-dG-RV-G-GFP. The MDCK cells were transiently transfected with the C.familiaris receptors Forty-eight hrs post transfection, cells were infected with the rVSV-dG-RV-G-GFP, MOI=5. Thirty hpi, the cells were imaged for fluorescence.* ***(B).*** *Representative histograms showing the GFP % of rVSV-dG-RV-G-GFP infected MDCK cells. MDCK cells were transiently transfected with C.familiaris receptors. Forty-eight hrs post*

transfection, cells were infected with rVSV-dG-RV-G-GFP, MOI=5. Thirty hpi, the cells collected and stained against the FLAG antibody (targeting the receptors) and followed by staining with Alexa Fluor 568 conjugated antibody for Flow cytometry analysis. GFP% was calculated from the receptor expressing cells, the empty vector transfected MDCK cells was used as control, cell control represented the un-infected cells. ***(C).*** *Graph showing the mean of the GFP% of MDCK cells infected and transfected with C.familiaris receptors compared to cells infected and transfected with the empty vector. The GFP % corresponds to the rVSV-dG-RV-G-GFP internalized to the transfected MDCK cells. The experiment was performed three times (n=3) independently. Data are representative of the mean and SEM of three biological replicates using one way ANOVA. *, P ≤ 0.05, ***, P ≤ 0.001, ****, P ≤ 0.0001.*

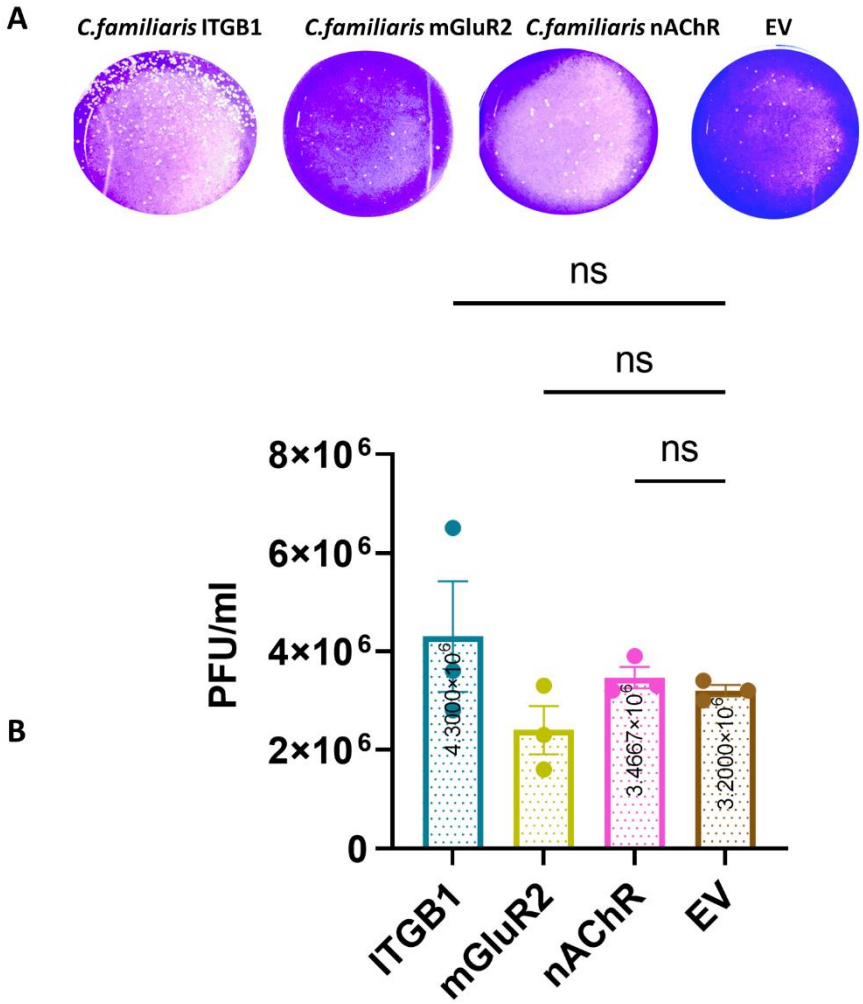

Figure 6.12 Replication of rVSV-dG-RV-G-GFP on MDCK cells overexpressing Canine receptors.

(A). Representative *plaque morphology of infected MDCK cells. MDCK cells transiently expressing the C.familiaris receptors, were infected with the rVSV-dG-RV-G-GFP MOI=5. Thirty hpi, the viral supernatants were collected for quantifying the released progeny virus. The released viruses were quantified using plaque assay on BHK-21 cells after 72 hrs.* ***(B).*** *Graph showing the difference of the mean PFU/mL of rVSV-*

dG-RV-G-GFP between MDCK expressing C.familiaris receptors and the MDCK cells infected and transfected with the empty vector. The experiment was performed three times (n=3) independently. Data are representative of the mean and SEM of three biological replicates using one way ANOVA. ns, non-significant, P > 0.05.

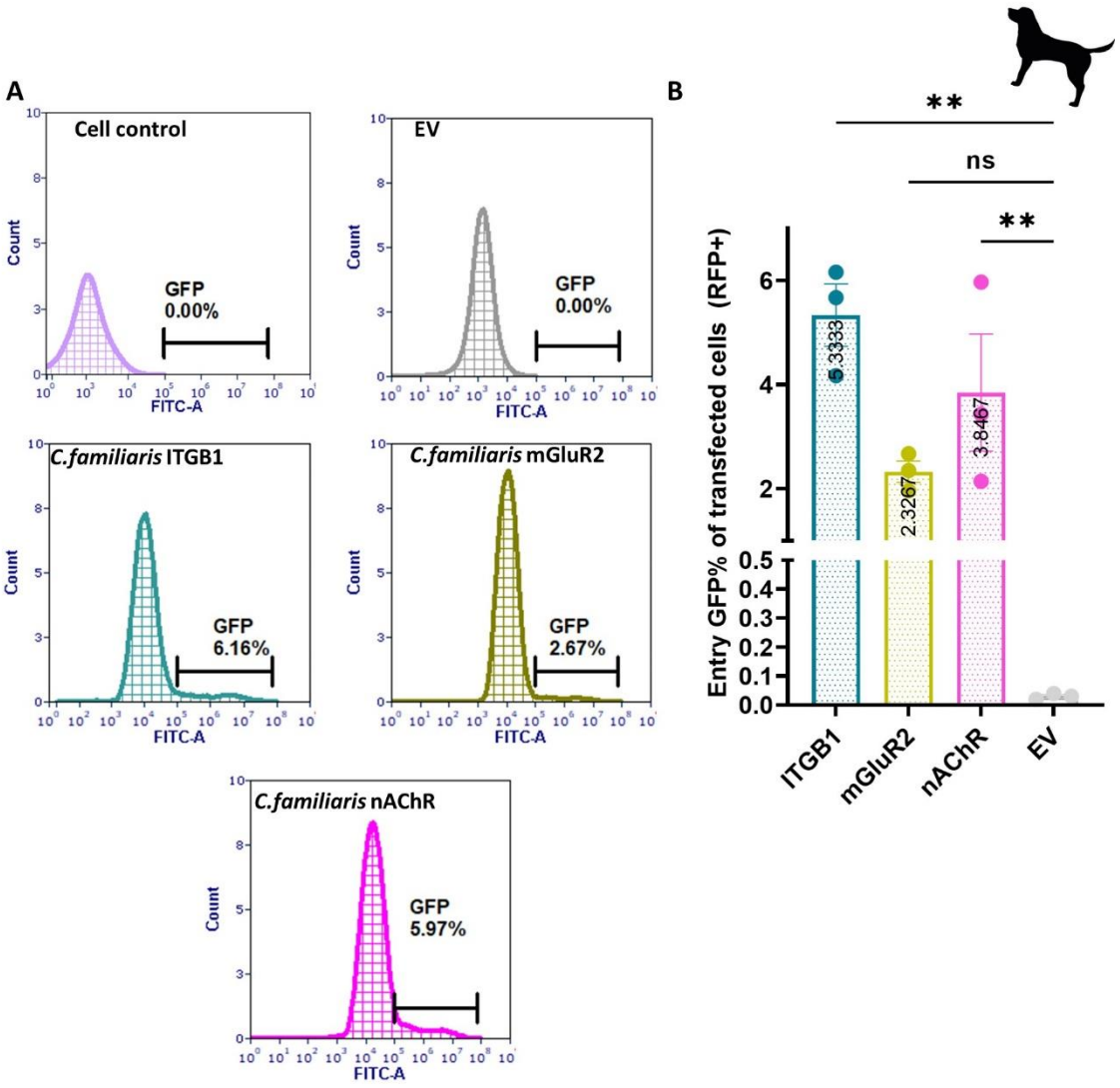

Figure 6.13 Entry of rVSV-dG-RV-G-GFP on MDCK cells expressing C.familaris receptors.

(A). *Representative histograms showing the GFP % of rVSV-dG-RV-G-GFP infected MDCK cells. The MDCK cells were transiently transfected with the C.familiaris receptors and empty vector. Fourty-eight hr post transfection, cells were infected with the rVSV-dG-RV-G-GFP MOI=5 for 2 hrs., then cells were washed, collected, and stained with anti-FLAG (targeting the FLAG-tagged receptor) and RV-G antibodies(targeting the virus RV-G), followed by staining with Alexa Fluor 568 and Alexa Fluor 468 conjugated antibodies, respectively for flow cytometry analysis. Flow cytometry data were analysed by FCS Express software. Cell control represented the un-infected cells.* ***(B.).*** *Graph showing the mean of the GFP% of MDCK cells infected and transfected with C.familiaris receptors and EV. The GFP % corresponds to the RV-G bound to*

*the transfected MDCK cells. The experiment was performed three times (n=3) independently. Data are representative of the mean and SEM of three biological replicates using one way ANOVA. ****, P ≤ 0.0001.*

6.2.9 The nAChR enhanced RV replication in bats, while ITGB1 resulted in more initial virus binding in dogs and humans.

Summarizing the results obtained from the replication and entry of the rVSV-dG-RV-G-GFP on different cell lines. In bats, entry, and replication of the rVSV-dG-RV-G-GFP was enhanced with the expression of the *P.alecto* nAChR. In dogs, and humans elevated levels of the RV -G binding was achieved in cells expressing the ITGB1. Likewise, enhanced progeny virus release was mediated on MDCK cells expressing *C.familiaris* ITGB1. While in human, the A549 cells ectopically expressing the *H.sapiens* nAChR resulted in more efficient virus release **(Figure 6.14).**

A

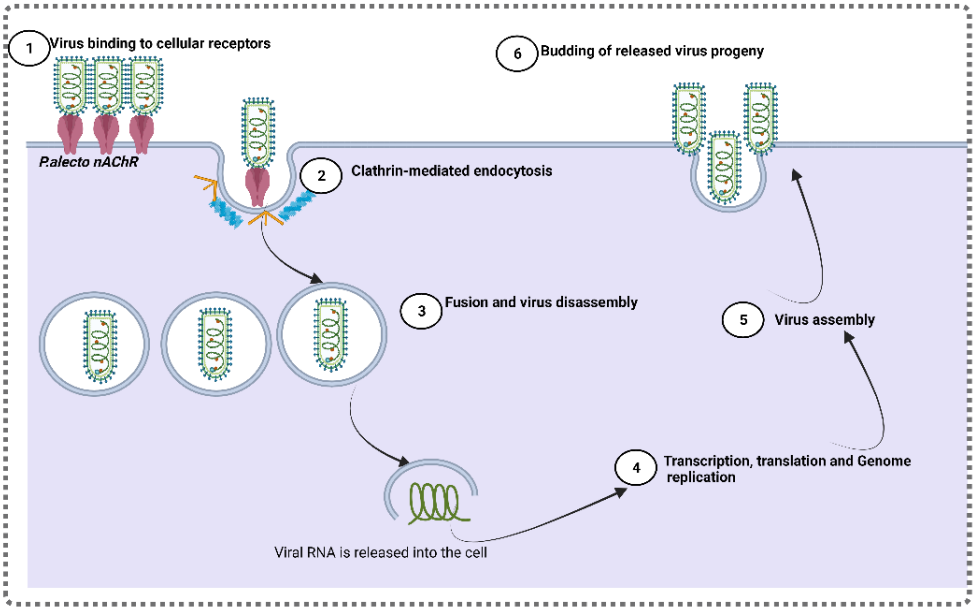
1 Virus binding to cellular receptors
6 Budding of released virus progeny
Palecto nAChR
2 Clathrin-mediated endocytosis
3 Fusion and virus disassembly
5 Virus assembly
4 Transcription, translation and Genome replication
Viral RNA is released into the cell

B

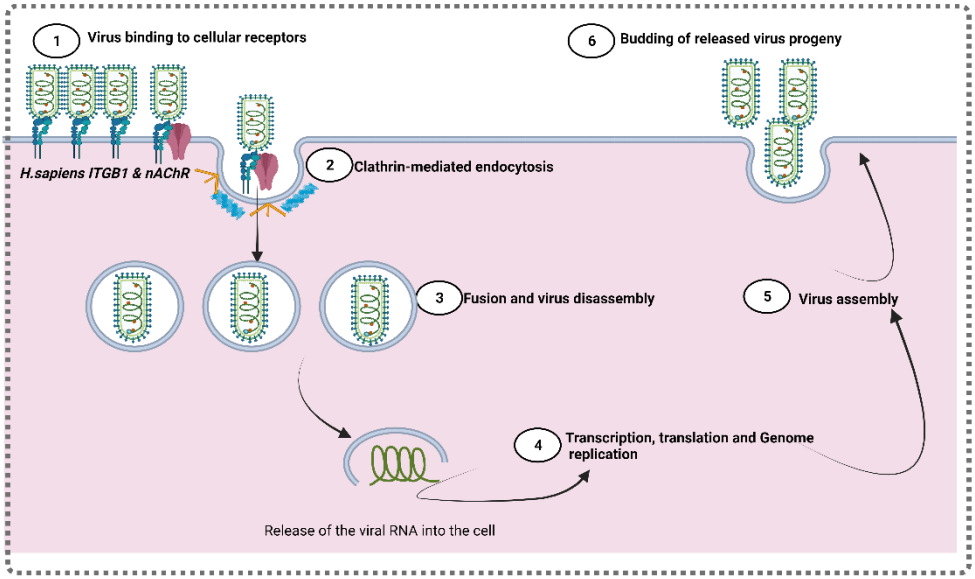
1 Virus binding to cellular receptors
6 Budding of released virus progeny
H.sapiens ITGB1 & nAChR
2 Clathrin-mediated endocytosis
3 Fusion and virus disassembly
5 Virus assembly
4 Transcription, translation and Genome replication
Release of the viral RNA into the cell

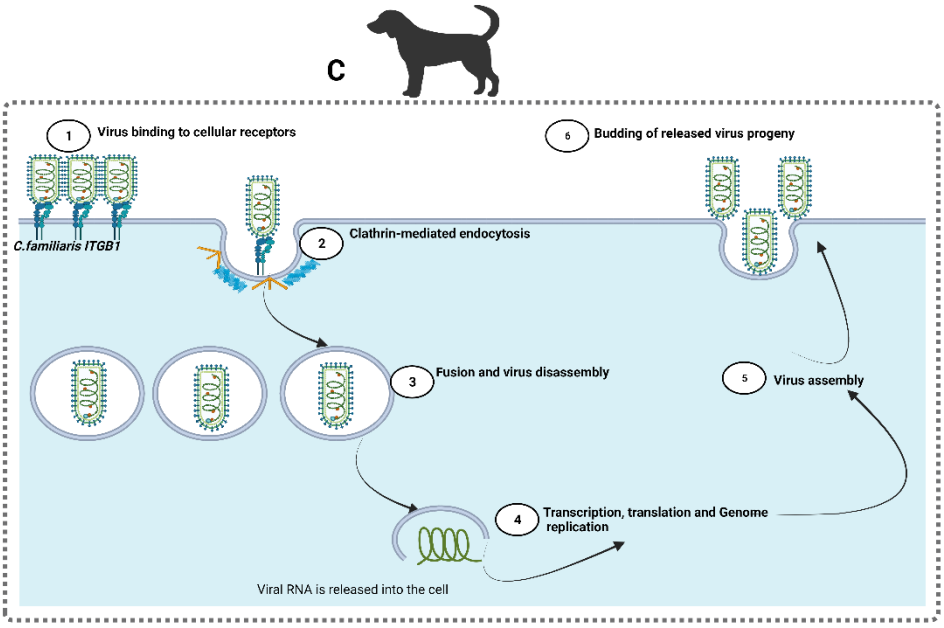

Figure 6.14 Schematic diagram summarizing the RV receptor preference for entry and replication among the bats, human and dog cell lines.

(A). *Schematic diagram showing the proposed entry and internalization of rVSV-dG-RV-G-GFP on Pa-Br cells (P.alecto brain cells), firstly, the overexpression of P.alecto nAChR allowed more virus entry which consequently resulted in more virus binding allowing virus internalization through the nAChR via receptor-mediated endocytosis, resulting in enhanced release of virus progeny.* ***(B).*** *Schematic diagram showing the entry of rVSV-dG-RV-G-GFP into A549 human lung cells, firstly, the surface H.sapiens ITGB1 allowed more virus binding and entry on the cellular surface. Afterwards, presumably, an interaction between the ITGB1 bound to the rVSV-dG-RV-G-GFP and the H.sapiens nAChR occurs, allowing the internalization of the ITGB1 virus complex through the nAChR, facilitating their internalization through receptor-mediated endocytosis and resulting in increased virus release.* ***(C).*** *Schematic diagram showing the entry and replication of rVSV-dG-RV-G-GFP on MDCK, canine kidney cells, the binding of the rVSV-dG-RV-G-GFP virus to the cells was enhanced by the abundance of C.familiaris ITGB1 on the cellular surface, this binding allowed the virus to enter and subsequently internalized via the ITGB1 through endocytosis, resulting in more released virus progeny.*

6.3 Discussion

Over the past years, the origin of the Ebola virus, SARS-CoV, MERS-CoV, Hendra virus and other viral diseases have been linked to the bats (Letko et al., 2020). With specific regard to the bat species belonging to the genus Pteropus which have been reported previously as reservoirs for the Hendra virus (Dlugolenski et al., 2013). Thus, we investigated the susceptibility of the *P.alecto* brain cell line to the RV infection. Remarkably, to the best of our knowledge we are the first to report here that the Pa-BR

cell line which is derived from the *P.alecto* brain could be infected with the RV. This finding is crucial in understanding the potential role that could be played by the *P.alecto* as potential virus reservoir of the RV wildlife. However, it is worth mentioning that the *in vitro* susceptibility of the bat species to the virus does not inevitably imply its susceptibility to the RV *in vivo* (Dlugolenski et al., 2013). Considering the numerous factors which influence the likelihood of the virus transmission in the field, among those the bat immune response, the ecological interaction which would allow the contact between the virus and the host and behavioural patterns (Letko et al., 2020). Further *in vivo* studies are deemed essential to understand the significance of the susceptibility of *P.alecto* to the virus infection and the explanation of the restricted RV reservoirs to the microbat species.

Most the human rabies cases are known to have originated from the cross-species transmission which requires the species host cell factors for establishment of infection into the new host (Wu et al., 2020). Thereby, in this chapter, understanding the host cell factors contributing to viral entry and replication of RV among human, canine, and bat cell lines, will gain more insight on the rabies viral tropism (Sakuma and Takeuchi, 2012).

As reported previously, the RV infection downregulated the expression of some of the host genes that could be involved in cell metabolism, protein synthesis and synaptic activity upon RV infection (Prosniak et al., 2001). Nonetheless, there are no recent studies that evaluated the regulation of the RV to the receptor gene expressions among the different hosts. Therefore, we aim to dissect the role played by the rVSV-dG-RV-G-GFP in the expression patterns of these genes upon the RV infection in different cell lines representing distinct species. In this study, we showed a notable downregulation of the nAChR-expressing genes in response to the RV infection among all the tested cell lines. However, the genes encoding the p75 and mGluR2 expression profiles were similarly downregulated among the bat and human cell lines. In contrast, the expression levels of the p75 and mGluR2 were less affected by the RV infection in MDCK cell line. Further analysis for the ITGB1 expression levels also showed downregulation in both human and MDCK cell lines, but not in bat cell lines which might be correlated to the absence of the integrin plexin domain in the *P.alecto* ITGB1 bat species **(Chapter 3, section 3.2.1)**. Based on these findings, the varying downregulation of the receptor gene profiles is a matter

of interest since it defines the underlined inter species variability in RV susceptibility. One might also conclude that all the tested cell lines which showed permissiveness to the rVSV-dG-RV-G-GFP infection modulated all the known receptor genes of RV with various levels of magnitude. Only the ITGB1 and NCAM mRNA levels showed no change in the bat cell lines despite their susceptibility to the infection. This finding also supports our previous results that not all the known receptors for RV are utilized during the infection **(Chapter 5)**. Additionally, it should be emphasized that the differences in the expression levels of the receptor genes were assessed after the first 24 h of the rVSV-dG-RV-G-GFP infection. Yet, further investigation to the temporal regulation of those genes by the RV infection might be required to gain more understanding of the mechanism by which the RV regulate those genes.

Given that our cell tropism data indicated that the RV infection is not restricted to the neural cells only, but the cells of intestinal epithelium and renal origins could also be infected suggesting the broad cellular tropism of RV. The main determinant of virus infection is the binding to the host cellular receptors which defines the virus tissue tropism and host range (Liu et al., 2021). To gain more understanding of the mechanism by which RV is transmitted through bats, dog, and human, we compared the role of the ectopically expressed RV receptor orthologs in the rVSV-dG-RV-G-GFP entry and replication. Unexpectedly, our results indicated that the RV entry and replication on different cell lines showed differential virus preference. The replication of the rVSV-dG-RV-G-GFP on the Pa-Br cells was enhanced by the overexpression of the *P.alecto* nAChR receptor. While on MDCK cells, the virus initial attachment and GFP expression was upregulated by the ectopic expression of the ITGB1. In human cell line, the initial attachment was augmented by the *H.sapiens* ITGB1, while its replication and release were amplified by the expression of the *H.sapiens* nAChR **(Figure 6.14)**. Given that the receptors were ectopically expressed, we cannot attribute the variation of levels of RV replication/entry to the abundance of receptors expressed by the cells. Multiple explanations could be postulated to this finding: varying receptor preference for the rVSV-dG-RV-GFP among different cell lines might be due to sequence differences in critical amino acid residues among the receptor orthologs nAChR, ITGB1 and mGluR2 (**Chapter 3**) that might have interfered with the ability of the G protein to bind and enter

different cell lines (Sato et al., 2012). One other possible scenario for differential receptor utilization of RV might be the cascade of events activated following the initial attachment to a specific receptor. For instance, when the virus interacts with its receptor, it could trigger a signal transduction process because of this interaction. This interaction may lead to the secretion of interferons and ultimately hinder the virus from being taken up effectively. This phenomenon might elucidate why cells that overexpress ITGB1 show increased viral binding, while enhanced virus replication is observed in cells transiently expressing nAChR, as is the case in human cells. lines.(Schneider-Schaulies, 2000). In summary, these findings could imply that for the virus to successfully cross into and infect other species, it may undergo evolutionary changes, such as mutations, to enhance its adaptation and overcome species barriers, thereby expanding its host range, and ensuring its survival. It is noteworthy that the glycoprotein strain used in this study was associated with dog-related genetic lineage. Therefore, future research should account for potential variations in how the G protein from a bat-related genetic lineage interacts with the receptor orthologs of different species.

Overall, it is important to note that the virus-receptor interaction represent one aspect of the complex interactions between the virus and host and many other factors influence the successful establishment of infection into new host species. Among those are the specific virus and host cell line being studied, the expression levels of other cellular factors, and the viral entry pathways which ultimately contribute to the fate of RV infections.(Feige et al., 2021b).

7 Chapter 7 Role of receptor co-factors and innate immune antagonizing viral proteins in mediating RV replication in bat cells

7.1 Introduction

Owing to their ability of hosting diverse range of viral zoonotic diseases without displaying clinical signs, bats have been associated with the emergence of viral diseases (Letko et al., 2020). Additionally, the limited tools including the availability of the bat cell lines has set more challenges for studying the bats' response to the viral diseases (Crameri et al., 2009). With specific concern in RV, many studies have addressed the role of the human receptors in initiating RV entry and internalization together with the innate immune response. Although, none of previous studies have shed light on the mechanism by which RV enter and replicate in bat cells. The information collated in previous chapters demonstrated the role of the bat receptors in RV replication and entry. However, more understanding of the other factors supporting virus replication is deemed essential. Thus, in this chapter, we aim to investigate the additional factors contributing to RV replication on Pa-BR cells. Among those are the host attachment factors and the role of the viral proteins as phosphoprotein and matrix proteins which are known to inhibit innate immune responses(Zhao and Pu, 2022).

7.1.1 Attachment factors

The attachment of the virus to the cell is the initial interaction between the virus and the cellular membrane. Understanding the role of the cellular factors involved in this step is crucial since it initiates a chain of dynamics, allowing the virus movement along the cellular membrane and their engagement with the receptors for internalization (Schneider-Schaulies, 2000). The existence of the cellular attachment factors results in physical forces bringing the virus surface protein in close contact to the host cell surface receptors (Shukla and Spear, 2001). One clear difference among the cellular attachment factors and the cellular receptors is that attachment factors just allow virus concentration on cell surface, in contrast to the receptors that mediate delivery of the virus genome into the cytoplasmic and cellular compartments (Taube et al., 2010).

7.1.1.1 Heparan sulphate proteoglycan (HS)

HS are glycosaminoglycans, with negatively charged heparin polysaccharides. They are abundantly present on the cell surface thus they are involved in multiple biological processes (Sasaki et al., 2018). Among their well characterized functions, is their role in

facilitating initial virus attachment to the cells surface through electrostatic binding to the viruses' glycoproteins. Thus, their role is limited to initial attachment without contributing to virus internalization (Sasaki et al., 2018). Thereby, allowing more concentration of the viruses near the cell surface to enable interaction with the additional surface molecules and consequently facilitate virus internalization (Jolly and Sattentau, 2013). HS has been reported as an essential attachment factor for SARS-CoV-2 for attachment to the cell membrane. HS serves as collector for the SARS-CoV-2 on cell surface, mediating its binding to the ACE2 receptor (Clausen et al., 2020). Moreover, the V3 loop of the human immunodeficiency virus (HIV) glycoprotein gp120 binds initially with the HS, followed by binding to the chemokine receptor CCR5 (Landi et al., 2011).

7.1.1.2 Gangliosides

Gangliosides belong to the amphipathic lipid family, which are composed of sialic acid with glycosphingolipids. Their hydrophobic ceramide tail allows them to remain anchored to the plasma membrane, extending their glycan hydrophilic portion extracellularly (Martínez et al., 2013). Variations among the types of gangliosides is due to differences in the number and type of carbohydrate building blocks.

Any virus entering the cell membrane encounters the glycocalyx which is formed of sugar antennas extending to the extracellular environment, beyond the cellular receptors (Tantirimudalige et al., 2022). Thus, it is crucial to identify how viruses interact with this sugar-based molecule.

Non-enveloped viruses such as Rota virus, polyomaviruses, and Simian virus 40 (SV40) have displayed their reliance on the gangliosides for virus entry (Martínez et al., 2013; You et al., 2015).

Dengue viruses, one of the enveloped viruses, is characterized by its high affinity to many attachment factors and cellular receptors supporting its initial attachment with the cellular membrane. The E protein of Dengue virus does not interact with GM1 gangliosides only (Tantirimudalige et al., 2022). However, for interaction to occur, the fully assembled contact of the virus is required to bind to the surface. Upon attachment with the gangliosides, it assists the virus movement across the cellular environment facilitating the binding to another receptor. Nevertheless, the depletion of the

gangliosides, reduce but does not completely abolish the viral infection (Tantirimudalige et al., 2022).

The role of the gangliosides on RV has been demonstrated in previous studies (Superti et al., 1986; Lafon, 2005). High virus infectivity was observed upon pre-incubating chicken embryo related cell (CER) cells with the gangliosides. Although reduced virus recovery resulted from the initial pre-incubation of the virus with the gangliosides, followed by inoculation on CER cells, suggesting competition between the RV and gangliosides (Superti et al., 1986; Lafon, 2005).

7.1.2 Viral proteins

The rabies virus genome is comprised of five structural proteins: N, P, M, G and L. In this chapter, we focused on P and M proteins due to their role in evading the innate immune response.

7.1.2.1 Phosphoprotein

The multifunction P protein is comprised of three domains: N-terminal, central dimerization, and C-terminal domains. Phosphoprotein plays the crucial role in evading the host innate immune response through preventing the production of IFN-α/β. The interference of the transcriptional activation of the IFN-α/β occurs as a result of preventing the phosphorylation of its essential transcription factors IRF7 and IRF3 (Scrima et al., 2023). Additionally, the retention of the Signal transducer and activator of transcription (STAT1 and STAT2) isoforms in the cytoplasm consequently inhibits the Janus kinase signal transducer and activator of transcription (JAK-STAT) signalling pathway. The P protein role in RV pathogenesis is not limited to antagonizing the IFN response. It also plays a significant role in RV replication through acting as a cofactor for the RNA dependent RNA Polymerase (RdRp) (Yin et al., 2021). The regulatory role played by the P protein in immune evasion and replication renders it a potential therapeutic target for antiviral drugs.

7.1.2.2 Matrix protein

The M protein is well known for its involvement in virus assembly and budding. The interaction of the M protein together with the ribonucleoprotein (RNP) complex and the

G proteins allow the recruitment of the RNP to the host cell membrane, enabling the budding of encapsulated viral particles (Yin et al., 2021).

Besides its role in virus budding, P and M proteins play simultaneously to inhibit the (JAK-STAT) pathway. Moreover, it is involved in inhibition of the NF-κB dependent gene regulatory factors through its interaction with the C-terminal in P43/Rel A subunit in NF-κB reaction (Yin et al., 2021).

7.1.3 Aims

- To codon optimize and clone the rabies viral structural proteins in the pCAGG expression vector fused with the HA tag at the C-terminus: pCAGG-P-HA and pCAAG-M-HA plasmids. Followed by validation of the expression and localisation in Pa-Br cells.
- To identify whether the ectopic expression of the viral proteins on Pa-Br would enhance the virus replication in Pa-Br cells.
- To evaluate whether supplementing the Pa-Br cells with the attachment factors (Hepran sulphate and gangliosides) would enhance or retain the rVSV-dG-RV-G-GFP replication in Pa-Br cells.
- To construct the functional domains of the bat ITGB1, mGluR2 that interacts with the RV-G on HEK 293 cells and the physical interaction of the *P.alecto* receptors with RV-G.

7.2 Results

7.2.1 The *P.alecto* RV receptors directly interact with RV glycoprotein.

In the previous chapter **(Chapter 6),** we demonstrated the ability of the rVSV-dG-RV-G-GFP to infect the *P.alecto* brain cells. Herein, to gain more understanding of the underlying mechanism by which the *P.alecto* enhances the rVSV-dG-RV-G-GFP replication, we studied the physical interaction between the RV-G and each of the *P.alecto* receptors. Immunoprecipitation assay (IP) was carried out to test the physical interaction between the bat receptors and the full-length RV-G using the each of the FLAG-tagged receptor proteins and the RV-G derived from the Egyptian strain (Gene ID: MK760770). Collectively, our results demonstrated that all the tested bat receptor proteins showed direct interaction with the RV-G (**Figure 7.1-7.5)**.

Firstly, co-transfecting HEK 293 cells with pCAGG-RV-G-HA with each of the following plasmids pCAGG-ITGB1-FLAG, pCAGG-mGluR2-FLAG, pCAGG-nAChR-FLAG-, pCAGG-

NCAM-FLAG-, pCAGG-p75-FLAG was carried out. Followed by confirmation of expression of each of the *P.alecto* FLAG tagged receptors and the HA-tagged RV-G in the cell lysates. Upon coupling the lysates with FLAG bound beads, all *P.alecto* receptors were capable of immunoprecipitating a 60 kDa band in HEK293 cells corresponding to the rabies surface glycoprotein **(Figures 7.1-7.5 A).** To further validate the physical interaction between the G proteins and the bat receptors, the HEK 293 cells were co-transfected with the pCAGG-RV-G-HA plasmid with each of the plasmids expressing *P.alecto* receptors (ITGB1, mGluR2, nAChR, NCAM and p75), followed by immunofluorescence assay. As demonstrated **(Figure 7.1-7.5 B),** the pCAGG-RV-G-HA was expressed as red fluorescence, while plasmids expressing the *P.alecto* receptors in pCAGG-FLAG were demonstrated as green fluorescence. The colocalization of the surface glycoprotein with the *P.alecto* cellular receptors was indicated by the orange fluorescence upon merging DAPI, green and red signals **(Figure 7.1-7.5 B)**. Corroborating these results with receptor mediated entry of RV indicated that all the tested *P.alecto* receptors showed direct interaction with the RV surface glycoprotein, explaining their functional role in mediating RV entry.

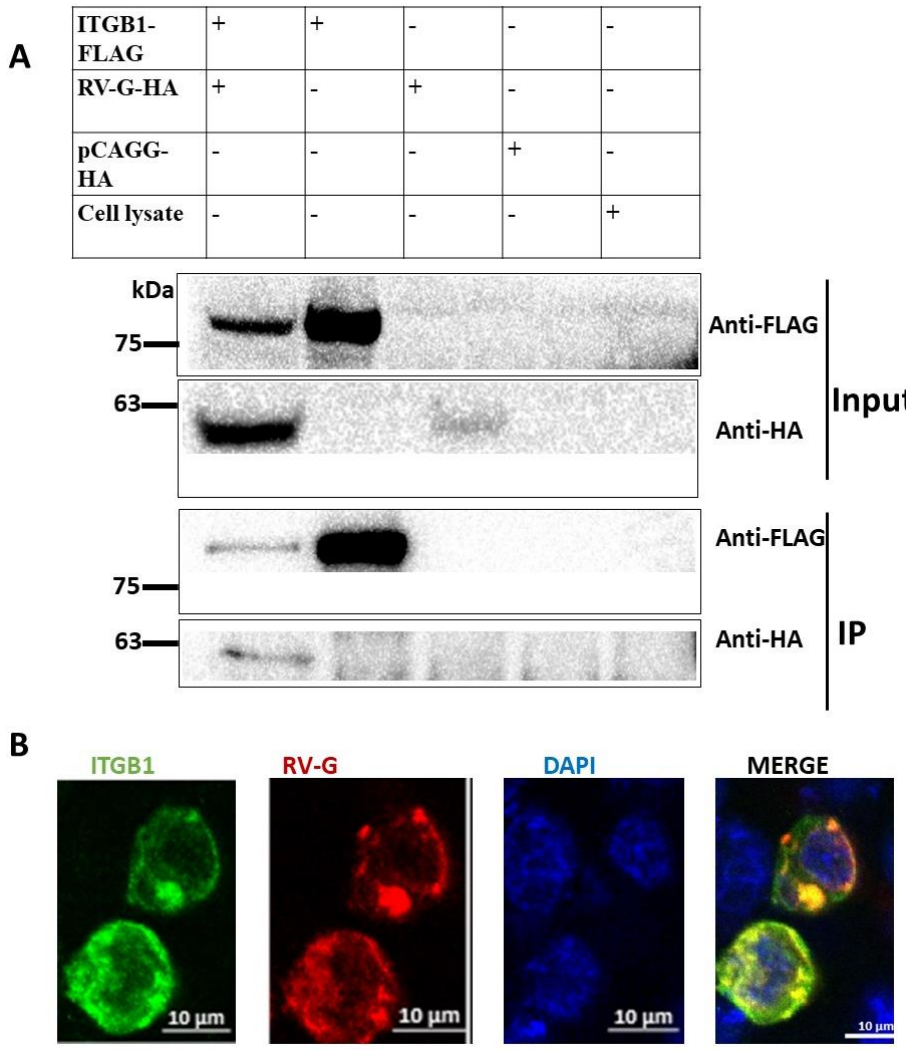

Figure 7.1 Interaction of P.alecto ITGB1 receptor with RV-G.

HEK 293 cells were transiently transfected with the P.alecto ITGB1-FLAG and RV-G-HA plasmids ***(A)*** *after 24 hrs, cell lysates were collected and subjected to western blot analysis (input) showing the expression of the FLAG-tagged ITGB1 and the HA-tagged RV-G. Upon coupling the lysates with the FLAG-bound beads, the ITGB1-FLAG (*~88 kDa) *pulled down the RV-G HA (*~60 kDa) *from the transfected HEK293 lysates. The pCAGG-HA, served as a negative control.* ***(B).*** *The HEK 293 cells were co-transfected with the P.alecto-ITGB1-FLAG and the RV-G-HA plasmids. After 24 hours, cells were fixed and stained with antibodies against FLAG (green) and HA tags (red), and the nuclei were stained with DAPI (blue). The yellow areas in the merged images show the cellular localization of P.alecto ITGB1 with the RV-G protein. Fluorescence signals were visualized by confocal immunofluorescence microscopy, scale bars, 10 µm. All experiments were performed two times (n=2) independently. Uncropped blots are shown in Chapter 9, Supplementary Figure 9.*

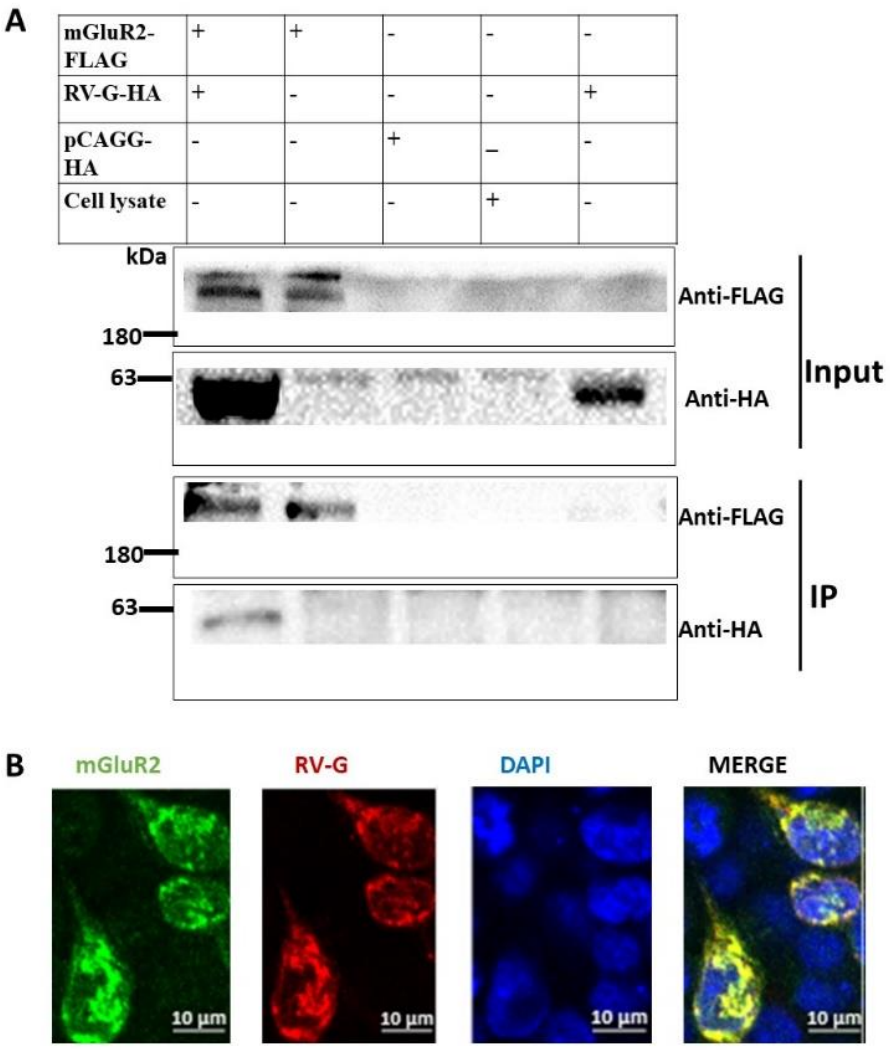

Figure 7.2 Interaction of P.alecto mGluR2 receptor with RV-G.

HEK 293 cells were transiently transfected with the P.alecto mGluR2-FLAG and RV-G-HA plasmids ***(A).*** *After 24 hrs, cell lysates were collected and subjected to western blot analysis (input) showing the expression of the FLAG-tagged mGluR2 and the HA-tagged RV-G. Upon coupling the lysates with the FLAG-bound beads, the mGluR2-FLAG (*~190-200 kDa) *pulled down the RV-G HA (*~60 kDa) *from the transfected HEK293 lysates. The pCAGG-HA, served as a negative control.* ***(B).*** *The HEK 293 cells were co-transfected with the P.alecto-mGluR2-FLAG and the RV-G-HA plasmids. After 24 hours, cells were fixed and stained with antibodies against FLAG (green) and HA tags (red), and the nuclei were stained with DAPI (blue). The yellow areas in the merged images show the cellular localization of P.alecto mGluR2 with the RV-G protein. Fluorescence signals were visualized by confocal immunofluorescence microscopy, scale bars, 10 µm. All experiments were performed two times (n=2) independently. Uncropped blots are shown in Chapter 9, Supplementary Figure 10.*

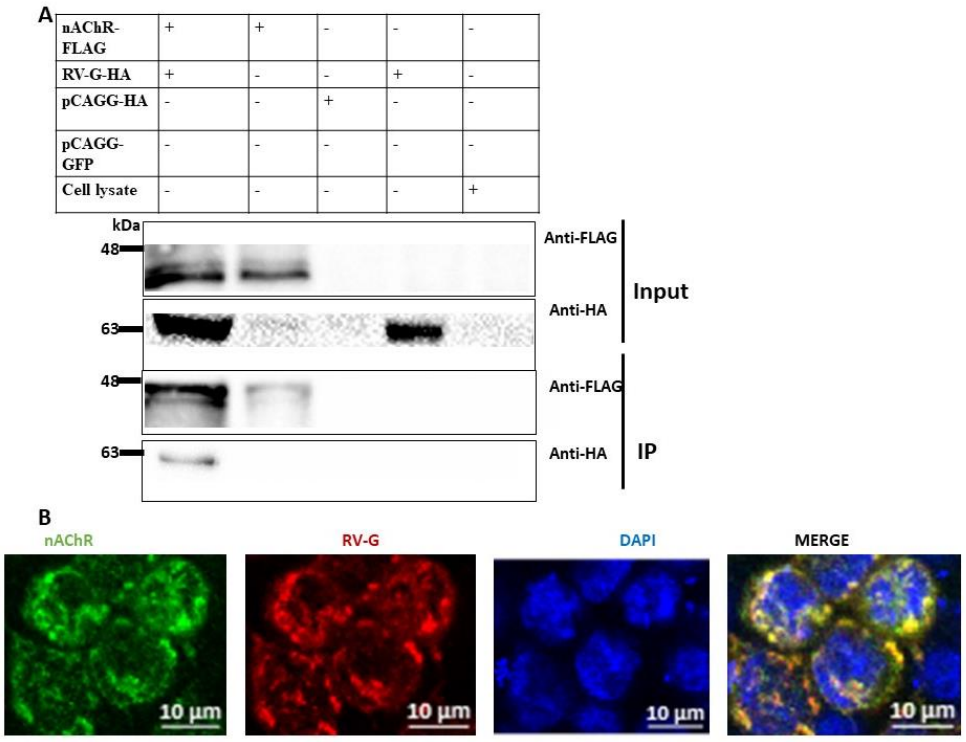

Figure 7.3 Interaction of P.alecto nAChR receptor with RV-G

HEK 293 cells were transiently transfected with the P.alecto nAChR-FLAG and RV-G-HA plasmids ***(A)*** *After 24 hrs, cell lysates were collected and subjected to western blot analysis (input) showing the expression of the FLAG-tagged nAChR and the HA-tagged RV-G. Upon coupling the lysates with the FLAG-bound beads, the nAChR -FLAG (*~45 kDa) *pulled down the RV-G HA (*~60 kDa) *from the transfected HEK293 lysates. The pCAGG-HA, served as a negative control.* ***(B).*** *The HEK 293 cells were co-transfected with the P.alecto nAChR -FLAG and the RV-G-HA plasmids. After 24 hours, cells were fixed and stained with antibodies against FLAG (green) and HA tags (red), and the nuclei were stained with DAPI (blue). The yellow areas in the merged images show the cellular localization of P.alecto nAChR with the RV-G protein. Fluorescence signals were visualized by confocal immunofluorescence microscopy, scale bars, 10 µm. All experiments were performed two times (n=2) independently. Uncropped blots are shown in Chapter 9, Supplementary Figure 11.*

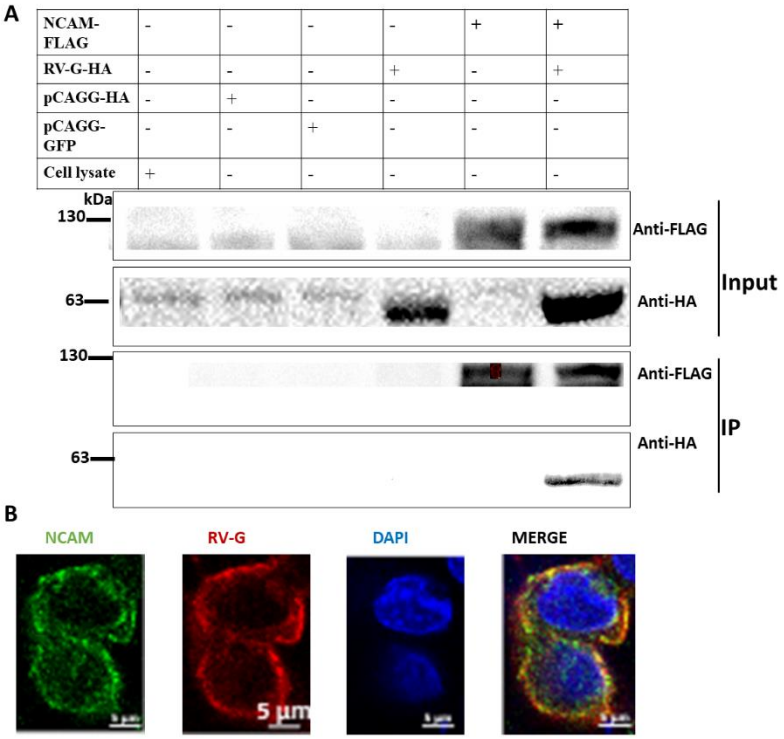

Figure 7.4 Interaction of P.alecto NCAM receptor with RV-G.

HEK 293 cells were transiently transfected with the P.alecto NCAM-FLAG and RV-G-HA plasmids ***(A)*** *After 24 hrs, cell lysates were collected and subjected to western blot analysis (input) showing the expression of the FLAG-tagged NCAM and the HA-tagged RV-G. Upon coupling the lysates with the FLAG-bound beads, the NCAM -FLAG (~120 kDa) pulled down the RV-G HA (~60 kDa) from the transfected HEK293 lysates. The pCAGG-HA, served as a negative control.* ***(B).*** *The HEK 293 cells were co-transfected with the P.alecto-NCAM-FLAG and the RV-G-HA plasmids. After 24 hours, cells were fixed and stained with antibodies against FLAG (green) and HA tags (red), and the nuclei were stained with DAPI (blue). The yellow areas in the merged images show the cellular localization of P.alecto NCAM with the RV-G protein. Fluorescence signals were visualized by confocal immunofluorescence microscopy, scale bars,* 5 *µm*. All experiments were performed two times (n=2) independently. *Uncropped blots are shown in Chapter 9, Supplementary Figure 12.*

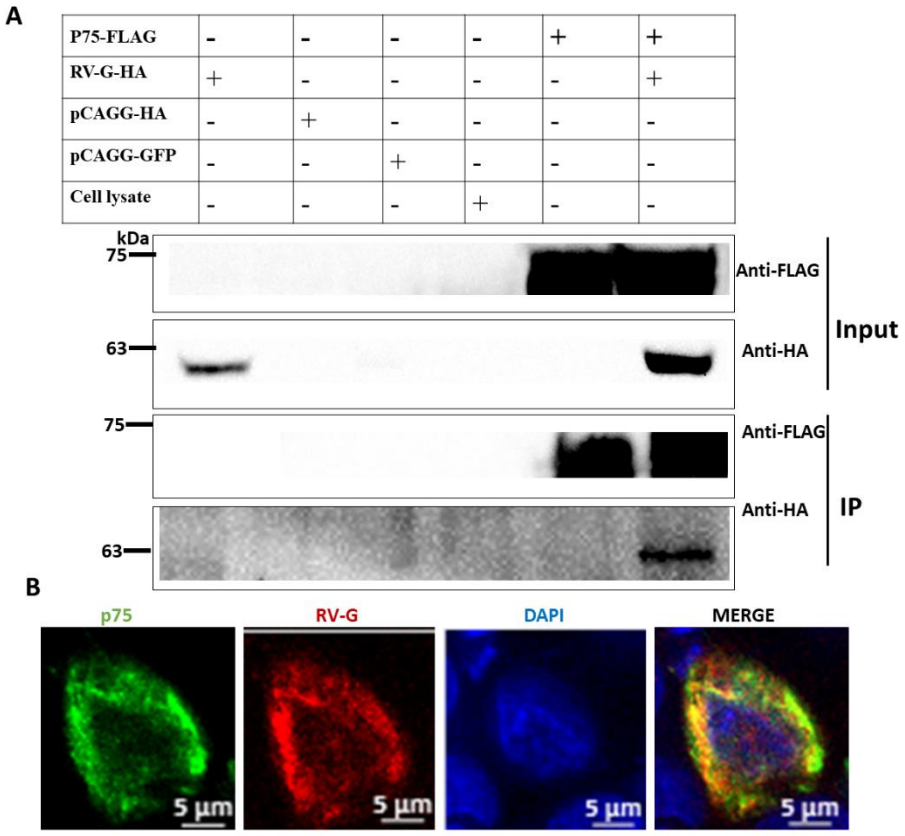

Figure 7.5 Interaction of P.alecto p75 receptor with RV-G.

HEK 293 cells were transiently transfected with the P.alecto p75 FLAG and RV-G-HA plasmids ***(A)*** *After 24 hrs, cell lysates were collected and subjected to western blot analysis (input) showing the expression of the FLAG-tagged p75 and the HA-tagged RV-G. Upon coupling the lysates with the FLAG-bound beads, the p75 FLAG (~60-75 kDa) pulled down the RV-G HA (~60 kDa) from the transfected HEK293 lysates. The pCAGG-HA, served as a negative control.* ***(B)****. The HEK 293 cells were co-transfected with the P.alecto p75 FLAG and the RV-G-HA plasmids. After 24 hours, cells were fixed and stained with antibodies against FLAG (green) and HA tags (red), and the nuclei were stained with DAPI (blue). The yellow areas in the merged images show the cellular localization of P.alecto p75 with the RV-G protein. Fluorescence signals were visualized by confocal immunofluorescence microscopy, scale bars, 5 µm. All experiments were performed two times (n=2) independently. Uncropped blots are shown in Chapter 9, Supplementary Figure 13.*

7.2.2 Functional domain in *P.alecto* ITGB1

Throughout our study, we have demonstrated that ITGB1 and mGluR2 play crucial roles in mediating the entry of the rVSV-dG-RV-G-GFP. Additionally, there is a lack of information on the role of the bat receptors in RV infection. From this perspective, we investigated the functional domains to elucidate the interaction site between the RV- and each of the *P.alecto* ITGB1 and mGluR2. To this end, we divided the *P.alecto* ITGB1

into two fragments, referred to as ITGB1-N-terminal-FLAG-COOH domain encompassing the a.a. residues from a.a. 1-412, and the EGF domain corresponding to the residues from 413-746 a.a. referred to as ITGB1-EGF-FLAG-COOH. Employing the traditional PCR cloning method, we amplified the corresponding domains followed by cloning in the pCAGG-FLAG plasmid. To confirm the insert and orientation of the clone we confirmed the existence of the insert of interest through sequence analysis **(Figure 7.6)**. Next, we verified the expression of the designed domain in HEK293 cells and subsequently assessed their cellular localization. The ITGB1-N terminal-FLAG-COOH showed perinuclear localization, while cytoplasmic diffusion was detected in the ITGB1-EGF-FLAG-COOH **(Figure 7.7-7.8 B**). To further dissect which domain is responsible for the interaction with the RV-G, we co-transfected HEK293 cells with the full-length pCAAG-RV-G-HA and each of the ITGB1-N terminal and ITGB1 EGF domains. Followed by IP assay. Our analysis indicated that both domains were capable of immunoprecipitating the 60 kDa band corresponding to the RV-G protein **(Figure 7.7-7.8 A).** Thus, further investigation to map the interaction site between the ITGB1 and the RV-G is required through further fragmentation of domains into functionally intact shorter portions.

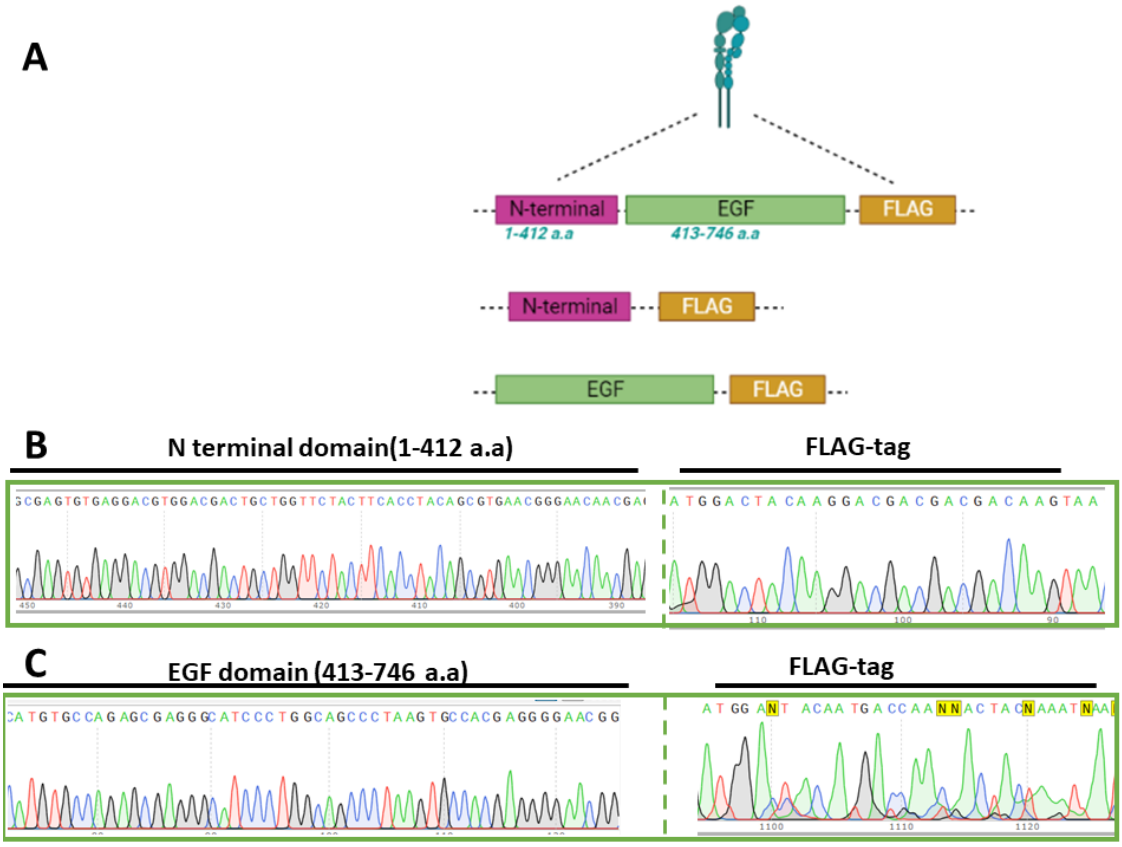

Figure 7.6 Sequence verification of the P.alecto ITGB1 domains.

(A) *Schematic illustration of ITGB1 Full length and domains that are designed and fragmented. The ITGB1-WT and each of the domains to be constructed are indicated. The FLAG tag is marked by a yellow box at the 3' end of each terminus and wild-type protein****. (B-C).*** *Representative Sanger sequence to confirm the cloning of the N-Terminus and EGF domains in pCAGG-FLAG vector. Each of the N-terminus and the EGF domains of the ITGB1 were subcloned in pCAAG-FLAG vector, following the cloning, the region corresponding to each of the N-terminus and EGF domains were amplified for sequence analysis.*

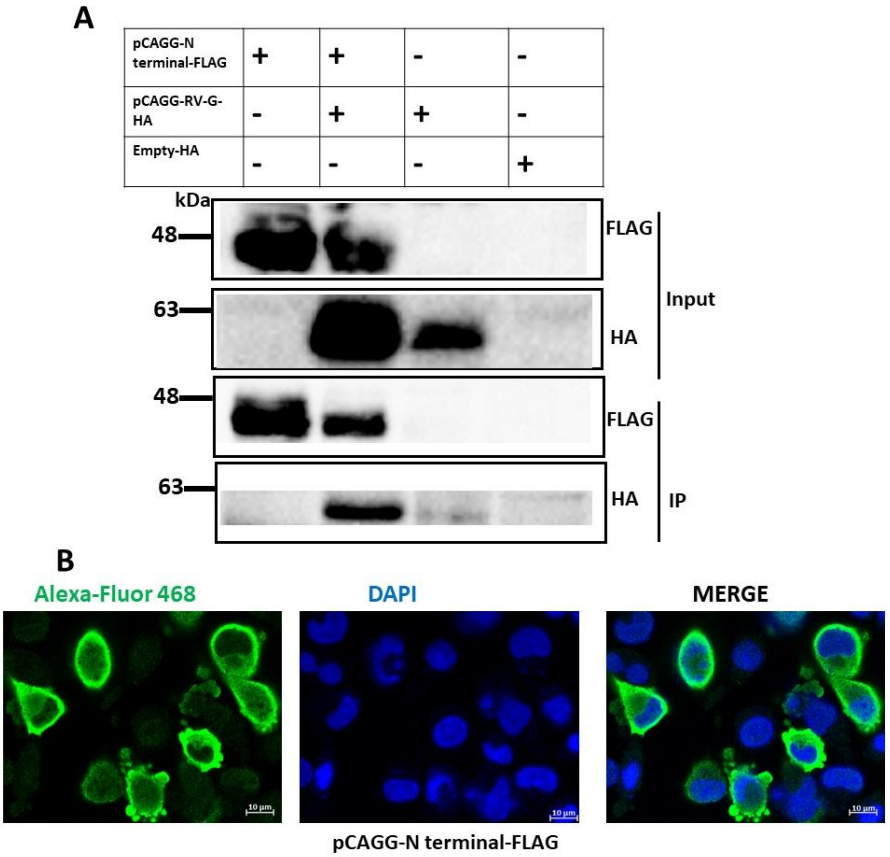

Figure 7.7 Expression and interaction of P.alecto ITGB1 N-Terminal domain with RV-G.

(A)*. HEK 293 cells were transiently transfected with the P.alecto ITGB1-N-Terminal-FLAG and RV-G-HA plasmids. After 24 hrs, cell lysates were collected and subjected to western blot analysis (input) showing the expression of the FLAG-tagged ITGB1-N-terminal domain and the HA-tagged RV-G. Upon coupling the lysates with the FLAG-bound beads, the ITGB1-N-Terminal (*~50 kDa*) FLAG pulled down the RV-G HA (*~60 kDa*) from the transfected HEK293 lysates. The pCAGG-HA, served as a negative control.* ***(B). The*** *HEK 293 cells were transfected with the P. alecto-ITGB1-N-Terminal FLAG plasmid. After 24 hours, cells were fixed and stained with antibodies against FLAG (green), and the nuclei were stained with DAPI (blue). Fluorescence signals were visualized by confocal immunofluorescence microscopy, scale bars, 10 µm. All experiments were performed two times (n=2) independently. Images were analysed using the ZenCore 3.4 software. Uncropped blots are shown in Chapter 9, Supplementary Figure 14.*

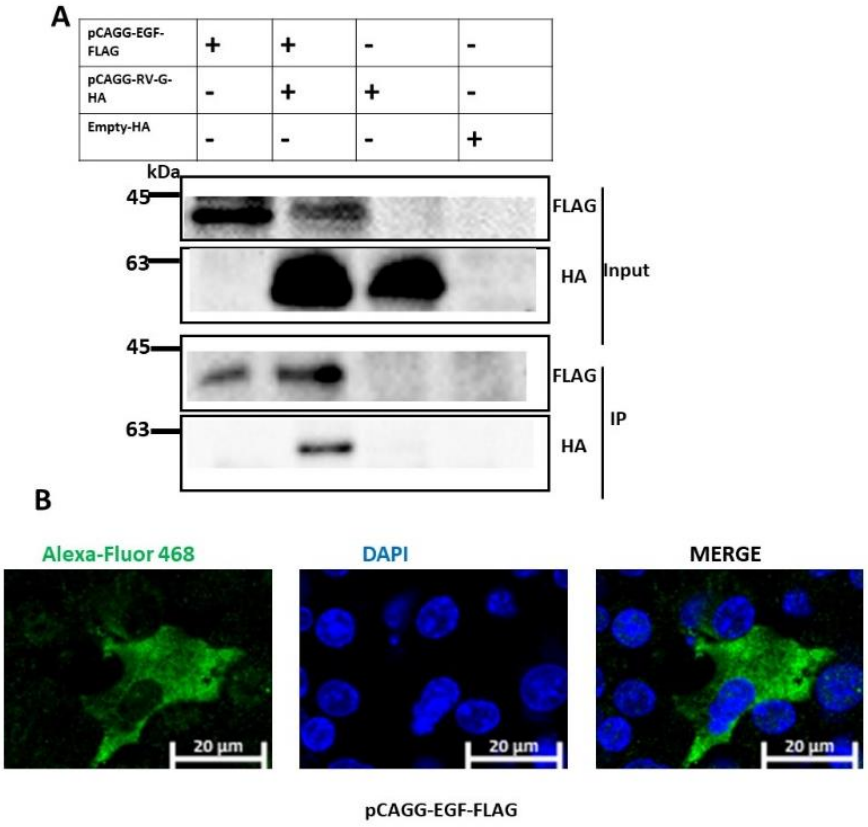

Figure 7.8 Expression and Interaction of P.alecto ITGB1 EGF domain with RV-G.

(A). HEK 293 cells were transiently transfected with the P.alecto ITGB1-EGF-FLAG and RV-G-HA plasmids. After 24 hrs, cell lysates were collected and subjected to western blot analysis (input) showing the expression of the FLAG-tagged ITGB1-EGF domain and the HA-tagged RV-G. Upon coupling the lysates with the FLAG-bound beads, the ITGB1-EGF FLAG (~40 kDa) *pulled down the RV-G HA (*~60 kDa) *from the transfected HEK293 lysates. The pCAGG-HA, served as a negative control. (B). The HEK 293 cells were transfected with the P. alecto-ITGB1-EGF FLAG plasmid. After 24 hours, cells were fixed and stained with antibodies against FLAG (green), and the nuclei were stained with DAPI (blue). Fluorescence signals were visualized by confocal immunofluorescence microscopy, scale bars, 20 µm. All experiments were performed two times (n=2) independently. Images were analysed using the ZenCore 3.4 software. Uncropped blots are shown in Chapter 9, Supplementary Figure 15.*

7.2.3 mGluR2 LBD domain act as functional domain in *P.alecto*

The mGluR2 is comprised of three domains as previously described (Wang et al., 2018). The ligand binding domain, the cysteine rich domain and the seven transmembrane domains (7-TM). Since these domains have been classified according to human mGluR2, we decided to investigate if the corresponding domains in the *P.alecto* mGluR2 would serve similarly as functional domains. Therefore, we divided the *P.alecto* mGluR2 receptor into two different domains: the first domain encompassing the first 484 a.a

residues and referred to as pCAGG-LBD-FLAG. The second domain to be constructed encompasses residues from 484 until 875 a.a, including both the CRD domain along the TM domain, referred to as pCAGG-CRD-TM-FLAG. Primers were designed to amplify the region of interest, followed by cloning the amplicons in pCAAG vector in fusion with the FLAG-tag. To verify the correct insertion of the cloned sequences in the vector, we carried out Sanger's sequencing and sequence analysis which confirmed the correct orientations of the insert and the FLAG sequences in the LBD domain. However, the cloning for the CRD was not successful. (**Figure 7.9 A-B).** To ensure proper expression of the pCAGG-LBD-FLAG in-frame with the FLAG tag, and its cellular localization, immunofluorescence was carried out. It was clearly noticed that the LBD domain displayed perinuclear distribution **(Figure 7.10 B).** Since none of the previous studies mapped the interaction domains for the mGluR2 with the surface G protein. Thus, we performed immunoprecipitation for the LBD domain to identify if it interacts with the RV-G protein. Notably, the LBD were capable of immunoprecipitating the G protein, indicating their interaction **(Figure 7.10-A).** The obtained results seem interesting as they indicate that the *P.alecto* LBD domain is functional, evidenced by its potential reactivity with the G protein. However, further splicing of the cloned fragment might be required to ascertain the region of interaction with RV-G.

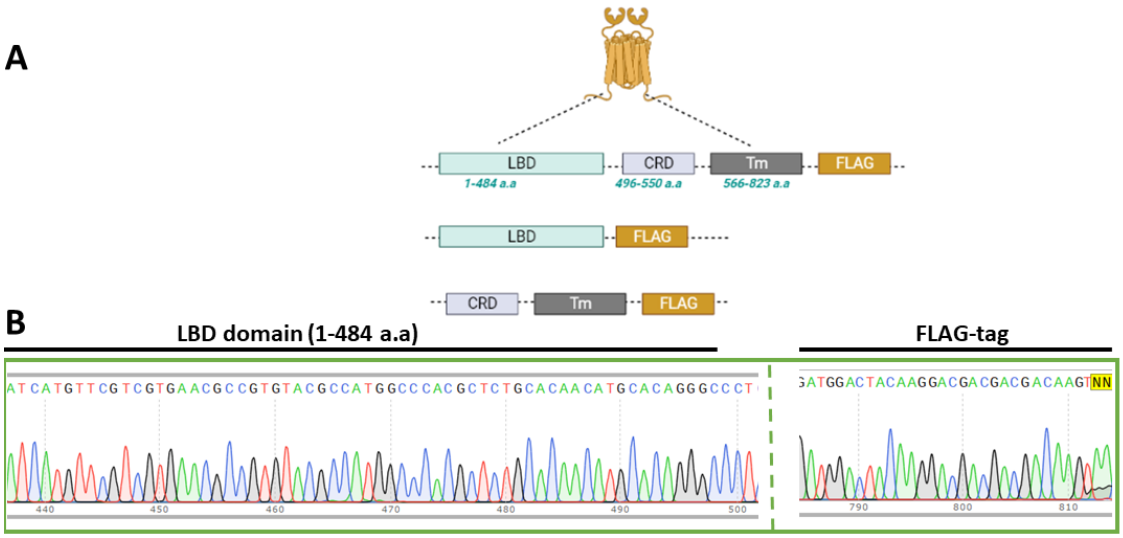

Figure 7.9 Sequence verification of mGluR2-LBD domain.

(A) *Schematic illustration of mGluR2 Full length and domains that are designed and fragmented. The mGluR2-WT and each of the domains to be constructed are indicated. The FLAG tag is marked by a yellow box at the 3' end of each terminus and wild-type protein.* ***(B).*** *Representative Sanger sequence to confirm*

the cloning of the LBD domain in the pCAGG-FLAG vector. The LBD domain of the mGluR2 was subcloned in pCAAG-FLAG vector, following the cloning, the region corresponding to LBD domain was amplified for sequence analysis.

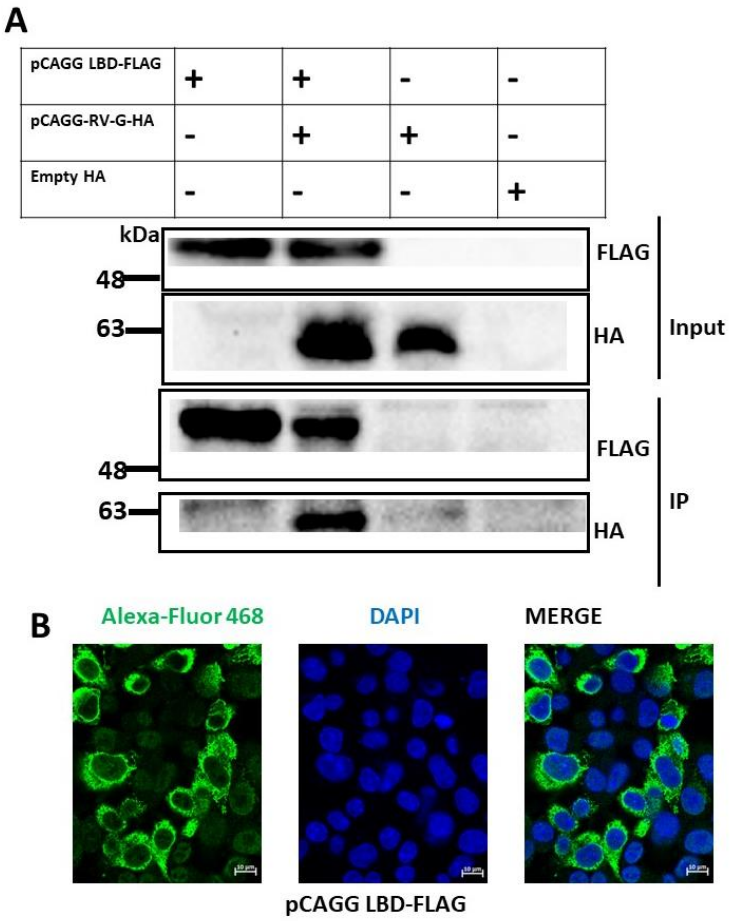

Figure 7.10. Expression and interaction of P.alecto mGluR2 LBD domain receptors with RV-G.

(A). *HEK 293 cells were transiently transfected with the P.alecto mGluR2-LBD-FLAG and RV-G-HA plasmids. After 24 hrs, cell lysates were collected and subjected to western blot analysis (input) showing the expression of the FLAG-tagged mGluR2 LBD- domain and the HA-tagged RV-G. Upon coupling the lysates with the FLAG-bound beads, the mGluR2-LBD FLAG (*~45 kDa) *pulled down the RV-G HA (*~60 kDa) *from the transfected HEK293 lysates. The pCAGG-HA, served as a negative control.* ***(B). The*** *HEK 293 cells were transfected with the P.alecto mGluR2 LBD FLAG plasmid. After 24 hours, cells were fixed and stained with antibodies against FLAG (green), and the nuclei were stained with DAPI (blue). Fluorescence signals were visualized by confocal immunofluorescence microscopy, scale bars, 10 µm. Images were analysed using the ZenCore 3.4 software. All experiments were performed two times (n=2) independently. Uncropped blots are shown in Chapter 9, Supplementary Figure 16.*

7.2.4 Role of the attachment factors on Pa-Br cells

Gangliosides and HS have been reported to be involved as attachment factors for multiple viruses (Sasaki et al., 2018; Tantirimudalige et al., 2022). To elucidate their role in supporting the rVSV-dG-RV-G-GFP in Pa-Br cells. We preincubated the Pa-BR cells with safe doses of HS or gangliosides, for 1 hr and 20 min; respectively. Followed by the inoculation of the rVSV-dG-RV-GFP (MOI=5). Thirty hpi, the GFP percentage was observed, and the virus release progeny was quantified by plaque assay. Our results showed non-significant difference between Pa-Br cells pretreated with either HS or gangliosides compared to the untreated, infected Pa-Br cells**. (Figure 7.11).**

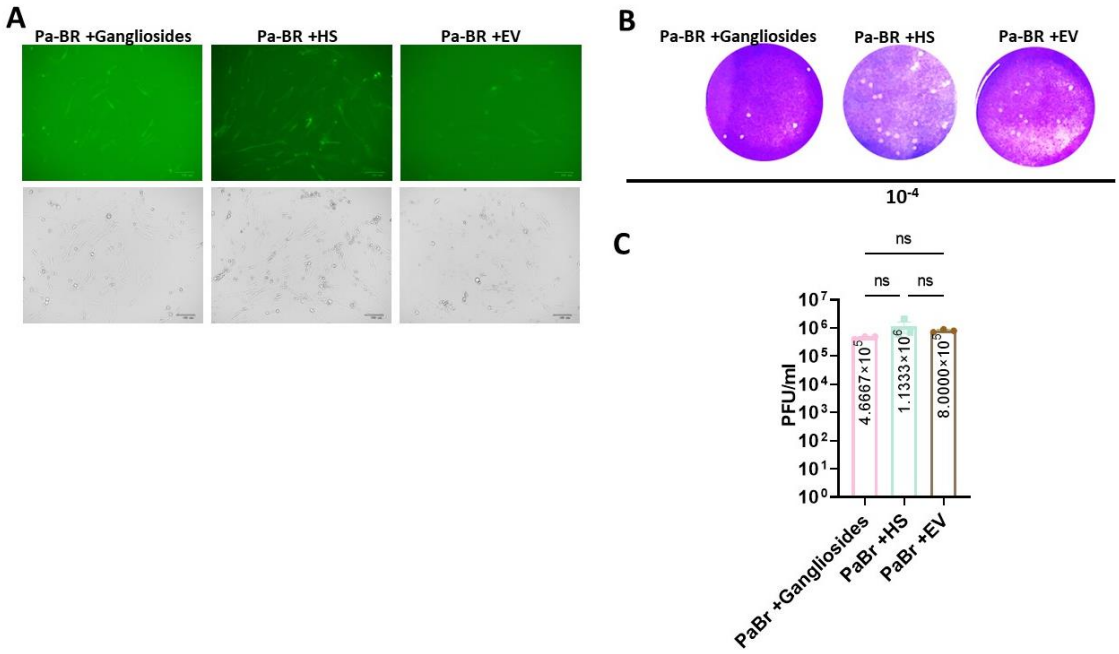

Figure 7.11 Effect of Gangliosides and Heparan sulphate on the rVSV-dG-RV-G-GFP infectivity on Pa-Br cells.

(A) *Representative microscopic fields green (upper), bright (lower) of Pa-Br cells infected with rVSV-dG-RV-G-GFP. Pa-Br cells were incubated with Gangliosides and Heparan sulphate for 1 hr at 37 ° C. One hr after incubation, cells were infected with rVSV-dG-RV-G-GFP (MOI=5). Thirty, hours post infection, viral supernatants were collected for plaque assay.* ***(B).*** *Representative plaque morphology of infected Pa-Br cells. Pa-Br cells were incubated with heparan sulphate and gangliosides for 1 hr and 20 min; respectively at 37 ° C, then cells were infected with the rVSV-dG-RV-G-GFP MOI=5. Thirty hpi, the viral supernatants were collected for quantifying the released progeny virus. The released viruses were quantified using plaque assay on BHK-21 cells after 72 hrs.* ***(C).*** *Graph showing the difference of the mean PFU/mL of rVSV-dG-RV-G-GFP between Pa-Br cells treated with heparan sulphate and cells treated with gangliosides. This*

experiment was performed three times independently (n=3). Data are representative of the mean and SEM of three biological replicates using one way ANOVA. ns, non-significant, P > 0.05.

7.2.5 HS inhibited the rVSV-dG-RV-G-GFP replication in overexpressed Pa-BR cells with *P.alecto* nAChR.

To further understand the tripartite relationship of the receptors together with the attachment factors and the rVSV-dG-RV-G-GFP. The Pa-Br cells were transiently transfected with each of the *P.alecto* ITGB1, *P.alecto* mGluR2 and *P.alecto* nAChR receptors. After 48 hpt, the cells were preincubated with the gangliosides or HS for 20 min and 1 hr; respectively, followed by infecting with the rVSV-dG-RV-G-GFP at MOI of 5. The virus progeny release was compared 30 hpi by plaque assay. Significantly reduced released virus was demonstrated on Pa-BR cells ectopically expressing the *P.alecto* nAChR and preincubated with the HS compared to untreated, infected Pa-Br cells. Indicating that preincubation of cells with the HS could have possibly antagonized the effect of the nAChR receptor. Whereas Pa-Br cells supplemented with HS or gangliosides and ectopically expressing the ITGB1, or *P.alecto* mGluR2 appeared to show no

significant difference in released virus progeny compared to non-treated cells. **(Figure 7.12)**.

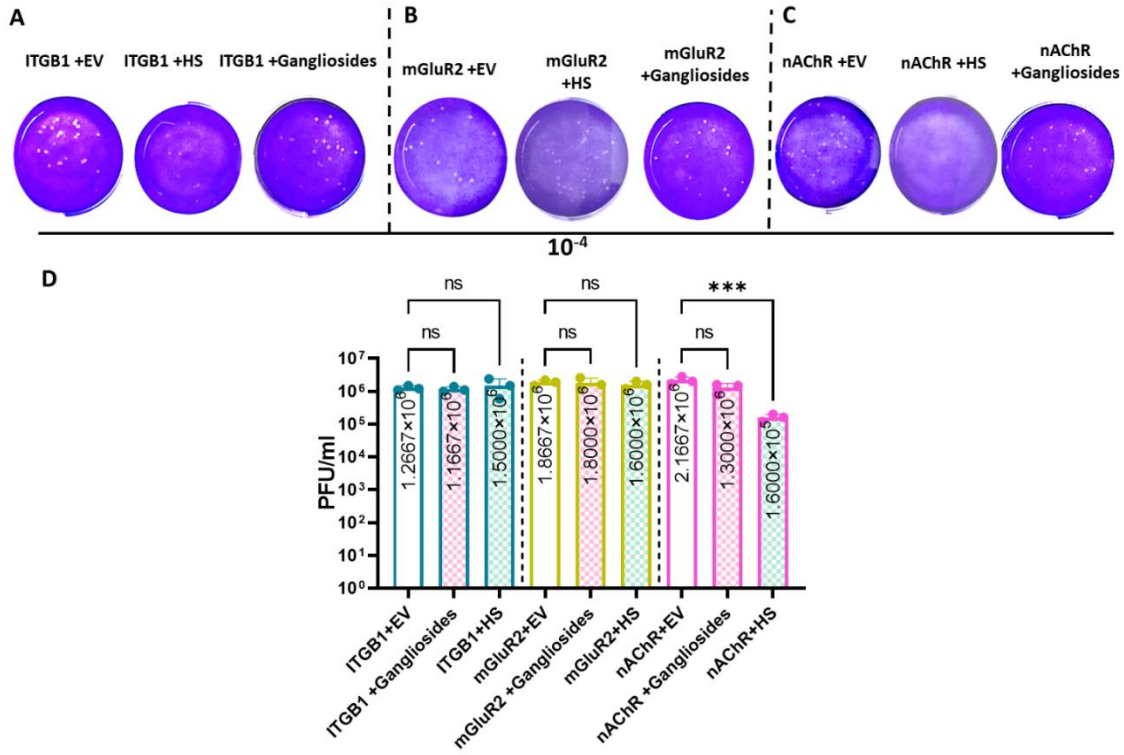

Figure 7.12 Effect of Gangliosides and Heparan sulphate on the rVSV-dG-RV-G-GFP infectivity on Pa-Br cells transfected with P.alecto receptors.

***(A)**. Representative plaque morphology of infected Pa-Br cells with rVSV-dG-RV-G-GFP. Pa-Br cells were transfected with P.alecto **(A)** ITGB1, **(B)** mGluR2 and **(C)** nAChR receptors. Forty-eight hrs post-transfection, cells were treated with heparan sulphate or gangliosides for 1 hr and 20 min; respectively at 37 °C, followed by infection with the rVSV-dG-RV-G-FP. Thirty hpi, the viral supernatants were collected for quantifying the released progeny virus. The released viruses were quantified using plaque assay on BHK-21 cells after 72 hrs. **(D).** Graph showing the difference of the mean PFU/mL of rVSV-dG-RV-G-GFP between Pa-Br cells transfected and treated with heparan sulphate and cells transfected treated with gangliosides, transfected Pa-Br cells expressing empty vector was used as control. This experiment was performed three times independently (n=3). Data are representative of the mean and SEM of three biological replicates using one-way ANOVA. ns, non-significant, P > 0.05, ***, P ≤ 0.001.*

7.2.6 Impact of P and M protein mediated inhibition of innate immunity on the entry of RV in Pa-Br cells.

Since the generated rVSV-dG-RV-G-GFP encodes the G protein of RV, carry the genome of VSV, we aim to dissect the roles of the P and M proteins of RV in regulating the infection of rVSV-dG-RV-G-GFP in Pa-BR cells. To this end, we codon optimized the full

length ORF of P and M protein belonging to the Egyptian strain. Then they were sub cloned in pCAGG plasmid with HA tag, referred to as pCAGG-M-HA-COOH and pCAGG-P-HA-COOH. To confirm proper expression of the proteins, the Pa-Br cells were transfected with pCAGG-M-HA-COOH and pCAGG-P-HA-COOH for western blot and IFA analysis. Assessment of the localization patterns of the RV-P and RV-M proteins indicated the cytoplasmic localization of the RV-M protein, while the P protein showed nuclear localization in Pa-Br cells. We further validated the expression of the RV-P and RV-M with WB which revealed the bands corresponding to the expected sizes **(Figure 7.13).**

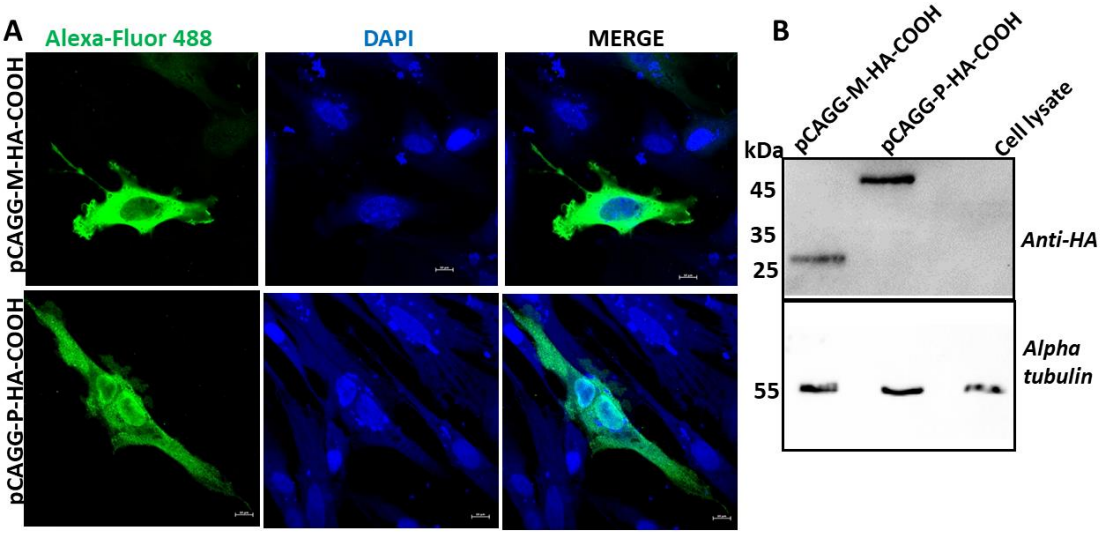

Figure 7.13. Expression of the RV proteins on Pa-Br cells

(A) *Pa-Br cells were transfected with plasmids encoding RV-M –HA and RV- P-HA plasmids; for 24 h, After 24, cells were fixed and stained with Anti-FLAG antibody and Alexa-Fluor 468 conjugated antibody (Green). Cell nuclei were stained by DAPI (Blue), fluorescence signals were visualized by confocal immunofluorescence microscopy, Scale bars size, 20 µm.* ***(B)*** *Pa-Br cells were transiently transfected with RV proteins (pCAGG-P-HA and pCAGG-M-HA plasmids). Thirty-six hrs post transfection, cells were lysed, and total proteins were extracted. The cell lysates are then subjected to SDS-PAGE and Western blot analysis. The HA-tagged viral proteins: pCAGG RV-M-HA (25 kDa) and pCAGG RV-P-HA (40 kDa) were detected using Rabbit Anti-HA as primary antibody and Goat anti-Rabbit HRP as secondary antibody. This experiment was performed two times independently (n=2). Cell lysate served as negative control. Uncropped blots are shown in Chapter 9, Supplementary Figure 17.*

7.2.7 The role of P and M proteins in rVSV-dG-RV-G-GFP replication.

Bats harbour multiple viruses without displaying of clinical signs, possibly due to their strong innate immune response against viruses. Thus, we evaluated whether the ectopic

expression of the P/M proteins in bat cells will be capable of modulating the bats antiviral response or not. We ectopically expressed the Pa-Br cells with P or/and M protein, and forty-eight hrs post transfection, the cells were infected with rVSV-dG-RV-G-GFP at MOI of 5. Supernatants were collected for quantification of the released virus using plaque assay. Our results demonstrated that the virus exhibited significantly higher levels in cells overexpressing P or M and P and M compared to empty vector control. The pa-BR cells co-expressing P and M allowed more virus production compared to cells solely expressing P or M only. Taken together, these results highlighted enhanced virus production on the Pa-BR cells by over expressing P/M proteins which are known for their effects of hijacking the innate immune responses **(Figure 7.14).**

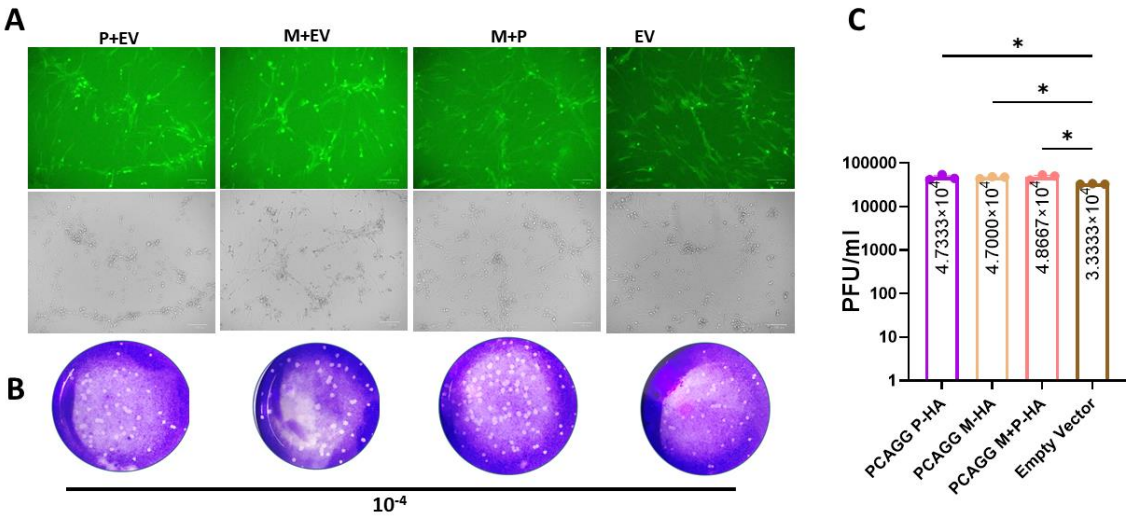

Figure 7.14 Effect of viral proteins on rVSV-dG-RV-G-GFP infectivity on Pa-Br cells

(A) *Representative microscopic fields green (upper), bright (lower) of Pa-Br cells infected with rVSV-dG-RV-G-GFP. Pa-Br cells were transfected with pCAGG-P-HA and pCAGG-M-HA vectors, forty-eight hrs post-transfection, the cells were infected with rVSV-dG-RV-G-GFP (MOI=5). Thirty hours post-infection, viral supernatants were collected for plaque assay.* ***(B).*** *Representative plaque morphology of infected Pa-Br cells with rVSV-dG-RV-G-GFP. Pa-Br cells were transfected with RV-P and RV-M expressing vectors. Forty-eight hrs post-transfection, cells were infected with rVSV-dG-RV-GFP. Thirty hpi, the viral supernatants were collected for quantifying the released progeny virus. The released viruses were quantified using plaque assay on BHK-21 cells after 72 hrs.* ***(C).*** *Graph showing the difference of the mean PFU/mL of rVSV-dG-RV-G-GFP between Pa-Br cells transfected with RV-P and RV-M or both. Pa-Br cells expressing empty vector was used as control. This experiment was performed three times independently (n=3). Data are representative of the mean and SEM of three biological replicates using one-way ANOVA *, P ≤ 0.05.*

7.3 Discussion

Bats have emerged as reservoirs for several zoonotic viral diseases which can be persistently infected without displaying clinical signs (Banerjee et al., 2020). Together with increasing the contact between bats and human which increased the possibilities of disease outbreaks and virus spillover among distinct species (Letko et al., 2020). Thus, in this chapter we studied additional factors that might be involved in the susceptibility of the bat cells to RV infection *in vitro*.

Most of the research focused on studying the RV receptors in human (Shuai et al., 2020; Wang et al., 2021, 2023), and none of previous studies have investigated the role of the RV receptors in bats. We have not only for the first time mapped the full spectrum of the RV interaction with bat receptors but also to further understood the underlying mechanism of the virus host receptor mediated entry and replication of rVSV-dG-RV-G-GFP in Pa-Br cells **(Chapter 6).** We evaluated the interaction of those proteins with the G protein through IP and co-IFA. All the IP and CO-IFA results demonstrated the physical interaction and co localization of the RV-G and the *P.alecto* receptors *in vitro*. These findings support the functional role in which those proteins play in the RV replication.

Next, we sought to identify the functional domains in the ITGB1 and mGluR2 owing to their crucial role in supporting rVSV-dG-RV-G-GFP entry and infectivity. A recent study has demonstrated the predominant interaction of the human ITGB1 ectodomain region (1-728 a.a) with the G protein. Thus, we sought to further divide the ITGB1 ectodomain in two regions; the N-terminal (1 a.a-412 a.a) and the EGF domain (413 a.a-746 a.a) and map which region is responsible for the G protein interaction. We hypothesized that interaction with the G protein would be limited to the N-terminal region. Although both domains were capable of immunoprecipitating the G protein probed with anti-FLAG.

To identify the mGluR2 functional domains involved in RV replication, we divided the *P.alecto* mGluR2 in to two different domains; the LBD domain and the CRD+TM domains. However, the cloning of the CRD+Tm domain was not successful, we were able to demonstrate direct physical interaction of the mGluR2 LBD domain with the RV-G.

As previously reported, RV uses multiple host cellular receptors for cellular entry and internalization (Lafon, 2005; Wang et al., 2018, 2023; Shuai et al., 2020). However, little

evidence is known about whether other factors could also contribute to the initiation of the attachment of RV-G to the cellular receptors. Among those is the heparan sulphate that has been previously reported to interact with the RV G protein (Sasaki et al., 2018). Our results indicated that the Pa-BR cells treated with HS followed by rVSV-dG-RV-G-GFP infection, resulted in non-significant released virus progeny compared to non-treated cells.

In contrast, the replication of the rVSV-dG-RV-G-GFP was significantly reduced upon infecting the Pa-Br cells ectopically expressing the bat nAChR that was preincubated with HS. This might be attributed to the direct and competitive binding of the HS to the surface G protein or to the nAChR receptor, subsequently hindering the interaction between RV-G and nAChR, and ultimately decreasing virus replication (Sasaki et al., 2018). Previously an antiviral effect of the HS has been reported on cells expressing NCAM which showed inhibited levels of RV infection in presence of the HS (Thoulouze et al., 1998).

Next, we evaluated the role of the coated Pa-Br cells with gangliosides which was simultaneously over expressing the *P.alecto* ITGB1 or *P.alecto* mGluR2 or *P.alecto* nAChR on sustaining the RV replication. The obtained results demonstrated that no significant difference between the treated cells compared to the empty vector control. In contrast to previous study which demonstrated that preincubating the chick embryo-related (CER) cells but not the RV with gangliosides, resulted in enhanced virus replication (Superti et al., 1986). Alternatively, many studies reported the role of gangliosides in enhancing virus replication. During Polyomavirus cycle, the gangliosides serve as entry receptors for the virus entry and spread of infection (You et al., 2015). Additionally, previous study demonstrated the functional role of the gangliosides for the productive entry of the Rotavirus (Martínez et al., 2013). One explanation for the non-significant role of the gangliosides observed in our study might be attributed to the nature of the bat cell line employed in this study. Another possibility might be the utilization of different G strain in our study compared to the previous study (Superti et al., 1986), which might differ in the amino acid binding sites to the gangliosides, resulting in loss of binding specificity (Taube et al., 2010). It should be also noted that the virus binding to the attachment factors differs according to whether the virus surface proteins are

presented in the form of recombinant protein or authentic virus form (Clausen et al., 2020). Ultimately studying the attachment factors involved in RV infection might enable targeting the virus complexed with attachment factor as therapeutic approach to prevent infection.

Further future studies are required, related to pre -incubating the rVSV-dG-RV-G-GFP, not the cell with HS or gangliosides which will give more insight on the underlying mechanism by which those factors inhibit or enhance the virus replication.

In our study, the replication and entry of the RV were demonstrated in the context of the replication competent VSV expressing the surface G protein of RV using reverse genetics. Thus, as an approach to mimic the wild-type rabies virus replication was carried out. We ectopically expressed the rabies phosphoprotein and matrix proteins on the Pa-Br cells, to investigate whether their ectopic expression would allow to modulate the Pa-BR antiviral response which would result in enhanced virus replication. As our results demonstrated the significantly increase in the virus progeny on the bat cells expressing the P/and or M proteins. Supporting the significant role of the phosphoprotein as the most crucial protein to counteract the cellular innate immunity through blocking the IRF3 phosphorylation (Scrima et al., 2023). Whereas M protein is a regulator for the NF-κB signalling through fixation of the RelAp43 (Khalifa et al., 2016). However, the exact mechanism of how the P and M on hijacking the immune response of the bat cells requires further investigation.

8 General Discussion

8.1 Summary

Despite the recent advancement in identifying novel RV receptors, there remains a knowledge gap in understanding the susceptibility of distinct species in relation to the heterogeneous array of the virus receptors encoded in these species. From this perspective, we aimed to address this gap of knowledge by conducting a comparative analysis of the virus receptor preference among humans, dog, and bats. Additionally, RV represents one of the highest-ranked viruses for spillover events (Grange et al., 2021). Understanding the host factors involved in virus transmission could aid in identifying the emerging infection in potential hosts.

While most viruses show selectively preserved employment of specific receptors to enter cells, RV demonstrates diverse utilization of receptors across various species. Thus, we aimed to understand the receptors essential for the RV replication cycle among different RV susceptible hosts including human, dog, and bats.

Firstly, we conducted a comparative analysis of protein sequences to identify variations in the RV receptors among humans, dogs, and bats. Two notable findings emerged from this analysis: the absence of the integrin plexin domain in the *P.alecto* ITGB1 sequence and the highly conserved interaction site within the nAChR across dogs, humans, and bats.

Subsequently, we retrieved the ORF sequences for the RV receptor corresponding to *P.alecto* as a model to investigate its potential as a reservoir for RV. We confirmed the expression of these receptors and verified their endogenous expression in the *P.alecto* brain cell line (Pa-BR). These results validated the functional role of these receptors in mammalian cells **(Chapter 3).**

To study the entry mechanisms of a neurotropic RV, we generated a replication competent VSV system encoding the RV surface G protein, which is the key determinant of RV tropism and host range (Kgaladi et al., 2013). Further, the rVSV-dG-RV-G-GFP was characterized for genetic stability through sequence analysis, growth kinetics, protein expression (RV-G and VSV-M proteins), and GFP expression levels. Additionally, we selected a cellular model (HaCaT cell) in which replication of rVSV-dG-RV-G-GFP was

impeded to allow the investigation of the RV receptor preference in an over-expression model system **(Chapter 4).**

Employing the established cellular model (HaCaT) cells, non-permissive for rVSV-dG-RV-G-GFP) in its nature form, we applied two independent approaches to identify the receptor preference of RV-G for cell entry. The first approach involved the ectopic expression of RV receptors of *P.alecto* in HaCaT cells individually or in combinations to elucidate RV receptor preference for viral entry. Results obtained from this approach clearly identified the role of the ectopically expressed P.*alecto* nAChR individually and the combinations of *P.alecto* ITGB1 and *P.alecto* mGluR2 receptors in promoting RV-G-binding and consequently enhanced virus progeny.

Based on the findings from the receptor preference approach, we selectively identified ITGB1, mGluR2, and nAChR for further functional analysis. For their role on RV replication. Genetic knockout of each of these receptors individually was performed on A549 cells, revealing that KO cells devoid of any of these receptors individually was still capable of sustaining the rVSV-dG-RV-G-GFP replication yet, to varying degrees **(Chapter 5).**

Further to the *in-silico* analysis which allowed the comparison of the receptor orthologs, we further validated the obtained findings experimentally. We conducted an *in vitro* investigation to examine the tropism of RV virus in human, bat, and dog cell lines. This was achieved by introducing (ectopic expression) orthologs of RV receptors into the respective cell lines. By comparing the selective receptor preference of RV in different cell lines, we obtained compelling results. Specifically, the findings indicated that RV selectively utilizes distinct receptors in various cell lines. For instance, virus replication was enhanced in Pa-Br cells ectopically expressing *P.alecto* nAChR, while MDCK cells overexpressing canine ITGB1 facilitated virus entry and replication in dog cell lines. On the other hand, A549 cells, ectopically expressing *H.sapiens* ITGB1 enhanced initial binding, while *H.sapiens* nAChR promoted virus internalization **(Chapter 6).**

Since the *P.alecto* proteins corresponding to RV receptors were firstly identified as functional receptors for RV in the current study. We assessed their physical interaction with the RV-G to gain more insight on their mechanistic role. The full-length *P.alecto* proteins interacted with the RV-G. Further investigation of the domains responsible for

the interaction of *P.alecto* ITGB1, mGluR2, was carried out. However, our results indicated further domain splicing is required but the obtained results demonstrated that the ITGB1 N-terminal and EGF domains interacted with RV-G. Furthermore, the mGluR2 LBD domain showed interaction with the RV-G.

Finally, we mapped other factors contributing to the replication of rVSV-dG-RV-G-GFP in Pa-BR cells. We observed that viral proteins such as phosphoprotein and matrix proteins, enhanced the virus replication possibly due to their role in evading the innate immune response (Scrima et al., 2023). Other attachment factors, including HS and gangliosides, were also studied. The ectopic expression of *P.alecto* nAChR resulted in less significant virus release compared to untreated empty vector control. However, HS and gangliosides pretreatment of the Pa-Br cells transiently expressing either the *P.alecto* ITGB1 or *P.alecto* mGluR2 failed to significant difference in released virus progeny compared to the untreated empty vector control **(Chapter 7).**

The findings obtained in this report have not identified one essential receptor on which the RV fully rely during its entry. However, the presented results can direct future research to answer arising research questions. This chapter will focus on the findings obtained from this study and relating them to previous studies to expand prior research. This would allow the explanation of our findings and gain insight on the implications of the obtained results for future research.

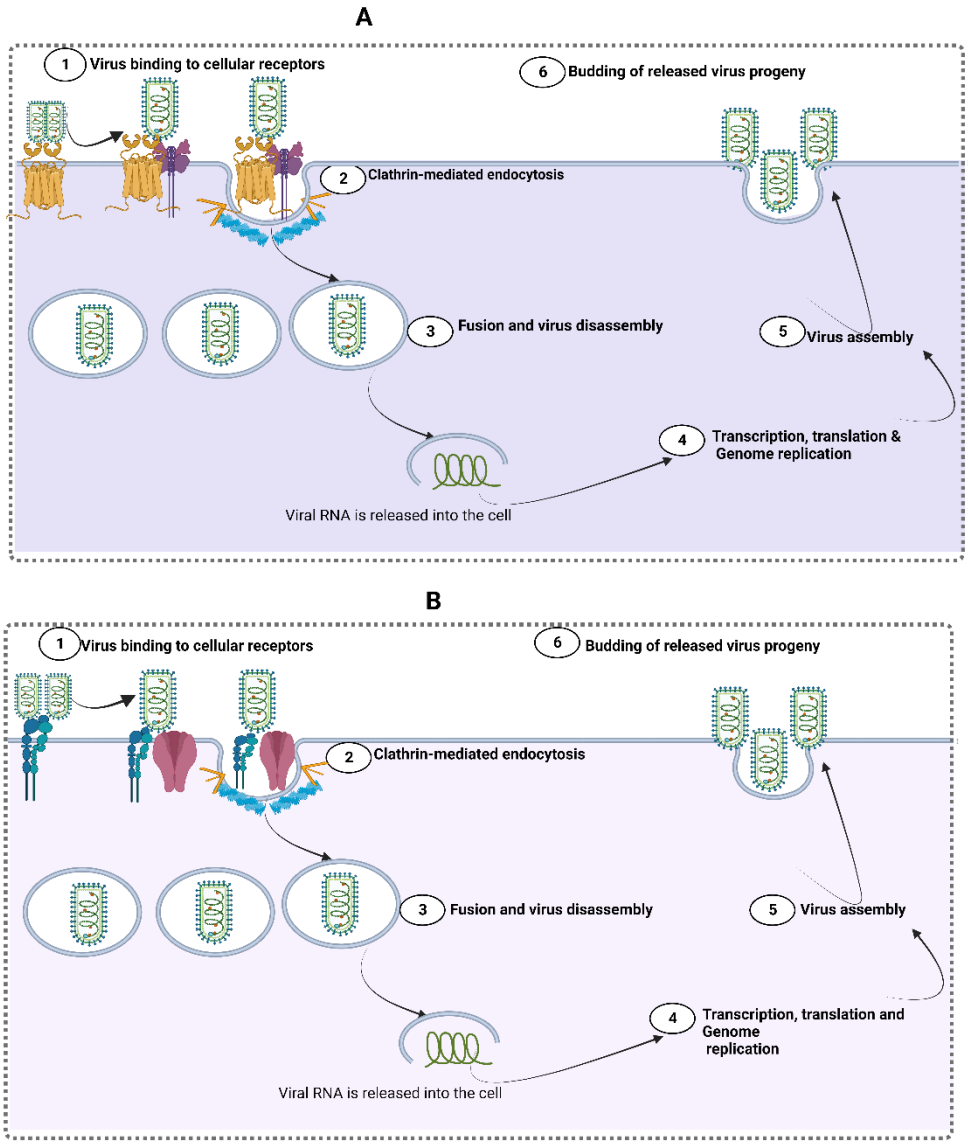

Figure 8.1 Schematic diagram showing the putative mechanism of the rVSV-dG-RV-G-GFP entry, and replication

(A) *Diagram showing the rVSV-dG-RV-G-GFP binding to the cell surface mGluR2 receptor, subsequently, the mGluR2-virus complex interacts with the transferrin receptor 1 mediating the virus internalization via receptor-mediated endocytosis, enabling virus replication and release of virus progeny.* ***(B)*** *Diagram showing the binding of the rVSV-dG-RV-G-GFP to the cell surface ITGB1 receptor, which subsequently interacts with the nAChR receptor promoting the virus internalization into the endocytic compartments, subsequently virus replication and release of the progeny virus occurs. These proposed models are conclusions from results in the current study along with conclusions from previous study (Wang et al., 2022).*

8.2 Identification of *P.alecto* as novel bat species that can be involved in maintaining the RV.

Owing to limited knowledge of the susceptibility of Megachiroptera species to RV, and the numerous challenges associated with the *in vivo* transmission studies. The development of the *in vitro* assays is crucial to determine the RV susceptibility and host range.

Fruit bats have been presumed to be the potential reservoirs for Marburg and Ebola viruses (Takadate et al., 2020). Rabies has been one of the viruses primarily discovered in bats, however most of bat related rabies viruses have been attributed to the vampire bats (suborder Microchiroptera) with no studies conducted on the possibility of the involvement of fruit bats (suborder Megachiroptera) in rabies transmission to human (Banyard et al., 2013).

Owing to the robust immune responses observed in fruit bats, particularly their enhanced interferon (IFN) capabilities, these bats may experience more efficient rates of virus transmission without displaying clinical signs. However, when these rapidly reproducing viruses are transmitted to other hosts lacking similar immune capacities as bats, they can potentially result in severe pathogenesis and virulence (Brook et al., 2020). In this study, we aimed to investigate the susceptibility of the *P.alecto* brain cell line to rVSV-dG-RV-G-GFP infection *in vitro*. We retrieved the protein sequences corresponding to RV receptors in bats and experimentally examined their functional roles in supporting rVSV-dG-RV-G-GFP infection in Pa-Br cells. Our findings demonstrated the ability of the tested *P.alecto* receptors to facilitate RV entry and replication. To the best of our knowledge, this study provides the first characterization of RV receptors in *P.alecto*, highlighting the functional roles of ITGB1, mGluR2, nAChR, NCAM, and p75 genes as functional proteins., indicating that all host receptor proteins required by RV are functional in *P.alecto* **(Chapter 3, section 3.2.9, Figure 3.9)**. Moreover, their physical interaction with the RV-G protein in immunoprecipitation assays confirmed their candidacy as receptors for RV *in vitro* **(Chapter 7, section 7.2.1, Figures 7.1-7.5)**. Collectively, our results provide the initial evidence of *P.alecto* brain cells (Pa-BR) susceptibility to rVSV-dG-RV-G-GFP infection and that *P.alecto* bats have the potential to serve as direct reservoirs for RV in humans. It is important to note that

fruit bats exhibit diverse foraging habitats and roosting sites, which may influence their contact with humans and RV *in vivo*, unlike vampire bats. Given the results presented in this study, further investigations are warranted, including the expansion of the bat surveillance in multiple geographical locations, particularly among fruit bat populations.

8.3 The *P.alecto* ITGB1 does not promote the replication of the rVSV-dG-RV-G-GFP in PA-BR cells as other receptors.

Integrins have been involved in facilitating the entry of multiple viruses with the Arg-Gly-Asp (RGD) motif as Rotavirus (RV), human metapneumovirus (HMPV), human cytomegalovirus (HHV-5) Epstein-Barr virus (HHV-4) and SARS-CoV-2 (Sigrist et al., 2020). Recent study suggested the involvement of the ITGB1 in RV peripheral entry in various human cells (N2a cell and HEK293). Besides, the co-existence of the ITGB1 with the RV in the thigh muscles upon injecting the mice with RV I/M, but not I/C through immunofluorescence (Shuai et al., 2020). Thus, we sought to assess the role of the *P.alecto* in the rVSV-dG-RV-G-GFP. As demonstrated in **(chapter 3, section 3.2.1, Figure 3.1),** the comparative genetic analysis revealed the amino acid sequence variation of the ITGB1 protein among bats, human and dogs. Our findings revealed the absence of the first 57 amino acid corresponding to the integrin plexin domain in bats. Further analysis has revealed the implications of the lack of the integrin plexin in which no discernible effect for the ITGB1 mRNA expression levels was observed in response to the rVSV-dG-RV-G-GFP compared to the mock Pa-BR cells **(Chapter 6, section 6.2.1, Figure 6.1**).

To further ascertain the minimal role of the ITGB1 in rVSV-dG-RV-G-GFP infection, the ectopic expression of the *P.alecto* ITGB1 in Pa-Br cells resulted in reduced released virus progeny and limited binding affinity to the RV-G compared to other *P.alecto* receptors as discussed in **chapter 6, section 6.2.2, Figures 6.2-6.44**.

These findings clearly dictate the differential RV receptor preference across the species and tissues infected. Additionally, it reveals that RV does not necessarily employ all known receptors during entry at least in our tested settings. This serves as an example of how the selective pressure acting on the host protein can modify the ability of the virus to infect cells.

8.4 Downregulating the nAChR and NCAM are not sufficient for RV infection.

In the current study, most of the tested cell lines have demonstrated permissiveness to rVSV-dG-RV-G-GFP rendering them susceptible to natural infection and unsuitable for assessing the host susceptibility of the virus. Therefore, we identified a non-permissive cell line, HaCaT cells, which do not support rVSV-dG-RV-G-GFP infection in its naïve form. This serves as a promising cellular model for studying host susceptibility i*n vitro*. Our hypothesis was that the ectopic expression of any of the RV receptors in HaCaT cells would enhance RV replication. Although our findings revealed that HaCaT cells did not exhibit GFP expression, which is indicative of viral replication. Alternatively, our analysis using plaque assays and binding studies demonstrated increased binding and release of viral progeny in HaCaT cells when nAChR was ectopically expressed, as well as in cells expressing combinations with either the mGluR2 or ITGB1**(Chapter 5, section 5.2.1.5, Figures 5.6, 5.9,5.10,5.11)**. As a result, we specifically focused on further investigating the role of these receptors in shaping the RV tropism among dogs and humans.

To gain more insights into the non-permissive nature of HaCaT cells towards RV infection, we assessed the endogenous expression of RV receptor genes in these cells and the influence of the rVSV-dG-RV-G-GFP on their regulation. Notably, our findings revealed the expression of RV cellular receptor genes in HaCaT cells. However, upon infection with rVSV-dG-RV-G-GFP, we observed a selective downregulation of the genes encoding nAChR and NCAM only. It is worth noting that despite this downregulation, it is evident that the exclusive modulation of these genes is insufficient to establish RV infection in HaCaT cell **(Chapter 5, section 5.2.1.1, Figure 5.3)**.

8.5 nAChR is essential, yet not sufficient for RV infection.

Downregulation of the RV cellular receptor genes serves as a common mechanism to counteract the superinfection of readily infected cells, facilitating the widespread dissemination of progeny virus to un-infected cells for uniform y spread of the progeny virus to uninfected cells (Id and Id, 2022). In similar fashion, RV employs this strategy by downmodulating the expression of these cellular genes involved in virus initial attachment and entry. Remarkably, the rVSV-dG-RV-G-GFP sustained the downregulation of the nAChR genes across all tested cell lines, including human, bat,

and dog cells, as well as various tissues such as epithelial, brain and keratinocytes, albeit with varying degrees of magnitude. These findings can be attributed to the highly conserved interaction site between nAChR and RV-G across different species, as elucidated in **(Chapter 3, Section 3.2.5, Figure 3.5).** The down-modulation of the nAChR was also observed in HaCaT cells in response to the rVSV-dG-RV-G-GFP infection, which is typically refractory to rVSV-dG-RV-G-GFP. Taken together, these findings provide clear evidence that the nAChR is essential for the rVSV-dG-RV-G-GFP, yet not sufficient for virus replication **(Chapter 5, section 5.2.1.1)**.

8.6 A549 cells with individual KO receptors, support the rVSV-dG-RV-G-GFP entry and replication.

To elucidate the critical receptors implicated in RV entry and infection, the proteins ITGB1, mGluR2, and nAChR were specifically chosen for further investigation based on the findings from the receptor preference analysis. Moreover, previous studies have demonstrated the role of NCAM and p75 as knockout targets (Hotta et al., 2006; Tuffereau et al., 2007). Earlier reports have shown that the transfection of short interfering RNA (siRNA) targeting mGluR2 or ITGB1 mRNA levels resulted in reduced RV infection rates *in vitro*, providing insights into the involvement of ITGB1 and mGluR2 as host factors in RV entry and internalization into cells (Wang et al., 2018; Shuai et al., 2020). In this study, we aimed to downregulate the expression of nAChR, ITGB1, and mGluR2 genes at the DNA level using CRISPR/Cas9 technology. Interestingly, even in the three generated KO cell lines, rVSV-dG-RV-G-GFP was still able to replicate, albeit to a lesser extent compared to wild-type (WT) cells. The replication of the virus in ITGB1 KO, nAChR KO, and mGluR2 KO cells was reduced by 3, 4, and 5 log, respectively, in comparison to WT A549 cells **(Chapter 5, section 5.2.2, Figures 5.15, 5.21,5.24)**. Furthermore, we explored at which stage the genetic ablation has affected the RV replication cycle. The findings obtained clearly demonstrated that initial virus binding to the KO ITGB1 cells showed a non-significant difference from the non-infected KO cells **(Chapter 5, section 5.2.2.5, Figure 5.21)**. These findings suggest that ITGB1 primarily participates in initial stages of the rVSV-dG-RV-G-GFP lifecycle, while mGluR2 influences virus internalization. These findings are consistent with previous reports highlighting the

effect of mGluR2 mRNA knockdown on virus internalization, without significant impact on cell binding (Wang et al., 2022).

Additionally, these results indicate that the role of the ITGB1, nAChR and mGluR2 as cellular factors contribute to virus replication and entry, but also suggest that they are not the sole receptors involved in RV entry. It could be suggested that RV utilizes these receptors in parallel manner rather than sequentially **(Figure 8.1)**. Further investigations should focus on generating triple knockout cell lines lacking all three receptors simultaneously, although cell growth presents a challenge.

8.7 mGluR2, crucial host factor in mediating the rVSV-dG-RV-G-GFP infection.

The current study focused on investigating the role of mGluR2, as a crucial host factor, in rVSV-dG-RV-G-GFP infection. In this report, results revealed that the cells that exhibited susceptibility to rVSV-dG-RV-G-GFP showed a downmodulation of the mGluR2 gene expression. However, non-permissive HaCaT cells maintained unchanged levels of mGluR2 expression following rVSV-dG-RV-G-GFP infection **(Chapter 5, section 5.2.1.1, Figure 5.3)**. Further support for the significance of the crucial role of the mGluR2 was provided by the substantial decreased in rVSV-dG-RV-G-GFP replication observed in mGluR2 KO cells compared to nAChR and ITGB1 KO cells **(Chapter 5, section 5.2.2.3, Figure 5.18)**. These findings align with a recent study which revealed that approximately 58% of mice with mGluR2 KO were protected upon infection with the RV street strain *in vivo* (Wang et al., 2022). Collectively, these results clearly highlight the key role of the mGluR2 in RV infection.

8.8 ITGB1, plays significant role in mediating the rVSV-dG-RV-G-GFP in different cell lines.

Integrin beta 1 has been identified recently as a cellular receptor involved in RV peripheral entry (Shuai et al., 2020). Investigating the exact role of ITGB1 in our study has demonstrated dramatically impaired entry of the rVSV-dG-RV-G-GFP in ITGB1 deficient A549 cells, which was non-significantly different from non-infected KO ITGB1 cells **(Chapter 5, section 5.2.2.5, Figure 5.21**). Moreover, transiently expressing the *H.sapiens* and *C. familiaris* ITGB1 orthologs in A549 and MDCK cells resulted in significantly higher Initial attachment of the rVSV-dG-RV-G-GFP compared to the empty

vector control (**Chapter 6, section, 6.2.5 and 6.2.8, Figures 6.8 and 6.13)**. Conclusively, it is evident that the ITGB1 plays significant role in mediating the initial rVSV-dG-RV-G-GFP attachment in different cell lines.

8.9 Entry of rVSV-dG-RV-G-GFP depends on multiple host factors.

Our obtained results demonstrated the capability of rVSV-dG-RV-G-GFP to enter and replicate in A549 cells genetically deficient in either ITGB1, mGluR2 or nAChR **(Chapter 5, section 5.2.2, Figures 5.15-5.24)**. Based on these findings, we hypothesized that the entry of RV depends on interaction with more than one host factor. Previous studies provided plausible explanation to this notion, which revealed the interaction between the ITGB1 and nAChR indicating the possibility of their dual role in promoting the RV entry (Shuai et al., 2020). Furthermore, although previous reports have suggested the involvement of mGluR2 in RV internalization (Wang et al., 2018), it is widely recognized that G protein-coupled receptors (GPCRs), including mGluR2, do not typically initiate the formation of clathrin-coated pits (Scott et al., 2002). Therefore, based on recent study which mapped the interaction between mGluR2 and TRf1, it has been deduced that the internalization of RV occurs through the interaction between mGluR2 and TRf1 (Wang et al., 2023). Further experimental investigations are required to substantiate this hypothesis. One significant inference of these findings might be that design of the RV antiviral drugs targeting host cellular factors may not effectively inhibit RV entry into cells. Instead, antiviral drugs that target the surface proteins of the virus may exhibit greater efficacy.

8.10 NCAM does not play a central role in rVSV-dG-RV-G-GFP

NCAM-120, identified as a receptor for RV since cells exhibited decreased surface NCAM expression upon incubation with the RV, resulting in increased virus attachment in resistant cells when NCAM-120 is expressed (Thoulouze et al., 1998; Hotta et al., 2006). The results obtained from our study indicated that however the RV infection resulted in downregulation of NCAM expression levels in HaCaT cells, it was insufficient to render them susceptible to RV infection. Also, it is noteworthy that the unchanged mRNA levels of NCAM genes on A549 cells did not impact their susceptibility to RV infection, suggesting that NCAM does not play a vital role in RV replication (**Chapter 5, section**

5.2.2.1, Figure 5.15). Our results are consistent with a previous study demonstrating that the expression of NCAM-120 in a resistant cell line (HEP-2) enhances virus binding and adsorption but does not permit virus release due to the production of IFN-beta one hour after infection (Matthias and Horstkorte, 2006).

8.11 The p75 is not essential for the rVSV-dG-RV-G-GFP

The involvement of the p75 in RV infection has been subject to debate with some studies demonstrating its role in promoting RV infection, while others indicating it may not be essential for RV infection (Tuffereau et al., 2007). From this perspective, we investigated the role of p75 and evaluated its expression levels in response to rVSV-dG-RV-G-GFP infection among different cell lines. In our study, we observed downregulation of p75 expression in all susceptible cells for RV infection, except in HaCaT cells where rVSV-dG-RV-G-GFP did not affect the p75 expression levels **(Chapter 5, section 5.2.1.1, Figure 5.3)**. Interestingly, ectopic expression of p75 in HaCaT cells individually or in combination with other receptors resulted in reduced virus release and binding to the G protein **(Chapter 5, section 5.2.1.4, Figure 5.12-5.13)**. However, it should be noted that p75 exhibited the highest capacity for G protein binding and virus release in Pa-BR cells **(Chapter 6, section 6.2.2, Figures 6.2-6.4)**. Collectively, the obtained results demonstrate the variability of the receptor selection of the RV-G in different cells and host. Moreover, these results clearly indicate that the p75 might promote more virus infectivity but is not essential for the RV replication.

8.12 Same virus strain does not exhibit uniform utilization of receptors across different species in RV.

Feline leukaemia virus subtype A (FELV-A) and subtype C (FELV-C) show differential host range, with the FELV-A strictly infecting feline, but broader host range is known to be demonstrated by the FELV-C. This variation in host range has been associated with a single variable domain within the surface envelope protein. Thus, similar receptor usage was displayed upon exchanging this region from the subtype A to that of subtype C. These findings suggested that the variability in the receptor usage between both subtypes lies in the virus envelope variable sequences among both subtypes (Bupp et al., 2005).

In this project, despite the same RV G strain was employed to elucidate the role of the cellular receptor orthologs in shaping RV tropism. Our results demonstrated that the entry and internalization of the rVSV-dG-RV-G-GFP in Pa-Br cell (bat), A549 (human) and MDCK (dog) showed selective preference of receptors. In bat cells, the virus entry and internalization were enhanced in cells ectopically expressing the *P.alecto* nAChR **(Chapter 6, section 6.2.2, Figures 6.2-6.4)**. Whereas MDCK cells ectopically expressing the canine ITGB1 promoted more virus entry and GFP expression **(Chapter 6, section 6.2.8, Figures 6.11-6.13)**. The *H.sapiens* ITGB1 and nAChR receptors simultaneously supported more virus entry and thereby enhanced virus infection **(Chapter 6, section 6.2.5, Figures 6.6-6.8)**. Based on the obtained findings, we can clearly exemplify that the crossing of the host species barrier is influenced by the variable cell lines expressing distinctive receptors which subsequently can be promoting more virus entry and replication compared to other species. Additionally, these findings dictate two main conclusions: Firstly, in bat and dog cell lines dependent function of receptors were maintained in which the *C.familiaris* ITGB1 and *P.alecto* nAChR mediated both virus initial attachment and membrane endocytosis, while in human cells, independent roles are played by the *H.sapiens* ITGB1 which facilitates virus entry and nAChR which promotes the virus internalization **(Chapter 6, Figure 6.14).** Secondly, the decisive role of the cellular receptors in discerning virus tropism, highlighting their potential role in virus cross-species transmission. Another plausible explanation for the variation in receptor selection among the cell lines could be attributed to the presence of abundant host factors within the cells, thereby facilitating preferential binding of the virus to the receptors compared to others. This concept aligns with previous studies suggesting that RV potentially relies on interaction of multiple receptors during the initial stages of viral entry (Shuai et al., 2020; Wang et al., 2022).

8.13 Effect of pre-treating Pa-BR cells with HS and gangliosides on rVSV-dG-RV-G-GFP replication.

Besides, the role of the host cellular receptors in mediating the entry of the rVSV-dG-RV-G-GFP, we also assessed the effect of preincubating the Pa-Br cells with HS prior to inoculation of the rVSV-dG-RV-G-GFP. The results obtained showed no significant difference in released virus progeny compared to un-treated infected Pa-Br cells. Only

the Pa-Br cells transiently expressing the *P.alecto* nAChR and treated with HS, showed significantly decrease in released virus compared to untreated empty vector. This might be attributed to the competitive binding of the HS to the RV-G; hindering its ability to bind the nAChR (Sasaki et al., 2018). Similar pattern was observed upon preincubating gangliosides with Pa-Br cells transiently transfected with either of the *P.alecto* receptors which resulted in non-significant difference in the virus progeny compared to untreated empty vector control. Future studies related to the underlying mechanism of the attachment factors in RV infectivity is required **(Chapter 7, section 7.2.5, Figures 7.11-7.12)**

8.14 *P.alecto* domain organization and their functional role in virus entry

Since the susceptibility of the *P.alecto* to RV infection has been identified for the first time in this study, further mapping of the functional domains of the *P.alecto* ITGB1, mGluR2 were demonstrated.

The human ITGB1 ectodomain (1-724 a.a) has been reported previously to be the region responsible for interaction with the RV-G (Shuai et al., 2020). Thus, we sought that further splicing of this region in the P.alecto ITGB1 might reveal which region is specifically responsible for RV binding. The IP results obtained has demonstrated the interaction of both the ITGB1 N terminal (1-412 a.a) region and ITGB1 EGF (413-746 a.a) region with the RV. **(Chapter 7, section 7.2.2, Figure 7.7-7.8)**.

Despite that the role of the mGluR2 in RV infection has been extensively studied (Wang et al., 2018, 2021). None of previous studies has elucidated the functional domain within the mGluR2. Herein, we tested the role of the *P.alecto* mGluR2, LBD domain in interacting with the RV-G. A physical interaction with the RV-G was observed with the LBD domain. (**Chapter 7, section 7.2.3, Figure 7.10)**.

Collectively, these results demonstrated the underlying mechanism of the *P.alecto* domains in enhancing virus binding. However, more understanding of the specific regions involved in RV-G interactions is deemed essential in future.

8.15 Future work

The findings of this study have provided answers to some research questions, while also raising additional research questions that necessitate further investigation.

Firstly, we have demonstrated the susceptibility of *P.alecto* to rVSV-dG-RV-G-GFP on Pa-Br cells. It is important to expand testing to assess the reservoir competence of *P.alecto* and its ability to transmit RV in real-life scenarios, as our conclusions are based on cell culture experiments.

In this study, we utilized rVSV-dG-RV-G-GFP, which express the G protein from a dog-related RV. It is essential to conduct further research employing a G protein strain belonging to a bat-related RV to evaluate whether similar receptor utilization occurs. This investigation would reveal the differential tropism of G protein sequences between dog-related and bat-related RV.

We have evaluated the endogenous expression of receptor genes in different cell lines in response to rVSV-dG-RV-GFP. However, a more detailed temporal evaluation in a time-dependent manner could provide additional insights into the influence of rVSV-dG-RV-G-FP, specifically at which step these genes are required in the virus replication cycle.

HaCaT cells served as a potential cellular model in this study, allowing us to study the host preference of RV due to their resistance to rVSV-dG-RV-G-GFP. However, further investigation is required to determine the restriction factors of HaCaT cells to RV infection.

Initially, we hypothesized that identifying a single essential receptor would enable us to identify an antiviral drug that targets the receptor-virus interaction, thereby preventing RV replication. However, the results obtained suggested that RV utilizes more than one receptor for entry, and none of the identified receptors has been deemed indispensable. Therefore, these findings strongly suggest that antiviral drugs targeting the host receptors would be less effective than those targeting the G protein.

Furthermore, since our knockout results did not completely result in abolishment of the rVSV-dG-RV-G-GFP Replication, a triple knockout including ITGB1, mGluR2, and nAChR might yield more plausible results regarding the potential dual receptor utilization by RV to enter host cells.

As this study reports the susceptibility of *P.alecto* to RV for the first time, the investigation into functional domains within ITGB1 and mGluR2 requires further

investigation. Further analysis of domain splicing would provide additional insights into the sites contributing to the essential RV-G interaction.

Additionally, we have identified other factors that affect rVSV-dG-RV-G-FP replication on Pa-Br cells, including phosphoprotein and matrix viral proteins that enhance virus replication, as well as the treatment of cells with HS prior to infection. Understanding the underlying mechanisms by which these factors promote virus replication is necessary.

9 Appendix

9.1 Materials

Chemicals, enzymes, antibodies, media, and instruments used in this study were used according to the manufacturer's recommendations.

9.1.1 Chemicals, consumables, and equipment

9.1.1.1 Chemicals

Chemical	Catalogue number	Manufacturer
Acetic acid	A6283	Sigma-Aldrich, St. Louis, USA
Acrylamide/Bis Solution (30%)	1610158	Bio-Rad, China
Agar-bacteriological Lennox L Agar	22700	Invitrogen, Life Technologies, USA
Agar-bacteriological Lennox L broth	12780	Invitrogen, Life Technologies, USA
Agarose-Low EEO	R1040	NBS-biologicals, Cambridge, UK (United Kingdom)
Ammonium persulfate (APS)	1610700	Bio-Rad, Japan
Ampicillin Na-Salt	A9518	Sigma-Aldrich, St. Louis, USA
Antibiotic-Antimycotic (100 X)	15240062	Gibco, Life Technologies, UK
BSA (Albumin Bovine Fraction V)	05482	Sigma-Aldrich, St. Louis, USA
Chloroform	C14960115	Fisher Scientific, UK
Crystal Violet	C0775	Sigma-Aldrich, St. Louis, USA
DAPI	62247	Thermo Scientific, USA
Dimethyl sulfoxide (DMSO)	175462	Fisher Scientific, UK
Dulbecco's MEM (DMEM)	31966-021	Gibco, Life Technologies, UK
EDTA	324503	Millipore, USA
Ethanol	2107463	Fisher Scientific, UK
Foetal bovine serum	10500-64	Gibco, Life Technologies, UK
Glycerol	G5516	Sigma-Aldrich, St. Louis, USA
Glycine	G8898	Sigma-Aldrich, St. Louis, USA
L-glutamine (200 mM)	25030-081	Gibco, life technologies, UK

MEM (10 X)	21430-020	Gibco, life technologies, UK
Methanol	2196137	Fisher Scientific, UK
Methylene blue	M9140	Sigma-Aldrich, St. Louis, USA
NP-40	85124	Thermo Scientific, USA
Nuclease free water	10977-035	Thermo Scientific, USA
NuPAGE (transfer buffer)	2270643	Novex, Life Technologies, USA
Opti-MEM	31985-070	Gibco, life technologies, UK
Paraformaldehyde	J19943-k2	Thermo Scientific, USA
Permeabilization buffer (10 X)	00833356	Thermo Scientific, USA
Pierce Protease inhibitor tablet	A32963	Thermo Scientific, USA
Potassium phosphate dibasic	P0662	Sigma-Aldrich, St. Louis, USA
Potassium phosphate monobasic	P5655	Sigma-Aldrich, St. Louis, USA
Protein G Sepharose® FF resin	PCG5182501	Generon, UK
Puromycin Dihydrochloride	A1113803	Gibco, China
SDS-sample buffer	1597380	Life Technologies, USA
SDS-solution 10%	1610416	Bio-Rad, USA
Skimmed milk powder	70166	Millipore, Switzerland
Sodium bicarbonate	S5761	Sigma-Aldrich, St. Louis, USA
Sodium chloride	S5886	Sigma-Aldrich, St. Louis, USA
Sodium dodecyl sulphate (SDS)	L3771	Sigma-Aldrich, St. Louis, USA
Sodium hydroxide	221465	Sigma-Aldrich, St. Louis, USA
Sodium phosphate dibasic	S5136	Sigma-Aldrich, St. Louis, USA
TEMED	1610801	Bio-Rad, USA
Tris-base	252859	Sigma-Aldrich, St. Louis, USA
Tris-EDTA 1X	BP2473	Fisher scientific, USA
Triton X-100	T8787	Sigma-Aldrich, St. Louis, USA
Trizma hydrochloride	RDD009	Sigma-Aldrich, St. Louis, USA
Trypsin 2.5%	15090-046	Gibco, Thermo Fisher, UK
Tween -20	P2287	Sigma-Aldrich, St. Louis, USA
VECTASHIELD antifade mounting buffer	ZH1108	Vector Laboratories, USA

Versene 1:5000 (1X)	15040-033	Gibco, Thermo Fisher, UK
β-mercaptoethanol	1610710	Bio-Rad, China

9.1.1.2 Consumables

Name	Feature	Manufacturer
0.45-, 0.2 um filter	E4780-1456	STAR LAB, UK
Blotting papers	170396	Bio-Rad, USA
Cell culture flasks	25 mL, 75 mL	Corning, Mexico
Cell culture plates	6-, 24-, 96- well	Corning, Mexico
Conical centrifuge tubes	15 mL, 50 mL	Corning, Mexico
Cryovials	1.8 mL	Corning, Mexico
Eppendorf tubes	1.5 mL	Sarstedt, Germany
Latex gloves	S, M, L	Fisher Scientific, Malaysia
Parafilm	13080	Star lab, Hamburg
PCR Tubes	0.2 mL	Applied Biosystem, UK
Petri dishes for bacteria	100 mm	Sarstedt, Germany
PVDF membrane	88518	Thermo Scientific, Ireland
qPCR-tube 0.1 mL	8-tube strips	Bio-Rad, USA
Sterile pipette tips	10, 200, 1000 µL	STAR LAB, UK
Strippette	5, 10, 25 mL	Corning, Mexico

9.1.1.3 Equipment

Name	Manufacturer
Autoclave	Astell, UK
Bacterial incubator 37 ^{o}C	SANYO, Switzerland
Balance	KERN EWJ, Sigma-Aldrich, USA
Cell culture Co_2 incubator	Panasonic, Japan
Centrifuge 5424 R	Eppendorf, Germany
Centrifuge Allegra X-30R	Beckman Coulter, UK
CFX96 Real-Time system	Bio-Rad, UK
ChemiDoc^{TM} MP imaging system	Bio-Rad, UK

Class 2 Microbiological Safety Cabinets	Contained Air Solution, BioMAT2, UK
CytoFLEX Flow Cytometer	Beckman Coulter, USA
Electrophoresis power supply	Power Ease 90w, life technologies, UK
Fluorescence microscope	LSM880, Zeiss, Jena Germany
Freezer -20 ^{o}C	Lab cold, UK
Freezer -80 ^{o}C	PHCbi, IL, USA
Fridge	Lab cold, UK
Heat block	Thermo Scientific, USA
Ice maker	Scotsman, UK
Inverted cell culture microscope	Primovert, ZEISS, Jena, Germany
Magnetic stirrer	Stuart™ Sigma, UK
Milli-Q	IQ 7000, France
NanoDrop 2000 spectrophotometer	Thermo Scientific, USA
Orbital shaker	SANYO, Switzerland
pH-meter	Hanna Instruments, UK
Pipettes	Gilson, P10, 100, 1000
PTC-200 Peltier Thermal Cycler	Universal Resource Trading Ltd, UK
Rotor SW Ti-32	Beckman Coulter, UK
Roller mixer	Stuart™ Sigma, UK
SDS-PAGE system	Bio-Rad, UK
Shaking bacterial incubator	New Brunswick Scientific, USA
Stripettor^{TM} Ultra	Corning, Mexico
Trans- blot turbo membrane blotter	Bio-Rad, UK
UV transilluminator	Syngene, UK
Vortex	SLS, lab basics, UK
ZOE^{TM} fluorescent cell imager	Bio-Rad, UK

9.1.1.4 Software

Software	Version	Company
BioEdit	7.2.5	Ibis Biosciences, Carlsbad, CA
CFX Manager™ Software	3.1	Bio-Rad, UK

CytExpert	2.4	Beckman Coulter Inc.
Graphpad prism 9	9	GraphPad Software Inc.
ImageJ (FIJI)	1.52	NIH (National Institutes of Health), Bethesda
MegaAlign	3.18	DNAStar, Madison, WI, USA
SnapGene®	3.2.1	GSL Biotech, Chicago, IL
ZEN Microscopy software	(blue) 3.6	Carl Zeiss Imaging, Jena
FCS Express	7	DeNovo Software, Los Angeles California.
Benchling		San Francisco, USA

9.1.1.5 Enzymes and markers.

Enzyme/marker	Catalogue number	Manufacturer
BbsI-HF®	R3539S	New England Biolabs, UK
EcoRI-HF®	R3101S	New England Biolabs, UK
GeneRuler 1 kb DNA Ladder	SM0311	Thermo Scientific, USA
GeneRuler 1 kb Plus DNA Ladder	N3200S	New England Biolabs, UK
KpnI-HF®	R3142S	New England Biolabs, UK
Pre-stained Protein Ladder (10-180 kDa)	ab116027	Abcam, USA
Q5-high fidelity DNA polymerase	M0491S	New England Biolabs, UK
T4 DNA ligase	M0202	New England Biolabs, UK
NheI-HF	R3131S	New England Biolabs, UK
MluI-HF	R3198S	New England Biolabs, UK

9.1.1.6 Kits and reagents

Kit and reagent	Cat. No.	Manufacturer
DNeasy blood & tissue kit	69504	QIAGEN, Germany
DreamTaq Green PCR Master Mix (2 X)	K1081	Thermo Scientific, USA
GeneJET Gel Extraction Kit	01237174	Thermo Fisher, Lithuania

LIVE/DEAD™ Fixable Violet Dead Cell Stain Kit	L34964	Thermo Fisher, USA
MAX Efficiency™ DH5α Competent Cells	18258012	Thermo Scientific, USA
Pierce™ ECL western blotting substrate	32106	Thermo Scientific, USA
QIAamp ® Viral RNA mini kit	52906	QIAGEN, Germany
QIAprep ® Spin Miniprep kit	27106	QIAGEN, Germany
RNeasy ® Mini Kit	74106	QIAGEN, Germany
SuperScript IV Reverse Transcriptase	18090010	Thermo Scientific, USA
SuperScript™ III Platinum™ SYBR™ Green One-Step qRT-PCR Kit	11736059	Thermo Scientific, USA
GoTaq® 1-Step RT-qPCR System	A6020	PROMEGA
TRIzol™ Reagent	15596026	Thermo Scientific, USA
TurboFect ™Transfection Reagent	R0532	Thermo Scientific, USA
Lipofectamine™ Transfection Reagent	18324012	Thermo Scientific, USA
SuperScript™ III Platinum™ One-Step qRT-PCR Kit	11732-088	Thermo Scientific, USA
SuperScript™ III Platinum™ One-Step qRT-PCR Kit	11732-020	Thermo Scientific, USA
Recombinant Protein G Sepharose beads FF Resin	423131	Generon, UK
Heparan sulphate proteoglycan	H4777	Sigma, UK
Ganglioside-Total	860053	Avanti POLAR Lipids inc, USA

9.1.2 Antibodies

Antibody	Cat. No	Dilution	Manufacturer
Alexa-fluor goat anti-mouse IgG (468)	A11001	1:5000	Invitrogen, USA
Alexa-fluor goat anti-mouse IgG (568)	A11004	1:5000	Invitrogen, USA
Alexa-fluor goat anti-rabbit IgG (468)	A11008	1:5000	Invitrogen, USA
Alexa-fluor goat anti-rabbit IgG (568)	A11011	1:5000	Invitrogen, USA

Goat polyclonal anti-rabbit IgG (HRP)	ab6721	1:2500	Abcam, UK
Goat polyclonal anti-rabbit IgG (HRP)	ab6789	1:2500	Abcam, UK
Mouse monoclonal anti-HA tag	ab18181	1:2500	Abcam, UK
Rabbit polyclonal anti-FLAG tag	F7425	1:2500	Sigma
Rabbit polyclonal anti-HA tag	ab137838	1:2500	Abcam, UK
Mouse RV Glycoprotein antibody	MCA2828	1:1500	BIO-RAD, USA
Mouse VSV M antibody	EB0011	1:1500	KERAFAST, USA

9.1.3 Solutions and Buffers

Name	Purpose	Composition
Annealing buffer	gRNA annealing	10 mM Tris, 1 mM EDTA, 50 mM NaCl
Blocking buffer	IFA blocking	5 % BSA in PBS
Blocking buffer	WB (Western Blot)	5% skimmed milk powder in PBST
Fixative	Cell fixation (Plaque assay, IFA)	4% paraformaldehyde (PFA) in PBS
Lysis buffer	WB/IP	10% NP-40, 1 mM EDTA, 150 mM NaCl, 20 mM Tris-HCl (pH. 7.4)
PBS	Washing and dilution	0.8% (w/v) NaCl, 0.02% (w/v) KCl, 0.02% (w/v) KH_2PO_4, 0.135% (w/v), $Na_2HPO_4 \cdot 2H_2O$
PBST	WB washing buffer	0.1% tween-20 in PBS
Permeabilization buffer	Permeabilization for IFA	0.1% Triton X 100 in H_2O

Plaque overlay media. (1:1)3% CMC	Plaque assay	Sterile bottled water (142 mL), 10X MEM (50 mL), Sodium Bicarbonate Solution (15 mL) (7.5%), L-glutamine/Gluta-Max (5 mL), Non-Essential Amino Acids (5 mL), HEPES (13 mL, 1M), FCS (20 mL), 3% CMC
Separating gel solution	SDS-PAGE	10% (w/v) acrylamide/bis-acrylamide stock solution, 0.1% (w/v) SDS, 375 mM Tris.HCl (pH 8.8), 0.05% (w/v) APS, 0.1% (v/v) TEMED
Stacking gel solution	SDS-PAGE	5% (w/v) acrylamide/bis-acrylamide, 0.1% SDS, 125 mM Tris·HCl (pH 6.8), 0.075% (w/v) APS, 0.15% (v/v) TEMED
TAE (10 X)	Gel electrophoresis	48.4 g of Tris base, 11.4 mL of glacial acetic acid (17.4 M), 3.7 g of EDTA, disodium salt in distilled water
FC Buffer	Flow cytometry	PBS (2% FBS)

9.1.4 Primers

9.1.4.1 Primers for cloning RV-G and qRT-PCR

Primer name	Sequence 5'-3'
RV-G FWD.	TGTTT*ACGCGT*CACTATGGTGCCCCAGGCCCTGCT
RV-G REV	ATGAAGAATCTG*GCTAGC*AGGATTTGAGTTACAGCCGTGTCTCGCC CCCGCTCTT
VSV-UP	GCCCACCATGGGAGCGTGGGTCCTGGATTCTATCAGCCACTTC
VSV down	TGGGACAACTCCAGTGAAAAGTTCTTCTCCTTTACTCAT
qPCR-VSV N-F	TGATCGACTTTGGATTGTCTTCTAA
qPCR-VSV-N R	TCTGGTGGATCTGAGCAGAAGAG
qPCR-VSV-N Probe	FAM-ATATTCTTCCGTCAAAAACCCTGCCTTCCA-TAM

9.1.4.2 Primers for CRISPR/Cas9 mediated KO

Primer name	Sequence 5'-3'
gHumGluR2 Exon2 F	CACCGGGTCGCATAAGAGCCGTCG
gHumGluR2 Exon2 R	AAACCGACGGCTCTTATGCGACCC
mGluR2 KO Up	CAGAAGGGCGGCCCAGCAGAGGACTGTGGTCCTGTC AATGAG
mGluR2 KO down	AAATCGACCACCATTATGTGACCAGGGCACTTTCTTAG CTTC
gHuITGB1 Exon4 F	CACCGAATCGCAAAACCAACTGCTG
gHuITGB1 Exon4 R	AAACCAGCAGTTGGTTTTGCGATT
ITGB1 KO up	CAATTTTCATTTATACCTATATTTTATATGTCA
ITGB1 KO down	AATTAATACTTTCTGAATCTTTAACAAAATTTACTTTGA A
gHunAChR-Exon1 F	CACCGACCGGAGCTTGTGTGGACCA
gHnAChR-Exon1 R	AAACTGGTCCACACAAGCTCCGGT
nAChR KO up	GTGTAAAACAATAGCTCTAGTGAGCCGACTCGCTTTC CAA
nAChR KO down	GCGTGTCTATCTTGAAGTCTTTGACCAGGCAGTTTCTA T
U6 Promoter	GAGGGCCTATTTCCCATGATT

9.1.4.3 Primers for relative quantification of RV receptor genes in Pa-Br cells

Primer name	Sequence 5'-3'
q*P.alecto* ITGB1 FWD	ATGCGACTGTTCTCTGGACA
q*P.alecto* ITGB1 REV	TATTGAAGGCTCGGCACTGA
qP.alecto mGluR2 FWD	AGTGCCCCGAAAACTTCAAC
q*P.alecto* mGluR2 REV	GATGATGTGCAGCTTGGGAG
q*P.alecto* nAChR FWD	TCTCCCCTGATCAAACACCC
q*P.alecto* nAChR REV	AATTCAATGAGCCGACCTGC
q*P. alecto* NCAM FWD	AGTTCGGAGCTGACCATCAA
q*P.alecto* NCAM REV	GAGTGTGACCTGTTCCTCCA

q*P.alecto* p75 FWD	AAGCTTGCAACTTGGGTGAG
q*P.alecto* p75 REV	CTCGTTCTGGTAGTAGCCGT
q*P.alecto 18S* FWD	CGGTACCACATCCAAGG
q*P.alecto 18S* REV	GCTGGAATTACCGCGGCT

9.1.4.4 Primers for relative quantification of *C. familiaris* RV receptor genes in MDCK cells

Primer name	**Sequence 5'-3'**
qdoITGB1 FWD	GTGCAACCCCAACTACACTG
qdoITGB1 REV	GTTCAGCACAGACACCAAGG
qdomGluR2 FWD	CAACCTCCTGCGGCTATTTC
qdo mGluR2 REV	CGCCATAGTCACCCTCAGAT
qdo nAChR FWD	CTACCACTTCGTCATGCAGC
qdo nAChR REV	ACGGTTAGAGACAGCAGGAC
qdo NCAM FWD	CAGCGATGACAGTTCTGAGC
qdo NCAM REV	GAGGCTTCACAGGTCAGAGT
qdo p75 FWD	GCAAGCAGAACAAGCAAGGA
qdop75 REV	GCTGTAGAGACCTCCATCCC
qdo beta actin FWD	CCGCCTATTCCAGGATTCTCT
qdo beta actin REV	GGACCTTCCCAACCCTGTTAG

9.1.4.5 Primers for relative quantification of *H. Sapiens* RV receptor genes in A549 cell lines

Primer name	**Sequence 5'-3'**
qhuITGB1 FWD	GAAGGGTTGCCCTCCAGA
qhuITGB1 REV	GCTTGAGCTTCTCTGCTGTT
qhumGluR2 FWD	TACTGGGCAGAAGGCTTCACTC
qhu mGluR2 REV	GGATGGCTTGGCAATGAAGATG
qhunAChR FWD	CTACCACTTCGTCATGCAGC
qhunAChR REV	TTTCCAATCAAGGGCACAGC
qhu NCAM FWD	AATGTGCCACCTACCATCCA

qhu NCAM REV	AGATGTACTCAGCCTCGTCG
qhu p75 FWD	ACTCACTGCACAGACTCTCC
qhup75 REV	CCCGAGCACATAGACTCCTT
qhu beta actin FWD	CCTCGCCTTTGCCGATCCG
qhu beta actin REV	GCCGGAGCCGTTGTCGACG

9.1.4.6 Primers for cloning the *P.alecto* ITGB1 and mGluR2 domains.

Primer name	Sequence 5'-3'
ITGB1-FWD1 N terminal	GCAAAGAATTCGCCACCATGCCCACAAGC
ITGB1-Rev1 N terminal	TAGCACGTCCTCACACTCGCAGATGAACTGGAGGATG
ITGB1-Fwd2 EGF	CCGGAATTCGCCACCATGTGCCAGAGCGAGGGCATCCCTGG CA
ITGB1-Rev2 EGF	CCGGGTACCAGTACCCACTTCCCCTCGTACTTAGG
LBD-EcoRI-Fwd1	CAAAGAATTCGCCACCATGGGCAGCCT
LBD REV V3	GGGGAGCTCTCTCAGGCTTGTGTCCAGGGTCAAC

9.1.5 Plasmids

Plasmid Name	Catalogue number	Company
pBS-N-ΦT Plasmid	EH1013	Kerafast, USA
pBS-P-ΦT Plasmid	EH1014	Kerafast, USA
pBS-L-ΦT Plasmid	EH1015	Kerafast, USA
pBS-G-ΦT Plasmid	EH1016	Kerafast, USA
VSV-dG-GFP-2.6 plasmid expression vector	EH1026	Kerafast, USA
pSpCas9(BB)-2A-Puro (PX459) V 2.0	62988	ADDGENE, UK

Thermocycler conditions for PCR Chapter 2, section 2.1.2.1

Step	Temperature and Duration	Number of cycles
Initial denaturation	98 °C/ 3 min	1
Denaturation	98 °C/ 30 sec	
Annealing	72 °C/ 1 min	35 cycles

Extension	72 °C/ 2 min	
Final extension	72 °C/10 min	1

PCR reaction profile for colony PCR described in **Chapter 2, section 2.1.2.7**

Step	**Temperature and Duration**	**Number of cycles**
Initial denaturation	95 °C/ 3 min	1
Denaturation	95 °C/ 30 sec	
Annealing	72 °C/ 1 min	35 cycles
Extension	72 °C/ 1 min	
Final extension	72 °C/10 min	1
Hold	4 °C /∞	

The PCR Profile for the RT-PCR **Chapter 2, section 2.1.2.11** was set as follows:

Step	**Temperature and Duration**	**Number of cycles**
Initial denaturation	95 °C/ 3 min	1
Denaturation	95 °C/ 30 sec	
Annealing	67.8 °C / 1 min	35 cycles
Extension	68 °C / 2 min	
Final extension	68 °C/10 min	1

The RT-qPCR profile of the quantitative One step RT-qPCR (TaqMan™), **Chapter 2, section 2.1.2.12:**

Temperature	**Duration**	**No of cycles**
50 °C	15 minutes	
95 °C	2 minutes	
95 °C	15 sec	40
60°C	30 sec	
Melt curve 65 °C to 95 °C increment 0.5 for 0.05 +plate read		

The RT-qPCR cycling protocol SYBR™ Green qPCR kit, described in **Chapter 2, section 2.1.2.16**, was carried out as follows:

Temperature	Temperature	Duration	No of cycles
Reverse transcriptase	50 °C	15 min	1
Initial denaturation	95 °C	5 min	1
Denaturation*	95 °C	10 sec	40
Annealing-Extension*	60 °C	30 sec	
Melt curve	65 °C to 95 °C	increment 0.05 °C each 5 sec	
Hold	4	∞	

*These streps were repeated.

9.2 Plasmid maps

9.2.1 RV cellular receptors plasmid

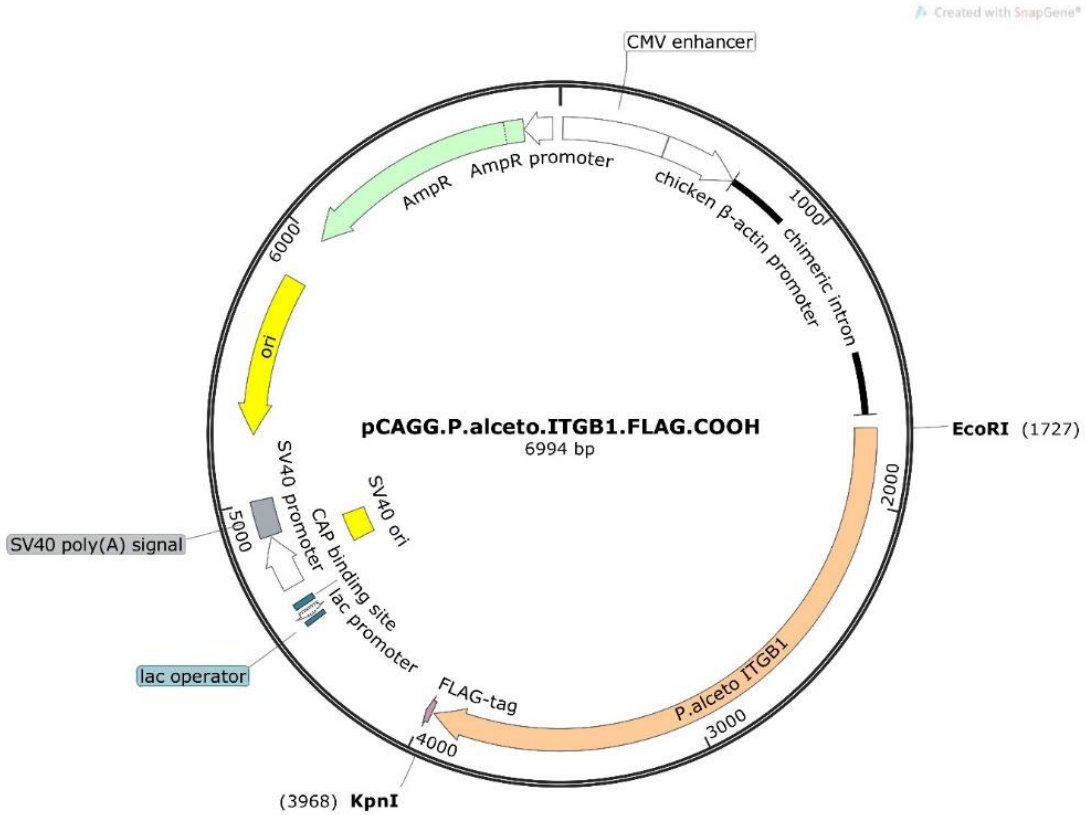

***Supplementary Figure 1**: Representative plasmid map encoding the codon optimized ORF of P.alecto ITGB1 in pCAGG-FLAG backbone between the EcoR-I and KpnI restriction sites.*

9.2.2 Viral plamsid

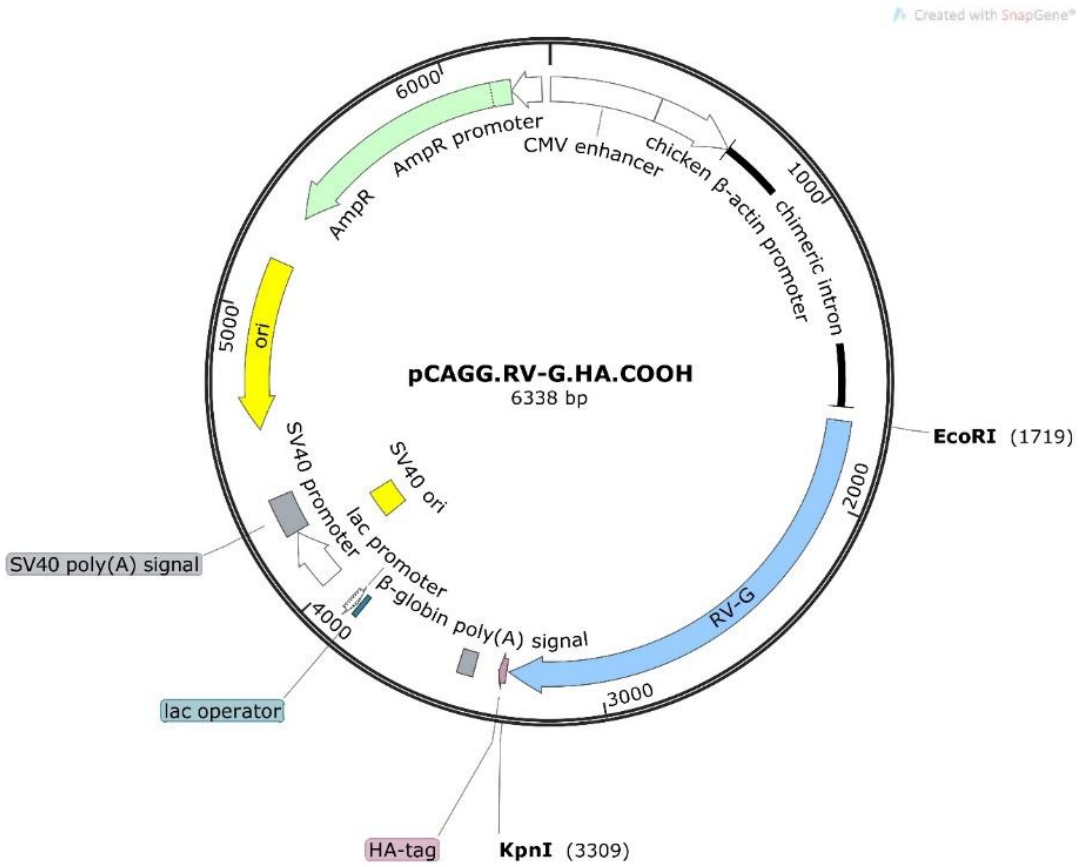

Supplementary Figure 2*: Representative plasmid map of the viral plasmids encoding the codon optimized RV-G in pCAGG-HA backbone between the EcoR-I and KpnI restriction sites.*

9.2.3 pVSV -dG-RV-G-GFP plasmid

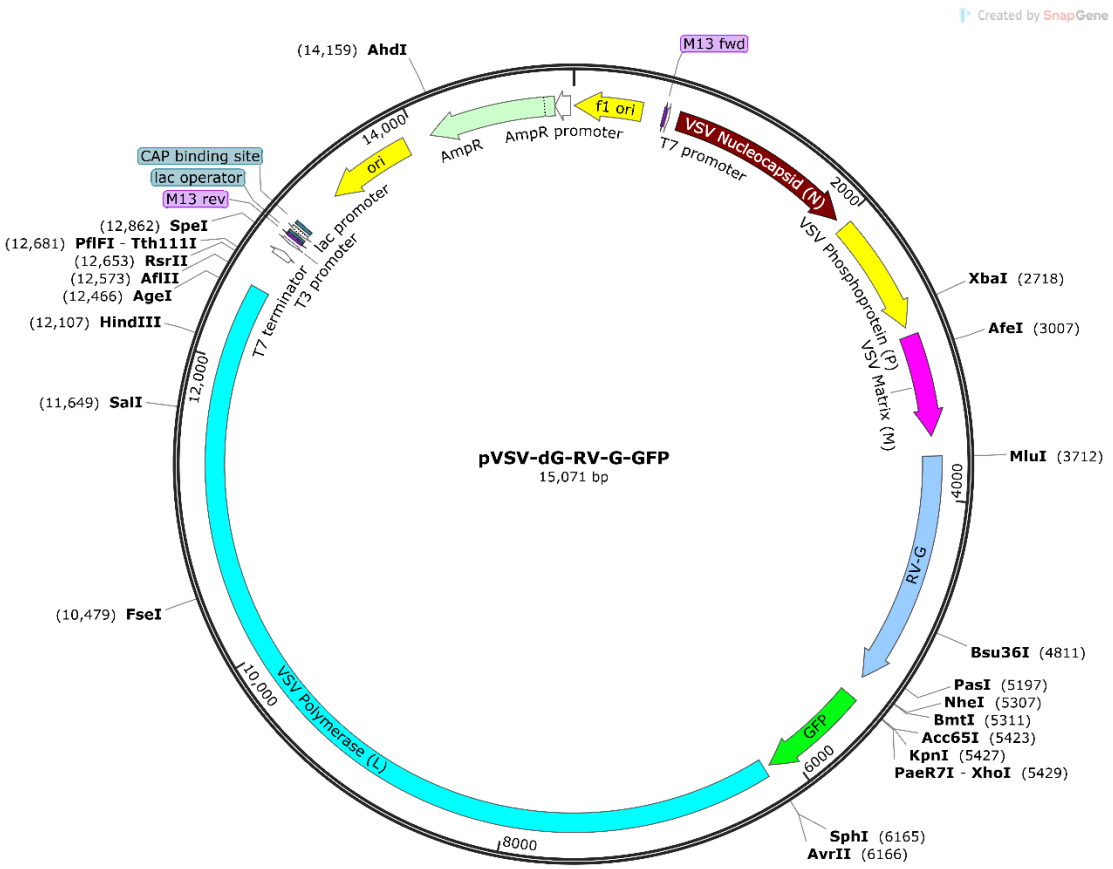

Supplementary Figure 3*: Plasmid map of the pVSV-dG-RV-G-GFP, encoding the antigenome sequence of VSV except for the VSV G gene which was replaced with the RV-G, cloned between the matrix and GFP genes and flanked with MluI and NheI restriction sites.*

9.2.4 VSV helper plasmid

***Supplementary Figure 4**: Representative plasmid map of the VSV helper plasmid encoding the nucleoprotein pBS-N-ΦT Pbs-n-pVSV-dG-RV-G-GFP. As shown in the map, the RV-G, cloned between the matrix and GFP genes flanked with MluI and NheI restriction sites.*

9.3 Uncropped western blots

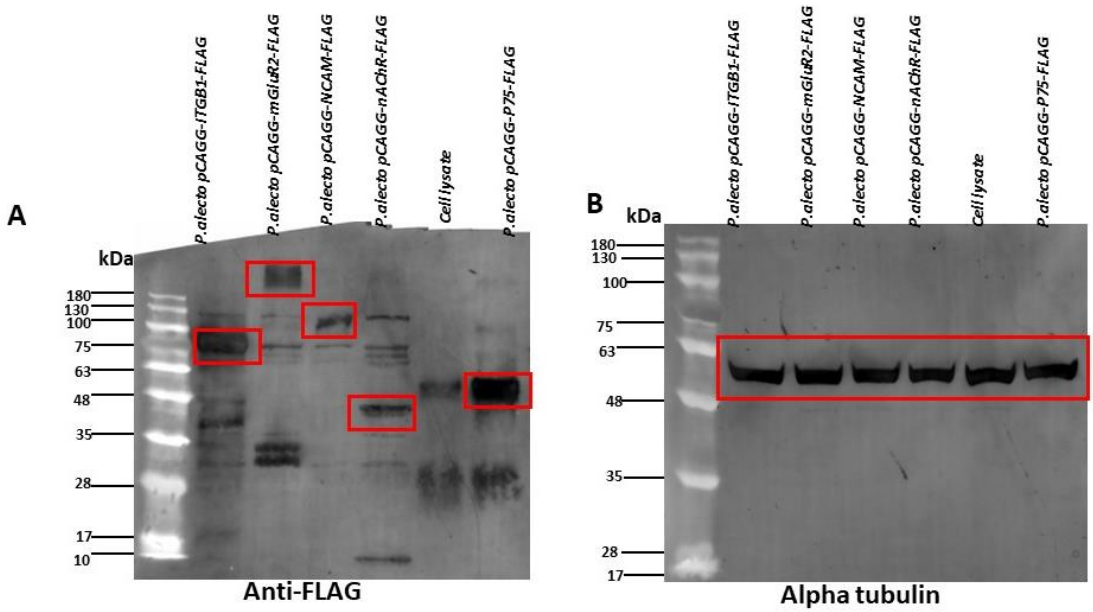

Supplementary Figure 5. *Uncropped images of the blots in* ***Chapter 3, Figure 3.9****.* ***(A)*** *Blot stained against the FLAG antibody.* ***(B)*** *Blot stained against the alpha tubulin antibody. Red boxes refer to the region used for figures. Position of the molecular mass markers is shown in kDa.*

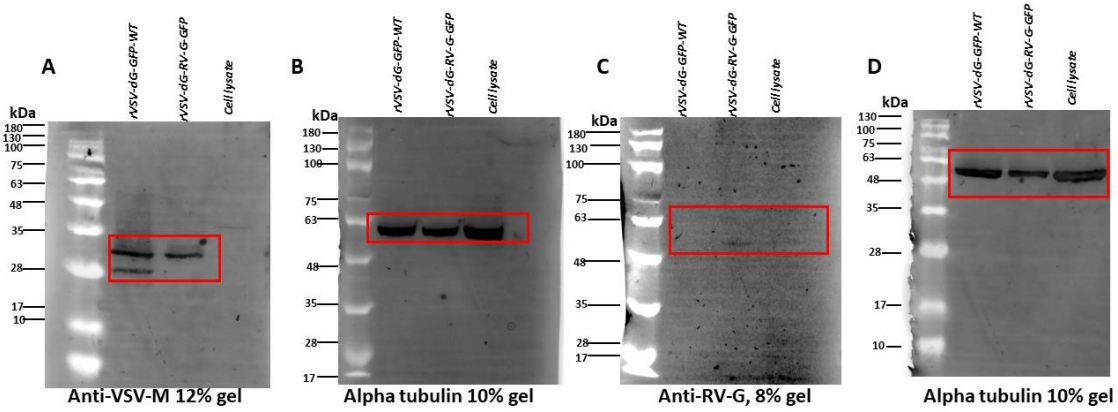

Supplementary Figure 6. *Uncropped images of blots used in* ***Chapter 4, Figure 4.5****.* ***(A)*** *Blot stained against the VSV-M antibody.* ***(B)*** *Blot stained against the alpha tubulin antibody* ***(C)*** *Blot stained against the RV-G antibody.* ***(D)*** *Blot stained against the alpha tubulin antibody. Red boxes refer to the region used for figures. Position of the molecular mass markers is shown in kDa.*

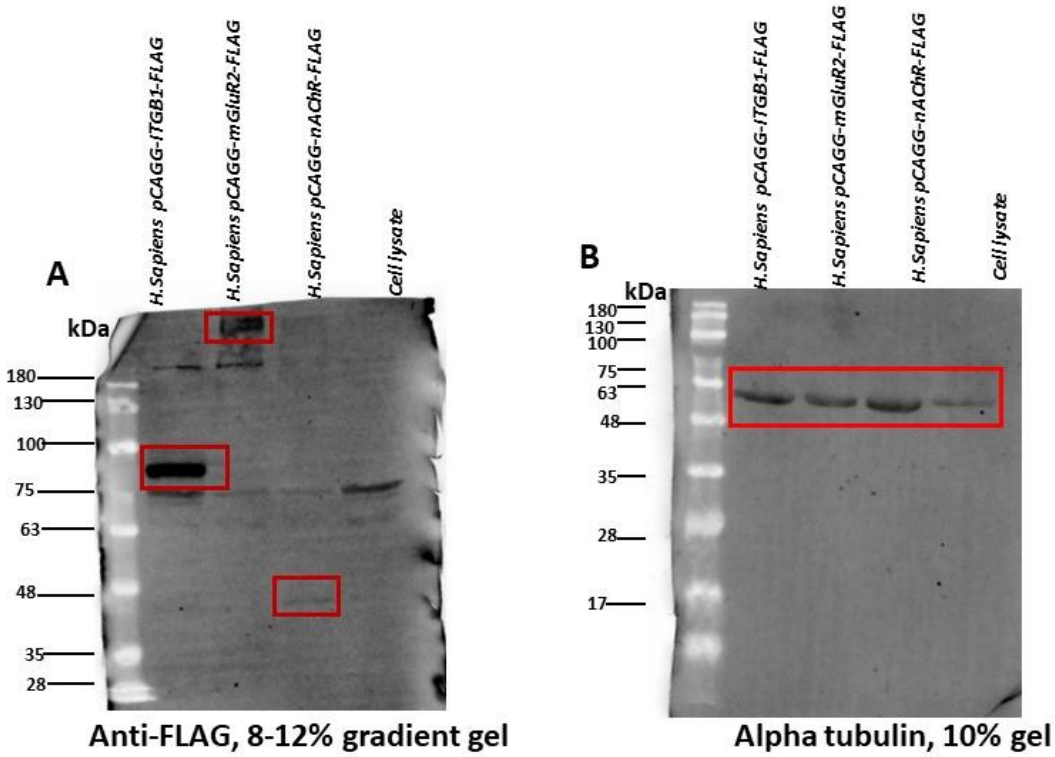

Supplementary Figure 7. *Uncropped images of blots used in* ***Chapter 6, Figure 6.5****.* ***(A)*** *Blot stained against the FLAG antibody.* ***(B)*** *Blot stained against the alpha tubulin antibody. Red boxes refer to the region used for figures. Position of the molecular mass markers is shown in kDa.*

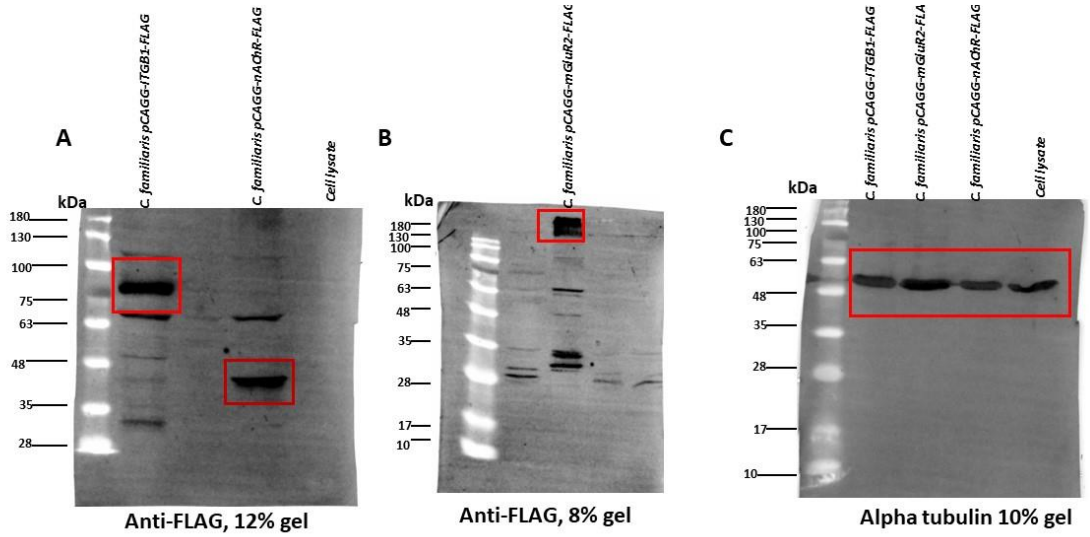

Supplementary Figure 8. *Uncropped images of blots used in* ***Chapter 6, Figure 6.10****.* ***(A-B)*** *Blots stained against the FLAG antibody.* ***(C)*** *Blot stained against the alpha tubulin antibody. Red boxes refer to the region used for figures. Position of the molecular mass markers is shown in kDa.*

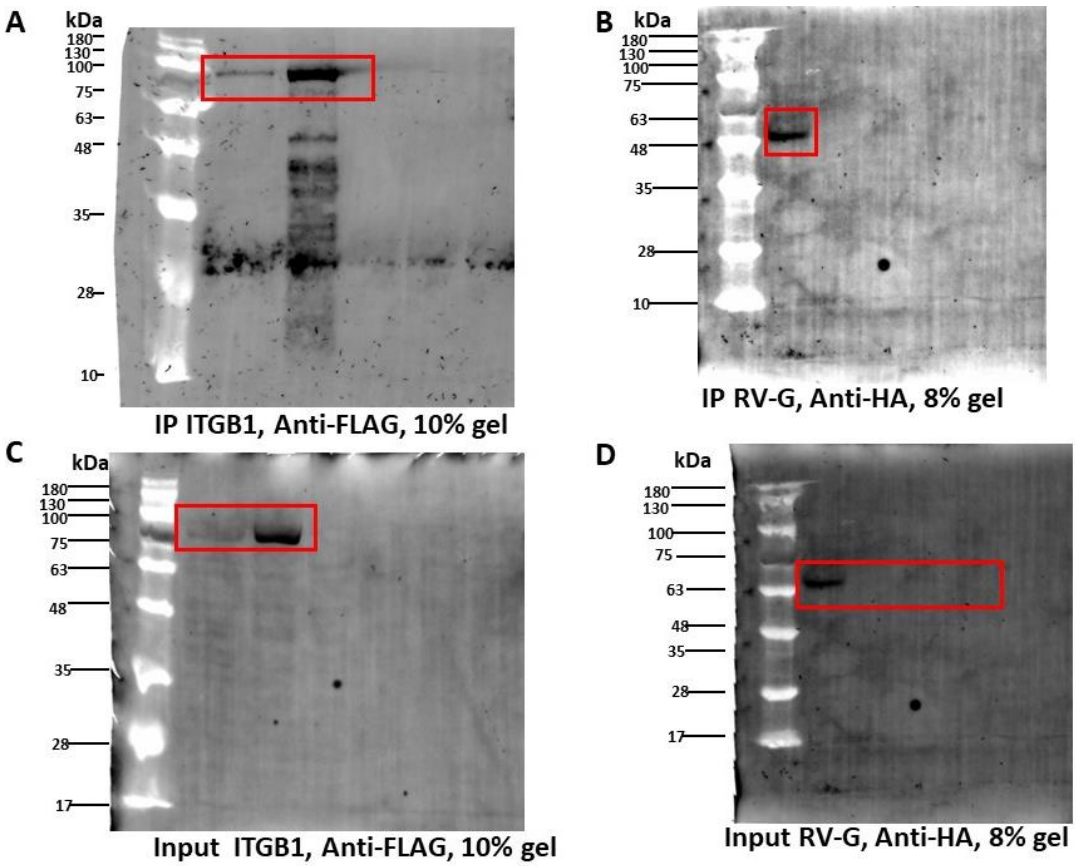

Supplementary Figure 9. *Uncropped images of blots used in* ***Chapter 7, Figure 7.1****.* ***(A, C)*** *Blots stained against the FLAG antibody.* ***(B, D)*** *Blots stained against the HA antibody. Red boxes refer to the region used for figures. Position of the molecular mass markers is shown in kDa.*

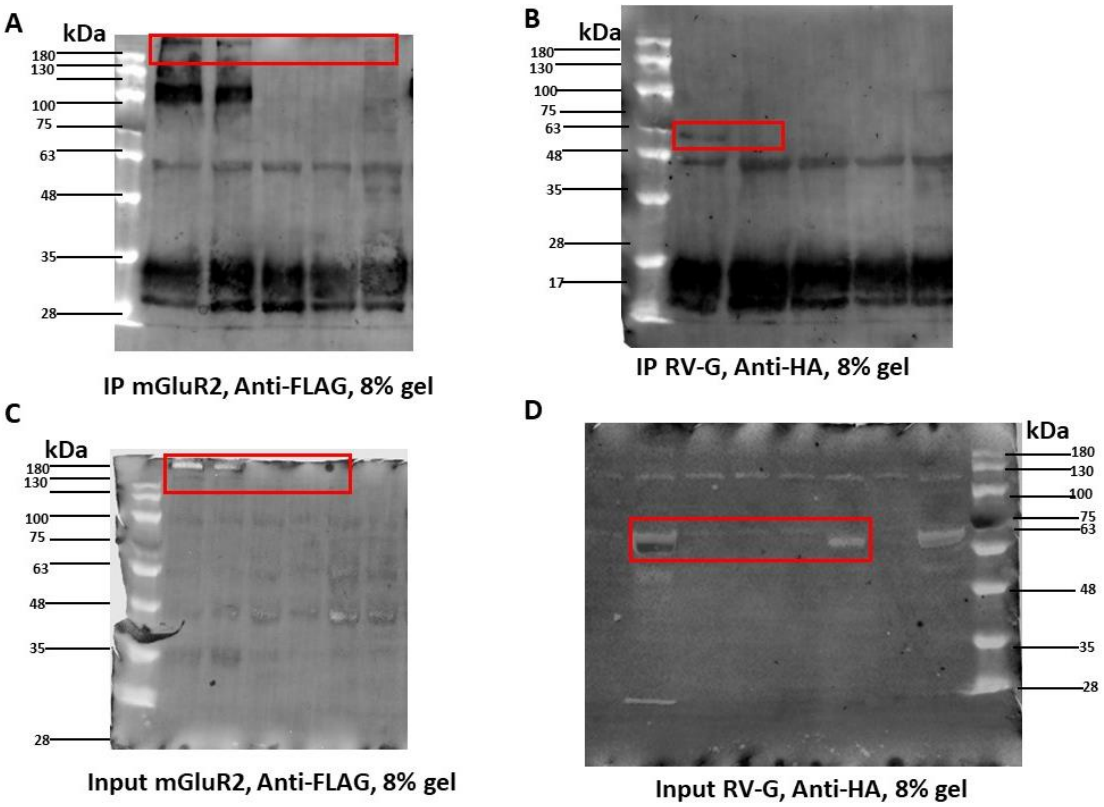

Supplementary Figure 10. *Uncropped images of blots used in* ***Chapter 7, Figure 7.2****.* ***(A, C)*** *Blots stained against the FLAG antibody.* ***(B, D)*** *Blots stained against the HA antibody. Red boxes refer to the region used for figures. Position of the molecular mass markers is shown in kDa.*

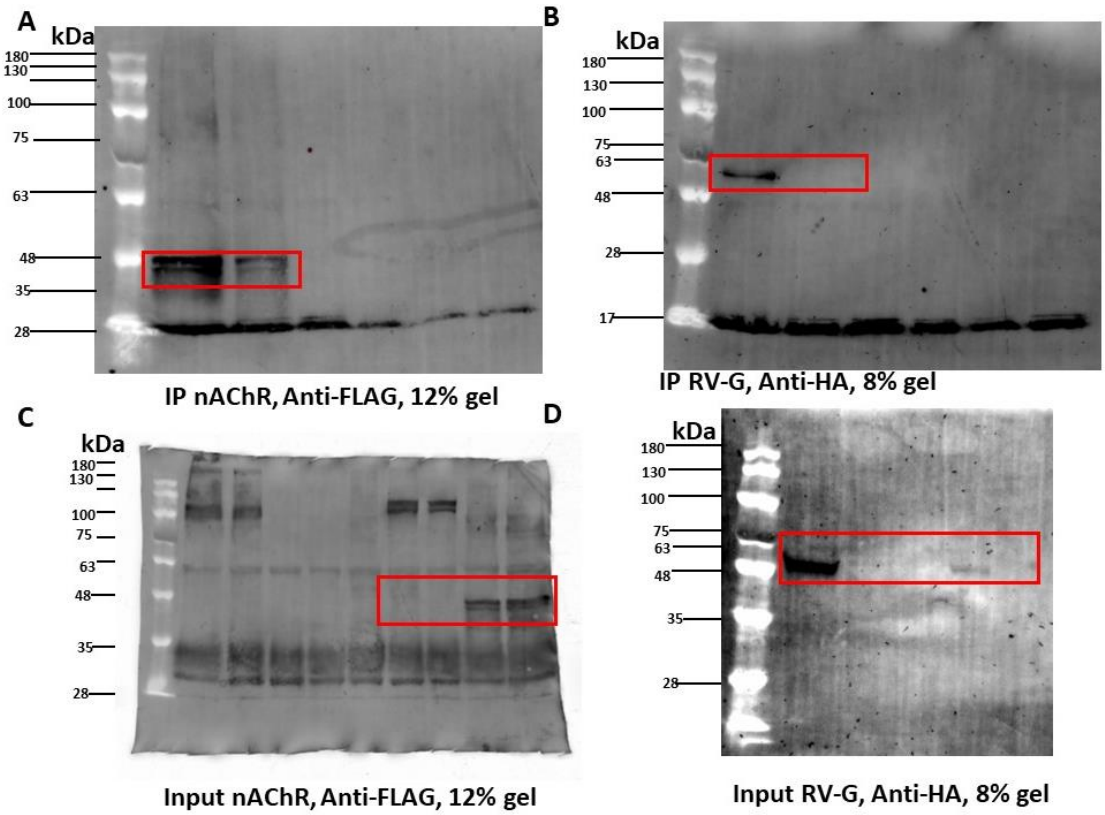

Supplementary Figure 11. *Uncropped images of blots used in* ***Chapter 7, Figure 7.3****.* ***(A, C)*** *Blots stained against the FLAG antibody.* ***(B, D)*** *Blots stained against the HA antibody. Red boxes refer to the region used for figures. Position of the molecular mass markers is shown in kDa.*

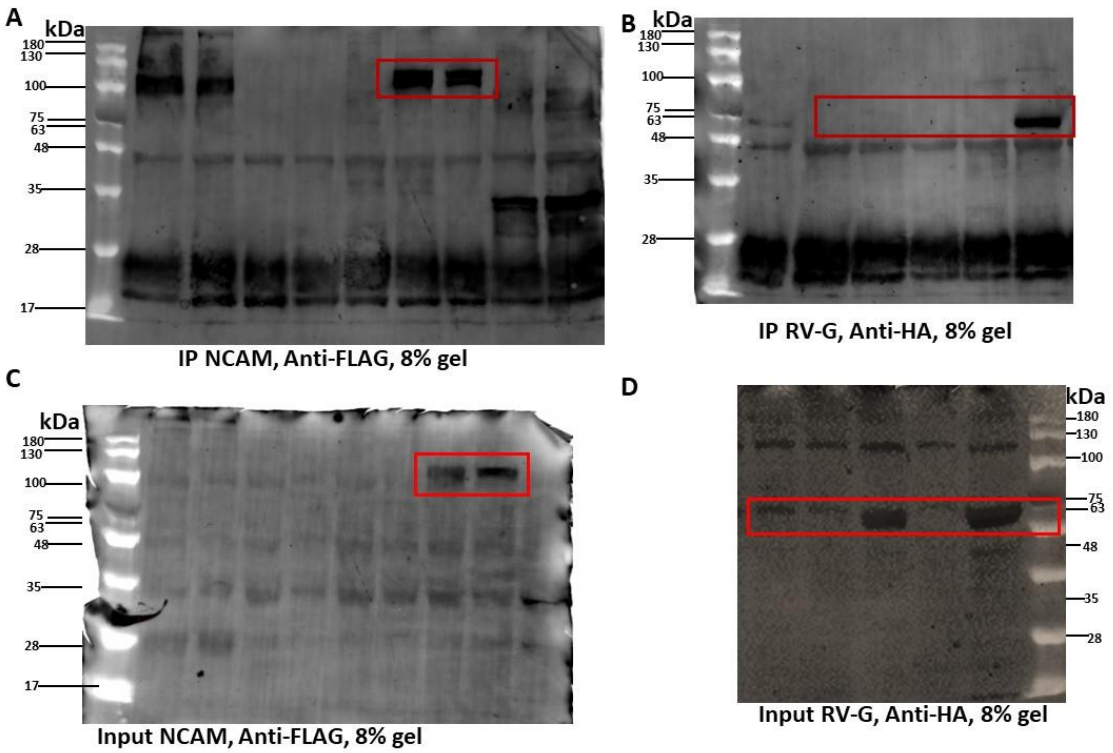

Supplementary Figure 12. *Uncropped images of blots used in* ***Chapter 7, Figure 7.4****.* ***(A, C)*** *Blots stained against the FLAG antibody.* ***(B, D)*** *Blots stained against the HA antibody. Red boxes refer to the region used for figures. Position of the molecular mass markers is shown in kDa.*

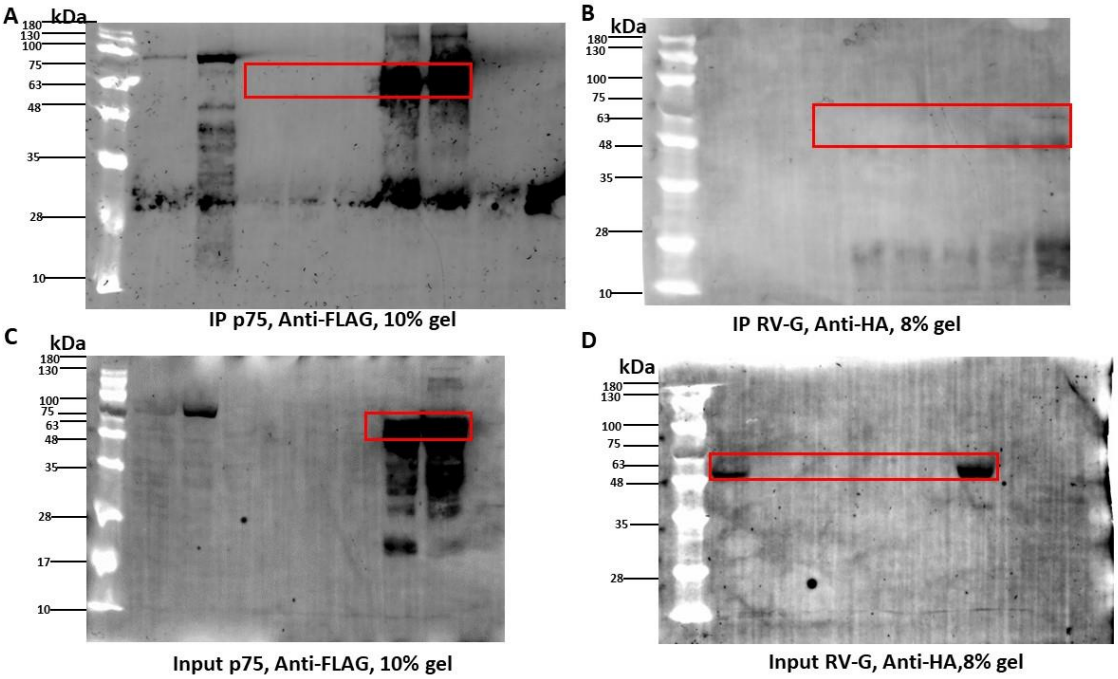

Supplementary Figure 13. *Uncropped images of blots used in* ***Chapter 7, Figure 7.5****.* ***(A, C)*** *Blots stained against the FLAG antibody.* ***(B, D)*** *Blots stained against the HA antibody. Red boxes refer to the region used for figures. Position of the molecular mass markers is shown in kDa.*

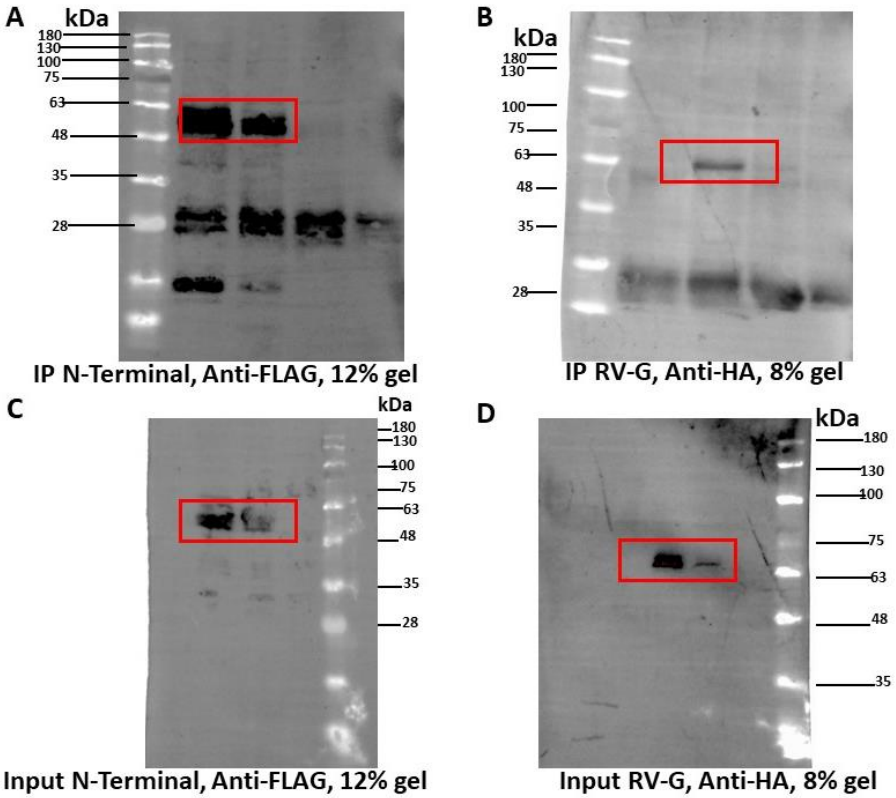

Supplementary Figure 14. *Uncropped images of blots used in* ***Chapter 7, Figure 7.7****.* ***(A, C)*** *Blots stained against the FLAG antibody.* ***(B, D)*** *Blots stained against the HA antibody. Red boxes refer to the region used for figures. Position of the molecular mass markers is shown in kDa.*

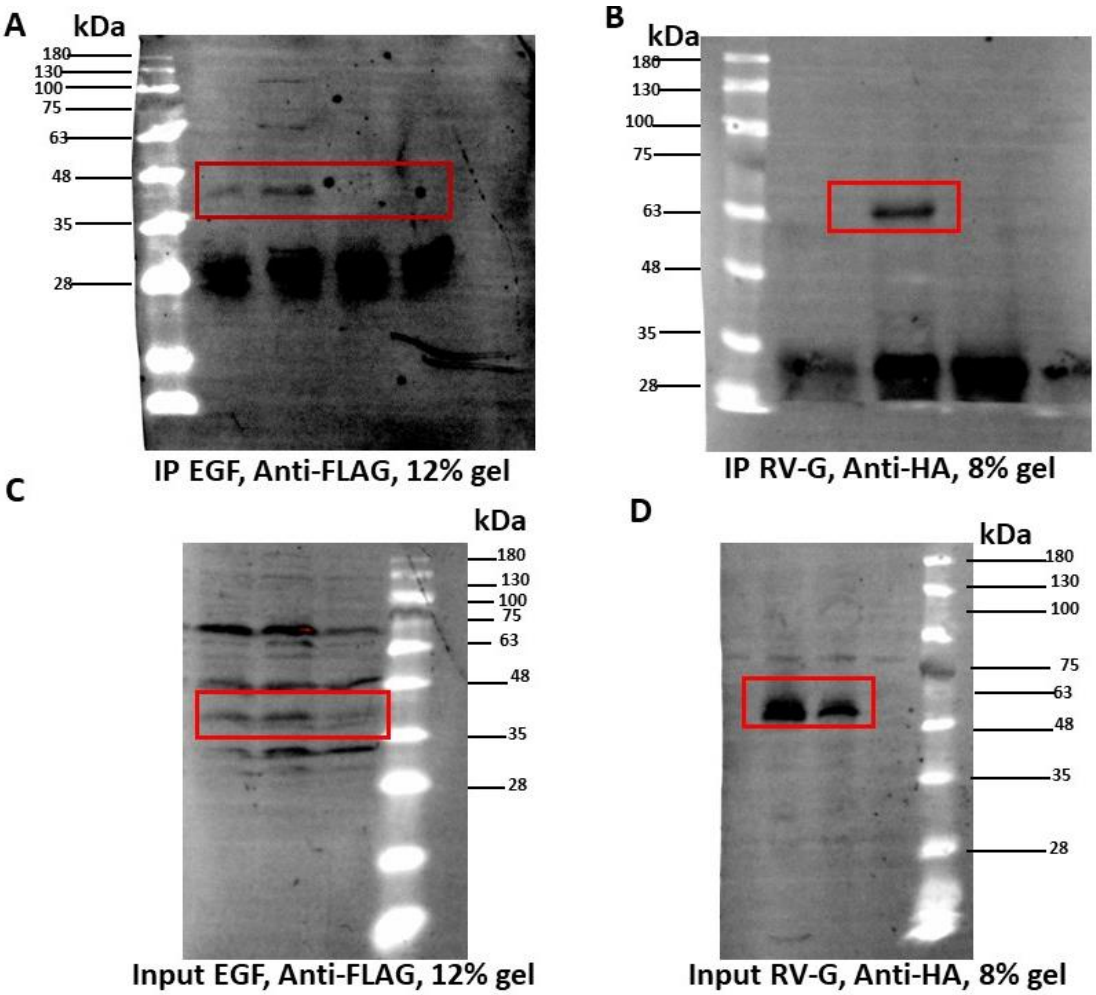

Supplementary Figure 15. *Uncropped images of blots used in* ***Chapter 7, Figure 7.8****.* ***(A, C)*** *Blots stained against the FLAG antibody.* ***(B, D)*** *Blots stained against the HA antibody. Red boxes refer to the region used for figures. Position of the molecular mass markers is shown in kDa.*

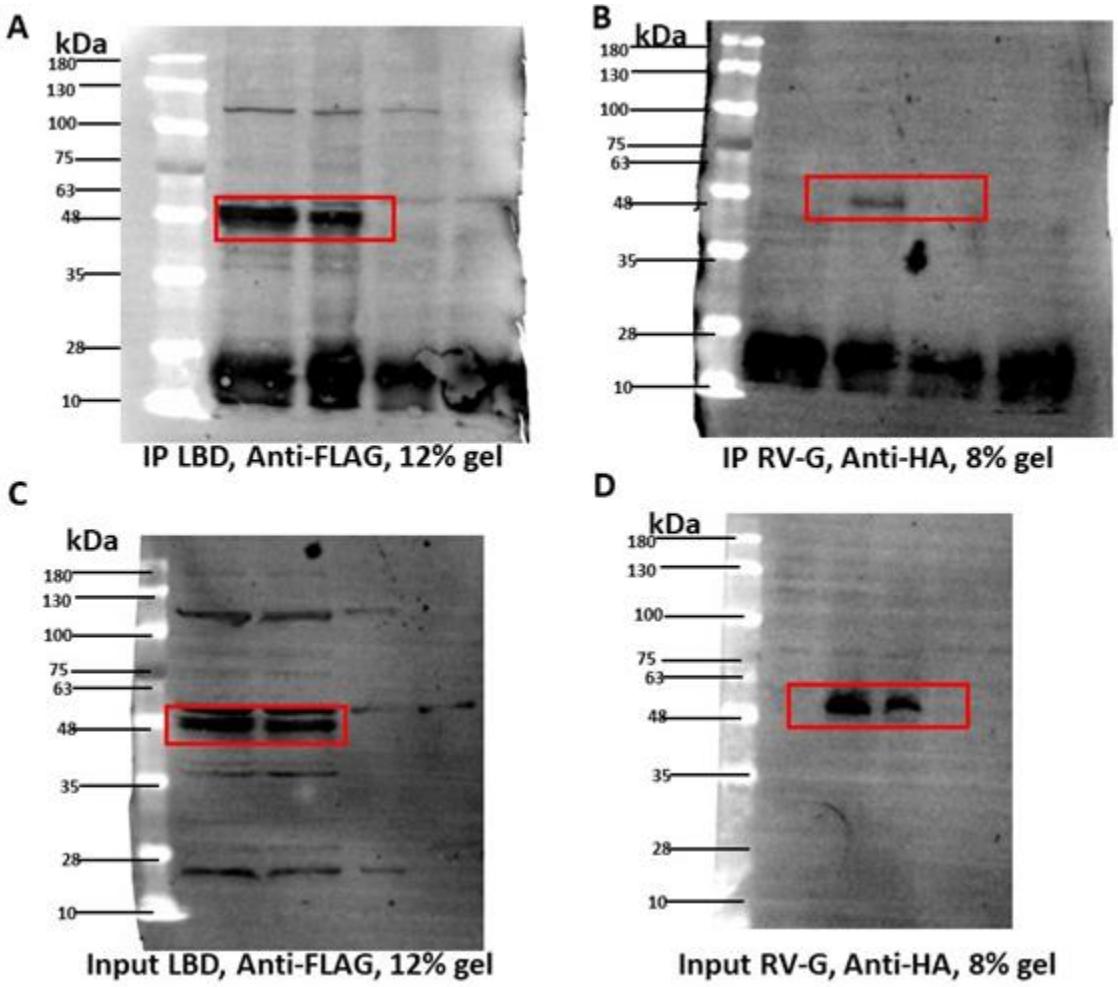

Supplementary Figure 16. *Uncropped images of blots used in* ***Chapter 7, Figure 7.10****.* ***(A, C)*** *Blots stained against the FLAG antibody.* ***(B, D)*** *Blots stained against the HA antibody. Red boxes refer to the region used for figures. Position of the molecular mass markers is shown in kDa.*

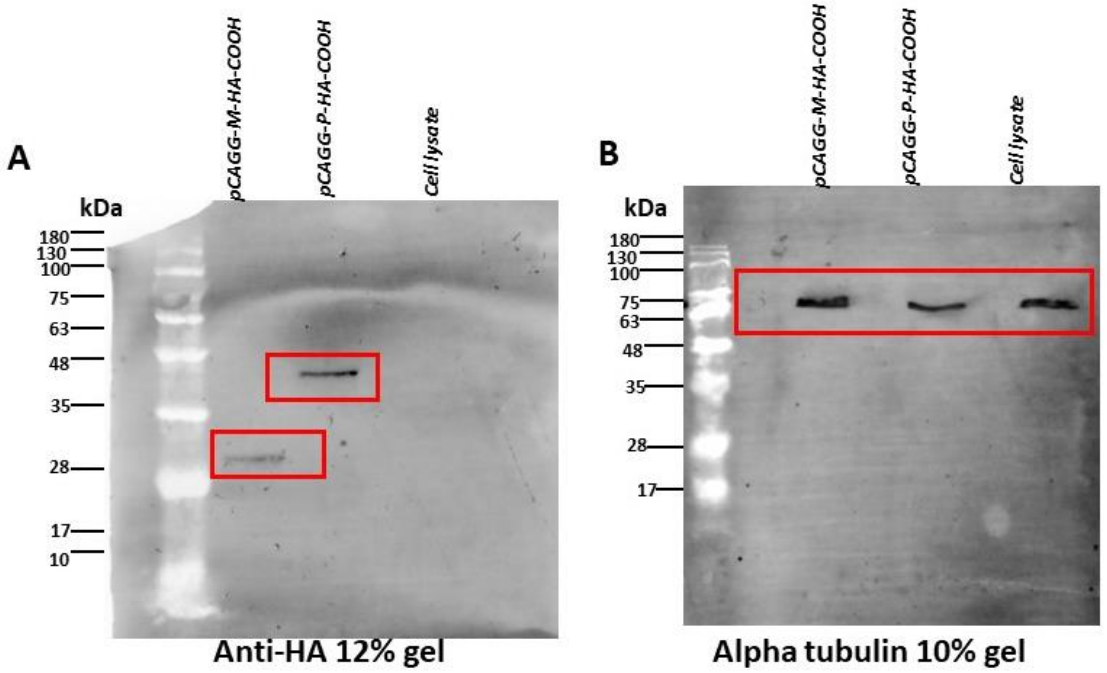

Supplementary Figure 17. *Uncropped images of blots used in* ***Chapter 7, Figure 7.13****.* ***(A)*** *Blot stained against the HA antibody.* ***(B)*** *Blot stained against the alpha tubulin antibody. Red boxes refer to the region used for figures. Position of the molecular mass markers is shown in kDa.*

9.4 Colony PCR and sequencing of the cloned sgRNAs in PX459 V2.0 vector

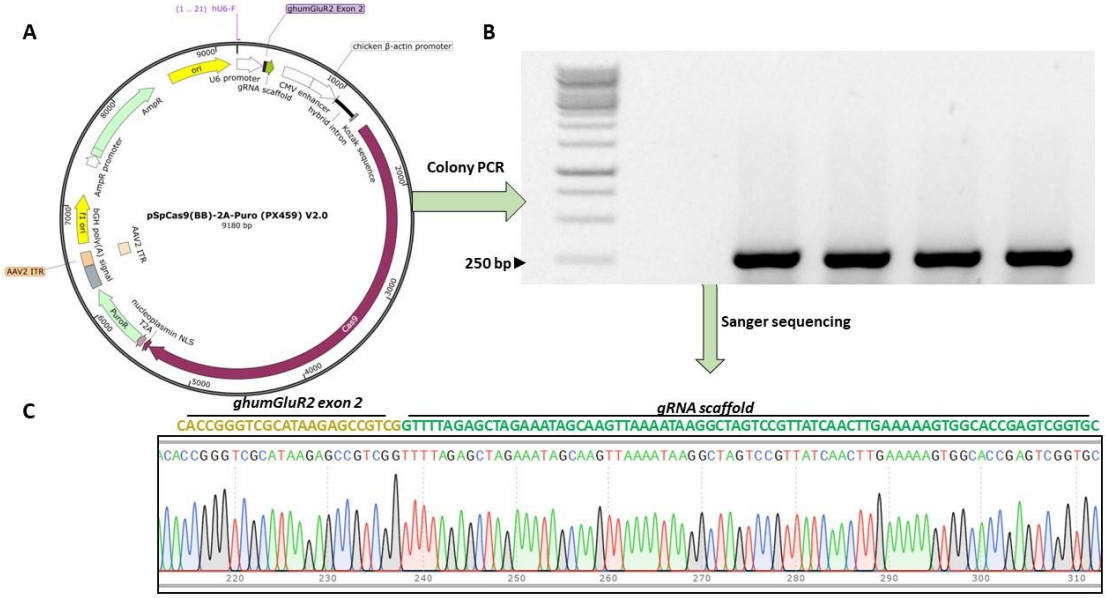

Supplementary Figure 18. *Verification of ghumGluR2 cloning in pSpCas9 PX459 V 2.0 plasmid.* ***(A)*** *Schematic diagram of the PX459 V 2.0 with the cloned humGluR2 gRNA map. (****B****) Gel electrophoresis image of colony PCR showing the successful cloning of the humGluR2 gRNA into the PX459 V 2.0 plasmid.* ***(C)*** *Sanger sequence confirmation of cloning the sgRNA humGluR2 into the PX459 V2.0 plasmid*

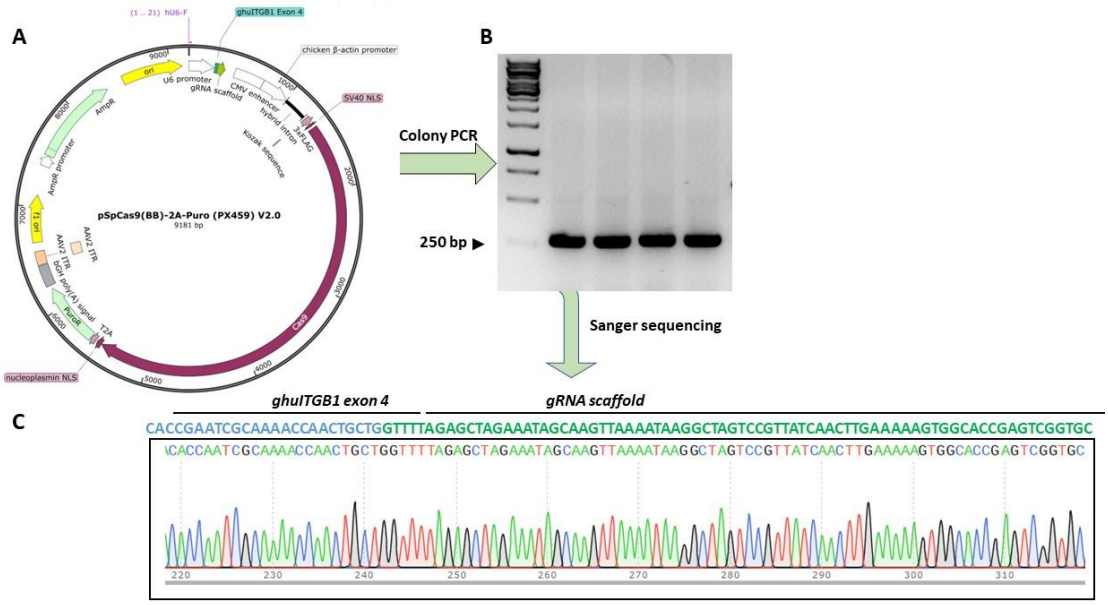

Supplementary Figure 19. *Verification of ghITGB1 cloning in pSpCas9 PX459 V 2.0 plasmid.* ***(A)*** *Schematic diagram of the PX459 V 2.0 with the cloned huITGB1 gRNA map. (****B****) Gel electrophoresis image of colony*

PCR showing the successful cloning of the huITGB1 gRNA into the PX459 V2.0 plasmid. ***(C)*** *Sanger sequence confirmation of cloning the sgRNA huITGB1 into the PX459 V 2.0 plasmid*

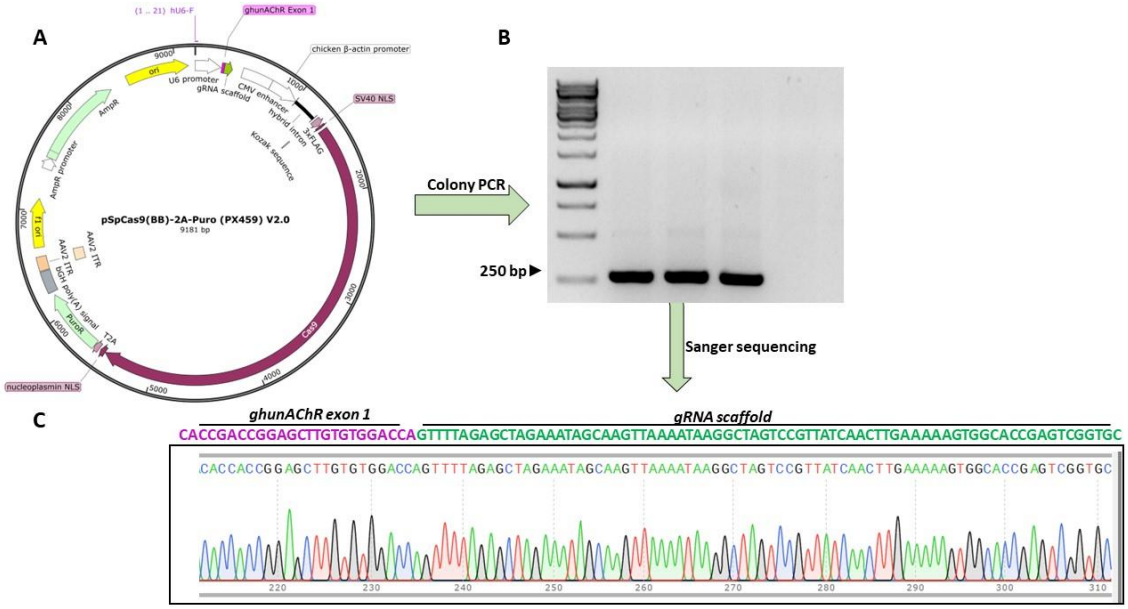

Supplementary Figure 20. *Verification of ghnAChR cloning in pSpCas9 PX459 V 2.0 plasmid.* ***(A)*** *Schematic diagram of the PX459 V 2.0 with the cloned hunAChR gRNA map. (****B****) Gel electrophoresis image of colony PCR showing the successful cloning of the hunAChR gRNA into the PX459 V2.0 plasmid.* ***(C)*** *Sanger sequence confirmation of cloning the sgRNA hunAChR into the PX459 V2.0 plasmid*

Supplementary Table 1, showing the mean fluorescence intensity (MFI) of Pa-Br cells, transfected with *P. alecto* receptors, and infected with rVSV-dG-RV-G-GFP MOI=5. This table corresponds to **Chapter 6, Figure 6.2**

Receptor	Geometric mean of fluorescence intensity
P. alecto ITGB1	634530.77
P. aalecto mGluR2	651483.53
P. alecto nAChR	883529.12
P. alecto NCAM	1075936.65
P. alecto p75	1409584.31
Empty vector	307545.62

10 References

Abdelmmageed, A. A., and Ferran, M. C. (2020). The Propagation, Quantification, and Storage of Vesicular Stomatitis (VSV). *Curr. Protoc. Cell Biol.* 58, 1–17. doi:10.1002/cpmc.110.The.

Albertini, A. A. V., Schoehn, G., Weissenhorn, W., and Ruigrok, R. W. H. (2008). Structural aspects of rabies virus replication. *Cell. Mol. Life Sci.* 65, 282–294. doi:10.1007/s00018-007-7298-1.

Almeida, R., and Duarte, C. B. (2014). p75NTR Processing and Signaling: Functional Role. *Handb. Neurotox.* 1–3, 1–2371. doi:10.1007/978-1-4614-5836-4.

Anderson, L. J., Nicholson, K. G., Tauxe, R. V., and Winkler, W. G. (1984). Human rabies in the United States, 1960 to 1979: Epidemiology, diagnosis, and prevention. *Ann. Intern. Med.* 100, 728–735. doi:10.7326/0003-4819-100-5-728.

Astorga, F., Escobar, L. E., Poo-Muñoz, D. A., and Medina-Vogel, G. (2015). Dog ownership, abundance and potential for bat-borne rabies spillover in Chile. *Prev. Vet. Med.* 118, 397–405. doi:10.1016/j.prevetmed.2015.01.002.

Athingo, R., Tenzin, T., Shilongo, A., Hikufe, E., Shoombe, K. K., Khaiseb, S., et al. (2020). Fighting dog-mediated rabies in Namibia—implementation of a rabies elimination program in the northern communal areas. *Trop. Med. Infect. Dis.* 5. doi:10.3390/tropicalmed5010012.

Banerjee, A., Baker, M. L., Kulcsar, K., Misra, V., Plowright, R., and Mossman, K. (2020). Novel Insights Into Immune Systems of Bats. *Front. Immunol.* 11, 1–15. doi:10.3389/fimmu.2020.00026.

Banyard, A. C., and Fooks, A. R. (2020). Rabies and Other Lyssaviruses (Rhabdoviridae). *Encycl. Virol. Vol. 1-5, Fourth Ed.* 1–5, 738–746. doi:10.1016/B978-0-12-809633-8.20936-9.

Banyard, A. C., Hayman, D. T. S., Freuling, C. M., Müller, T., Fooks, A. R., and Johnson, N. (2013). *Bat rabies*. doi:10.1016/B978-0-12-396547-9.00006-7.

Barker, P. A. (1998). p75 NTR : A study in contrasts. *Cell Death Differ.* 5, 346–356.

Barrass, S. V, and Butcher, S. J. (2020). Advances in high - throughput methods for the identification of virus receptors. *Med. Microbiol. Immunol.* 209, 309–323.

doi:10.1007/s00430-019-00653-2.

Battle, G. M. (2016). PDBePISA : Identifying and interpreting the likely biological assemblies of a protein structure. 1–12. Available at: https://www.semanticscholar.org/paper/PDBePISA-%3A-Identifying-and-interpreting-the-likely-Battle/2154b7c24212f0c21793a008a7255d328d6d4b23.

Begeman, L., GeurtsvanKessel, C., Finke, S., Freuling, C. M., Koopmans, M., Müller, T., et al. (2018). Comparative pathogenesis of rabies in bats and carnivores, and implications for spillover to humans. *Lancet Infect. Dis.* 18, e147–e159. doi:10.1016/S1473-3099(17)30574-1.

Beier, K. T., Saunders, A. B., Oldenburg, I. A., Sabatini, B. L., Cepko, C. L., Smith, J. C., et al. (2013). Vesicular stomatitis virus with the rabies virus glycoprotein directs retrograde transsynaptic transport among neurons *in vivo*. *Front. Neural Circuits* 7, 1–13. doi:10.3389/fncir.2013.00011.

Blackburn, D., Minhaj, F. S., Hammoud, R. Al, Orciari, L., Miller, J., Maness, T., et al. (2022). Human Rabies — Texas , 2021. *Morb. Mortal. Wkly. Rep.* 71, 2021–2023.

Blanco, E. (2013). Structure and Physics of Viruses. 68, 631–665. doi:10.1007/978-94-007-6552-8.

Bonifacino, J. S., Gershlick, D. C., and Dell'Angelica, E. C. (2016). Immunoprecipitation. *Curr. Protoc. Cell Biol.* 71, 7.2.1-7.2.24. doi:10.1002/cpcb.3.

Borucki, M. K., Chen-Harris, H., Lao, V., Vanier, G., Wadford, D. A., Messenger, S., et al. (2013). Ultra-Deep Sequencing of Intra-host Rabies Virus Populations during Cross-species Transmission. *PLoS Negl. Trop. Dis.* 7. doi:10.1371/journal.pntd.0002555.

Both, L., Banyard, A. C., van Dolleweerd, C., Horton, D. L., Ma, J. K. C., and Fooks, A. R. (2012). Passive immunity in the prevention of rabies. *Lancet Infect. Dis.* 12, 397–407. doi:10.1016/S1473-3099(11)70340-1.

Boulant, S., Stanifer, M., and Lozach, P. Y. (2015). Dynamics of virus-receptor interactions in virus binding, signaling, and endocytosis. *Viruses* 7, 2794–2815.

doi:10.3390/v7062747.

Brinkman, E. K., Chen, T., Amendola, M., and Steensel, B. Van (2014). Easy quantitative assessment of genome editing by sequence trace decomposition. *Nucleic Acids Res.* 1, 1–8. doi:10.1093/nar/gku936.

Bupp, K., Sarangi, A., and Roth, M. J. (2005). Probing Sequence Variation in the Receptor-Targeting Domain of Feline Leukemia Virus Envelope Proteins with Peptide Display Libraries. *J. Virol.* 79, 1463–1469. doi:10.1128/jvi.79.3.1463-1469.2005.

Burland (2000). Sequence Analysis Using DNASTAR ' s Lasergene Software Suite. *Methods Mol. Biol.* 132, 71–91. doi:doi: 10.1385/1-59259-192-2:71.

Cai, M., Liu, H., Jiang, F., Sun, Y., Wang, W., An, Y., et al. (2022). Analysis of the evolution, infectivity and antigenicity of circulating rabies virus strains. *Emerg. Microbes Infect.* 11, 1474–1487. doi:10.1080/22221751.2022.2078742.

Callaway, H. M., Zyla, D., Larrous, F., de Melo, G. D., Hastie, K. M., Avalos, R. D., et al. (2022). Structure of the rabies virus glycoprotein trimer bound to a prefusion-specific neutralizing antibody. *Sci. Adv.* 8, 1–13. doi:10.1126/sciadv.abp9151.

Chauhan, R. P., and Gordon, M. L. (2021). Deciphering transmission dynamics and spillover of avian influenza viruses from avian species to swine populations globally. *Virus Genes* 57, 541–555. doi:10.1007/s11262-021-01873-6.

Cho, M., and Seok, H. (2020). Prediction of cross-species infection propensities of viruses with receptor similarity. *Infect. Evol.*

Clausen, T. M., Sandoval, D. R., Spliid, C. B., Pihl, J., Perrett, H. R., Painter, C. D., et al. (2020). SARS-CoV-2 Infection Depends on Cellular Heparan Sulfate and ACE2. *Cell* 183, 1043-1057.e15. doi:10.1016/j.cell.2020.09.033.

Coffin, J. M. (2013). Virions at the Gates: Receptors and the Host-Virus Arms Race. *PLoS Biol.* 11. doi:10.1371/journal.pbio.1001574.

Conceicao, C., Thakur, N., Human, S., Kelly, J. T., Logan, L., Bialy, D., et al. (2020). The SARS-CoV-2 Spike protein has a broad tropism for mammalian ACE2 proteins.

PLoS Biol. 18, 1–27. doi:10.1371/journal.pbio.3001016.

Cragnolini, A. B., and Friedman, W. J. (2008). The function of p75NTR in glia. *Trends Neurosci.* 31, 99–104. doi:10.1016/j.tins.2007.11.005.

Crameri, G., Todd, S., Grimley, S., McEachern, J. A., Marsh, G. A., Smith, C., et al. (2009). Establishment, immortalisation and characterisation of pteropid bat cell lines. *PLoS One* 4. doi:10.1371/journal.pone.0008266.

Cremer, H., Lange, R., Christoph, A., Plomann, M., Vopper, G., Roes, J., et al. (1994). Inactivation of the N-CAM gene in mice results in size reduction of the olfactory bulb and deficits in spatial learning. *Nature* 367, 455–459. doi:10.1038/367455a0.

Cureton, D. K., Massol, R. H., Saffarian, S., Kirchhausen, T. L., and Whelan, S. P. J. (2009). Vesicular Stomatitis Virus Enters Cells through Vesicles Incompletely Coated with Clathrin That Depend upon Actin for Internalization. *PLoS Pathog.* 5. doi:10.1371/journal.ppat.1000394.

DeLano (2002). Pymol: An open-source molecular graphics tool. *{CCP4} Newsl. Protein Crystallogr.* 40, 1–8. Available at: http://www.ccp4.ac.uk/newsletters/newsletter40/11_pymol.pdf.

Ding, N. Z., Xu, D. S., Sun, Y. Y., He, H. Bin, and He, C. Q. (2017). A permanent host shift of rabies virus from Chiroptera to Carnivora associated with recombination. *Sci. Rep.* 7, 1–9. doi:10.1038/s41598-017-00395-2.

Dlugolenski, D., Jones, L., Tompkins, S. M., Crameri, G., Wang, L. F., and Tripp, R. A. (2013). Bat cells from Pteropus alecto are susceptible to influenza A virus infection and reassortment. *Influenza Other Respi. Viruses* 7, 900–903. doi:10.1111/irv.12128.

Doudna, J. A., and Charpentier, E. (2014). The new frontier of genome engineering with CRISPR-Cas9. *Science (80-.).* 346. doi:10.1126/science.1258096.

Edson X. Albuquerque, Edna F. R. Pereira, Manickavasagom Alkondon, and S. W. R. (2009). Mammalian Nicotinic Acetylcholine Receptors: From Structure to Function. *Physiol. Rev.* 89, 73–120.

doi:10.1152/physrev.00015.2008.Mammalian.

Escobar, L. E., Villa, A. V., Satheshkumar, P. S., Nakazawa, Y., and Vuurst, P. Van De (2023). Revealing the complexity of vampire bat rabies " spillover transmission ." *Infect. Dis. Poverty* 12, 1–9. doi:10.1186/s40249-023-01062-7.

Fan, L., Zhang, L., Li, J., and Zhu, F. (2022). Advances in the progress of monoclonal antibodies for rabies. *Hum. Vaccines Immunother.* 18. doi:10.1080/21645515.2022.2026713.

Feige, L., Kozaki, T., Melo, G. D. De, and Guillemot, V. (2021a). Cell-type specific innate immune responses shape rabies virus.

Feige, L., Kozaki, T., Melo, G. D. de, Guillemot, V., Larrous, F., Ginhoux, F., et al. (2021b). Cell-type specific innate immune responses shape rabies virus tropism. *bioRxiv*, 2021.07.26.453802. Available at: https://www.biorxiv.org/content/10.1101/2021.07.26.453802v1%0Ahttps://www.biorxiv.org/content/10.1101/2021.07.26.453802v1.abstract.

Feng, T., Zhang, J., Chen, Z., Pan, W., Chen, Z., Yan, Y., et al. (2022). Glycosylation of viral proteins: Implication in virus–host interaction and virulence. *Virulence* 13, 670–683. doi:10.1080/21505594.2022.2060464.

Feng, Y., Ma, J., Sun, S., Chi, L., Kou, Z., and Tu, C. (2021). Epidemiology of Animal Rabies — China, 2010–2020. *China CDC Wkly.* 3, 815–818. doi:10.46234/ccdcw2021.202.

Finke, S., and Conzelmann, K. K. (2005). Replication strategies of rabies virus. *Virus Res.* 111, 120–131. doi:10.1016/j.virusres.2005.04.004.

Finn, R. D., Coggill, P., Eberhardt, R. Y., Eddy, S. R., Mistry, J., Mitchell, A. L., et al. (2016). The Pfam protein families database: Towards a more sustainable future. *Nucleic Acids Res.* 44, D279–D285. doi:10.1093/nar/gkv1344.

Fisher, C. R., Streicker, D. G., and Schnell, M. J. (2018). The spread and evolution of rabies virus : conquering new frontiers. *Nat. Rev. Microbiol.* 16, 241–255. doi:10.1038/nrmicro.2018.11.

Fisher, C. R., Streicker, D. G., Schnell, M. J., and Health, A. (2019). The spread and

evolution of rabies virus: conquering new frontiers. *Nat Rev Microbiol* 16, 241–255. doi:10.1038/nrmicro.2018.11.The.

Fooks, A. R., Cliquet, F., Finke, S., Freuling, C., Hemachudha, T., Mani, R. S., et al. (2017). Rabies. *Nat. Rev. Dis. Prim.* 3. doi:10.1038/nrdp.2017.91.

Fooks, A. R., Shipley, R., Markotter, W., Tordo, N., Freuling, C. M., Müller, T., et al. (2021). Renewed public health threat from emerging lyssaviruses. *Viruses* 13, 1–10. doi:10.3390/v13091769.

Gao, Y., Zhang, Y., Shinya, K., Deng, G., Jiang, Y., Li, Z., et al. (2009). Identification of amino acids in HA and PB2 critical for the transmission of H5N1 avian influenza viruses in a mammalian host. *PLoS Pathog.* 5, 1–11. doi:10.1371/journal.ppat.1000709.

Garbutt, M., Liebscher, R., Wahl-Jensen, V., Jones, S., Möller, P., Wagner, R., et al. (2004). Properties of Replication-Competent Vesicular Stomatitis Virus Vectors Expressing Glycoproteins of Filoviruses and Arenaviruses. *J. Virol.* 78, 5458–5465. doi:10.1128/jvi.78.10.5458-5465.2004.

Gaudin, Y., Moreira, S., Bénéjean, J., Blondel, D., Flamand, A., and Tuffereau, C. (1999). Soluble ectodomain of rabies virus glycoprotein expressed in eukaryotic cells folds in a monomeric conformation that is antigenically distinct from the native state of the complete, membrane-anchored glycoprotein. *J. Gen. Virol.* 80, 1647–1656. doi:10.1099/0022-1317-80-7-1647.

Giuliano, C. J., Lin, A., Girish, V., and Sheltzer, J. M. (2019a). Generating Single Cell–Derived Knockout Clones in Mammalian Cells with CRISPR/Cas9. *Curr. Protoc. Mol. Biol.* 128, 1–25. doi:10.1002/cpmb.100.

Giuliano, C. J., Lin, A., Girish, V., and Sheltzer, J. M. (2019b). Generating Single Cell – Derived Knockout Clones in Mammalian Cells with CRISPR / Cas9. 1–25. doi:10.1002/cpmb.100.

Gluska, S., Zahavi, E. E., Chein, M., Gradus, T., Bauer, A., Finke, S., et al. (2014). Rabies Virus Hijacks and Accelerates the p75NTR Retrograde Axonal Transport Machinery. *PLoS Pathog.* 10. doi:10.1371/journal.ppat.1004348.

Gould, A. R., Hyatt, A. D., Lunt, R., Kattenbelt, J. A., Hengstberger, S., and Blacksell, S. D. (1998). Characterisation of a novel lyssavirus isolated from Pteropid bats in Australia. *Virus Res.* 54, 165–187. doi:10.1016/S0168-1702(98)00025-2.

Grange, Z. L., Goldstein, T., Johnson, C. K., Anthony, S., Gilardi, K., Daszak, P., et al. (2021). Ranking the risk of animal-to-human spillover for newly discovered viruses. *Proc. Natl. Acad. Sci. U. S. A.* 118, 1–8. doi:10.1073/pnas.2002324118.

Grove, J., and Marsh, M. (2011). The cell biology of receptor-mediated virus entry. *J. Cell Biol.* 195, 1071–1082. doi:10.1083/jcb.201108131.

Guo, Y., Duan, M., Wang, X., Gao, J., Guan, Z., and Zhang, M. (2019). Early events in rabies virus infection—Attachment, entry, and intracellular trafficking. *Virus Res.* 263, 217–225. doi:10.1016/j.virusres.2019.02.006.

Guth, S., Visher, E., Boots, M., and Brook, C. E. (2019). Host phylogenetic distance drives trends in virus virulence and transmissibility across the animal-human interface. *Philos. Trans. R. Soc. B* 374. doi:10.1098/rstb.2019.0296.

Hampson, K., Coudeville, L., Lembo, T., Sambo, M., Kieffer, A., Attlan, M., et al. (2015). Estimating the Global Burden of Endemic Canine Rabies. *PLoS Negl. Trop. Dis.* 9, 1–20. doi:10.1371/journal.pntd.0003709.

Hanke, L., Schmidt, F. I., Knockenhauer, K. E., Morin, B., Whelan, S. P., Schwartz, T. U., et al. (2017). Vesicular stomatitis virus N protein-specific single-domain antibody fragments inhibit replication. *EMBO Rep.* 18, 1027–1037. doi:10.15252/embr.201643764.

Hastie, E., Cataldi, M., Marriott, I., and Grdzelishvili, V. Z. (2013). Understanding and altering cell tropism of vesicular stomatitis virus. *Virus Res.* 176, 16–32. doi:10.1016/j.virusres.2013.06.003.

Hayes, M. A., and Piaggio, A. J. (2018). Assessing the potential impacts of a changing climate on the distribution of a rabies virus vector. *PLoS One* 13, 1–17. doi:10.1371/journal.pone.0192887.

Hoffman, G. M., Ghanayem, N. S., Amlie-lefond, C. M., Schwabe, M. J., Chusid, M. J., Rupprecht, C. E., et al. (2005). Survival after Treatment of Rabies with Induction

of Coma. *N. Engl. J. Med.* 352, 2508–2514.

Holmes, E. C., Woelk, C. H., Kassis, R., and Bourhy, H. (2002). Genetic constraints and the adaptive evolution of rabies virus in nature. *Virology* 292, 247–257. doi:10.1006/viro.2001.1271.

Honigschmid, P., Bykova, N., Schneider, R., Ivankov, D., and Frishman, D. (2018). Evolutionary Interplay between Symbiotic Relationships and Patterns of Signal Peptide Gain and Loss. *Genome Biol. Evol.* 10, 928–938. doi:10.1093/gbe/evy049.

Horstkorte, R., Büttner, B., and Bork, K. (2012). *NCAM1*. doi:10.1007/978-1-4419-0461-4.

Hotta, K., Motoi, Y., Okutani, A., Kaku, Y., and Noguchi, A. (2006). Role of GPI-anchored NCAM-120 in rabies virus infection. *Microbes Infect.* 9, 167–174. doi:10.1016/j.micinf.2006.11.003.

Hu, R., Tang, Q., Tang, J., and Fooks, A. R. (2009). Rabies in China: An update. *Vector-Borne Zoonotic Dis.* 9, 1–11. doi:10.1089/vbz.2008.0046.

Hueffer K, Khatri S, Rideout S (2017). Rabies virus modifies host behaviour through a snake-toxin like region of its glycoprotein that inhibits neurotransmitter receptors in the CNS. *Sci. Rep.* 7, 1–8. doi:10.1038/s41598-017-12726-4.

Id, M. H., and Id, D. F. (2022). PLOS COMPUTATIONAL BIOLOGY Superinfection exclusion : A viral strategy with short-term benefits and long-term drawbacks. 1–18. doi:10.1371/journal.pcbi.1010125.

Jackson, A. C. (2013). "History of Rabies Research," in *Rabies*, 1–15. doi:10.1016/B978-0-12-396547-9.00001-8.

Jochmans, D., and Neyts, J. (2019). The path towards effective antivirals against rabies. *Vaccine* 37, 4660–4662. doi:10.1016/j.vaccine.2017.12.051.

Johnson, C. K., Hitchens, P. L., Pandit, P. S., Rushmore, J., Evans, T. S., Young, C. C. W., et al. (2020). Global shifts in mammalian population trends reveal key predictors of virus spillover risk. *Proc. R. Soc. B Biol. Sci.* 287. doi:10.1098/rspb.2019.2736.

Johnson, N., Vos, A., Freuling, C., Tordo, N., Fooks, A. R., and Müller, T. (2010). Human rabies due to lyssavirus infection of bat origin. *Vet. Microbiol.* 142, 151–159. doi:10.1016/j.vetmic.2010.02.001.

Jolly, C. L., and Sattentau, Q. J. (2013). Attachment factors. *Adv. Exp. Med. Biol.* 790, 1–23. doi:10.1007/978-1-4614-7651-1_1.

Kapadia, S. U., Simon, I. D., and Rose, J. K. (2008). SARS vaccine based on a replication-defective recombinant vesicular stomatitis virus is more potent than one based on a replication-competent vector. *Virol. J.* 376, 165–172. doi:10.1016/j.virol.2008.03.002.

Kapp, T. G., Rechenmacher, F., Neubauer, S., Maltsev, O. V., Cavalcanti-Adam, E. A., Zarka, R., et al. (2017). A comprehensive evaluation of the activity and selectivity profile of ligands for RGD-binding integrins. *Sci. Rep.* 7, 1–13. doi:10.1038/srep39805.

Karlin, A. (2002). EMERGING STRUCTURE OF THE RECEPTORS. *Nat. Rev. Neurosci.* 3, 102–114. doi:10.1038/nrn731.

Kgaladi, J., Nel, L. H., and Markotter, W. (2013). Comparison of pathogenic domains of rabies and African rabies-related lyssaviruses and pathogenicity observed in mice. *Onderstepoort J. Vet. Res.* 80, 1–13. doi:10.4102/ojvr.v80i1.511.

Khalifa, Y. Ben, Luco, S., Besson, B., Sonthonnax, F., Archambaud, M., Grimes, J. M., et al. (2016). The matrix protein of rabies virus binds to RelAp43 to modulate NF- κ B-dependent gene expression related to innate immunity. *Nat. Publ. Gr.*, 1–13. doi:10.1038/srep39420.

Khalifa, M. E., Unterholzner, L., and Munir, M. (2021). Structural and Evolutionary Insights Into the Binding of Host Receptors by the Rabies Virus Glycoprotein. *Front. Cell. Infect. Microbiol.* 11, 1–13. doi:10.3389/fcimb.2021.736114.

Kim, P., Jang, Y. H., Kwon, S. Bin, Lee, C. M., Han, G., and Seong, B. L. (2018). Glycosylation of hemagglutinin and neuraminidase of influenza a virus as signature for ecological spillover and adaptation among influenza reservoirs. *Viruses* 10, 1–18. doi:10.3390/v10040183.

Kumlin, U., Olofsson, S., and Dimock, K. (2008). Sialic acid tissue distribution and influenza virus tropism. 147–154. doi:10.1111/j.1750-2659.2008.00051.x.

Kuzmin, I. V., Shi, M., Orciari, L. A., Yager, P. A., Velasco-Villa, A., Kuzmina, N. A., et al. (2012). Molecular inferences suggest multiple host shifts of rabies viruses from bats to mesocarnivores in Arizona during 2001-2009. *PLoS Pathog.* 8. doi:10.1371/journal.ppat.1002786.

Lafon, M. (2005). Rabies virus receptors. *J. Neurovirol.* 11, 82–87. doi:10.1080/13550280590900427.

Landi, A., Iannucci, V., Van Nuffel, A., Meuwissen, P., and Verhasselt, B. (2011). One Protein to Rule them All: Modulation of Cell Surface Receptors and Molecules by HIV Nef. *Curr. HIV Res.* 9, 496–504. doi:10.2174/157016211798842116.

Langevin, C., Jaaro, H., Bressanelli, S., Fainzilber, M., and Tuffereau, C. (2002). Rabies virus glycoprotein (RVG) is a trimeric ligand for the N-terminal cysteine-rich domain of the mammalian p75 neurotrophin receptor. *J. Biol. Chem.* 277, 37655–37662. doi:10.1074/jbc.M201374200.

Laskowski, R. A., Jabłońska, J., Pravda, L., Vařeková, R. S., and Thornton, J. M. (2018). PDBsum: Structural summaries of PDB entries. *Protein Sci.* 27, 129–134. doi:10.1002/pro.3289.

Lawson, N. D., Stillman, E. A., Whitt, M. A., and Rose, J. K. (1995). Recombinant vesicular stomatitis viruses from DNA. *Proc. Natl. Acad. Sci. U. S. A.* 92, 4477–4481. doi:10.1073/pnas.92.10.4477.

Lentz, T., Burrage, T., Smith, A., Crick, J., and Tignor, G. (1982). Is the acetylcholine receptor a rabies-virus receptor? *Science (80-.).* 215, 182–184. doi:10.1016/0166-2236(82)90227-2.

Lentz, T. L. (1990). Rabies virus binding to an acetylcholine receptor α-subunit peptide. *J. Mol. Recognit.* 3, 82–88. doi:10.1002/jmr.300030205.

Leroy, H., Han, M., Woottum, M., Bracq, L., Xie, M., and Benichou, S. (2020). Virus-Mediated Cell-Cell Fusion. *Int. J. Mol. Sci.* 21, 1–28.

Letko, M., Seifert, S. N., Olival, K. J., Plowright, R. K., and Munster, V. J. (2020). Bat-

borne virus diversity, spillover and emergence. *Nat. Rev. Microbiol.* 18, 461–471. doi:10.1038/s41579-020-0394-z.

Li, Y., Liu, D., Wang, Y., Su, W., Liu, G., and Dong, W. (2021). The Importance of Glycans of Viral and Host Proteins in Enveloped Virus Infection. *Front. Immunol.* 12, 1–12. doi:10.3389/fimmu.2021.638573.

Liu, Y., Hu, G., Wang, Y., Ren, W., Zhao, X., Ji, F., et al. (2021). Functional and genetic analysis of viral receptor ACE2 orthologs reveals a broad potential host range of SARS-CoV-2. *Proc. Natl. Acad. Sci. U. S. A.* 118, 1–9. doi:10.1073/pnas.2025373118.

Longdon, B., Brockhurst, M. A., Russell, C. A., Welch, J. J., and Jiggins, F. M. (2014). The Evolution and Genetics of Virus Host Shifts. *PLoS Pathog.* 10. doi:10.1371/journal.ppat.1004395.

Ma, X., Monroe, B. P., Wallace, R. M., Orciari, L. A., Gigante, C. M., Kirby, J. D., et al. (2021). Rabies surveillance in the United States during 2019. *J. Am. Vetreinary Assoc.* 258.

Maginnis, M. S. (2018a). Virus–Receptor Interactions: The Key to Cellular Invasion. *J. Mol. Biol.* 430, 2590–2611. doi:10.1016/j.jmb.2018.06.024.

Maginnis, M. S. (2018b). Virus–Receptor Interactions: The Key to Cellular Invasion. *J Mol Biol* 430, 2590–2611. doi:https://doi.org/10.1016/j.jmb.2018.06.024.

Majid, A. M., and Barber, G. N. (2006). Recombinant Vesicular Stomatitis Virus (VSV) and Other Strategies in HCV Vaccine Designs and Immunotherapy. *Genomes Mol. Biol.*, 423–450. Available at: http://www.ncbi.nlm.nih.gov/pubmed/21250380.

Marth, J. D., and Grewal, P. K. (2008). Mammalian glycosylation in immunity. *Nat. Rev. Immunol.* 8, 874–887. doi:10.1038/nri2417.

Martínez, M. A., López, S., Arias, C. F., and Isa, P. (2013). Gangliosides Have a Functional Role during Rotavirus Cell Entry. *J. Virol.* 87, 1115–1122. doi:10.1128/jvi.01964-12.

Matthias, S., and Horstkorte, R. (2006). Phosphorylation of the neural cell adhesion

molecule on serine or threonine residues is induced by adhesion or nerve growth factor. *J. Neurosci. Res.* 84, 142–150. doi:10.1002/jnr.20854.

Mazzitelli, M., Palazzo, E., Maione, S., and Neugebauer, V. (2018). Group II Metabotropic Glutamate Receptors: Role in Pain Mechanisms and Pain Modulation. *Front. Mol. Neurosci.* 11, 1–11. doi:10.3389/fnmol.2018.00383.

McFadden, G., Mohamed, M. R., Rahman, M. M., and Bartee, E. (2009). Cytokine determinants of viral tropism. *Nat. Rev. Immunol.* 9, 645–655. doi:10.1038/nri2623.

Michael R. Green, J. S. (2012). *Molecular Cloning*.

Mitchell, A., Chang, H. Y., Daugherty, L., Fraser, M., Hunter, S., Lopez, R., et al. (2015). The InterPro protein families database: The classification resource after 15 years. *Nucleic Acids Res.* 43, D213–D221. doi:10.1093/nar/gku1243.

Mollentze, N., Biek, R., and Streicker, D. G. (2014). The role of viral evolution in rabies host shifts and emergence. *Curr. Opin. Virol.* 8, 68–72. doi:10.1016/j.coviro.2014.07.004.

Morgene, M. F., Maurin, C., Pillet, S., Berthelot, P., and Mor, F. (2018). HaCaT epithelial cells as an innovative novel model of rhinovirus infection and impact of clarithromycin treatment on infection kinetics. *Virol. J.* 523, 27–34. doi:10.1016/j.virol.2018.07.025.

Morimoto, K., Foley, H. D., McGettigan, J. P., Schnell, M. J., and Dietzschold, B. (2000). Reinvestigation of the role of the rabies virus glycoprotein in viral pathogenesis using a reverse genetics approach. *J. Neurovirol.* 6, 373–381. doi:10.3109/13550280009018301.

Munis, A. M., Bentley, E. M., and Takeuchi, Y. (2020). A tool with many applications: vesicular stomatitis virus in research and medicine. *Expert Opin. Biol. Ther.* 20, 1187–1201. doi:10.1080/14712598.2020.1787981.

Natesan, K., Isloor, S., Vinayagamurthy, B., Ramakrishnaiah, S., Doddamane, R., and Fooks, A. R. (2023). Developments in Rabies Vaccines: The Path Traversed from Pasteur to the Modern Era of Immunization. *Vaccines* 11, 1–28.

doi:10.3390/vaccines11040756.

Nevo, J. (2010). Novel Players in the Integrin Signaling Orchestra: TCPTP and MDGI. *Thromb. J.*, 1–97. Available at: https://www.researchgate.net/publication/48330882_Novel_Players_in_the_Integrin_Signaling_Orchestra_TCPTP_and_MDGI/figures?lo=1.

Ng, W. M., Fedosyuk, S., English, S., Augusto, G., Berg, A., Thorley, L., et al. (2022). Structure of trimeric pre-fusion rabies virus glycoprotein in complex with two protective antibodies. *Cell Host Microbe* 30, 1219-1230.e7. doi:10.1016/j.chom.2022.07.014.

Noah, D. L., Drenzek, C. L., Smith, J. S., Krebs, J. W., Orciari, L., Shaddock, J., et al. (1998). Epidemiology of human rabies in the United States, 1980 to 1996. *Ann. Intern. Med.* 128, 922–930. doi:10.7326/0003-4819-128-11-199806010-00012.

Okumura, A., and Harty, R. N. (2011). *Rabies Virus Assembly and Budding*. 1st ed. Elsevier Inc. doi:10.1016/B978-0-12-387040-7.00002-0.

Omasits, U., Ahrens, C. H., Müller, S., and Wollscheid, B. (2014). Protter: Interactive protein feature visualization and integration with experimental proteomic data. *Bioinformatics* 30, 884–886. doi:10.1093/bioinformatics/btt607.

Pantsar, T., and Poso, A. (2018). Binding affinity via docking: Fact and fiction. *Molecules* 23, 1DUMMY. doi:10.3390/molecules23081899.

Perez, M., Clemente, R., Robison, C. S., Jeetendra, E., Jayakar, H. R., Whitt, M. A., et al. (2007). Generation and Characterization of a Recombinant Vesicular Stomatitis Virus Expressing the Glycoprotein of Borna Disease Virus . *J. Virol.* 81, 5527–5536. doi:10.1128/JVI.02586-06.

Piccinotti, S., Kirchhausen, T., and Whelan, S. P. J. (2013). Uptake of Rabies Virus into Epithelial Cells by Clathrin-Mediated Endocytosis Depends upon Actin. *J. Virol.* 87, 11637–11647. doi:10.1128/jvi.01648-13.

Plowright, R. K., Parrish, C. R., McCallum, H., Hudson, P. J., Ko, A. I., Graham, A. L., et al. (2017). Pathways to zoonotic spillover. *Nat. Rev. Microbiol.* 15, 502–510. doi:10.1038/nrmicro.2017.45.

Prosniak, M., Hooper, D. C., Dietzschold, B., and Koprowski, H. (2001). Effect of rabies virus infection on gene expression in mouse brain. *Proc. Natl. Acad. Sci. U. S. A.* 98, 2758–2763. doi:10.1073/pnas.051630298.

Pulmanausahakul, R., Li, J., Schnell, M. J., and Dietzschold, B. (2008). The Glycoprotein and the Matrix Protein of Rabies Virus Affect Pathogenicity by Regulating Viral Replication and Facilitating Cell-to-Cell Spread. *J. Virol.* 82, 2330–2338. doi:10.1128/jvi.02327-07.

Qiao, Y. chao, Wang, F., He, Y. ling, Yang, Q., Yang, J., and Wei, Y. sheng (2021). Regional and age difference of human rabies prevalence of the past fourteen years in China. *Prev. Vet. Med.* 187, 105161. doi:10.1016/j.prevetmed.2020.105161.

Rao, X., Huang, X., Zhou, Z., and Lin, X. (2013). An improvement of the 2ˆ(-delta delta CT) method for quantitative real-time polymerase chain reaction data analysis. *Biostat. Bioinforma. Biomath.* 3, 71–85. Available at: http://www.ncbi.nlm.nih.gov/pubmed/25558171%0Ahttp://www.pubmedcentral.nih.gov/articlerender.fcgi?artid=PMC4280562.

Ren, J., Yao, L., Sun, J., and Gong, Z. (2015). Zagreb regimen, an abbreviated intramuscular schedule for rabies vaccination. *Clin. Vaccine Immunol.* 22, 1–5. doi:10.1128/CVI.00531-14.

Rey, F. A., and Lok, S. (2018). Review Common Features of Enveloped Viruses and Implications for Immunogen Design for Next-Generation Vaccines. *Cell* 172, 1319–1334. doi:10.1016/j.cell.2018.02.054.

Reznik, S. E., Tiwari, A. K., and Jr, C. R. A. (2020). Potential Use of Sofosbuvir in the Prophylaxis for Rabies. *Front. Pharmacol.* 11, 2012–2015. doi:10.3389/fphar.2020.00472.

Rio, D. C., Ares, M., Hannon, G. J., Nilsen, T. W., Rio, D. C., Jr, M. A., et al. (2010). Purification of RNA Using TRIzol (TRI Reagent). *Cold Spring Harb Protoc* 6, 2010–2013. doi:10.1101/pdb.prot5439.

Roberts, A., and Rose, J. K. (1998). Recovery of negative-strand RNA viruses from

plasmid DNAs: A positive approach revitalizes a negative field. *Virology* 247, 1–6. doi:10.1006/viro.1998.9250.

Sadeuh-Mba, S. A., Momo, J. B., Besong, L., Loul, S., and Njouom, R. (2017). Molecular characterization and phylogenetic relatedness of dog-derived Rabies Viruses circulating in Cameroon between 2010 and 2016. *PLoS Negl. Trop. Dis.* 11, 1–21. doi:10.1371/journal.pntd.0006041.

Sajjanar, B., Saxena, S., Bisht, D., Kumar, A., Reddy, G. B. M., Singh, R., et al. (2016). Neuropeptides Effect of nicotinic acetylcholine receptor alpha 1 (nAChR α 1) peptides on rabies virus infection in neuronal cells. *Neuropeptides* 57, 59–64. doi:10.1016/j.npep.2015.11.090.

Sasaki, M., Anindita, P. D., Ito, N., Sugiyama, M., Carr, M., Fukuhara, H., et al. (2018). The role of heparan sulfate proteoglycans as an attachment factor for rabies virus entry and infection. *J. Infect. Dis.* 217, 1740–1749. doi:10.1093/infdis/jiy081.

Sato, H., Yoneda, M., Honda, T., and Kai, C. (2012). Morbillivirus receptors and tropism: Multiple pathways for infection. *Front. Microbiol.* 3, 1–9. doi:10.3389/fmicb.2012.00075.

Schneider-Schaulies, J. (2000). Cellular receptors for viruses: Links to tropism and pathogenesis. *J. Gen. Virol.* 81, 1413–1429. doi:10.1099/0022-1317-81-6-1413.

Schnell, M. J., Buonocore, L., Whitt, M. A., and Rose, J. K. (1996). The minimal conserved transcription stop-start signal promotes stable expression of a foreign gene in vesicular stomatitis virus. *J. Virol.* 70, 2318–2323. doi:10.1128/jvi.70.4.2318-2323.1996.

Schnell, M. J., McGettigan, J. P., Wirblich, C., and Papaneri, A. (2010). The cell biology of rabies virus: Using stealth to reach the brain. *Nat. Rev. Microbiol.* 8, 51–61. doi:10.1038/nrmicro2260.

Scott, M. G. H., Benmerah, A., Muntaner, O., and Marullo, S. (2002). Recruitment of Activated G Protein-coupled Receptors to Pre-existing Clathrin-coated Pits in Living Cells *. *J. Biol. Chem.* 277, 3552–3559. doi:10.1074/jbc.M106586200.

Scrima, N., Le Bars, R., Nevers, Q., Glon, D., Chevreux, G., Civas, A., et al. (2023). Rabies virus P protein binds to TBK1 and interferes with the formation of innate immunity-related liquid condensates. *Cell Rep.* 42. doi:10.1016/j.celrep.2022.111949.

Shen, H., Fang, S. G., Chen, B., Chen, G., Tay, F. P. L., and Liu, D. X. (2009). Towards construction of viral vectors based on avian coronavirus infectious bronchitis virus for gene delivery and vaccine development. *J. Virol. Methods* 160, 48–56. doi:10.1016/j.jviromet.2009.04.023.

Shepherd, J. G., Davis, C., Streicker, D. G., and Thomson, E. C. (2023). Emerging Rhabdoviruses and Human Infection. *Biology (Basel).* 12, 878. doi:10.3390/biology12060878.

Shuai, L., Wang, J., Zhao, D., Wen, Z., Ge, J., He, X., et al. (2020). Integrin β1 Promotes Peripheral Entry by Rabies Virus. *J. Virol.* 94, 1–17. doi:10.1128/jvi.01819-19.

Shukla, D., and Spear, P. G. (2001). Herpesviruses and heparan sulfate: an intimate relationship in aid of viral entry. *J. Clin. Invest.* 108, 503–510. doi:10.1172/jci13799.

Sigrist, C. J. A., Bridge, A., and Mercier, P. Le (2020). A potential role for integrins in host cell entry by SARS-CoV-2. *Antiviral Res.* 177.

Skog, M. S., Nystedt, J., Korhonen, M., Anderson, H., Lehti, T. A., Pajunen, M. I., et al. (2016). Expression of neural cell adhesion molecule and polysialic acid in human bone marrow-derived mesenchymal stromal cells. *Stem Cell Res. Ther.* 7, 1–12. doi:10.1186/s13287-016-0373-5.

Slate, D., Algeo, T. P., Nelson, K. M., Chipman, R. B., Donovan, D., Blanton, J. D., et al. (2009). Oral rabies vaccination in North America: Opportunities, complexities, and challenges. *PLoS Negl. Trop. Dis.* 3, 1–9. doi:10.1371/journal.pntd.0000549.

Slate, D., Rupprecht, C. E., Rooney, J. A., Donovan, D., Lein, D. H., and Chipman, R. B. (2005). Status of oral rabies vaccination in wild carnivores in the United States.

Virus Res. 111, 68–76. doi:10.1016/j.virusres.2005.03.012.

Song, M., Tang, Q., Rayner, S., Tao, X. Y., Li, H., Guo, Z. Y., et al. (2014). Human rabies surveillance and control in China, 2005-2012. *BMC Infect. Dis.* 14, 1–9. doi:10.1186/1471-2334-14-212.

Song, M., Tang, Q., Wang, D., Mo, Z., Guo, S., Li, H., et al. (2009). Epidemiological investigations of human rabies in China. *BMC Infect. Dis.* 8, 1–8. doi:10.1186/1471-2334-9-210.

Superti, F., Hauttecoeur, B., Morelec, M. J., Goldoni, P., Bizzini, B., and Tsiang, H. (1986). Involvement of gangliosides in rabies virus infection. *J. Gen. Virol.* 67, 47–56. doi:10.1099/0022-1317-67-1-47.

Takadate, Y., Kondoh, T., Igarashi, M., Maruyama, J., Manzoor, R., Ogawa, H., et al. (2020). Niemann-Pick C1 Heterogeneity of Bat Cells Controls Filovirus Tropism. *Cell Rep.* 30, 308-319.e5. doi:10.1016/j.celrep.2019.12.042.

Tani, H., Morikawa, S., and Matsuura, Y. (2012). Development and applications of VSV vectors based on cell tropism. *Front. Microbiol.* 2, 1–7. doi:10.3389/fmicb.2011.00272.

Tantirimudalige, S. N., Raghuvamsi, P. V., Sharma, K. K., Wei Bao, J. C., Anand, G. S., and Wohland, T. (2022). The ganglioside GM1a functions as a coreceptor/attachment factor for dengue virus during infection. *J. Biol. Chem.* 298, 102570. doi:10.1016/j.jbc.2022.102570.

Tao, X., Liu, S., Zhu, W., and Rayner, S. (2021). Rabies surveillance and control in China over the last twenty years. *Biosaf. Heal.* 3, 142–147. doi:10.1016/j.bsheal.2020.11.004.

Tarantola, A., Tejiokem, M. C., and Briggs, D. J. (2019). Evaluating new rabies post-exposure prophylaxis (PEP) regimens or vaccines. *Vaccine* 37, A88–A93. doi:10.1016/j.vaccine.2018.10.103.

Taube, S., Jiang, M., and Wobus, C. E. (2010). Glycosphingolipids as receptors for non-enveloped viruses. *Viruses* 2, 1011–1049. doi:10.3390/v2041011.

Tell, J. G., Coller, B. G., Dubey, S. A., Jenal, U., Lapps, W., Wang, L., et al. (2020).

Environmental Risk Assessment for rVSV Δ G-ZEBOV-GP , a Genetically Modified Live Vaccine for Ebola Virus Disease.

Theobald, D. L., and Wuttke, D. S. (2007). Divergent Evolution Within Protein Superfolds Inferred from Profile-based Phylogenetics Douglas. *J Mol Biol* 354, 722–737.

Thomas, P., and Smart, T. G. (2005). HEK293 cell line: A vehicle for the expression of recombinant proteins. *J. Pharmacol. Toxicol. Methods* 51, 187–200. doi:10.1016/j.vascn.2004.08.014.

Thoulouze, M.-I., Lafage, M., Schachner, M., Hartmann, U., Cremer, H., and Lafon, M. (1998). The Neural Cell Adhesion Molecule Is a Receptor for Rabies Virus. *J. Virol.* 72, 7181–7190. doi:10.1128/jvi.72.9.7181-7190.1998.

Thwaites, R. S., Uruchurtu, A. S. S., Siggins, M. K., Liew, F., Russell, C. D., Moore, S. C., et al. (2020). Info _ Outline. *Crit. Rev. Clin. Lab. Sci.* 8, 1–5. Available at: https://doi.org/10.1016/j.medcli.2020.05.012%0Ahttps://doi.org/10.1080/10408363.2020.1776675%0Ahttps://doi.org/10.1007/s11033-021-06148-9%0Ahttp://dx.doi.org/10.1038/s41584-021-00608-z%0Ahttp://dx.doi.org/10.1038/s41409-020-0931-4%0Ahttps://doi.org/10.118.

Topiol, S., Sabio, M., and Uberti, M. (2011). Exploration of structure-based drug design opportunities for mGluRs. *Neuropharmacology* 60, 93–101. doi:10.1016/j.neuropharm.2010.08.001.

Tovchigrechko, A., and Vakser, I. A. (2006a). GRAMM-X public web server for protein-protein docking. *Nucleic Acids Res.* 34, 310–314. doi:10.1093/nar/gkl206.

Tovchigrechko, A., and Vakser, I. A. (2006b). GRAMM-X public web server for protein – protein docking. *Nucleic Acids Res.* 34, 310–314. doi:10.1093/nar/gkl206.

Tuffereau, C., Benejean, J., Alfonso, A.-M. R., Flamand, A., and Fishman, M. C. (1998a). Neuronal Cell Surface Molecules Mediate Specific Binding to Rabies Virus Glycoprotein Expressed by a Recombinant Baculovirus on the Surfaces of Lepidopteran Cells. *J. Virol.* 72, 1085–1091. doi:10.1128/jvi.72.2.1085-

1091.1998.

Tuffereau, C., Bénéjean, J., Blondel, D., Kieffer, B., and Flamand, A. (1998b). Low-affinity nerve-growth factor receptor (P75NTR) can serve as a receptor for rabies virus. *EMBO J.* 17, 7250–7259. doi:10.1093/emboj/17.24.7250.

Tuffereau, C., Schmidt, K., Langevin, C., Lafay, F., Dechant, G., and Koltzenburg, M. (2007). The Rabies Virus Glycoprotein Receptor p75 NTR Is Not Essential for Rabies Virus Infection . *J. Virol.* 81, 13622–13630. doi:10.1128/jvi.02368-06.

Vaidya, S. A., Manning, S. E., Dhankhar, P., Meltzer, M. I., Rupprecht, C., Hull, H. F., et al. (2010). Estimating the risk of rabies transmission to humans in the U.S.: A delphi analysis. *BMC Public Health* 10. doi:10.1186/1471-2458-10-278.

Walker, P. J., Firth, C., Widen, S. G., Blasdell, K. R., Guzman, H., and Vasilakis, N. (2015). Evolution of Genome Size and Complexity in the Rhabdoviridae. *PLoS Pathog.* 11, 1–25. doi:10.1371/journal.ppat.1004664.

Walker, P. J., Freitas-Astua, J., Bejerman, N., Blasdell, K. R., Breyta, R., Dietzgen, R. G., et al. (2022). ICTV Virus Taxonomy Profile: Rhabdoviridae 2022. *J. Gen. Virol.* 103, 2021–2022. doi:10.1099/jgv.0.001689.

Wang, J., Wang, Z., Liu, R., Shuai, L., Wang, X., Luo, J., et al. (2018). Metabotropic glutamate receptor subtype 2 is a cellular receptor for rabies virus. *PLoS Pathog.* 14, 1–21. doi:10.1371/journal.ppat.1007189.

Wang, J., Yang, G., Wang, X., Wen, Z., Shuai, L., Luo, J., et al. (2021). SARS-CoV-2 uses metabotropic glutamate receptor subtype 2 as an internalization factor to infect cells. *Cell Discov.* 7. doi:10.1038/s41421-021-00357-z.

Wang, X., Wen, Z., Cao, H., Luo, J., Shuai, L., Wang, C., et al. (2023). Transferrin Receptor Protein 1 Is an Entry Factor for Rabies Virus. *J. Virol.* 1.

Wang, X. X., Wen, Z., Cao, H., Luo, J., Shuai, L., Wang, C., et al. (2022). Transferrin Receptor Protein 1 Cooperates with mGluR2 To Mediate the Internalization of Rabies Virus and SARS-CoV-2. *J. Virol.* 1.

Warren, C. J., and Sawyer, S. L. (2019). How host genetics dictates successful viral zoonosis. *PLoS Biol.* 17, 1–19. doi:10.1371/journal.pbio.3000217.

Wei, C.-J., Boyington, J. C., Dai, K., Houser, K. V., Pearce, M. B., Kong, W.-P., et al. (2010). Cross-Neutralization of 1918 and 2009 Influenza Viruses: Role of Glycans in Viral Evolution and Vaccine Design. *Sci Transl. Med.* 24, 139–148. doi:10.1126/scitranslmed.3000799.Cross-Neutralization.

Wertz, G. W., Moudy, R., and Ball, L. A. (2002). Adding Genes to the RNA Genome of Vesicular Stomatitis Virus: Positional Effects on Stability of Expression. *J. Virol.* 76, 7642–7650. doi:10.1128/jvi.76.15.7642-7650.2002.

Whitt, M. A. (2010). Generation of VSV pseudotypes using recombinant ΔG-VSV for studies on virus entry, identification of entry inhibitors, and immune responses to vaccines. *J. Virol. Methods* 169, 365–374. doi:10.1016/j.jviromet.2010.08.006.

Wojczyk, B. S., Takahashi, N., Levy, M. T., Andrews, D. W., Abrams, W. R., Wunner, W. H., et al. (2005). N-glycosylation at one rabies virus glycoprotein sequon influences N-glycan processing at a distant sequon on the same molecule. *Glycobiology* 15, 655–666. doi:10.1093/glycob/cwi046.

Wunner, W. H., and Briggs, D. J. (2010). Rabies in the 21st century. *PLoS Negl. Trop. Dis.* 4, 4–6. doi:10.1371/journal.pntd.0000591.

Xu, H., Hao, X., Wang, S., Wang, Z., Cai, M., Jiang, J., et al. (2015). Real-time imaging of rabies virus entry into living vero cells. *Sci. Rep.* 5, 1–12. doi:10.1038/srep11753.

Yang, F., Lin, S., Ye, F., Yang, J., Qi, J., Chen, Z. Z., et al. (2020). Structural Analysis of Rabies Virus Glycoprotein Reveals pH-Dependent Conformational Changes and Interactions with a Neutralizing Antibody. *Cell Host Microbe* 27, 441-453.e7. doi:10.1016/j.chom.2019.12.012.

Yang, J., Zhang, Y., Rohini, K., Srikumar, P. S., Anbarasu, K., Structural, L., et al. (2010). I-TASSER: a unified platform for automated protein structure and function prediction. *Nat. Protoc.* 5, 725–738. doi:10.1038/nprot.2010.5.I-TASSER.

Yin, J., Wang, X., Mao, R., Zhang, Z., Gao, X., Luo, Y., et al. (2021). Research Advances

on the Interactions between Rabies Virus Structural Proteins and Host Target Cells : Accrued Knowledge from the Application of Reverse Genetics Systems. *Viruses* 13.

Yin, W., Dong, J., Tu, C., Edwards, J., Guo, F., Zhou, H., et al. (2013). Challenges and needs for China to eliminate rabies. *Infect. Dis. poverty* 2, 1. doi:10.1186/2049-9957-2-23.

You, J., O'Hara, S. D., Velupillai, P., Castle, S., Levery, S., Garcea, R. L., et al. (2015). Ganglioside and Non-ganglioside Mediated Host Responses to the Mouse Polyomavirus. *PLoS Pathog.* 11, 1–19. doi:10.1371/journal.ppat.1005175.

Zeiler, F. A., and Jackson, A. C. (2015). Critical Appraisal of the Milwaukee Protocol for Rabies : This Failed Approach Should Be Abandoned. *Can. J. Neurol. Sci.* 43. doi:10.1017/cjn.2015.331.

Zhang, Y., Yan, Y., Li, S., Yuan, F., and Wen, D. (2023). Broad Host Tropism of Flaviviruses during the Entry Stage.

Zhao, C., and Pu, J. (2022). Influence of Host Sialic Acid Receptors Structure on the Host Specificity of Influenza Viruses. *Viruses* 14. doi:10.3390/v14102141.

Zhou, H., Vong, S., Liu, K., Li, Y., Mu, D., Wang, L., et al. (2016). Human Rabies in China , 1960-2014 : A Descriptive Epidemiological Study. *PLoS Negl. Trop. Dis.* 10, 1–12. doi:10.1371/journal.pntd.0004874.